

SYNCHROTRON RADIATION IN NATURAL SCIENCE

Bulletin of the Polish Synchrotron Radiation Society
Volume 9, Number 1-2, June 2010



Includes: Programme and Abstracts of the of the 10th International Symposium and School on Synchrotron Radiation in Natural Science (ISSRNS-10)



Organised by: Polish Synchrotron Radiation Society (PTPS)
in cooperation with Adam Mickiewicz University (Poznań, Poland)

Sponsored by: Ministry of Science and Higher Education

SYNCHROTRON RADIATION IN NATURAL SCIENCE

Bulletin of the Polish Synchrotron Radiation Society

Address: al. Lotników 32/46, 02-668 Warsaw, Poland, phone/fax (0) 228436034, e-mail: paszk@ifpan.edu.pl

Editor

Wojciech Paszkowicz (Editor)
Institute of Physics
Polish Academy of Sciences
al. Lotników 32/46
02-668 Warsaw
e-mail: paszk@ifpan.edu.pl

Editorial Board

Andrzej Burian
Institute of Physics
Silesian University
ul. Uniwersytecka 4
40-007 Katowice
e-mail: burian@us.edu.pl

Edward A. Görllich
Institute of Physics
Jagellonian University
ul. Reymonta 4
30-059 Kraków
e-mail: ufgoerli@cyf-kr.edu.pl

Krystyna Jabłońska
Institute of Physics
Polish Academy of Sciences
al. Lotników 32/46
02-668 Warsaw
e-mail: jablo@ifpan.edu.pl

Bogdan J. Kowalski
Institute of Physics
Polish Academy of Sciences
al. Lotników 32/46
02-668 Warsaw, Poland
e-mail: kowab@ifpan.edu.pl

Maciej Kozak
Faculty of Physics
A. Mickiewicz University
ul. Umultowska 85
61-614 Poznań
e-mail: mkozak@amu.edu.pl

Wojciech Kwiatek
Institute of Nuclear Physics
Polish Academy of Sciences
ul. Radzikowskiego 152
31-342 Cracow
e-mail:
wojciech.kwiatek@ifj.edu.pl

Bronisław A. Orłowski
Institute of Physics
Polish Academy of Sciences
al. Lotników 32/46
02-668 Warsaw
e-mail: orbro@ifpan.edu.pl

Paweł Piszora
Faculty of Chemistry
A. Mickiewicz University
ul. Grunwaldzka 6
60-780 Poznań
e-mail: pawel@amu.edu.pl

Anna Wolska
Institute of Physics
Polish Academy of Sciences
al. Lotników 32/46
02-668 Warsaw
e-mail: wolska@ifpan.edu.pl

Danuta Żymierska
Institute of Physics
Polish Academy of Sciences
al. Lotników 32/46
02-668 Warsaw
e-mail: zymier@ifpan.edu.pl

Note for contributors: Contributions in English (preferred) or in Polish should be sent to the Editor. The topics include: synchrotron and alternative radiation sources, beamline instrumentation, experimental and theoretical results connected with application of various methods and approaches (x-ray scattering, x-ray diffraction, x-ray absorption, fluorescence and photoelectron spectroscopies, magnetic dichroism, etc.) in connection with application of synchrotron radiation in physics, chemistry, crystallography, materials science and life sciences.

Figure on the cover page: The constructor's impression of Polish synchrotron (Drawing by PROBADEX, cf. page 1, this issue).

SYNCHROTRON RADIATION IN NATURAL SCIENCE is published and distributed by the Polish Synchrotron Radiation Society (PSRS). Typesetting and cover design by W. Paszkowicz.

Detailed information on PSRS is given on cover page 3.

Acknowledgements: This issue of the journal was sponsored by Ministry of Science and Higher Education (Poland) through the grant 643/DWB/P/2010.

ISSN 1644-7190

Volume 9, No. 1-2, 2010, © Polish Synchrotron Radiation Society

Skład, łamanie i druk:
ORKA Media Sp. z o.o.
e-mail: orkamedia@orkamedia.pl

CONTENTS

M.J. Stankiewicz, E.A. Görlich, K. Królas	Synchrotron light source in Poland!		1
	Synchrotron Light News		2
Regular contributions			
Z. Dauter, A. Wlodawer, M. Jaskólski	Promieniowanie rentgenowskie ze źródeł synchrotronowych jako katalizator rozwoju krystalografii białek		4
M. Jaskólski	From atomic resolution to molecular giants: An overview of crystallographic studies of biological macromolecules with synchrotron radiation		17
H. Tomizawa	Advanced metaheuristic algorithms for laser optimization		24
M. Jaskólski	Dr. Zbigniew Dauter receives the highest science award from the Polish Academy of Sciences		28
D. Żymierska, B. Orłowski	The jubilee of our conferences		29
D. Żymierska	News from the Polish Synchrotron Radiation Society		32
K. Lawniczak-Jablonska, R. Nietubyć, R. Sobierajski	On FEL in Ryn		34
	Zapowiedzi wydawnicze (forthcoming books)		35
ISSRNS-10 – 10th International School and Symposium on Synchrotron Radiation in Natural Science 2010			
	ISSRNS 2010 – Information		37
	ISSRNS 2010 – programme		38
	Welcome		41
ISSRNS-10 – Invited lectures and oral presentations			
W. Minor	Impact of 3 rd generation synchrotron sources on structural biology	L01	42
A. Marcelli	Biological applications of synchrotron radiation infrared spectromicroscopy	L02	43
P. Ghigna, S. Pin, G. Spinolo	Synchrotron radiation in solid state chemistry	L03	44
U. Pietsch, A. Davydok, S. Breuer, A. Biermanns, L. Geelhaar	X-ray strain evaluation at individual semiconductor nanowires	L04	45
P. Hoffmann, C. Pettenkofer	Chemical nature of N-ions incorporated into epitaxial ZnO films	O01	46
U. Heinemann, B. König, E. Lanka, A. Schütz, D. Carstanjen, K.E.A. Max	Use of synchrotron radiation in studies of protein structure and nucleic acid binding	L05	47
K. Shimada	Many-body interactions in solids studied by high-resolution ARPES using synchrotron radiation	L06	48
Y. Cerenius	First phase beamlines on MAX IV	L08	50
D. Einfeld	Trends in state of the art storage ring based SR sources	L09	51

B.J. Kowalski, M.A. Pietrzyk, W. Knoff, R. Nietubyć, K. Nowakowska-Langier, J. Sadowski, A. Łusakowski, T. Story	Photoelectron spectroscopy in studies of the band structure of IV-VI spintronic materials	L10ext	52
S. Thies, T.-L. Lee, F. Bottin, . Gloskovskii, W. Drube, J. Zegenhagen	Site specific XPS: Structural and electronic properties investigated by X-ray standing waves	L11ext	54
K. Lawniczak-Jablonska, A. Wolska, M.T. Klepka, J. Gosk, A. Twardowski, D.Wasik, A. Kwiatkowski, J. Sadowski	The shape anisotropy of the MnSb inclusions formed in GaSb matrix as probed by XMCD	O02ext	56
H. Amenitsch	Applications of SAXS and GISAXS in bionanotechnology	L12	58
M. Roessle, D.I. Svergun	Structural studies of biological macromolecules in solution using synchrotron small-angle X-ray scattering	L13	59
M. Reconditi, G. Piazzesi, M.Irving, V. Lombardi	SAXS studies of the muscle cell to identify the force-generating myosin molecules	O03	60
H. Drozdowski, K. Nowakowski, Z. Błaszczak	Determination of electron radial distribution function for liquid cyclohexylamine by X-ray diffraction	O04	61
K.O. Kvashnina, S.M. Butorin, A. Kotani, P. Glatzel	X-ray absorption and emission spectroscopy of rare-earth materials	L14ext	62
A. Kuczumow, J. Nowak, R. Chałas	Microchemical and structural regular variability of apatites in "overbuilt" enamel and dentin of human molar teeth	L15	64
J. Ivančo, D. Karnaushenko, P. Schäfer, D.R.T. Zahn, W. Braun, E. Majková	Top metal contact on an organic film: Indium on copper phthalocyanine	O05	65
A. Ghaffar, W. Pichl, G. Krexner, I. Zizak	Confinement-induced structural changes of lithium and sodium in nano-porous silica glass	O06	66
V. Petříček, M. Dušek	Jana2006 as a tool for solution and refinement of non-standard crystal structures	L16	67
J. Gapiński, A. Patkowski	Application of X-ray scattering and diffraction techniques to studies of highly charged colloid suspensions in the vicinity of the crystallization point	L17	68
M.S. Žbik, R.L. Frost	Synchrotron based transmission X-ray microscopy reveals smectite fine structure in an aqueous environment	O07	69
V. Lombardi, M. Linari, M. Reconditi, E. Brunello, L. Fusi, T.C. Irving, T. Narayanan, G. Piazzesi, M. Irving	X-ray interference measurements of the molecular motor of muscle with nanometer-microsecond resolution	L18	70
M. Cholewa	High resolution X-ray microprobes and their applications	L19	71
T. Ślęzak, M. Zając, M. Ślęzak, K. Matlak, N. Spiridis, K. Freindl, D. Wilgocka-Ślęzak, R. Ruffer, J. Korecki	Depth-resolved magnetization structure at the spin reorientation transition in Fe/W(110) ultrathin films studied by the nuclear resonant scattering of synchrotron radiation	O08	72
W. Wierzchowski, K. Wieteska, D. Klinger, R. Sobierajski, J. Pełka, T. Balcer	X-ray topographic investigation of the deformation field around spots irradiated by FLASH single pulses	O09	73
M.J. Stankiewicz, E.A. Görlich, K. Królas	Polish Synchrotron – present status	L20	74
M. Eriksson, A. Wawrzyniak, P. Goryl	The accelerators for the Polish Light Source and MAX IV	L21	75
J. Szade,, B.A. Orłowski, B.J. Kowalski, E. Görlich, K. Tomala, P. Starowicz	Soft X-ray Spectroscopy - first beamline at Polish synchrotron	L22	76
B. Kaulich, A. Gianoncelli, M. Kiskinova	Transmission and emission soft X-ray spectromicroscopies for life and nanosciences at Elettra	L23	77

R. Nietubyć, E. Dynowska, R. Mirowski, K. Nowakowska-Langier, J. Pełka, P. Romanowski, J. Witkowski	Growth of niobium film on sapphire(001)	O10	78
J. Szlachetko, M. Cotte, J. Morse, . Salome, M. Pajek, P. Jagodzinski, J.–Cl. Dousse, J. Hozowska, Y. Kayser, J. Susini	Application of wavelength-dispersive spectroscopy at ID21 X-ray Microscopy beamline of ESRF: New possibilities for micro-fluorescence and micro-XANES analysis	O11	79
W. Paszkowicz	Properties of rare earth orthovanadates under high pressure	O12	80
L. Walczak, V. Joco, G. Goryl, .A. Valbuena, T. Balasubramanian, P. Segovia, M. Szymonski, E.G. Michel	Electronic structure and crystalline structure of vicinal beryllium surfaces	O13	81
C.V. Ciobanu	Genetic algorithms for structural optimization problems at the nanoscale	L24	82
AJ. Martinez-Blanco, V. Joco, C. Quiros, P. Segovia, E.G. Michel	Application of genetic algorithms to surface X-ray diffraction analysis	L25	83
H. Tomizawa	Strategy of metaheuristics algorithms for laser optimization	L26	84
W. Sławiński, R. Przeniosło, I. Sosnowska, M. Bieringer	Magnetoelastic coupling in $\text{CaMn}_7\text{O}_{12}$	O14	85
M. Zając, T. Ślęzak, M. Ślęzak, K. Freindl, P. Cierniak, E. Partyka-Jankowska, J. Korecki	In situ high temperature magnetic and dynamic properties of Fe(110) nanostructures studied with nuclear resonant scattering techniques	O15	86
M. Amati, M. Kazemian Abyaneh, M.M. Dalmiglio, L. Gregoratti, M. Kiskinova	Recent achievement in characterization of micro- and nano-materials by scanning photoemission imaging and spectromicroscopy	O16	87
ISSRNS-10 – Poster presentations			
P. Romanowski, A. Shalimov,, J. Bak-Misiuk, A. Misiuk, W. Caliebe	Structural and magnetic properties of Si single crystals implanted with Mn	P01ext	88
M. Wojcik, J. Gaca, A. Turos, P. Caban, W. Strupiński, K. Pałowska	HRXRD and RBS/channeling determination of the correlation between radiation damage and interplanar spacing in GaN epilayers	P02	90
R. Bacewicz, A. Pietnoczka, W. Zalewski, A. Antonowicz, T. Słupiński	Local structure in Te doped GaAs	P03	91
B.A. Orlowski, P. Dziawa, K. Gas, S. Mickievicius, M. Szot, J.B. Pelka, M.A. Pietrzyk, B.J. Kowalski, S. Thiess, W. Drube	High energy photoemission from covered layer	P04	92
B.A. Orlowski, A. Szczerbakow, B.J. Kowalski, M.A. Pietrzyk, K. Gas, M. Szot, W. Szuszkiewicz, V. Domukhovski, S. Mickevicius, R.L. Johnson, S. Thiess, W. Drube	Electronic structure of ternary $\text{Pb}_{1-x}\text{Cd}_x\text{Te}$ crystal by means of photoemission spectroscopy	P05	93
B. Marciniak, M. Kozak, K. Dettlaff, M. Naskrent	Influence of ionizing radiation on disulfiram in the solid state	P06	94
K. Mazur, J. Sarnecki, W. Wierzchowski, K. Wieteska, A. Turos	Topographic X-ray characterization of GGG homoepitaxial layers with introduced divalent ions of transition-metals	P07	95
J. Bak-Misiuk, E. Dynowska, P. Romanowski, A. Kulik, W. Caliebe	Structural characterization of Mn^+ ion-implanted GaSb	P08	96

I. Capan, J. Bak-Misiuk, A. Misiuk, P. Dubček, S. Bernstorff, P. Romanowski	Synchrotron and X-ray studies of spongy-like buried layers produced in silicon by helium implantation	P09	97
V.G. Vlasenko, A.S. Burlov, Y.V. Zubavichus, I.S. Vasilchenko, A.I. Uraev, A.D. Garnovskii	XAFS study of novel type of metallochelates of phenylazoderivatives of Schiff bases	P10	98
E. Guziewicz, M. Lukasiewicz, L. Wachnicki, K. Kopalko, B.S. Witkowski, J. Sadowski, M. Godlewski	Synchrotron photoemission study of (Zn,Co)O films with uniform Co distribution	P11ext	99
E. Dynowska, J. Bak-Misiuk, P. Romanowski, J. Domagala, J. Sadowski, T. Wojciechowski, A. Kwiatkowski, W. Caliebe	Structural and magnetic properties of GaSb:MnSb granular layers	P12	101
Cz. Ślusarczyk	Crystallization and melting behavior of poly(ethylene oxide) and its blend with styrene-based ionomer using time-resolved SAXS/WAXS experiments	p13	102
M. Ślęzak, A. Koziół, K. Matlak, T. Ślęzak, M. Zając, R. Ruffer, J. Korecki	Growth and spin structure of ultrathin Fe films on W(110)	P14ext	103
L. Hawelek, A. Brodka, J.C. Dore, V. Honkimaki, A. Burian	Structural studies of disordered carbons - comparison of simulations and high-energy X-ray diffraction data	P15	105
S. Grebinskij, M. Senulis, H. Tvardauskas, V. Bondarenka, V. Lissauskas, K. Sliuziene, B. Vengalis, B.A. Orłowski, R.L. Johnson, S. Mickevicius	Valence band study of LaNiO _{3-δ} thin films	P16	106
M.S. Walczak, K. Ławniczak-Jablonska, A. Wolska, M. Sikora, A. Sienkiewicz, L. Suárez, A. Kosar, M.J. Bellemare, D.S. Bohle	XANES study of the synthetic equivalent of hemozoin dissolved in organic solvents before and after interaction with chloroquine	P17	107
M. Kowalik, M. Sikora, A. Kołodziejczyk, Cz. Kapusta	XANES and X-ray photoemission of the La _{0.67} (Ca,Pb) _{0.33} (Mn _{1-x} Fe _x)O ₃ compounds	P18ext	108
J. Klasa, O. Borkiewicz, J. Flis, M. Manecki	Synchrotron-based X-ray diffraction of the pyromorphite-vanadinite and mimetite-vanadinite series	P19	110
W. Zalewski, A. Pietnoczka, J. Antonowicz, R. Bacewicz	Local atomic order in Zr-Cu metallic glasses studied by X-ray absorption fine structure method	P20	111
J. Gaca, M. Wójcik, M. Bugajski, K. Kosiel	The determination of the chemical composition profile of the GaAs/AlGaAs heterostructures designed for quantum cascade lasers by means of synchrotron radiation	P21	112
W. Szczerba, M. Radtke, U. Reinholz, H. Iesemeier, A.F. Thünemann, R. Fenger, K. Rademann	XAFS on CTAB-stabilized gold nanoparticles	P22	113
M. Gajda, J. Kowalska, A. Banaś, K. Banaś, W.M. Kwiatek, R. Kostogryś, Ł. Mateuszuk, S. Chłopicki, J.A. Litwin, K. Appel	Distribution of selected elements in atherosclerotic plaques of apoe/ldlr-double knockout mice subjected to dietary and pharmacological treatments	P23	114
A. Kubala-Kukuś, J. Szlachetko,, M. Pajek, J. Susini, M. Salome	Lateral distribution of elements in the multielemental standard samples studied by the synchrotron radiation based micro X-ray fluorescence	P24	115
H. Drozdowski, K. Nowakowski, Z. Błaszczak	X-ray diffraction investigation of cyclohexane derivatives at 293 K	P25	116
P. Jagodziński, M. Pajek, J. Szlachetko, D. Banaś, A. Kubala-Kukuś, J.-Cl. Dousse, J. Hoszowska, Y. Kayser	Simulations of polycapillary-based wavelength dispersive X-ray flat-crystal spectrometer	P26	117

E. Piskorska-Hommel, V. Holý, A. Wolska, A. Gust, C. Kruse, H. Kröncke, J. Falta, D. Hommel, H. Renevier, F. d'Acapito	Influence overgrowth parameters on the local structure in CdSe quantum dots studied by fine structure method	P27ext	118
M. Krupinski, M. Perzanowski, A. Polit, Y. Zabala, A. Zarzycki, M. Marszalek	EXAFS and XRD studies of crystallographic grains in nanocrystalline FePd:Cu thin films	P28	120
A. Jarmuła, A. Dowierciał, P. Wilk, W.R. Rypniewski, W. Rode	Thymidylate synthase in complex with N(4)-hydroxy-2'-deoxycytidine 5'-monophosphate: Crystal structure and molecular modeling	P29	121
T. Tataryn, D. Savytskii, E. Schmidbauer, C. Paulmann, U. Bismayer	Domain configurations and conductivity in LSGM	P30ext	122
V.A. Shuvaeva, Y.V. Zubavichus, A.A. Chernyshov, K.A. Lyssenko	XAFS and X-RAY diffraction study of the cubic phase of Ni ₃ B ₇ O ₁₃ Br	P31	125
A. Wolska, M.T. Klepka, K. Lawniczak-Jablonska, D. Arvanitis, A. Misiuk	EXAFS and XMCD investigations on the Mn ⁺ implanted silicon crystals	P32ext	126
A. Wolska, K. Lawniczak-Jablonska, M.T. Klepka, M. Kulik, R. Jakiela	Another approach to the Mn ion implantation into the GaSb crystals	P33ext	128
M.T. Klepka, A. Wolska, K. Lawniczak-Jablonska, S. Filipek, R. Sato	EXAFS investigations on novel Laves phase hydrides	P34ext	130
K. Polewski, J. Trunk, J.C. Sutherland	Luminescence from adenine in argon matrices at 12 K	P35	132
J. Szlachetko, M. Cotte, J. Morse, M. Salome, J. Susini	Multi-modal X-ray fluorescence detection at the ID21 X-ray microscopy beamline	P36	133
J. Szlachetko, M. Kavčič, M. Žitnik, K. Bučar	Lifetime broadening-free L ₃ X-ray absorption spectrum of Xe measured by X-ray resonant inelastic scattering	P37	134
B. Mierzwa, K. Zelga, W. Bury, K. Sokołowski, J. Lewiński, R. Nietubyć, Z. Kaszkur	EXAFS and XRD structure analysis of ZnO nanoclusters formed via selective oxygenation of organozinc compounds	P38ext	135
W. Paszkowicz, P. Piszora, Y. Cerenius, S. Carlson, B. Bojanowski, H. Dąbkowska	High-pressure diffraction study of SmVO ₄ : Compressibility and zircon-scheelite phase transition	P39	137
W.M. Kwiatek, J. Czapla, M. Podgórczyk, A. Kisiel, J. Konior, A. Balerna	First approach to studies of sulphur electron DOS in prostate cancer cell lines and tissues studied by XANES	P40	138
P. Olszowy, M. Kozak, S. Pikus, B. Buszewski	Characterisation of nanoporous polymeric SPME coatings with use of SAXS measurements	P41	139
P. Zajdel, I. Jendrzewska, J. Goraus, H. Duda, T. Goryczka, A. Kita	Influence of nickel doping on physical properties of ZnCr ₂ Se ₄	P42	140
M. Brancewicz, A. Andrejczuk, E. Żukowski, L. Dobrzyński, S. Kaprzyk	Reconstruction of the spherical electron momentum density distribution in Mg by the maximum entropy method	P43	141
D. Klinger, R. Sobierajski, M. Jurek, J. Krzywinski, J.B. Pelka, D. Żymierska, R. Minikayev, B. Kozankiewicz, J. Chalupský, L. Juha, V. Hájková, J. Cihelka, T. Burian, L. Vyšín, H. Wabnitz, W. Caliebe, K. Tiedtke, S. Toleikis, T. Tschentscher, R. London, S. Hau-Riege, K. Sokolowski-Tinten, N. Stojanovic, J. Hajdu, A.R. Khorsand, A.J. Gleeson, K. Nowakowska-Langier	Studies of structural changes induced by UV and VUV laser pulses	P44ext	142

M. Żabska, K. Jaśkiewicz, A. Kiersnowski, K. Szustakiewicz, S. Rathgeber, J. Piękowski	Spontaneous exfoliation and self-assembly phenomena in polyvinylpyrrolidone/synthetic layered silicate nanocomposites	P45	144
P. Piszora, W. Nowicki, J. Darul, C. Lathe	Hexagonal boron nitride as a pressure transmitting medium in the high-pressure high-temperature X-ray diffraction experiment	P46	145
J. Darul, W. Nowicki, D. Trots	Synthesis of multimetallic layered materials and characterization of the calcination products	P47	146
I.N. Demchenko, T. Tyliszczak, M. Chernyshova, K.M. Yu, J.D. Denlinger, D. Speaks, P. Olalde-Velasco, O. Hemmers, W. Walukiewicz, G. Derkachov, K. Lawniczak-Jablonska	Modification of the local structure of oxygen in CdO under irradiation	P48	147
D. Wardecki, R. Przeniosło, A.N. Fitch, M. Bukowski, R. Hempelmann	Studies of microstructure in annealed nanocrystalline chromium by using synchrotron radiation diffraction	P49	148
M. Basiura-Cembala, B. Goderis	A synchrotron study of polymorphic phase transition in nylon 6	P50	149
M. Taube, Z. Pietralik, A. Szymańska, A. Grubb, M. Kozak	Low resolution structure in solution of native human cystatin C	P51	150
Z. Pietralik, M. Taube, M. Balcerzak, A. Skrzypczak, M. Kozak	SAXS studies of DMPC and DPPC-dimeric surfactant lipoplexes	P52	151
O. Ermakova, W. Wierzchowski, K. Wieteska, W. Graeff, R.J. Iwanowski, H. Dąbkowska, M.H. Heinonen, P. Romanowski, J. Bąk-Misiuk, W. Paszkowicz	Characterization of LuVO ₄ :Yb single crystals	P53	152
K. Szpotkowski, A. Wypych, S. Jurga, M. Kozak	Phospholipid/surfactant bicellar phase studied by SAXS, FTIR and DS	P54	153
M. Taube, Z. Pietralik, A. Szymańska, M. Kozak	Solution scattering studies of human cystatin C mutants	P55	154
E. Werner-Malento, R. Minikayev, C. Lathe, H. Dąbkowska, W. Paszkowicz	High-pressure diffraction study of selected four-component synthetic garnets	P56	155
M. Taube, M. Hilgendorff, Z. Pietralik, M. Giersig, M. Kozak	SAXS studies of Fe ₃ O ₄ /SiO ₂ nanoparticles for nanosensing	P57	156
V. Lamzin	Mapping the protein world: Over 1500 biomolecular structures solved on-line at EMBL-Hamburg	L07	157
J. Härtwig	Challenges in X-ray optics for modern X-ray sources	L27ext	158
	Subject index		160
	Authors index		162
	Conference proceedings list		164
	Jobs and postdocs at ESRF		164



APARATURA naukowa i badawcza

Aplikacje • Sprzedaż • Serwis

- Spektrometry magnetycznego rezonansu jądrowego NMR
- Spektrometry paramagnetycznego rezonansu elektronowego EPR
- Spektrometry masowe FTMS, MALDI-TOF(-TOF), ESI-(Q-)TOF, pułapki jonowe
- Spektrometry i dyfraktometry rentgenowskie XRF, XRD, SCD
- Spektrometry optyczne OES
- Analizatory CS i ON/H

think forward

www.bruker.pl

ul. Niepodległości 82d, 44-370 Pszów
tel./fax: (032) 455 88 90, 0 601 500 167
www.testchem.pl, e-mail: biuro@testchem.pl

Prasy
laboratoryjne

Kruszarki
laboratoryjne

Próbobiorniki

Układy
chłodzenia

Młynki
laboratoryjne

Mieszalniki

Dzielniki próby



TESTCHEM

Synchrotron light source in Poland!

On the 9th of April 2010 the Minister of Science and Higher Education Prof. Barbara Kudrycka and the Rector of Jagiellonian University Prof. Karol Musioł signed in the interior of Jagiellonian University Collegium Maius the contract on realization of the project "National Centre of Electromagnetic Radiation for research applications (the stage I)" - *The Synchrotron Project*.



Figure 1. The Minister of Science and Higher Education Prof. Barbara Kudrycka and the Rector of Jagiellonian University Prof. Karol Musioł signing the contract.
Photo by A.Wojnar

The synchrotron installation will consist of:

- Electron injection system including electron source and 400-700 eV linear accelerator,
- 96 m circumference, 1.5 GeV, 500 mA storage ring with 12 bending magnets separated by 3.5 m long straight sections,
- 1 undulator based experimental beamline with a multi-grating monochromator and VUV - Soft X-ray electron spectroscopy end-station.

The building complex, apart of the synchrotron installation will also accommodate all the necessary auxiliary facilities *e.g.* workshops, preparatory laboratories, staff and administration offices.

The Centre with the budget of 143 740 000 PLN is scheduled to be commissioned in September 2014.

Novel concepts have been applied to the linear accelerator and the storage ring design which is based on the integrated bending magnets technology developed by the accelerator team at MAX-lab in Lund with whom the Memorandum of Understanding was signed in 2009.

The participation of the MAX-lab experts is fundamental to the project. The innovative design of the machine allows for creating a very powerful instrument at a very competitive price.

It will be able to provide radiation from both the bending magnets and insertion devices at the wavelength from infrared (IR) to X-ray region (with critical energy of not less than 5 keV at SCW), also opening possibilities of research in THz frequencies.

Although the project includes only one experimental beamline it is assumed that the search for funds for the range of new beamlines will start immediately. These can be either bending magnet, undulator or wiggler (superconducting) based facilities.

The Centre will be situated within the Jagiellonian University's III Campus area, the new location for the Science Faculties and the site of the Jagiellonian Center of Innovation – Life Science Park.

The idea of building a synchrotron light source in Poland has started about 12 years ago. Today it has materialized. The success should be billed to the entire Polish community of synchrotron radiation users who, for many years, through their outstanding research at synchrotron facilities abroad supported the case of the Polish Synchrotron.

Over the years many people were directly involved in repeated attempts for setting up Polish synchrotron facility. They have their big share in the last success.

The names of the final group members, who in 2009-2010 were working on defining, completing and submitting the successful *Synchrotron Project* application are: E.A. Görlich, K. Królas, M.J. Stankiewicz, J. Szwed, and K. Tomala, all from the Institute of Physics, and Michał Młynarczyk from the administration of the Jagiellonian University.



Figure 2. April 2010 - Jagiellonian University III Campus - the plot allocated for the Polish Synchrotron (50°01'21" N:19°53'37" E). *Photo by M.J. Stankiewicz*



Figure 3. September 2014 - the constructor's impression of the facility. *Drawing by PROBADEX*

M.J. Stankiewicz, E.A. Görlich, K. Królas

*Institute of Physics, Jagiellonian University,
ul. Reymonta 4, 30-059 Kraków, Poland*

SYNCHROTRON LIGHT NEWS

NEWS

Magnetic molecules for information technology: single molecular magnets (February 2009). Scientists from France and Italy (M. Mannini *et al.*, "Magnetic memory of a single-molecule quantum magnet wired to a gold surface", *Nature Mater.* 8, 2009, 194) show, using X-ray absorption spectroscopy and X-ray magnetic circular dichroism synchrotron-based techniques, that the Fe₄ complexes retain magnetic hysteresis at gold surfaces. The study has been performed at the SOLEIL Synchrotron (Saint Aubin, France). (WP)

Contrast Material-enhanced Synchrotron Radiation Computed Tomography (CT) helps in fine mapping of glioma circulation (March 2009). D. Balvay *et al.* (*Radiology* 250, 2009, 692), representing eight scientific and medical institutions from France, demonstrate an interesting opportunity for application of synchrotron radiation to *in vivo* analyze the tumor zone organization. Classical computed tomography is unable to show dynamic processes that are important to understand the angiogenesis that takes place during tumor formation. Knowledge on these processes is very important from medical point of view. In this paper, the authors show that fine mapping of the glioma microcirculation is feasible through step-by-step imaging data analyses. The experimental part of the study was performed at ESRF synchrotron source. (WK)

Studies of plant cells using synchrotron radiation (April 2009). T Punshon, M.L. Guerinot and A. Lanzirrotti (*Annals of Botany* 103, 2009, 665) have reviewed the applications of synchrotron X-ray fluorescence microprobes in studies of plant cells. The method is concluded to be capable to provide fundamental information on plant cells (also in the *in vivo* studies) in the sub-micrometer scale. (WP)

Kai Siegbahn prize¹ for Eli Rotenberg (September 2009). On September 30th, 2009, during the 10th International Conference on Synchrotron Radiation Instrumentation (Melbourne 2009), the winner of the 2009 Kai Siegbahn prize, Dr. Eli Rotenberg (Lawrence Berkeley National Lab., USA), was announced. A ceremony was organized on October 2nd, 2009 at the Dept. of Physics of the University of Uppsala where the laureate was invited. The prize was awarded for the creation of the ARPES "Electronic Structure Factory" end-station at the Advanced Light Source (USA) and its artful application to the understanding of quantum

electronic properties of nano-phase and reduced dimensionality materials. (WP)

Inauguration of the world's most brilliant synchrotron radiation source: Official starting shot for PETRA III (November 2009). The world's most brilliant and modern storage-ring-based synchrotron radiation source was officially inaugurated in November 2009 (the first X-ray beam was generated in May 2009). The facility will give unique opportunities for the studies of matter, including the nano and biomaterials. The total cost of the modernisation of PETRA II and the construction of the new experimental hall for PETRA III was 233 million EUR. (WP)

High reflectivity of synthetic diamond (January 2010). Y.V. Shvyd'ko *et al.* (High-reflectivity high-resolution X-ray crystal optics with diamonds, *Nature Phys.* 6, 2010, 196) demonstrate, using the data obtained at NSLS synchrotron source in US, the high reflectivity value of synthetic diamond crystals under Bragg condition and discuss the role of diamond for hard X-ray optics and for construction of elements of future free electron laser radiation sources. (WP)

Review of synchrotron-radiation methods applied to electrochemical systems (on line January 2010). An interesting review of structural characterization techniques applied for electrochemical systems using synchrotron-radiation appears in *TrAC Trends in Analytical Chemistry* (2010, in press). The researchers working in Australia, R. De Marco and J.-P. Vadera, demonstrate how various techniques can be useful in *in-situ* studies of batteries and fuel cells properties and what specialised tools are used in this field. (WP)

Iron containing sensory dendrites constitute an avian magnetometer system of birds (Feb. 2010). A team led by researchers from Frankfurt University in collaboration with HASYLAB/DESY, Univ. of Oldenburg, and Helmholtz-Zentrum Berlin discovered that iron containing sensory dendrites in the inner dermal lining of the upper beak are a candidate structure for an avian magnetometer system of birds. The physicochemical studies were performed at DORIS III, using microscopic X-ray absorption spectroscopy. The composition of the involved iron minerals in the dendrites is found to be identical in several bird species. For details see G. Falkenberg *et al.*, "Avian magnetoreception: elaborate iron mineral containing dendrites in the upper beak seem to be a common feature of birds". *PLoS ONE* 5 (2010) e9231. (WP)

Applications and trends in analytical chemistry using SR FT-IR microspectroscopy (on line March 2010). M.C. Martin *et al.* (*TrAC Trends in Analytical Chemistry*, 2010, in press) present an interesting review of applications and trends in analytical chemistry using synchrotron-based Fourier-transform IR spectromicrospectroscopy techniques. (WP)

¹ The aim of the Kai Siegbahn Prize is to recognize and encourage outstanding experimental achievement in synchrotron radiation research with a significant component of instrument development. Particular preference will be given to the development of synchrotron radiation spectroscopies.

Commercial table-top source operating in the 13–50 nm range (March 2010). I. Mc Kinnie and H. Kapteyn announced (*Nature Photonics* 4, 2010, 149) an introduction of a commercial table-top source operating in the range of 13–50 nm (extreme ultraviolet and soft x-rays). The principle of operation consists in high-harmonic generation of ultrafast Ti:Sapphire laser coupled with the extreme ultraviolet ultrafast source (XUUS) phase-matched high harmonics generation (HHG) gas capillary system. The 50 nm light is produced through the 15th harmonic, and 13 nm light through the 61st harmonic. The emission of 20 fs fully coherent pulses with a useful flux of 10^{12} photons per second produces brightness comparable to that of a classical synchrotron sources making it possible to perform tasks previously accessible only using large-scale synchrotrons, with additional ability to perform time resolved experiments with femtosecond time resolution. (JP)

Copernicus Medal for Dr. Zbigniew Dauter (March 2010). In March 2010, Dr. Zbigniew Dauter from the Advanced Photon Source (Argonne National Laboratory, USA), received the Nicolaus Copernicus Medal, the highest distinction awarded by the Polish Academy of Sciences. The award recognizes Dr. Dauter's contribution to the development of protein crystallographic methodology involving synchrotron radiation. Zbigniew Dauter graduated from Gdańsk University of Technology, where he also obtained his PhD degree. His habilitation (DSc), was awarded by A. Mickiewicz University, Poznań. Dr. Dauter spent a number of years at several synchrotron centers (EMBL c/o DESY, Hamburg; NSLS, Brookhaven; APS, Argonne) conducting structural biological research and supervising external users of macromolecular crystallography beamlines. For details, see p. 28, this issue. (MJ)

Dr. Zbigniew Dauter during the award ceremony.

Photo: M. Mlekicki



Polish synchrotron project accepted (April 2010). On 9th of April 2010, Minister of Science and Higher Education Prof. Barbara Kudrycka and Rector of Jagellonian University Prof. Karol Musioł, signed the Polish Synchrotron Project. According to the schedule, the machine will be built at the new Jagellonian University Campus and commissioned in September 2014. See p. 1 (this issue) for details. (MS)

Phosphorus in the cell can be quantified (July 2010). D.R. Núñez-Milland, S.B. Baines, S. Vogt and B.S. Twining show ("Quantification of phosphorus in single cells using synchrotron X-ray fluorescence", *Synchrotron Rad.* 17, 2010, in print) that phosphorus, an important component of the cell, can be quantified using

synchrotron X-ray fluorescence (SXRF). The authors discuss also the importance of choice of the standard used in this study. (WP)

FUTURE CONFERENCES & WORKSHOPS

Polish Crystallographic Conversatorium (June 2010). 52nd "Konwersatorium Krystalograficzne" will be held on 24-25 June 2010 r., followed by a Meeting and Workshop of Polish Crystallographic Society (25-26 June 2010), <http://komkryst.int.pan.wroc.pl/kk2010/kk2010.htm>.

Free Electron Laser Meeting (August 2010). 32nd International Free Electron Laser Conference will be organised on 23-27.08.2010 in Malmö (Sweden). <http://www.maxlab.lu.se/maxlab/conference/fel2010/index.html>.

European crystallographic conferences (August & September 2010) ECM-26, 26th European Crystallographic Meeting (Aug. 29 - Sept. 2, 2010) and EPDIC-12, 12th European Powder Diffraction Conference (Aug. 27-30), both will be held in Darmstadt, Germany.

Synchrotron Radiation Instrumentation Meeting (September 2010). The Sixteenth Pan-American Synchrotron Radiation Instrumentation (SRI) Conference, is planned for 21-24.09.2010, Argonne, IL (USA).

DISCUS nanoparticle modeling workshop (September 2010). DISCUS nanoparticle modeling workshop is organized from Sept. 23 to Sept. 26, 2010 in Erlangen (Germany). Details are available at <http://discus.sourceforge.net>.

Workshop on Extreme Condition Studies using Synchrotron Radiation and Neutrons (September 2010). A workshop "Synchrotron Radiation and Neutrons for Extreme Condition Studies" (Hercules Specialised Course, HSC12) will be organized in Grenoble, 27th Sept. to 2nd Oct, 2010.

MAXlab User Meeting (November 2010). MAX-lab 23rd Annual User Meeting, will be held in Lund, Sweden, November 8 - 10, 2010.

International Conference on X-ray Absorption Fine Structure, Beijing, China (2012). The 15th International Conference on X-ray Absorption Fine Structure (XAFS15) will be held in Beijing, China, in 2012. It is hosted by Institute of High Energy Physics, Chinese Academy of Sciences. The scope of the conference aims at XAFS and all the related techniques and topics. <http://www.xafs15.org/>.

More news at: <http://www.lightsources.org/cms/>.

News in this issue were prepared by: M. Jaskólski (MJ), A. Mickiewicz University; Marek Stankiewicz (MS), Jagellonian University; W. Paszkowicz (WP), Institute of Physics PAS; Jerzy B. Pelka (JP), Institute of Physics PAS; W. Kwiatek (WK), Institute of Nuclear Physics PAS.

PROMIENIOWANIE RENTGENOWSKIE ZE ŹRÓDEŁ SYNCHROTRONOWYCH JAKO KATALIZATOR ROZWOJU KRYSZTALOGRAFII BIAŁEK

Zbigniew Dauter^{1*}, Alexander Wlodawer^{2#} i Mariusz Jaskolski^{3,4\$}

¹ *Synchrotron Radiation Research Section, Macromolecular Crystallography Laboratory, NCI,
Argonne National Laboratory, Argonne, IL 60439, USA*

² *Protein Structure Section, Macromolecular Crystallography Laboratory, National Cancer Institute,
Frederick, MD 21702, USA*

³ *Zakład Krystalografii, Wydział Chemii, Uniwersytet im. A. Mickiewicza, Poznań*

⁴ *Centrum Badań Biokrystalograficznych, Instytut Chemii Bioorganicznej PAN, Poznań*

Streszczenie: Promieniowanie rentgenowskie ze źródeł synchrotronowych stało się dostępne dla badań biostrukturalnych na początku lat 70. XX wieku. Jego wprowadzenie całkowicie zrewolucjonizowało dyfrakcyjny eksperyment rentgenowski w krystalografii białek. W artykule omówione są najważniejsze fakty związane z początkami wykorzystania promieniowania synchrotronowego w krystalografii makromolekuł, kluczowe aspekty rewolucji naukowej, jaka się dzięki temu dokonała, oraz perspektywy dalszego rozwoju biologii strukturalnej opartej o promieniowanie synchrotronowe jako podstawowe narzędzie badawcze.

Keywords: synchrotron radiation; protein crystallography; structural biology
Słowa kluczowe: promieniowanie synchrotronowe; krystalografia białek; biologia strukturalna;

e-mail: () zdauter@anl.gov, (#) wlodawer@nih.gov, (\$) mariuszj@amu.edu.pl*

Wstęp

Narodziny krystalografii rentgenowskiej niemal dokładnie 100 lat temu oraz jej wielki tryumf pod koniec lat 50. XX wieku polegający na rozszyfrowaniu pierwszych struktur białkowych – to kamienie milowe na drodze do zrozumienia funkcjonowania cząsteczek życia na poziomie atomowym. Oczywiście jest, że sukces krystalografii białek byłby niemożliwy bez odpowiednio silnych źródeł promieniowania rentgenowskiego umożliwiających pomiar dyfrakcji od kryształów makromolekuł. Stosowane początkowo klasyczne źródła promieni X – różnego rodzaju lampy rentgenowskie emitujące promieniowanie elektromagnetyczne w wyniku bombardowania elektronami termicznymi anody wykonanej z miedzi lub molibdenu, wymagały zazwyczaj wielotygodniowego naświetlania kryształów białek. Sytuacja zmieniła się radykalnie z początkiem lat 1970. na skutek zastosowanie znacznie silniejszych źródeł synchrotronowych promieniowania rentgenowskiego. W następnych rozdziałach nakreślimy, na tle osobistych doświadczeń i wspomnień, historię

badań kryształów makromolekularnych z użyciem promieniowania synchrotronowego oraz podamy zarys rozwoju metodologii tej dyscypliny, którego katalizatorem były synchrotrony, jako potężne narzędzie badawcze biologii strukturalnej.

Początki krystalografii białek

Krystalografia białek pojawia się w annałach nauki w roku 1840, kiedy to Hünefeld opisał powstałe na drodze przypadku kryształy hemoglobiny dżdżownicy, które nazwał "kryształami krwi" [1]. Warto odnotować, że na początku XX wieku Reichert i Brown opublikowali imponującą monografię o krystalizacji hemoglobiny, udokumentowaną około 600 zdjęciami mikroskopowymi kryształów [2]. W roku 1946 Nagrodą Nobla w dziedzinie chemii przyznaną w istocie za krystalizację białek, podzielili się Sumner, Northrop i Stanley.

Krystalografia białek rozumiana jako nauka strukturalna jest jednak znacznie młodsza i datuje swoje powstanie na koniec lat 50. XX wieku, kiedy to John

Kendrew opublikował pierwszą w dziejach strukturę białka, mioglobiny wieloryba [3]. Choć był to początkowo model o bardzo niskiej rozdzielczości 6 Å, został on stosunkowo szybko ulepszony do bardzo przyzwoitej rozdzielczości 2 Å [4]. Mniej więcej w tym samym czasie strukturę hemoglobiny opublikował Max Perutz [5]. Perutz, który jest niekwestionowanym ojcem krystalografii białek, rozpoczął swoje pionierskie badania struktury hemoglobiny w roku 1937. Jednak pierwsze badania rentgenowskie miały miejsce jeszcze wcześniej, na początku lat 30. XX wieku, kiedy to w laboratorium Williama Astbury'ego wykonano zdjęcia dyfrakcji na włóknach białek [6], a w laboratorium Desmonda Bernala na monokryształach. Pierwsze zdjęcie dyfrakcji rentgenowskiej na kryształach pepsyny przyniosło rozczarowanie, ale Bernal szybko zorientował się, że jeśli kryształy zabezpieczy się przed wysychaniem, dyfrakcja będzie doskonała [7]. Warto przytoczyć wnikliwą uwagę Bernala, zainspirowaną pierwszymi zdjęciami rentgenowskimi pepsyny, które "ukazały bardzo duże komórki elementarne i bogactwo refleksów, obserwowanych również przy wysokich kątach rozproszenia odpowiadających odległościom $d=2$ Å [w prawie Bragga], co z kolei dowodzi, że cząsteczki białek mają nie tylko z grubsza taki sam kształt i rozmiary, ale że posiadają one identyczną strukturę z dokładnością do wymiarów atomowych" [8]. Jednak mimo tak obiecującego początku, pierwsze kroki, a nawet dekady, krystalografii białek były bardzo trudne, a postęp niezwykle wolny, o czym świadczy okres 22 lat jakich potrzebował Perutz na rozwiązanie struktury hemoglobiny. Z następnymi strukturami sytuacja była nieco lepsza, lecz mimo to w roku 1971, kiedy utworzono Bank Struktur Białkowych (Protein Data Bank, PDB) znalazła się w nim "zawrotna" liczba zaledwie 7 struktur [9]. W 1973 roku znano już strukturę ponad 10 białek, choć w PDB zdeponowano tylko 9 struktur. Wszystkie rozwiązano stosując rentgenografię monokryształów. Poza mioglobina i hemoglobina, początkową zawartość PDB stanowił również cytochrom b_5 , trzustkowy inhibitor trypsyny BPTI, subtylizyna, α -chymotrypsyna, karboksypeptydaza $A\alpha$, dehydrogenaza mleczanowa oraz rubredoksyna [10]. Należy podkreślić, że w początkowym okresie biologii strukturalnej oprócz krystalografii ważną rolę odegrała również dyfrakcja rentgenowska na włóknach. Ikoniczne odkrycie biologii strukturalnej XX wieku – struktury podwójnej helisy DNA [11], oparte było między innymi na zdjęciach rentgenowskich włókien DNA rejestrowanych przez Rosalind Franklin i innych [12].

Trudne początki krystalografii białek miały niewątpliwie swoją przyczynę w jaskrawej dysproporcji pomiędzy "niebotycznymi" celami i mniej niż skromnymi możliwościami ich realizacji. Wśród głównych niedomagań eksperymentalnych najważniejszy był chyba brak wystarczająco silnych źródeł promieniowania rentgenowskiego, wydłużający astronomicznie czas potrzebny do wykonania pomiarów dyfrakcyjnych, a najczęściej po prostu takie pomiary uniemożliwiający. Z początku postęp był stopniowy i wiązał się z udoskonaleniem lamp rentgenowskich, a

potem z wprowadzeniem generatorów z wirującą anodą. W latach 1970. nastąpił jednak dramatyczny skok jakościowy, który całkowicie zmienił oblicze krystalografii białek. Opóźnione w czasie, bo widoczne od lat 1980. konsekwencje tej zmiany odzwierciedla na przykład wykres ilustrujący tempo przyrostu zawartości PDB (Rys. 1) [13]. Ten "skok kwantowy" wiązał się w pierwszym rzędzie z zastosowaniem synchrotronów jako źródeł promieniowania rentgenowskiego. W tym samym czasie nałożyły się też inne czynniki, które pomogły krystalografii białek nabrać tempa, takie jak wprowadzenie programowalnych maszyn cyfrowych oraz rozwój inżynierii genetycznej i biotechnologii, jednak zdecydowanie dostęp do nowych źródeł promieniowania rentgenowskiego należy uznać za czynnik najważniejszy.

Synchrotron jako narzędzie biologii strukturalnej

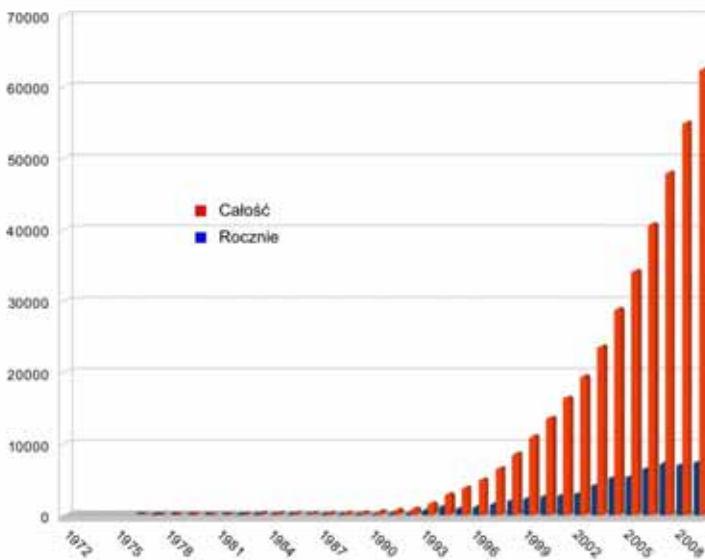
Synchrotrony, tj. przyspieszacze cyklotronowe cząstek elementarnych zostały początkowo zbudowane jako narzędzie dla fizyków wysokich energii badających subatomową strukturę materii. W instalacjach takich naładowanym cząstkom elementarnym (np. elektronom) nadawano ogromne energie, przyspieszając je do prędkości podświetlnych (relatywistycznych) i zmuszając do poruszania się po torze zamkniętym w płaszczyźnie horyzontalnej. Doprowadzając tak wysokoenergetyczne elektrony i jony do kolizji, fizycy mieli nadzieję odkryć nowe cząstki elementarne, które w wyniku takich zderzeń powstają. Z praw Maxwella wynika jednak, że poddane przyspieszeniu cząstki obdarzone ładunkiem będą emitować promieniowanie elektromagnetyczne. Z punktu widzenia fizyków wysokich energii, ten efekt synchrotronowy był kłopotliwą uciążliwością, powodując straty energii i pociągając za sobą konieczność ciągłego pompowania energii i nowych elektronów do urządzenia. Każdy synchrotron składa się z próżniowego tunelu w kształcie pierścienia oraz z umieszczonych na jego obwodzie potężnych elektromagnesów, których pole magnetyczne zakrzywia tor elektronów, wprowadzając je na w przybliżeniu kołową orbitę. Mówiąc dokładniej, synchrotron ma kształt ogromnego wielokąta z prostoliniowymi odcinkami toru pomiędzy sąsiednimi magnesami zakrzywiającymi. Po wstrzyknięciu (z akceleratora liniowego) do pierścienia i początkowym przyspieszeniu krążące elektrony mają stałą energię (i prędkość liniową) lecz doznają przyspieszenia kąтового przelatując przez pole magnetyczne. Elektromagnesy zakrzywiające są więc źródłem promieniowania elektromagnetycznego o bardzo szerokim zakresie długości fali, od mikrofal do twardego promieniowania rentgenowskiego. W odcinkach prostoliniowych toru, pomiędzy magnesami zakrzywiającymi, można umieścić tzw. urządzenia wstawkowe, wigglery lub undulatory. Są to multipole magnetyczne, w których przelatujące elektrony doznają dodatkowych przyspieszeń kątowych, emitując w efekcie promieniowanie silniejsze niż w zwykłym magnesie zakrzywiającym. W undulatorze promieniowanie pochodzące od każdej pary biegunów

magnetycznych daje wzmocnienie interferencyjne, dzięki czemu uzyskujemy w efekcie silne piki promieniowania rentgenowskiego, których długość fali zależy od odległości (przerwy) pomiędzy biegunami. Szczegółowa teoria zjawiska emisji promieniowania synchrotronowego (SR, synchrotron radiation) została opracowana już w latach 1940. [14].

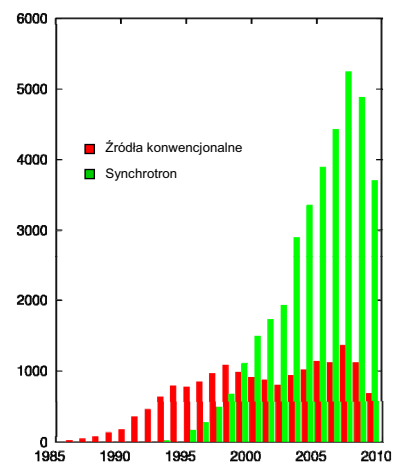
Fizycy wysokich energii, tj. główni użytkownicy instalacji synchrotronowych w początkowym okresie ich wdrażania do badań naukowych, traktowali badaczy starających się wykorzystać promieniowanie synchrotronowe na zasadzie pasożytów. W takiej właśnie roli funkcjonowali w ośrodkach synchrotronowych Hamburga, Stanford, czy Nowosybirsk krystalografowie białek. Wkrótce jednak, gdy zdano sobie sprawę z możliwości jakie oferuje promieniowanie synchrotronowe dla badania materii metodami rozproszeniowymi i dyfrakcyjnymi, zaczęły powstawać instalacje synchrotronowe nowej generacji, przeznaczone wyłącznie do wytwarzania promieniowania elektromagnetycznego. Te urządzenia drugiej generacji były nie tyle tradycyjnymi synchrotronami, co pierścieniami akumulacyjnymi o obwodzie rzędu 1 km, w których "przechowuje" się elektrony (lub pozytony) o energii rzędu 2-3 GeV. Prąd elektronowy w tych urządzeniach (rzędu kilkuset mA) z czasem zanika, konieczne są więc dodatkowe zastrzyki elektronów co kilka lub kilkanaście godzin. Urządzenia takie zbudowano w Daresbury w Anglii (SRS), w Hamburgu w Niemczech (DORIS), w Orsay we Francji

(LURE), w Tsukuba w Japonii (Photon Factory), oraz na Uniwersytetach Stanforda (SSRL) i Cornella (CHESS), w Brookhaven (NSLS) i w Berkeley (ALS) w USA. Od początku swojej działalności były one i są nadal wykorzystywane z bardzo pozytywnym skutkiem do zaawansowanych eksperymentów, w tym do eksperymentów krystalografii białek.

Zalety promieniowania synchrotronowego nie ograniczają się do wysokiej intensywności i możliwości wybrania z emitowanego spektrum pożądanej długości fali. Cząstki elementarne w pierścieniu akumulacyjnym zgrupowane są w pakiety, więc i promieniowanie synchrotronowe emitowane jest nano- lub pikosekundowymi impulsami, które rozdziela czas mikrosekund. Ta struktura czasowa wraz z opcją wykorzystania całego zakresu (polichromatycznego) widma rentgenowskiego, stwarzają unikalną możliwość, realizowaną w tzw. metodzie Lauego, przeprowadzenia pomiarów dyfrakcyjnych w niesłychanie krótkim czasie, a tym samym monitorowania w czasie rzeczywistym procesów kinetycznych zachodzących w kryształach białka, np. przebiegu reakcji enzymatycznych [15]. Co więcej, ponieważ cząstki elementarne krążą w płaszczyźnie poziomej, emitowane promieniowanie jest spolaryzowane, z wektorem elektrycznym drgającym w płaszczyźnie równikowej, co może być wykorzystane w badaniu efektów anizotropowych [16]. Wyczerpujący przegląd zastosowań promieniowania synchrotronowego w krystalografii białek podał Helliwell [17].



A



B

Rys. 1. Przyrost struktur zdeponowanych w Banku Danych Białkowych PDB. (A) Przyrost roczny (kolor niebieski) i całkowita zawartość bazy (czerwony). (B) Rocznie deponowane struktury z rozbiem na uzyskane przy pomocy promieniowania synchrotronowego (zielony) i źródeł konwencjonalnych (czerwony). Dane dla roku 2009 są niepełne. Diagram (B) przygotował dr W. Minor.

Źródła promieniowania synchrotronowego dla badań biostrukturalnych we wczesnym okresie

W Europie pomysł wykorzystania SR jako narzędzia badawczego zrodził się pierwotnie w środowisku biofizyków zajmujących się badaniem molekularnego mechanizmu skurczu mięśnia za pomocą metod dyfrakcyjnych. W doświadczeniach tych rejestrowano małąkąową dyfrakcję na cienkich pseudokrystalicznych włóknkach mięśni. W latach 1960. zajmowały się tym problemem dwie grupy, jedna kierowana przez Hugh Huxleya w Cambridge w Anglii (mięśnie żaby), druga przez Kena Holmesa w Heidelbergu w Niemczech (mięśnie owada). Oba zespoły stosowały promieniowanie $\text{Cu } K\alpha$ z nowoczesnego jak na owe czasy urządzenia, generatora rentgenowskiego z wirującą anodą. Wyniki były jednak mizerne, gdyż próbki mięśni były bardzo małe i dawały nikłą dyfrakcję. W roku 1969 do zespołu Holmesa dołączył jako doktorant Gerd Rosenbaum, młody fizyk, który jako student-dyplomant w grupie spektroskopii UV zetknął się wcześniej z działającym już wtedy w ośrodku DESY (Deutsches Elektronen-Synchrotron) w Hamburgu synchrotronem. Uzyskawszy od swojego promotora zadanie zbudowania lepszego źródła rentgenowskiego do badania włóknkach mięśniowych, Rosenbaum wpadł na pomysł wykorzystania promieniowania synchrotronowego [18]. Zespół wzmocniony przez Jeana Witza ze Strasburga zbudował stację pomiarową wyposażoną w ogniskującą monochromator kwarcowy pracujący w próżni, w regulowane szczeliny wiązki i w inne akcesoria. Maszyna ta była bardzo niewygodna w użyciu, m.in. z powodu skomplikowanego systemu zabezpieczeń. Jednym z jego elementów było telefoniczne zgłoszenie w centralnym punkcie kontroli otwarcia głównego okienka rentgenowskiego. Było to jednak możliwe tylko w czasie krótkich przerw pomiędzy eksperymentami fizyki cząstek elementarnych. Pierwsze obrazy dyfrakcji na włóknkach mięśnia owada zarejestrowano w 1970 roku. Według szacunku Rosenbauma ówczesny wiązka promieniowania synchrotronowego była kilkaset razy bardziej intensywna niż z generatora z wirującą anodą [19]. Po tym sukcesie dyrekcja DESY zachęciła Holmesa i Rosenbauma do zbudowania w osobnym budynku linii pomiarowej do badań materiału biologicznego [20]. Konstrukcję tę zrealizowano w roku 1971.

Na początku lat 1970. John Kendrew, wówczas dyrektor nowej organizacji EMBO (European Molecular Biology Organization), zrozumiał, że promieniowanie synchrotronowe stanowi wyjątkową szansę dla biologii strukturalnej i molekularnej. Z jego osobistej inicjatywy utworzono EMBL (European Molecular Biology Laboratory), ponadnarodową instytucję powołaną do prowadzenia takich badań w dziedzinie biologii molekularnej, które wymagałyby współpracy i finansowania w skali międzynarodowej. Doświadczenia wymagające promieniowania synchrotronowego były wprost idealnym przykładem dla idei EMBL. W roku 1975 na mocy umowy pomiędzy DESY i EMBL powołano w Hamburgu Placówkę EMBL posadowioną

na jednym kwadrancie nowozbudowanego synchrotronu DORIS.

Mniej więcej w tym samym czasie równolegle prowadzone były prace nad biostrukturalnym zastosowaniem promieniowania synchrotronowego w instalacji synchrotronowej w Nowosybirsku należącej do Akademii Nauk Związku Radzieckiego. Zbudowano tam stosunkowo prostą linię pomiarową wyposażoną w monochromator grafitowy lecz bez żadnej możliwości ogniskowania wiązki. Na linii tej zarejestrowano dane dyfrakcyjne dla kilku kryształów małowielkościowych oraz dla włókn DNA. Podobno uzyskano również dyfrakcję na kryształach małego białka aktynoksantyny, lecz szczegóły tego eksperymentu nie zostały opublikowane [21].

Pierwsza synchrotronowa linia dla krystalografii białek w Stanford

W USA możliwość zastosowania promieniowania synchrotronowego jako narzędzia badawczego pojawiła się po raz pierwszy w maju 1974 roku wraz z uruchomieniem projektu SSRP (Stanford Synchrotron Radiation Project), przemianowanego później na SSRL, który obejmował stację eksperymentalną zbudowaną przy niedawno ukończonym pierścieniu akumulacyjnym SPEAR. Pierwsza linia pomiarowa wykorzystywała wiązkę rentgenowską z magnesu zakrzywiającego o rozbieżności 11.5 miliradiana i służyła pomiarom w pięciu różnych obszarach badań. Podobnie jak w DESY, przy budowie linii BL1-4 nacisk położono na rozpraszanie rentgenowskie na włóknach. W Stanford jednak wysoki priorytet miała również krystalografia białek. Inną równolegle rozwijaną metodą badawczą była absorpcja EXAFS [22], możliwa w praktycznym zastosowaniu tylko dzięki promieniowaniu synchrotronowemu.

Adaptacja linii BL1-4 do pomiarów krystalograficznych była oczkiem w głowie Keitha Hodgsona, świeżo powołanego profesora na Wydziale Chemii Uniwersytetu Stanforda. Z początku grupa zapaleńców realizujących ten projekt była niewielka, wchodziło w jej skład dwoje doktorów, Margueritte Yevitz Bernheim i Alexander Włodawer, oraz doktorant James Phillips. Dr Julia Goodfellow dołączyła rok później.

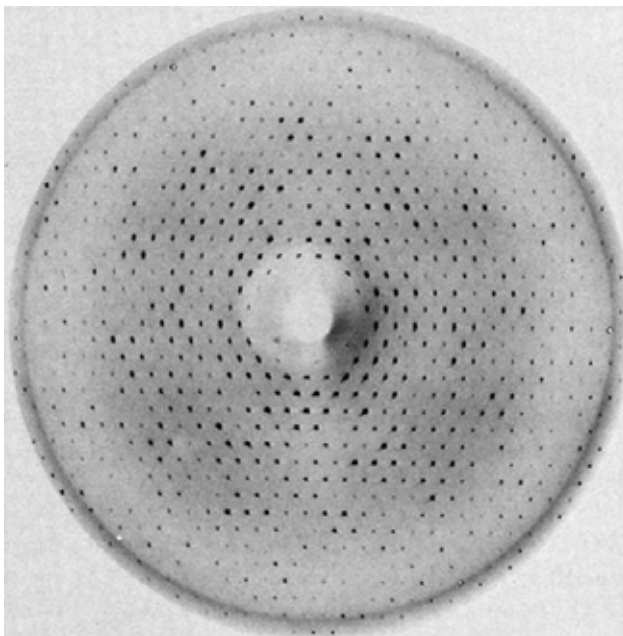
Wyposażenie tej stacji było dość prymitywne i sprowadzało się w zasadzie do kamery precesyjnej, na której rejestrowało się zdjęcia z wykorzystaniem błon do radiologii. Wiązało się to oczywiście z obróbką fotograficzną, a najbliższa ciemnia fotograficzna, na głównym kampusie Stanford, oddalona była o kilka mil. Wymagało to uciążliwych wycieczek w oficjalnym wehikule, jakim wtedy dysponował program SSRL. Był to odzyskany z "demobilu" po wojnie koreańskiej wojskowy pojazd opancerzony подарowany przez Marynarkę Wojenną USA. Humorystyczny aspekt był tym większy, że żadna z osób obsługujących ten wehikul nie posiadała w tym czasie paszportu USA!

Najbardziej uciążliwym aspektem pracy z promieniowaniem synchrotronowym w tamtym czasie była dla krystalografów, ale też dla innych badaczy wykorzystujących twarde promienie rentgena, "pasożytnicza" natura ich eksperymentów. To fizycy narzucali reguły gry i oni decydowali o parametrach operacyjnych synchrotronu. Gwoli sprawiedliwości trzeba odnotować, że te doświadczenia fizyków cząstek elementarnych zaowocowały Nagrodą Nobla przyznaną Burtonowi Richterowi dwa lata później. Na nieszczęście cząstka ψ , którą odkrył, pojawiała się, gdy synchrotron pracował przy energii 1.55 GeV – zbyt niskiej dla generowania użytecznego dla krystalografów promieniowania rentgenowskiego. Z drugą odkrytą cząstką elementarną, ψ' , było niewiele lepiej, gdyż wymagała energii 1.86 GeV, podczas gdy do wytwarzania użytecznego promieniowania rentgenowskiego potrzebna była energia co najmniej 2 GeV. Tak więc sukces fizyków opóźnił sukces krystalografów o dobre kilka miesięcy.

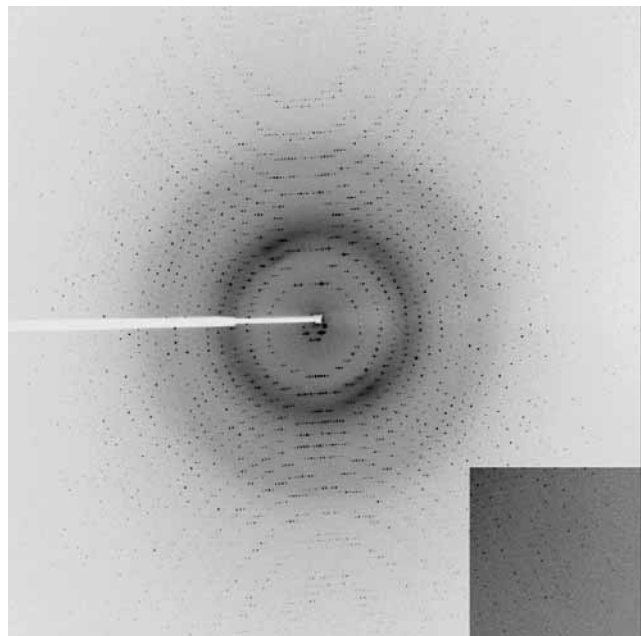
Pierwsze wyniki kosztowały wiele czasu i wysiłku i dostarczyły raczej dowodu na poparcie "strategii synchrotronowej" niż użytecznych danych doświadczalnych jako takich [23]. Dla azuryry udało się co prawda uzyskać trójwymiarowe dane dyfrakcyjne, ale dla pozostałych białek testowych, tj. rubredoksyny, czynnika wzrostu nerwów (NGF) i L-asparaginazy, zarejestrowano jedynie warstwie zerowe refleksów. Jako ciekawostkę można podać, że na rozwiązanie struktury kryształów NGF i asparaginazy przyszło

czekać ponad 15 lat! Czasy naświetlania dochodziły do 5 godz., ale ponieważ na standardowych źródłach promieniowania rentgenowskiego nie otrzymywano żadnej dyfrakcji, nawet taki wynik należało uznać za sukces. Już w początkowej fazie stosowania promieniowania synchrotronowego zwrócono uwagę na możliwość pomiarów przy różnych długościach fali, co pozwoliłoby ominąć problem pochodnych z atomami ciężkimi [24].

Dalszy postęp odnotowano rok później, gdy we współpracy z grupą Lyle'a Jensa wykazano możliwość uzyskania informacji fazowej na podstawie analizy danych dyfrakcyjnych dla rubredoksyny, białka wiążącego żelazo, którego próg absorpcji położony przy 1.75 Å pozwalał na zarejestrowanie stosunkowo silnego sygnału anomalnego. Dodatkowym atutem była grupa przestrzenna, $R3$, mająca niecentrosymetryczną projekcję osiową, a więc dająca różnice w parach Bijvoeta również na warstwie $hk0$ (Rys. 2A). Można więc było ustalić położenie jonów żelaza, przynajmniej na projekcji, posługując się tylko jednym zdjęciem precesyjnym [25]. Doświadczenia te nie należały jednak do łatwych. Kryształ justowano przy pomocy zdjęć rentgenowskich, co wymagało wchodzenia do stacji pomiarowej poprzez cały system zabezpieczeń co kilka minut. Ponieważ zaś długość życia wiązki synchrotronowej nie przekraczała 2 godzin, był to najdłuższy czas, jaki można było poświęcić na sen. Najdłuższy z przeprowadzonych eksperymentów trwał 5 dni i 6 nocy i doprowadził do całkowitego wyczerpania... jego uczestników.



A



B

Rys. 2. Obrazy dyfrakcji rentgenowskiej dla kryształów białek zarejestrowane dawniej i dziś. (A) Zdjęcie precesyjne warstwy $hk0$ kryształu rubredoksyny zarejestrowane w SSRL w Stanford w 1975 roku przy czasie ekspozycji 5 godzin. (B) Obraz dyfrakcyjny kryształu proteinazy K zarejestrowany na linii pomiarowej 19ID synchrotronu APS w Argonne pod Chicago. Na pokazanym z większym kontrastem fragmencie mozaikowego detektora CCD (prawy dolny narożnik) widać refleksy o rozdzielczości 1.07 Å. Ekspozycja trwała 2 sek. z wiązką rentgenowską atenuowaną do 10% intensywności.

Krystalografia białek w DESY

Przez pierwsze dwie dekady swojej pracy pierścien DORIS działał w dwóch trybach. Albo służył eksperymentom fizyki wysokich energii, kiedy w pierścieniu krążyły w przeciwnych kierunkach wiązki elektronów i pozytonów, albo działał jako generator promieniowania synchrotronowego wyłącznie w oparciu o elektrony.

Po pewnym czasie Placówka EMBL dorobiła się pięciu linii pomiarowych: trzech w głównym budynku eksperymentalnym DORIS (HASYLAB) wykorzystujących prąd elektronowy i dwóch w swoim własnym budynku (zwanym "bunkier 4") wykorzystujących prąd pozytonowy. Linie pozytonowe mogły być używane tylko w trybie "pasożytniczym", ale były znacznie bardziej "prywatne", rzadko odwiedzane przez BHP-owców HASYLAB-u. Na liniach w HASYLAB-ie działały urządzenia do pomiarów SAXS (X33), EXAFS (X32) i krystalografii białek (X31), podczas gdy w "bunkrze 4" była linia krystalograficzna (X11) i SAXS-owska (X13). Linia X31 działała w oparciu o magnes zakrzywiający i była wyposażona w podwójny monochromator tunelowy umożliwiający wygodną zmianę długości fali. Inaczej było na linii X11, wyposażonej w pojedynczy monochromator trójkątny, przez co zmiana długości fali była w praktyce rzadko stosowana. Zaletą linii X11 była natomiast znacznie większa intensywność wiązki. Obie stacje były wyposażone w goniometr i kamerę rentgenowską, którymi można było sterować zdalnie. Do końca lat 1980. obrazy dyfrakcyjne rejestrowane były na błonach fotograficznych w kasetach z 8 ładunkami montowanymi na kamerach Arndta-Wonacotta produkcji firmy Enraf-Nonius. Ciemnie fotograficzne były w pobliżu stacji pomiarowych, co znacznie ułatwiało życie eksperymentatorom.

Grupą krystalografii białek EMBL w Hamburgu kierował początkowo Hans-Dieter Bartunik, który potem utworzył niezależną placówkę Instytutu Maxa Plancka w DESY posiadającą własną linię pomiarową BW6. W 1985 roku grupę EMBL w Hamburgu stanowili Christian Betzel, Zbigniew Dauter i Kyriacos Petratos, a jej szefem (do 1996) był Keith Wilson, zastąpiony później przez Victora Lamzina i Matthiasa Wilmannsa. Z upływem czasu grupa znacznie się powiększyła i liczy obecnie ponad 10 osób na stanowiskach naukowych.

Ładowanie kaset (zwykle trzema błonami przedzielonymi przekładkami) oraz skrupulatne oznaczanie i opisywanie filmów w 100% zajmowało jedną osobę. Do obróbki fotograficznej potrzebna była druga para rąk. Taka praca non-stop nierzadko trwała ponad jedną dobę. W annałach nauki nie ma wzmianki ile ubrań zniszczyły odczynniki chemiczne w ciemni, gdy niecierpliwy eksperymentator chciał widzieć wynik podglądając na wpuł wywołane błony. Czasami wiązało się to z humorystycznymi sytuacjami. Wysłany w pojedynkę przez renomowane laboratorium zielony jeszcze student bardzo skrupulatnie "wywoływał" w ciemni wszystkie papierki z przekładek, podczas gdy filmy wyrzucił do kosza na śmieci...

Nastrzyk cząstek elementarnych do pierścienia odbywał się co 2-3 godziny. Po każdej takiej operacji należało ręcznie otworzyć wszystkie grodzie bezpieczeństwa. Procedury te często kolidowały z przerwami na posiłek personelu EMBL. Pod czujnym okiem BHP-owców z HASYLAB-u wszystko musiało przebiegać stricte według przepisów. W bardziej "prywatnych" warunkach linii X11 duży czerwony przycisk otwierający okienka był często wciśnięty na stałe za pomocą przemysłowego urządzenia zbudowanego z długiej linijki i korka, podczas gdy personel delektował się wolnym czasem w pobliskiej "bibliotece" (restauracja lub pub w pobliżu DESY).

W życiu użytkowników linii krystalograficznych EMBL nastąpił dramatyczny przełom w roku 1989, gdy Jules Hendrix i Arno Lentfer (pracujący wówczas w EMBL) skonstruowali pierwszy automatyczny skaner płyty obrazowej (IP), który stał się prototypem dla późniejszych detektorów MAR IP. Koniec z pracą w ciemni, koniec walki z densytometrami! Nowy detektor był ubóstwiany. Pierwszym początkom towarzyszyły jednak niespodzianki. Pierwszy pomiar wykonał Alex Teplyakov dla kryształu termityzy. Po nocy spędzonej na linii X31 narzekał, że po każdej ekspozycji musiał ręcznie "wkłapywać" nazwę zbioru na klawiaturze, choć jedyna różnica dotyczyła kolejnego numeru. Następnego dnia Michael Böhm, autor programu sterującego zmodyfikował kod, dając wytchnienie palcom eksperymentatora. Jednak przy bliższej inspekcji obrazy dyfrakcyjne posiadały kłopotliwą cechę: sąsiednie piksele miały bardzo często identyczną intensywność. Krótka rozmowa z Michałem wyjaśniła zagadkę. Jako ekspert w technikach obrazowania, przeoczył fakt, że podczas transformacji spiralnego odczytu detektora do współrzędnych kartezjańskich bardzo często dany piksel miał dwóch "najbliższych sąsiadów". Następnego dnia algorytm działał już poprawnie nie tylko w odniesieniu do kształtu (ważnego w obrazowaniu) ale też co do wartości liczbowych. Potencjalnie znacznie poważniejszy problem wypłynął, gdy otrzymano pierwsze mapy gęstości elektronowej dla dUTPazy sfazowane za pomocą sygnału anomalnego pochodnej rてciowej. Otóż wszystkie atomy C β modelu białka sterczały poza gęstością elektronową, podczas gdy sam łańcuch główny ulokowany był w niej idealnie. I tu dyskusja z Michałem Böhmem wyjaśniła powód i odtąd już wszystkie zbiory danych zapisywane były w poprawnym, prawoskrętnym układzie współrzędnych.

Pierścien DORIS przeszedł poważną przebudowę w roku 1989. Zamknięto program eksperymentów fizyki wysokich energii, a synchrotron DORIS stał się dedykowanym źródłem promieniowania synchrotronowego generowanego przez prąd pozytonowy krążący w kierunku dawnego prądu elektronów. Wymagało to przebudowy linii X11 i X13 w odwrotnym kierunku. W tym samym czasie postawiono nowy budynek eksperymentalny HASYLAB-u, w którym znalazły się nie tylko linie X11 i X13, ale także nowe linie wigglerowe BW7A i BW7B. Kolejną linię wigglerową, BW6, zbudował dla Instytutu Maxa Plancka

Hans-Dieter Bartunik. Tak wygląda z grubsza sytuacja EMBL w DESY obecnie. Miały miejsce różnego rodzaju udoskonalenia, np. większość skanerów IP zastąpiły detektory CCD, ale najważniejsza zmiana nastąpi w najbliższym czasie, kiedy zostaną oddane do użytku nowe linie pomiarowe zbudowane przy ogromnym pierścieniu synchrotronowym PETRA III. Synchrotron ten, pracujący przy energii 6 GeV stanie się źródłem promieniowania synchrotronowego o ogromnej jasności.

Selenometionina i dostrojona dyfrakcja anomalna (MAD) – metoda "jak ułai" dla promieniowania synchrotronowego

Możliwość dostrojenia długości fali λ promieniowania synchrotronowego do warunków konkretnego eksperymentu jest chyba najbardziej wyjątkową cechą tego promieniowania, która zrewolucjonizowała metodykę rozwiązywania struktur makromolekularnych. U sedna sprawy leży krystalograficzny problem fazowy, który uniemożliwia proste "wylczenie" struktury na podstawie zarejestrowanych intensywności refleksów i wymaga dodatkowej informacji o fazie każdej z fal rozproszonych. Jeśli nie ma adekwatnego modelu dla metody podstawienia cząsteczkowego – pozostaje eksperyment jako źródło informacji o brakujących fazach. Klasyczna metoda podstawienia izomorficznego (MIR) opracowana przez Perutza wymaga dodatkowych pomiarów dyfrakcyjnych dla kryształów pochodnych izomorficznych, w których cząsteczki białka zostały wyznaczone bardzo ciężkimi, bogatymi w elektrony atomami. (Klasyczne atomy ciężkie są kationami metali, lecz w pomysłowym wariantcie tej metody można użyć również anionów halogenkowych [26].) Jeszcze za czasów Perutza zdano sobie sprawę, że atomy z odpowiednimi właściwościami elektronowymi mogą odcisnąć swoje piętno na obrazie dyfrakcyjnym nie tylko poprzez wysoką liczbę elektronów, ale również przez rezonansową absorpcję kwantów rentgenowskich, co wiąże się ze zjawiskiem anomalnej dyspersji, tj. z zależnością atomowego czynnika rozpraszania f od długości fali λ : $f = f^0 + f'(\lambda) + if''(\lambda)$. Zjawisko anomalnej dyspersji było wykorzystywane w krystalografii białek jako pomocnicze źródło informacji fazowej, jednak jego systematyczne zastosowanie było niemożliwe z racji braku zgodności pomiędzy dostępną w doświadczeniu długością fali (np. Cu $K\alpha$ 1.54178 Å) a progami absorpcji typowych pierwiastków MIR.

Sytuację zmieniło diametralnie promieniowanie synchrotronowe i możliwość precyzyjnego dostrojenia długości fali. Dobranie konkretnej długości fali jest *de facto* stosowane na każdej monochromatycznej linii promieniowania synchrotronowego i polega na ustawieniu pod właściwym kątem urządzenia monochromatyzującego. Na nowoczesnych liniach synchrotronowych instaluje się monochromatory podwójne (lub jeden kryształ z wyciętym w środku tunelem), dzięki czemu wiązka opuszcza monochromator zawsze pod tym samym kątem. Inne wymogi eksperymentalne to wysoka precyzja i powtarzalność tak w odniesieniu do długości fali jak i parametrów

geometrycznych. Ponieważ efekty anomalne są zwykle małe, pomiary intensywności refleksów muszą być bardzo dokładne, ale ten wymóg obowiązuje w praktyce na każdej synchrotronowej linii pomiarowej. Istnieje obecnie bardzo dużo linii synchrotronowych umożliwiających pomiary przy dostrojonej długości fali.

W typowym doświadczeniu nastawionym na wykorzystanie sygnału anomalnego mierzy się kompletne dane dyfrakcyjne przy takich długościach fali, dla których efekty f'' (maksimum absorpcji) i f' (próg absorpcji) są maksymalne, plus dodatkowo przy jeszcze jednej długości fali, z dala od progu absorpcji. Od pomiarów przy kilku długościach fali wzięła się angielska nazwa metody dostrojonej dyfrakcji anomalnej, Multiwavelength Anomalous Diffraction (MAD). Do praktyki krystalograficznej weszła dzięki przełomowym pracom z lat 1986-1991 [27-32], choć na możliwość pomiarów przy kilku długościach fali zwracano już uwagę wcześniej [24,33,34]. Podstawy teoretyczne metody MAD podał Jerome Karle [35], a ich przełożenia na praktyczne algorytmy laboratoryjne dokonał Wayne Hendrickson [36]. Według tego formalizmu wkłady do rozpraszania zależne i niezależne od długości fali zostają rozdzielone w układzie równań algebraicznych, których rozwiązanie daje poszukiwane fazy refleksów. Ponieważ w metodzie MAD to czynnik fizyczny (zmiana długości fali) a nie chemiczny (użycie ciężkiego atomu) jest źródłem informacji fazowej, wszystkie pomiary można przeprowadzić na tym samym kryształ, co znakomicie upraszcza pomiary i zwiększa ich dokładność.

Pierwsze testy metody MAD z zastosowaniem promieniowania synchrotronowego przeprowadzono dla kryształów białek o znanych strukturach, mianowicie dla derywatyzowanej terbem parwalbuminy [37], dla zawierających żelazo cytochromu c' [28] i hemoglobiny [38], oraz dla zawierającej miedź azuryny [29]. Prawdopodobnie pierwszą nową strukturę rozwiązano metodą MAD wykorzystując obecność miedzi w białku CBP, które przez ponad 20 lat nie dawało się złamać innymi metodami [27]. Atomy rozpraszające anomalnie w tych testach, choć naukowo interesujące, nie nadawały się do rutynowego zastosowania, gdyż wymagały uciążliwych eksperymentów derywatyzacyjnych (przykład z terbem) lub szczęśliwego zbiegu okoliczności (obecność żelaza lub miedzi). Ponieważ w metodzie MAD długość fali jest precyzyjnie dostrojona do rezonansu z atomem rozpraszającym anomalnie, można ją zastosować również dla pierwiastków o stosunkowo słabym sygnale anomalnym, jeśli tylko próg absorpcji leży w dostępnym zakresie długości fali. W praktyce są to pierwiastki cięższe od wanadu. Tak więc, atomy w metodzie MAD nie muszą być bardzo ciężkie, a szczególnie dobrym przykładem jest selen, którego efekty anomalne wynoszą $f'' = 5$ i $f' = -9$ elektronów. Efekty te obserwuje się przy wartościach λ różniących się zaledwie o 0.0002 Å (równoważne 2.5 eV) w pobliżu $\lambda = 0.979$ Å, co ilustruje wysokie wymagania eksperymentalne odnośnie precyzji i powtarzalności ustawienia długości fali.

Atrakcyjność selenu polega na tym, że można go stosunkowo łatwo wprowadzić do białka zastępując selenometioniną (Se-Met) naturalny aminokwas metioninę (Met) [31]. Dzięki postępom inżynierii genetycznej takie podstawienie odbywa się dziś rutynowo i może być nawet przeprowadzone automatycznie. Jako bakterii-fabryki (zwykle *Escherichia coli*) produkującej pożądaną białko używa się w tym celu szczepu auktroficznego uzależnionego od metioniny. Jeśli w pożywce zamiast Met będzie Se-Met, syntetyzowane białko będzie wyznakowane selenem we wszystkich pozycjach sekwencji zajętych przez metioninę. Można również użyć zwykłych bakterii, w których zablokowano szlak biosyntezy metioniny. Ponieważ Met pojawia się w sekwencjach białkowych z częstością 2,5%, zwykle w wyznakowanym białku jest dość atomów Se do zastosowania metody MAD. Metoda Se-Met MAD świadczy dziś tryumfy jako metoda z wyboru w badaniu białek o całkowicie nowej strukturze, choć początkowo przyjmowana była ostrożnie, raczej jako ciekawostka naukowa. Pierwszą strukturą białkową rozwiązana metodą Se-MAD była streptawidyna w kompleksie z biotyną [39], której pojedynczy atom siarki zastąpiono selenem. Pierwszym sukcesem klasycznego podejścia Se-Met MAD była struktura rybonukleazy H [30] rozwiązana w celu rozwikłania pełnego mechanizmu enzymatycznego odwrotnej transkryptyazy retrowirusa HIV.

Brom, którym można wygodnie modyfikować zasady nukleinowe, może spełnić w badaniach strukturalnych kwasów nukleinowych tę samą rolę co selen w krystalografii białek. Jeszcze bardziej atrakcyjny jest jon bromkowy, który można wprowadzać do kryształów makromolekuł w wyniku szybkiego nasączenia [26], dzięki czemu metoda Br-MAD ma potencjalne zastosowanie w "wysokoprzepustowej" krystalografii synchrotronowej.

W klasycznej metodzie MAD należy zarejestrować dane przy co najmniej dwóch długościach fali. Coraz popularniejsze staje się jednak podejście z jedną długością fali (SAD), gdyż wysoka dokładność pomiarów synchrotronowych pozwala na wyekstrahowanie słabego sygnału anomalnego nawet gdy jest on zagłuszany wysokim poziomem szumu.

W laboratorium NCI po raz pierwszy zastosowaliśmy metodę Se-Met MAD w 1994 roku do rozwiązania struktury domeny katalitycznej integrazy retrowirusowej [40]. Pomiary zostały wykonane na linii F1 synchrotronu CHESS (Uniwersytet Cornell). Była to jedna z pierwszych, jeśli nie pierwsza struktura rozwiązana metodą MAD przez zewnętrznych użytkowników tej linii.

Promieniowanie synchrotronowe jako motor postępu metodologicznego

Promieniowanie synchrotronowe stało się siłą napędową dla szeregu nowoczesnych rozwiązań metodologicznych w krystalografii białek. Jedną z takich innowacji, która

walnie przyczyniła się do poprawy jakości danych synchrotronowych, było wprowadzenie rutynowego chłodzenia kryształów do temperatury ok. 100 K w celu zapobieżenia nagrzewaniu się próbki w czasie pomiaru i zredukowania rozkładu kryształu wywołanego efektami jonizacyjnymi. Choć kriokrystalografią interesowano się od samego początku badań białkowych, do praktyki wprowadził ją dopiero Håkon Hope pod koniec lat 1980 [41]. Początkowo chłodzenie obejmowało w zasadzie czas pomiaru, lecz praktyka wykazała, że jest to również idealny sposób przechowywania i transportu kryształów białek. Metody niskotemperaturowe znalazły jedno z pierwszych zastosowań przy badaniach dyfrakcyjnych kryształów rybosomów [42]. W rozwiązaniach technicznych niską temperaturę w miejscu kryształu uzyskuje się na dyfraktometrze dzięki strumieniowi gazowego azotu o temperaturze 100 K dostarczanego z odpowiedniej dyszy. Ten sposób chłodzenia wymusił zupełnie inny system montowania kryształów do pomiarów dyfrakcyjnych. Popularne dawniej zatopione kapilary zawierające kryształ w obecności kropelki roztworu macierzystego wyszły już całkowicie z użycia. Zamiast tego kryształ zawieszany się w błonce z roztworu macierzystego w miniaturowej pętelce wykonanej z włókienka nylonowego. Umieszczenie pętelki z kryształem w strumieniu zimnego azotu powoduje momentalne zeszklenie wody, co redukuje niepożądane rozpraszanie tła oraz znakomicie utrudnia penetrację kryształu przez wolne rodniki i tym samym przedłuża jego żywotność w intensywnej wiązce rentgenowskiej [43]. Specjalne dodatki zwane krioprotektantami (np. gliceryna) utrudniają krystalizację soli oraz wody zawartych w kryształach białkowych.

W laboratorium NCI wprowadziliśmy pomiary niskotemperaturowe bardzo wcześnie, choć nie wszystko szło gładko od samego początku. Na przykład z powodu braku standardów technicznych w tym czasie, sami zaprojektowaliśmy i wykonaliśmy specjalne precyzyjne podstawki magnetyczne do szybkiego montowania "kriopętelek" na goniometrze bezpośrednio w strumieniu chłodzącego azotu. Później bardzo podobne podstawki stały się standardem w całej kriobiokrystalografii za sprawą wdrożenia komercyjnego, m.in. przez firmę Hampton Research.

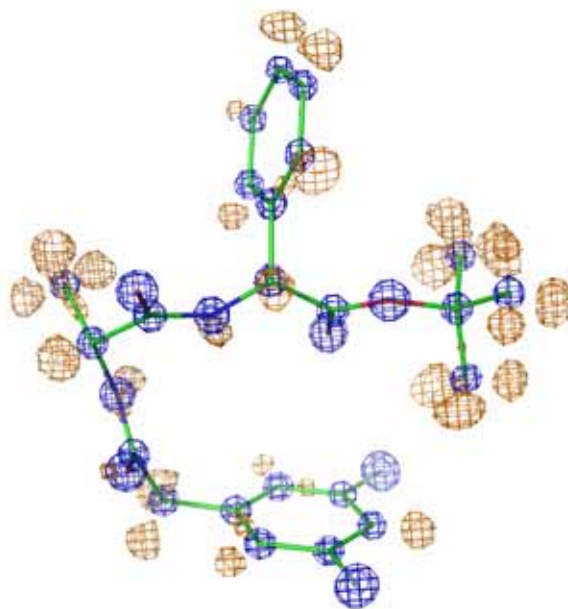
Ogromna intensywność promieniowania rentgenowskiego generowanego przez synchrotrony prowadzi zwykle do bardzo szybkiego zniszczenia porządku krystalicznego, co skutkuje gwałtownym spadkiem rozdzielczości obrazu dyfrakcyjnego. Z punktu widzenia chemicznego winne są wolne rodniki generowane w oddziaływaniu promieniowania jonizującego z materią, które w wypełnionym w połowie wodą kryształach białkowych mają fantastyczne możliwości błyskawicznego rozejścia się po całym kryształach i nieodwracalnej degradacji zawartego w nim delikatnego materiału białkowego. Warunki niskotemperaturowe, dzięki którym obszar wodny ulega zestaleniu, wprowadzono aby przeciwdziałać łatwej dyfuzji wolnych rodników, ale problem powrócił przy źródłach trzeciej generacji. Niska temperatura może spowolnić wtórne efekty wolnorodnikowe, ale nie jest w stanie zapobiec

zjawiskom pierwotnym, tj. rozrywaniu wiązań kowalencyjnych na skutek absorpcji kwantów promieniowania X, widocznemu w rozpadzie mostków dwusiarczkowych i dekarboksylacji reszt kwasu asparaginowego i glutaminowego [44]. Okazuje się jednak, że "nie ma tego złego, co by na dobre nie wyszło", gdyż efekty uszkodzeń radiacyjnych mogą być wykorzystane do uzyskania informacji fazowej metodą RIP (Radiation-damage Induced Phasing) [45], w podobny sposób jak izomorficzna zmiana chemiczna wykorzystywana jest w metodzie MIR.

Tzw. krystalografia Lauego jest tym działem biokrystalografii, który stał się możliwy wyłącznie dzięki promieniowaniu synchrotronowemu. W metodzie tej nieruchomy kryształ naświetlany jest błyskiem białego (tj. polichromatycznego) promieniowania rentgenowskiego, dzięki czemu możliwe jest zarejestrowanie niemal kompletnego obrazu dyfrakcyjnego w czasie zaledwie nanosekundowym. Pionierami tej metody są Keith Moffat [46], John Helliwell [17] i Janos Hajdu [47]. Można ją wykorzystać do badania struktury indywidualów o krótkim czasie życia (np. produktów pośrednich reakcji enzymatycznych) lub to monitorowania kinetyki przemian w kryształach białek, np. wiązania lub dysocjacji ligandów w mioglobinie [48]. Jeśli uda się znaleźć sposób na uwolnienie reakcji wszystkich cząsteczek białka w kryształach w tym samym momencie (np. w wyniku błysku laserowego), wówczas wykonując nanosekundowe zdjęcia w odstępach mikrosekund można będzie zarejestrować przebieg przemiany trwającej np. jedną milisekundę.

Bez promieniowania synchrotronowego niemożliwe byłoby rutynowe osiąganie rozdzielczości atomowej (zdefiniowanej jako 1.2 Å), a tym bardziej subatomowej, dla kryształów białek (Rys. 2B). Obecnie w PDB jest ponad 1000 struktur o rozdzielczości lepszej niż 1.2 Å, w tym około 20 struktur, dla których zarejestrowano dane o rozdzielczości co najmniej 0.8 Å (wszystkie z użyciem SR). Te struktury o najwyższej rozdzielczości są jak klejnoty w skarbcu biologii strukturalnej. Pozwalają one zlokalizować precyzyjnie każdy atom cząsteczki dzięki dobrze zdefiniowanym maksimum na mapie gęstości elektronowej, a nawet ukazują elektrony wiązań i atomy wodoru (Rys. 3). Ten ostatni aspekt jest bardzo ważny, gdyż atomy wodoru, choć odgrywają kluczową rolę w mechanizmach reakcji enzymatycznych, nie mogą być zlokalizowane w strukturach o niższej rozdzielczości. Rekordową rozdzielczość 0.54 Å osiągnięto dla małego białka zwanego krambiną [49]. Jednak w grupie rekordzistów są też większe białka, np. lizozym czy reduktaza aldozy, których struktury wyznaczono z rozdzielczością 0.65 Å [50] i 0.66 Å [51]. Przy tym poziomie rozdzielczości struktury makromolekularne nie tylko osiągają ale przekraczają standardy typowe dla krystalografii małych cząsteczek. W dwóch pionierskich projektach dotyczących krambiny [49] i reduktazy aldozy [52], udało się uokładnić parametry multipolowe makrocząsteczek, które ukazują rozkład elektronów na orbitalach wiążących i deformację ładunku atomów w odniesieniu do przybliżonego atomu sferycznego. Te

bezprecedensowe osiągnięcia umożliwiają opis makrocząsteczek na nieznanym dotąd poziomie dokładności.



Rys. 3. Fragment struktury inhibitora γ -sekreazy uokładnionej z rozdzielczością 0.7 Å na podstawie synchrotronowych danych dyfrakcyjnych. Niebieska mapa gęstości elektronowej pokazuje precyzyjną definicję atomów niewodorowych modelu. Różnicowa mapa pomarańczowa ujawnia położenia atomów wodoru, które nie zostały jeszcze ujęte w modelu. Rysunek przygotował A. Czerwiński.

Kolejnym obszarem nauki, gdzie postęp zależy krytycznie od dostępności promieniowania synchrotronowego dla pomiarów dyfrakcyjnych, jest genomika strukturalna, która stawia sobie za cel masowe rozwiązywanie maksymalnej liczby nowych struktur białkowych w jak najkrótszym czasie. Niektóre centra genomiki strukturalnej rozwiązują obecnie jedną strukturę białkową co drugi dzień [53]. Ilość danych jaka się za tym kryje nie mogłaby być nigdy osiągnięta przy pomocy konwencjonalnych źródeł promieniowania rentgenowskiego.

Dziedziną o szczególnym znaczeniu dla przemysłu farmaceutycznego, ale i dla zwykłego człowieka, jest poszukiwanie nowych molekuł-kandydatów, które dałyby w wyniku optymalizacji lek doskonały. Często molekułę "początkową" znajduje się prowadząc reakcję "celu farmakologicznego" (np. enzymu) z kockajlem możliwych molekuł [54]. Wyselekcjonowanie najlepszych spośród setek kandydatów odbywa się poprzez badanie struktury utworzonych kompleksów. Podejście to jest możliwe tylko w trybie "wysokoprzepustowym" przy użyciu promieniowania synchrotronowego.

"Podróże w nieznane"

Na koniec warto wymienić kilka niezwykłych osiągnięć, możliwych jedynie dzięki wykorzystaniu promieniowania synchrotronowego. Przykładowo, możliwe było zarejestrowanie obrazu dyfrakcyjnego od kryształów o gigantycznych wymiarach komórki elementarnej, 1255 Å w przypadku rdzenia cząstki reowirusowej [55] i 1123 Å w przypadku adaptora klatryny [56]. Stosując mikrowiązkę synchrotronową zarejestrowano dane dyfrakcyjne o rozdzielczości 2 Å dla naturalnych krystalitów o wielkości 2 μm zawierających cypowirus, wydobytych z komórek owadzych [57].

I wreszcie badania z wykorzystaniem promieniowania synchrotronowego uwieńczone Nagrodą Nobla. W roku 2009 nagrodę w dziedzinie chemii uzyskali Venkatraman Ramakrishnan, Thomas Steitz i Ada Yonath za wyjaśnienie na podstawie badań krystalograficznych struktury atomowej i funkcji rybosomu [58-61]. Ada Yonath przez 30 lat, a dwie pozostałe grupy przez kilkanaście lat zmagaly się z kryształami rybosomów, wykorzystując w tym celu niemal każdą synchrotronową linię białkową na świecie. Również wcześniejsze Nagrody Nobla z chemii uhonorowały badania z użyciem promieniowania synchrotronowego, poczynając od Johna Walkera (1997), który wyjaśnił mechanizm syntezy ATP [62,63]. Dane dyfrakcyjne dla kryształów ATPazy F₁ zarejestrowano na

synchrotronie SRS w Daresbury używając płyty obrazowej podarowanej przez Hendrixa i Lentfera. Dane rejestrowano dla ogromnej liczby nietrwałych kryształów, montowanych w kapilarach i chłodzonych do 4°C. Kolejne związane z promieniowaniem synchrotronowym Nagrody Nobla otrzymali Roderick MacKinnon (2003) za określenie struktury i działania błonowego kanału potasowego [64] oraz Roger Kornberg (2006) za wyjaśnienie podstaw strukturalnych transkrypcji DNA [65].

Perspektywy zastosowań promieniowania synchrotronowego w krystalografii białek

W latach 1990. postęp naukowy i techniczny doprowadził do powstania źródeł synchrotronowych trzeciej generacji charakteryzujących się większą średnicą pierścienia (~1 km) oraz znacznie wyższą jasnością i stabilnością promieniowania. Urządzenia takie zbudowano w Grenoble (ESRF), Chicago (APS) i w Japonii (Spring8), a nieco później w Szwajcarii (SLS), Wielkiej Brytanii (DIAMOND), Francji (SOLEIL) i Niemczech (PETRA III). W ten sposób liczba linii synchrotronowych do badań dyfrakcyjnych makromolekuł (Rys. 4) osiągnęła 100 (Tabela 1), przy czym dalsze są w budowie lub w stadium projektowym. Źródła synchrotronowe są dziś podstawowym źródłem danych dyfrakcyjnych dla krystalografii białek (Rys. 1B).



Rys. 4. Stacja pomiarowa ID14 do badań krystalograficznych makromolekuł synchrotronu ESRF w Grenoble. Zawieszony w małej pętli kryształ białka umieszczony jest jednocześnie w wiązce promieniowania rentgenowskiego i w strumieniu ochłodzonych par azotu. Obraz dyfrakcyjny rejestruje kamera CCD. Zdjęcie uzyskano dzięki uprzejmości dr D. Halla.

Tabela 1. Linie synchrotronowe służące krystalografii białek.

1	ALS (Advanced Light Source), Lawrence Berkeley National Laboratory	Berkeley, USA	4.2.2, 5.0.1, 5.0.2, 5.0.3, 8.2.1, 8.2.2, 8.3.1
2	APS (Advanced Photon Source), Argonne National Laboratory	Argonne, USA	14BM-C, 14BM-D, 14ID-B, 17BM, 17ID, 19BM, 19ID, 21ID-D, 21ID-E, 21ID-F, 21ID-G, 22BM, 22ID, 23BM-B, 23ID-B, 23ID-D, 24BM, 24ID-C, 24ID-E, 31ID
3	Australian Synchrotron	Melbourne, Australia	MX1, MX2
4	BESSY II	Berlin, Niemcy	14.1, 14.2, 14.3
5	BSRF	Beijing, Chiny	3W1A, 1W2B
6	CAMD (Center for Advanced Microstructures and Devices),	Baton Rouge, USA	GCPC
7	CHESS (Cornell High Energy Synchrotron Source), Cornell University	Ithaca, USA	A1, F1, F2
8	CSRF (Canadian Synchrotron Radiation Facility)	Saskatoon, Kanada	08ID-1
9	DIAMOND	Harwell Chilton Science Campus, Wlk. Brytania	I02, I03, I04, I04-1, I24
10	ELETTRA	Trieste, Włochy	5.2R
11	EMBL/MPG (European Molecular Biology Laboratory/Max-Planck Gesellschaft); DESY	Hamburg, Niemcy	BW7A, BW7B, X11, X12, X13, BW6
12	ESRF (European Synchrotron Radiation Facility)	Grenoble, Francja	ID14-1, ID14-2, ID14-4, ID23-1, ID23-2, ID29
13	LNLS (National Synchrotron Light Laboratory)	Campinas, Brazylia	D03, W01B
14	MAX, Lund University	Lund, Szwecja	I711, I911-2, I911-3, I911-4, I911-5,
15	NSLS (National Synchrotron Light Source), Brookhaven National Laboratory	Brookhaven, USA	X3A, X4A, X4C, X6A, X8C, X12B, X12C, X25, X26C, X29A
16	NSRRC (National Synchrotron Radiation Research Center)	Hsinchu, Tajwan	BL13B1, BL13C1, BL17B2
17	PAL,	Pohang, Korea	4A, 6B, 6C1
18	Photon Factory,	Tsukuba, Japonia	BL-5A, BL-6A, BL-17A, BL18-B, AR-NW12A
19	SLS (Synchrotron Light Source), Paul Scherrer Institute	Villigen, Szwajcaria	X06SA, X10SA, X06DA
20	SOLEIL	Saint-Aubin, Francja	PROXIMA1, PROXIMA2
21	Spring-8, Super Photon Ring 8	Japonia	BL12B2, BL24XU, BL26B1, BL26B 2, BL32B2, BL38B1, BL40B2, BL41XU, BL44XU, BL45XU
22	SSRL (Stanford Synchrotron Light Source), Stanford University	USA	BL1-5, BL7-1, BL9-1, BL9-2, BL11-1, BL12-2

Jeszcze bardziej zaawansowane są urządzenia czwartej generacji o charakterze akceleratorów liniowych typu laserowego, budowane w Hamburgu oraz działające już w Stanford. Jasność dostarczanego przez nie promieniowania rentgenowskiego jest o 10 rzędów wielkości większa, umożliwiając badanie ogromnych kompleksów makromolekularnych, całych komórek biologicznych, oraz nanomateriałów nieperiodycznych [66]. W laserze rentgenowskim na swobodnych elektronach (XFEL), strumień elektronów nie krąży w pierścieniu lecz jest przyspieszany do prędkości podświetlnych w akceleratorze liniowym o długości do kilku kilometrów, przechodząc przez szereg wnęk rezonansowych lub przez bardzo długi undulator. Ponieważ dochodzi do rezonansu pomiędzy elektronami a polem elektromagnetycznym przez nie wywołanym, możliwa jest akcja laserowa czyli efekt amplifikacji światła. Poziom energii generowanego w tych

urządzeniach promieniowania rentgenowskiego jest tak ogromny, że nie wiemy jeszcze, czy umieszczone w nim makromolekuły biologiczne "przeżyją" wystarczająco długo, aby eksperymentator zdążył zarejestrować swoje dane. Podobne problemy biologia synchrotronowa skutecznie rozwiązała w przeszłości, więc i z tymi wyzwaniami na pewno sobie poradzi. Rewolucja, którą zapoczątkowało wprowadzenie promieniowania synchrotronowego jako narzędzia badawczego w biologii strukturalnej dopiero się zaczęła. Bez wątplenia czekają nas jeszcze odkrycia, o jakich nam się nawet nie śniło, prowadzące do lepszego zrozumienia struktur i mechanizmów atomowych, które określamy jako "życie". A lepsze zrozumienie to nie tylko satysfakcja intelektualna uczonych, ale również postęp cywilizacyjny, szczególnie w obszarach takich jak zdrowie, a więc dotyczących nas wszystkich.

Literatura

- [1] F.L. Hünefeld, in *Chemismus in der Thierischen Organisation*, (Leipzig, 1840), p. 160.
- [2] E.T. Reichert, A.P. Brown, *The differentiation and specificity of corresponding proteins and their vital substances in relation to biological classification and organic evolution*. (Carnegie Institution of Washington, Washington DC, 1909).
- [3] J.C. Kendrew, G. Bodo, H.M. Dintzis, R.G. Parrish, H. Wyckoff, D.C. Phillips, "A three-dimensional model of the myoglobin molecule obtained by x-ray analysis", *Nature* **181** (1958) 662–666.
- [4] J.C. Kendrew, R.E. Dickerson, B.E. Strandberg, R.G. Hart, D.R. Davies, D.C. Phillips, V.C. Shore, "Structure of myoglobin. A three-dimensional Fourier synthesis at 2 Å resolution", *Nature* **185** (1960) 422–427.
- [5] M.F. Perutz, M.G. Rossmann, A.F. Cullis, H. Muirhead, G. Will, A.C.T. North, "Structure of haemoglobin. A three-dimensional fourier synthesis at 5.5-Å resolution, obtained by X-ray analysis", *Nature* **185** (1960) 416–421.
- [6] W.T. Astbury, A. Street, "X-ray studies of the structure of hair, wool, and related fibres", *Phil. Trans. Roy. Soc. A* **230** (1932) 75–101.
- [7] J.D. Bernal, D. Crowfoot, "X-ray photographs of crystalline pepsin.", *Nature* **133** (1934) 794–795.
- [8] J.D. Bernal, "Structure of proteins", *Nature* **143** (1939) 663–667.
- [9] Protein Data Bank, *Nature New Biol.* **233** (1971) 223.
- [10] Protein Data Bank, *Acta Crystallogr. B* **29** (1973) 1746.
- [11] J.D. Watson, F.H.C. Crick, "Molecular structure of nucleic acids; a structure for deoxyribose nucleic acid", *Nature* **171** (1953) 737–738.
- [12] R.E. Franklin, R.G. Gosling, "Molecular configuration in sodium thymonucleate", *Nature* **171** (1953) 740–741.
- [13] H.M. Berman, J. Westbrook, Z. Feng, G. Gilliland, T.N. Bhat, H. Weissig, I.N. Shindyalov, P.E. Bourne, "The Protein Data Bank", *Nucleic Acids Res.* **28** (2000) 235–242.
- [14] J. Schwinger, "On the classical radiation of accelerated electrons.", *Phys. Rev.* **12** (1949) 1912–1925.
- [15] D. Bourgeois, A. Royant, "Advances in kinetic protein crystallography", *Curr. Opin. Struct. Biol.* **15** (2005) 538–547.
- [16] M. Schiltz, G. Bricogne, "Exploiting the anisotropy of anomalous scattering boosts the phasing power of SAD and MAD experiments", *Acta Crystallogr. D* **64** (2008) 711–729.
- [17] J.R. Helliwell, *Macromolecular Crystallography With Synchrotron Radiation*, (Cambridge University Press, 1992).
- [18] C. Abad-Zapatero, "Notes of a protein crystallographer; our unsung heroes", *Structure* **12** (2004) 523–527.
- [19] G. Rosenbaum, K.C. Holmes, J. Witz, "Synchrotron radiation as a source for x-ray diffraction", *Nature* **230** (1971) 434–437.
- [20] K.C. Holmes, G. Rosenbaum, "How X-ray diffraction with synchrotron radiation got started", *J. Synchrotron Rad.* **5** (1998) 147–153.
- [21] T.D. Mokulskaya, M.A. Mokulskii, A.A. Nikitin, V.V. Anashin, G.N. Kuplipanov, V.A. Lukashev, A.N. Skrinkii, "[Utilization of the storage ring VEPP-3 for X-ray studies]", *Dokl. Akad. Nauk SSSR* **218** (1974) 824–827.
- [22] F.W. Lytle, "The EXAFS family tree: a personal history of the development of extended X-ray absorption fine structure", *J. Synchrotron Rad.* **6** (1999) 123–134.
- [23] J.C. Phillips, A. Wlodawer, M.M. Yevitz, K.O. Hodgson, "Applications of synchrotron radiation to protein crystallography: preliminary results", *Proc. Natl. Acad. Sci. USA* **73** (1976) 128–132.
- [24] A. Herzenberg, H.S.M. Lau, "Anomalous scattering and the phase problem", *Acta Crystallogr.* **22** (1967) 24–28.
- [25] J.C. Phillips, A. Wlodawer, J.M. Goodfellow, K.D. Watenpugh, L.C. Sieker, L.J. Jensen, K.O. Hodgson, "Applications of synchrotron radiation to protein crystallography II: Anomalous scattering, absolute intensity and polarization", *Acta Crystallogr.* **A33** (1977) 445–455.
- [26] Z. Dauter, M. Dauter, K.R. Rajashankar, "Novel approach to phasing proteins: derivatization by short cryo soaking with halides", *Acta Crystallogr.* **D56** (2000) 232–237.
- [27] J.M. Guss, E.A. Merritt, R.P. Phizackerley, B. Hedman, M. Murata, K.O. Hodgson, H.C. Freeman, "Phase determination by multiple-wavelength x-ray diffraction: crystal structure of a basic 'blue' copper protein from cucumbers", *Science* **241** (1988) 806–811.
- [28] S. Harada, M. Yasui, K. Murakawa, N. Kasai, Y. Satow, "Crystal-structure analysis of cytochrome-C' by the multiwavelength anomalous diffraction method using synchrotron radiation", *J. Appl. Crystallogr.* **19** (1986) 448–452.
- [29] Z.R. Korszun, "The tertiary structure of azurin from *Pseudomonas denitrificans* as determined by Cu resonant diffraction using synchrotron radiation", *J. Mol. Biol.* **196** (1987) 413–419.
- [30] W. Yang, W.A. Hendrickson, R.J. Crouch, Y. Satow, "Structure of ribonuclease H phased at 2 Å resolution by MAD analysis of the selenomethionyl protein", *Science* **249** (1990) 1398–1405.
- [31] W.A. Hendrickson, J.R. Horton, D.M. LeMaster, "Selenomethionyl proteins produced for analysis by multiwavelength anomalous diffraction (MAD): a vehicle for direct determination of three dimensional structure", *EMBO J.* **9** (1990) 1665–1672.
- [32] W.A. Hendrickson, "Determination of macromolecular structures from anomalous diffraction of synchrotron radiation", *Science* **254** (1991) 51–58.
- [33] Y. Okaya, R. Pepinsky, "New formulation and solution of the phase problem in X-ray analysis of noncentric crystals containing anomalous scatterers", *Phys. Rev.* **103** (1956) 1645–1647.
- [34] C.M. Mitchell, "Phase determination by the two-wavelength method of Okaya & Pepinsky", *Acta Crystallogr.* **10** (1957) 475–476.
- [35] J. Karle, "Some developments in anomalous dispersion for the structural investigation of macromolecular systems in biology.", *Int. J. Quant. Chem.* **S7** (1980) 357–367.
- [36] W.A. Hendrickson, "Analysis of protein structure from diffraction measurements at multiple wavelengths.", *Trans Am. Crystallogr. Assoc.* **21** (1985) 11–21.
- [37] R. Kahn, R. Fourme, R. Bosshard, M. Chiadmi, J.L. Risler, O. Dideberg, J.P. Wery, "Crystal structure study of Opsanus tau parvalbumin by multiwavelength anomalous diffraction", *FEBS Lett.* **179** (1985) 133–137.

- [38] W.A. Hendrickson, J.L. Smith, R.P. Phizackerley, E.A. Merritt, "Crystallographic structure analysis of lamprey hemoglobin from anomalous dispersion of synchrotron radiation", *Proteins* **4** (1988) 77–88.
- [39] W.A. Hendrickson, A. Pahler, J.L. Smith, Y. Satow, E.A. Merritt, R.P. Phizackerley, "Crystal structure of core streptavidin determined from multiwavelength anomalous diffraction of synchrotron radiation", *Proc. Natl. Acad. Sci. USA* **86** (1989) 2190–2194.
- [40] G. Bujacz, M. Jaskólski, J. Alexandratos, A. Wlodawer, G. Merkel, R.A. Katz, A.M. Skalka, "High resolution structure of the catalytic domain of the avian sarcoma virus integrase", *J. Molec. Biol.* **253** (1995) 333–346.
- [41] H. Hope, "Cryocrystallography of biological macromolecules: a generally applicable method", *Acta Crystallogr. D* **44** (1988) 22–26.
- [42] H. Hope, F. Frolow, K. von Bohlen, I. Makowski, C. Kratky, Y. Halfon, H. Danz, P. Webster, K.S. Bartels, H.G. Wittmann, "Cryocrystallography of ribosomal particles", *Acta Crystallogr. B* **45** (1989) 190–199.
- [43] T.-Y. Teng, "Mounting of crystals for macromolecular crystallography in a free-standing thin film.", *J. Appl. Cryst.* **23** (1990) 387–391.
- [44] M. Weik, R.B. Ravelli, G. Kryger, S. McSweeney, M.L. Raves, M. Harel, P. Gros, I. Silman, J. Kroon, J.L. Sussman, "Specific chemical and structural damage to proteins produced by synchrotron radiation", *Proc. Natl. Acad. Sci. USA* **97** (2000) 623–628.
- [45] R.B. Ravelli, H.K. Leiros, B. Pan, M. Caffrey, S. McSweeney, "Specific radiation damage can be used to solve macromolecular crystal structures", *Structure* **11** (2003) 217–224.
- [46] K. Moffat, D. Szebenyi, D. Bilderback, "X-ray Laue Diffraction from Protein Crystals", *Science* **223** (1984) 1423–1425.
- [47] J. Hajdu, P.A. Machin, J.W. Campbell, T.J. Greenhough, I.J. Clifton, S. Zurek, S. Gover, L.N. Johnson, M. Elder, "Millisecond X-ray diffraction and the first electron density map from Laue photographs of a protein crystal", *Nature* **329** (1987) 178–181.
- [48] M. Milani, M. Nardini, A. Pesce, E. Mastrangelo, M. Bolognesi, "Hemoprotein time-resolved X-ray crystallography", *IUBMB Life* **60** (2008) 154–158.
- [49] C. Jelsch, M.M. Teeter, V. Lamzin, V. Pichon-Pesme, R.H. Blessing, C. Lecomte, "Accurate protein crystallography at ultra-high resolution: Valence electron distribution in crambin", *Proc. Natl. Acad. Sci. USA* **97** (2000) 3171–3176.
- [50] J. Wang, M. Dauter, R. Alkire, A. Joachimiak, Z. Dauter, "Triclinic lysozyme at 0.65 Å resolution", *Acta Crystallogr. D* **63** (2007) 1254–1268.
- [51] E.I. Howard, R. Sanishvili, R.E. Cachau, A. Mitschler, B. Chevrier, P. Barth, V. Lamour, M. Van Zandt, E. Sibley, C. Bon, D. Moras, T.R. Schneider, A. Joachimiak, A. Podjarny, "Ultra-high resolution drug design I: details of interactions in human aldose reductase-inhibitor complex at 0.66 Å", *Proteins* **55** (2004) 792–804.
- [52] B. Guillot, C. Jelsch, A. Podjarny, C. Lecomte, "Charge-density analysis of a protein structure at subatomic resolution: the human aldose reductase case", *Acta Crystallogr. D* **64** (2008) 567–588.
- [53] M. Grabowski, M. Chruszcz, M.D. Zimmerman, O. Kirillova, W. Minor, "Benefits of structural genomics for drug discovery research", *Infect. Disord. Drug Targets* **9** (2009) 459–474.
- [54] T.L. Blundell, B.L. Sibanda, R.W. Montalvo, S. Brewerton, V. Chelliah, C.L. Worth, N.J. Harmer, O. Davies, D. Burke, "Structural biology and bioinformatics in drug design: opportunities and challenges for target identification and lead discovery", *Philos. Trans. Roy. Soc. Lond. B Biol. Sci.* **361** (2006) 413–423.
- [55] K.M. Reinisch, M.L. Nibert, S.C. Harrison, "Structure of the reovirus core at 3.6 Å resolution", *Nature* **404** (2000) 960–967.
- [56] E.E. Heldwein, E. Macia, J. Wang, H.L. Yin, T. Kirchhausen, S.C. Harrison, "Crystal structure of the clathrin adaptor protein 1 core", *Proc. Natl. Acad. Sci. U S A* **101** (2004) 14108–14113.
- [57] F. Coulibaly, E. Chiu, K. Ikeda, S. Gutmann, P.W. Haeberl, C. Schulze-Briese, H. Mori, P. Metcalf, "The molecular organization of cypovirus polyhedra", *Nature* **446** (2007) 97–101.
- [58] B.T. Wimberly, D.E. Brodersen, W.M. Clemons, Jr., R.J. Morgan-Warren, A.P. Carter, C. Vornrhein, T. Hartsch, V. Ramakrishnan, "Structure of the 30S ribosomal subunit", *Nature* **407** (2000) 327–339.
- [59] F. Schluenzen, A. Tocilj, R. Zarivach, J. Harms, M. Gluehmann, D. Janell, A. Bashan, H. Bartels, I. Agmon, F. Franceschi, A. Yonath, "Structure of functionally activated small ribosomal subunit at 3.3 Å resolution", *Cell* **102** (2000) 615–623.
- [60] N. Ban, P. Nissen, J. Hansen, P.B. Moore, T.A. Steitz, "The complete atomic structure of the large ribosomal subunit at 2.4 Å resolution", *Science* **289** (2000) 905–920.
- [61] M. Selmer, C.M. Dunham, F.V. Murphy, A. Weixlbaumer, S. Petry, A.C. Kelley, J.R. Weir, V. Ramakrishnan, "Structure of the 70S ribosome complexed with mRNA and tRNA", *Science* **313** (2006) 1935–1942.
- [62] J.P. Abrahams, A.G.W. Leslie, R. Lutter, J.E. Walker, "Structure at 2.8 Å resolution of F₁-ATPase from bovine heart mitochondria", *Nature* **370** (1994) 621–628.
- [63] J.P. Abrahams, A.G. Leslie, "Methods used in the structure determination of bovine mitochondrial F₁ ATPase", *Acta Crystallogr. D* **52** (1996) 30–42.
- [64] Y. Jiang, A. Lee, J. Chen, M. Cadene, B.T. Chait, R. MacKinnon, "Crystal structure and mechanism of a calcium-gated potassium channel", *Nature* **417** (2002) 515–522.
- [65] P. Cramer, D.A. Bushnell, R.D. Kornberg, "Structural basis of transcription: RNA polymerase II at 2.8 angstrom resolution", *Science* **292** (2001) 1863–1876.
- [66] M. Bergh, G. Hultdt, N. Timneanu, F.R. Maia, J. Hajdu, "Feasibility of imaging living cells at subnanometer resolutions by ultrafast X-ray diffraction", *Q. Rev. Biophys.* **41** (2008) 181–204.

FROM ATOMIC RESOLUTION TO MOLECULAR GIANTS: AN OVERVIEW OF CRYSTALLOGRAPHIC STUDIES OF BIOLOGICAL MACROMOLECULES WITH SYNCHROTRON RADIATION

M. Jaskólski ^{1,2, *}

¹ Department of Crystallography, Faculty of Chemistry, A. Mickiewicz University and

² Center for Biocrystallographic Research, Institute of Bioorganic Chemistry,
Polish Academy of Sciences, Poznań, Poland

Keywords: protein crystallography, macromolecular models, structural genomics, ribosome structure, drug design

*) e-mail: mariuszj@amu.edu.pl

Protein crystals have huge unit cells (~100 Å) filled not only with ordered protein molecules but also in about 50% with liquid water. The phase problem in protein crystallography can be solved by molecular replacement (using a suitable model molecule), by isomorphous replacement (using heavy atom derivatives), or by multiwavelength anomalous diffraction (using resonant scattering of synchrotron-generated X-rays by anomalous atoms, such as Se). X-ray diffraction by protein crystals produces thousands of reflections but since the models are very complex (many thousands of atoms), paucity of data is a serious problem and stereochemical restraints are necessary. In consequence, the highest possible resolution (minimum d -spacing in Bragg's Equation) should always be the experimental goal. Protein structures determined by crystallography are deposited in Protein Data Bank, which currently holds more than 65 000 entries. Recent methodological advancements, stimulated by a wide-spread use of powerful synchrotron sources and by structural genomics, have resulted in rapid acceleration of the structure elucidation process, and in addition help to obtain better data. Protein crystallography has produced atomic models of gigantic macromolecular assemblies, including the ribosome. It is also providing accurate targets for structure-guided development of drugs.

1. Introduction¹

1.1. X-ray diffraction pictures of protein crystals

When we look at the X-ray diffraction pattern of a protein crystal, we usually see an intensity-weighted reciprocal lattice with myriads of spots or reflections. But, two other things are also striking: (i) the reflections are very closely spaced and (ii) their intensity falls off rather quickly as we move away from the center, *i.e.*, from the direction of the primary beam. The former property, *i.e.*, small distances in reciprocal space (corresponding to small angles θ), stems directly from Bragg's Law, $\lambda = 2d \sin\theta$, and reflects the fact that protein crystals have very large unit cells in direct space (large d), necessary to accommodate the gigantic macromolecules. The latter property is the consequence of the fact that scattering of X-rays by atoms, f_j , while appreciable (proportional to the number of electrons) in the forward direction, declines quickly with the scattering angle θ . An example X-ray diffraction image of a protein crystal is shown in Fig. 1. Other examples can be found in several excellent handbooks on protein crystallography, for instance [1], or in Ref. [2].

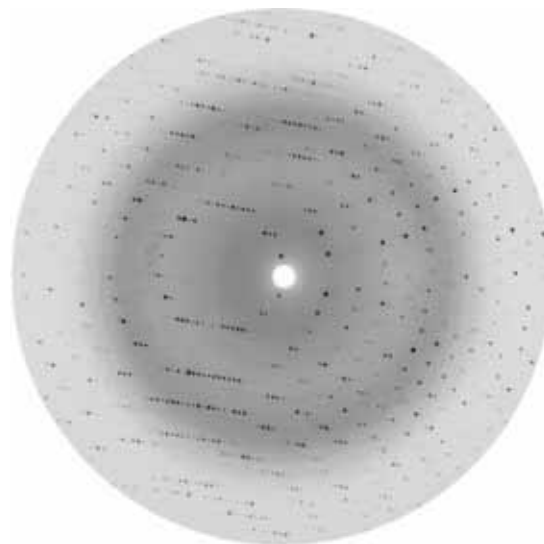


Figure 1. An X-ray diffraction pattern recorded for a protein crystal using synchrotron radiation. The resolution on this image increases radially from the center (which coincides with the position of the primary beam) and corresponds, at the edge of the detector, to $d_{\min} = 2.4 \text{ \AA}$. To increase the resolution captured on the detector, we would have to swing the detector away from the primary beam, or move the detector closer to the crystal, or increase its diameter, or alternatively use X-rays with shorter wavelength. Courtesy of Dr. Szymon Krzywda.

#) Reprinted with permission from *Acta Physica Polonica A* 117, 2 (2010) 257-263.

1.2. Water content in protein crystals

Usually, there is also another curious feature in the X-ray photographs of protein crystals, namely, a very strong background visible as a diffuse dark ring at a certain angle with the primary beam. This feature is due to the scattering of X-rays by disordered water molecules, which always accompany protein molecules in their crystals. The protein-to-water volume ratio is typically 1:1. This property of protein crystals is on the one hand a blessing for the protein crystallographer, because it guarantees that protein molecules even in crystalline form are in their native aqueous environment and thus they have a native structure. But it can be a curse on the other hand, because with weak, water-shielded direct protein-protein contacts the degree of molecular order can be less than perfect, which in consequence leads to a poor diffraction and to a poor structure determination. Even more importantly, the water channels in protein crystals are excellent routes for the diffusion of free radicals (generated by the ionizing X-ray radiation), which can degrade the delicate protein material very quickly.

Bulk water in protein crystals is "structured" as liquid water, *i.e.*, we have an endless network of tetrahedrally arranged water molecules connected by hydrogen bonds, whose donor/acceptor properties fluctuate throughout the entire network. Typical O...O distances in those hydrogen bonds are 2.7 Å. This leads to a great number of 1–3 O...O vectors, whose directions, but not the length (4.4 Å), can change. Those repeated distances lead to scattering of X-rays with the intensity distribution that has a maximum at a certain angle θ .

With tuneable X-ray radiation, such as obtained in a synchrotron, the "water ring" recorded on a flat detector perpendicular to the primary beam can be bigger or smaller depending on the wavelength λ of the radiation (typically about 1 Å), but even at a constant λ we can change its radius by moving the detector in and out. It would appear that it would be advantageous to move the detector far from the crystal, because then the closely spaced diffraction spots would become well separated. While we indeed do want to achieve a physical resolution of diffraction spots on the detector, there is a different consideration, connected with another meaning of the term "resolution", which prompts us to move the detector as close to the crystal as possible. We will explain this in the next section.

2. Fourier transformation, the phase problem, and electron density maps

To understand the reason for moving the detector as close to the crystal as possible, we must first realize that X-rays are scattered by electrons, primarily by electrons in atomic cores, but also by bonding electrons. The X-ray diffraction image is a Fourier transform of the scattering object, *i.e.*, of the electron distribution (also called electron density) in the crystal. To be able to calculate back the information about the electron density is of a

great importance to us. In chemistry, everything is explained by electrons: the nature of different atoms and bonds between them in chemical molecules. It is thus very fortunate that we have a mathematical apparatus, the inverse Fourier transform, allowing us to calculate electron density maps (Fig. 2) in the crystallographic unit cell. Electron density maps will tell us all we want to know about the chemical molecules that build up our crystal.

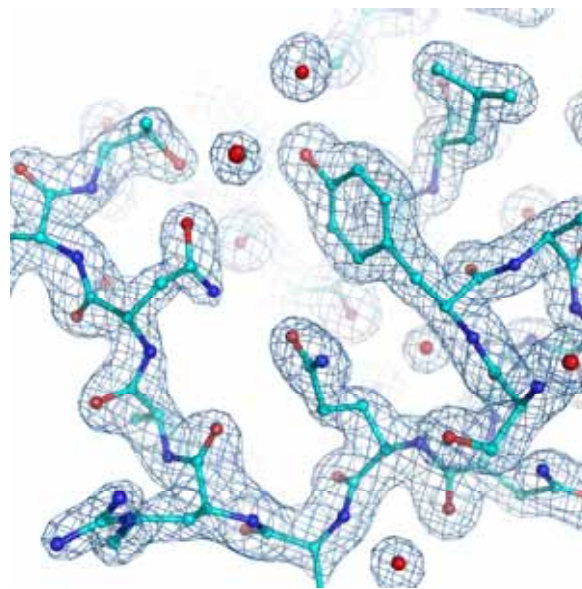


Figure 2. An electron density map calculated from the diffraction pattern of a protein crystal revealing the atomic architecture of the biomolecule. The high resolution (1.6 Å) of this $2F_o - F_c$ map allows even for water molecules (red spheres), which accompany proteins in their crystals, to be visualized. *Courtesy of Agnieszka Wojtkowiak.*

However, there is a serious obstacle on our way from the diffraction pattern to the electron density map, $\rho(xyz)$, *i.e.*, to the crystal structure. It is known as the phase problem because in the simple Fourier formula $\rho(xyz) = \sum F(hkl) \exp[-2\pi i(hx+ky+lz)]$, the complex entities $F(hkl)$, called the structure factors, are known from the diffraction experiment with respect to their amplitudes, calculated simply as $|F(hkl)| = \sqrt{I(hkl)}$ (where $I(hkl)$ is the intensity of reflection hkl), but not with respect to their phases $\phi(hkl)$.

In protein crystallography, the Fourier coefficients of electron density maps are usually of the form $\{(2|F_o| - |F_c|), \phi\}$, where F_o is the observed structure factor and F_c is the corresponding value calculated from some atomic model. The phase ϕ is usually also obtained through Fourier transformation of a model, except when some experimental phase information must be generated for structures without a suitable model. In essence, the " $2F_o - F_c$ " map can be considered as a sum of " F_o " (representing the experimental reality) and " $F_o - F_c$ "

(representing the difference between the reality and the current model) maps. Alternatively, difference " $F_o - F_c$ " Fourier maps can also be computed to facilitate modeling aimed at model correction. In all cases where the phases are derived from an atomic model, the model will strongly influence (or bias) the appearance of the electron density maps; therefore independent experimental information is always very important.

3. Solution of the phase problem in protein crystallography

The formidable task of estimating the phases of many thousands of individual reflections can be accomplished in macromolecular crystallography on three ways, each of which relies to some extent on a peculiar inverse Fourier transform, $P(uvw) = \sum |F(hkl)|^2 \exp[-2\pi i(hu + kv + lw)]$, known as the Patterson function, so named after its inventor, Arthur Lindo Patterson [3]. While the desirable function $\rho(xyz)$ represents the distribution of atoms in the crystal unit cell, $P(uvw)$ (which mathematically represents an autocorrelation function or the convolution of the atomic structure with its centrosymmetric image) represents the distribution of all interatomic vectors. It is clear that for large structures, such as protein structures that contain thousands of atoms, the Patterson function is astronomically complex, containing millions of vectors. But it is easily calculated, and with a judicious use, it can be of a great help. The Patterson function finds the most straightforward application in the method of molecular replacement, invented by Michael Rossmann and David Blow [4]. Here, we have an approximate atomic model of our macromolecule from which we can generate all interatomic vectors. The problem of solving an unknown crystal structure is then reduced to confronting this set of vectors with the experimental Patterson function in order to find the correct rotation and translation of the model in the unit cell of the unknown structure.

The other two methods solve the phase problem by first locating in the unit cell of a small number of special atoms (special, because they must scatter X-rays in a special way), which become the starting point for deciphering the complete structural puzzle. The classic and historically first method of isomorphous replacement, developed by the pioneer of protein crystallography, Max Perutz [5], uses a very heavy, electron-rich metal atoms, which are attached to protein molecules in an isomorphous way, i.e., without altering the crystal structure. If we are lucky, the differences in the diffraction pattern of the derivative and native crystals can reveal (via a Patterson function) the locations of the heavy atoms, which are the first, very crude, approximation of the complete structure. With one heavy atom derivative, the Single Isomorphous Replacement (SIR) approach narrows the possible solutions of the phase problem but does not give a unique solution. With more derivatives, the Multiple Isomorphous Replacement method (MIR) leads to a unique solution. An interesting variant of the isomorphous replacement method has been introduced by

Dauter [6], who recommends using the simple and safe halide anions, such as Br^- or I^- , instead of the highly toxic heavy metals.

The third method is based on a somewhat similar principle but it uses, as phasing markers, atoms that do not need to be very heavy but must scatter X-rays in an anomalous way. Anomalous scattering occurs when the energy of X-ray quanta is tuned to (i.e., is in resonance with) the electronic energy levels of the scattering atom. In resonance conditions, the atomic scattering factor becomes a complex quantity, $f_j = f_o + f' + if''$, and thus introduces (through the anomalous correction if'') an extra phase shift that can be detected and used for the calculation of the unknown reflection phases. To exploit the method of anomalous scattering, we must be able to tune the wavelength of the X-ray beam, something that is possible with synchrotron radiation, and have a special atom type in our crystal structure. The normal protein atoms (C, N, O, H, and S) are not good for anomalous scattering. Therefore, a trick is usually used to introduce into the protein molecule several selenium (Se) atoms, which can be excellent anomalous scatterers of synchrotron radiation with precisely tuned λ . Typically, the experiment is conducted at several carefully adjusted wavelengths, as recommended by Wayne Hendrickson [7], which gives the method its name, Multiwavelength Anomalous Diffraction or (MAD), and allows to solve the phase problem in an algebraic way. However, with ingenuity and very accurate X-ray diffraction data, it is also possible to attempt protein structure determination using X-ray data measured in a SAD mode, at a Single wavelength, even with such weak anomalous scatterers as sulfur (in protein crystals) or phosphorus (in nucleic acids crystals) [8].

4. A digression: preparation of protein material for crystallographic studies

The trick with the Se atoms in MAD is to replace in the make-up of our protein the natural sulfur-containing amino acid methionine with its close chemical cousin containing selenium. The replacement is possible if we harness bacteria to manufacture our protein and supply them with selenomethionine (Se-Met) instead of methionine (Met). Although it sounds very bizarre, this method is a commonplace practice of genetic engineering. In fact, the majority of protein samples used nowadays for crystallographic studies are obtained not by isolation from the source organism, but recombinantly in *Escherichia coli* cells. Once we know the coding sequence of the protein of interest (this information is provided by genome sequencing projects, but it is also available from smaller-scale experiments), the corresponding DNA molecule (a clone) is synthesized (chemically or enzymatically using Polymerase Chain Reaction, or PCR) and introduced into a special circular DNA molecule called plasmid. Plasmids are autonomous fragments of the bacterial genome, capable of independent replication, and coding specialized traits. When a bacterial cell is transformed with an artificial plasmid, it can be turned into a factory, producing

predominantly the desired protein. If additionally the bacteria is forced to grow on Se-Met medium, selenium-labeled proteins will be produced. They are then purified by chromatography and they can be used for crystallization experiments. Se-Met proteins usually crystallize and behave very much like their natural variants. In particular, bacteria tolerate selenomethylated proteins quite well, although the situation is different with higher organisms.

5. Protein structure refinement and stereochemical restraints

Even if we solve the phase problem, the electron density map still has to be interpreted by an atomic model, and this model has to be refined. In the refinement, we calculate the structure factors using the Fourier transform $F_c(hkl) = \sum f_j \exp[-B_j(\sin\theta/\lambda)^2] \exp[2\pi i(hx_j + ky_j + lz_j)]$ and introduce adjustments into our model to bring the calculated values F_c to an optimal agreement with experimental measurements, F_o . Although in principle different algorithms can be used for model optimization (for instance, the least-squares method), protein crystallographers mostly employ the maximum likelihood method [9]. Quite often, the model refinement is combined with molecular dynamics simulation at elevated temperature (this approach is called "simulated annealing") to facilitate better convergence and to avoid false energy minima [10].

For each atom of the model, corrections are made to its coordinates x , y , z and to a parameter, the atomic displacement parameter or the temperature factor (B), that describes the amplitude of its vibrations in the crystal lattice. Atomic vibrations, even if we assume harmonic motion, are anisotropic, and should be described by a symmetric second-rank tensor with six parameters. In most cases, there are not enough experimental data to justify such a complicated model and atomic vibrations are treated isotropically, assuming the same displacement in all directions and a spherical approximation of the vibration ellipsoid (one B_{iso} parameter per atom).

Although it looks very straightforward, the refinement is a difficult step, mainly because of the huge number of parameters. For instance, a protein with a molecular mass of 50 kDa (average size) would consist of about 3500 non-H atoms and a simple isotropic model would require $4 \times 3500 = 14000$ parameters! Compare this with merely 8500 reflections that we would have if the resolution was poor (3 Å). Not infrequently, the number of model parameters will be close to the total number of available experimental data, making the problem barely solvable from the mathematical point of view. And, remember that in order to describe the crystal structure adequately, we also need to take care of at least some water molecules around the protein (provided, of course, that the experimental data justify such a model). To improve the situation, two approaches are possible. First, we could fix some of the model parameters or constrain them. This is, however, a dangerous trick because if a

parameter is constrained wrongly, it will never be corrected. A better solution is to supplement the refinement with extra equations, called restraints, which represent our prior knowledge about the stereochemistry of the macromolecule under refinement. We can, for instance, require that the bond lengths (or angles, or other geometrical parameters) of our model have reasonable values. A list of stereochemical standards (and their uncertainties) for the use in protein structure refinement has been compiled by Engh and Huber [11] from their analysis of the structural data contained in the Cambridge Structural Database (CSD) [12]. The use of restraints has the additional appeal because the used equations approximate geometrical distortions of protein molecules using Hooke's Law, which intuitively allows to interpret the stereochemical restraining as energy minimization.

6. Data and model resolution

The best strategy for successful refinement is, however, very simple: get more data! But how can this be achieved? Experimentally, more diffraction spots can be registered by increasing the "acceptance angle" 2θ at our detector. Through Bragg's Equation, an increase of θ_{max} is equivalent to a decrease of d_{min} , the minimum spacing of the lattice planes which still reflect the X-rays. This minimum d -value, expressed in Å, is called the resolution limit of our data. Optical considerations show that it is equivalent to the optical resolution of our model. In other words, if we collect diffraction data to 2.0 Å resolution, we can see in our electron density maps features that are more than 2 Å apart, but we will not be able to distinguish, for instance, atoms that are more closely spaced. Fortunately, we know the basic stereochemistry of our macromolecules, so it is possible to construct an atomic interpretation of the electron density map even if it does not have a true atomic resolution, but it is obvious that our main struggle should be to obtain experimental data with the highest possible resolution, because only then will we be able to see our structure atom-for-atom, refine anisotropic displacement parameters and see fine features that are not visible, or blurred by restraints, in poorly resolved maps. High-brilliance synchrotron sources of X-ray radiation are essential for a reliable measurement of the weak high-resolution data.

As a criterion for atomic resolution, 1.2 Å has been accepted [13] because 1.2 Å is the shortest covalent bond in proteins (C=O) not involving H atoms. One might think that it is a trivial thing to collect high-resolution data, a mere technicality. But this is not so because it is usually the crystal that "determines" the maximum resolution. In most cases there is no point in increasing θ_{max} , simply because there is nothing to measure beyond a certain limit. The reasons are several: the atomic scattering factors, f_j , fall-off with 2θ quite rapidly, the atomic vibrations smear out the electrons making scattering less effective. But most importantly, protein crystals have only a limited degree of crystalline order (connected with the mixed water-protein composition of

their interior) which bears directly on their ability to scatter X-rays coherently.

At very low resolution ($d_{\min} > 3.0 \text{ \AA}$) it may be only possible to trace the main chain of the protein. At 2.7 \AA , medium resolution is achieved. At this level, modeling of the solvent structure may be cautiously attempted, as the hydrogen-bonded water molecules can be already distinguished. 2.0 \AA is an accepted limit of high resolution. At 1.5 \AA one might start contemplating anisotropic refinement, and at 1.0 \AA the weakly scattering hydrogen atoms will start to be discernible, as their C–H, N–H, *etc.* distances are of this order. 0.54 \AA resolution is the current record achieved for a (small) protein structure [14].

7. Deposition and validation of macromolecular structures

Experimentally determined macromolecular structures are deposited in the Protein Data Bank (PDB) [15], which is a global archive of biostructural information freely and publicly available to the scientific community. When the PDB was created in 1971, there were merely seven protein structures in it. Today it stores more than 65 000 structures, most of them of proteins, and most of them determined by single crystal X-ray diffraction.

In assessing the quality of a protein structure [16], one should first check the resolution of the experimental data. The lower the d_{\min} value is, the better. High resolution ($d_{\min} < 2.0 \text{ \AA}$) should be always sought. The agreement with experimental data is usually measured by the crystallographic *R*-factor, defined as $R = \frac{\sum | |F_o| - |F_c| |}{\sum |F_o|}$. Well refined macromolecular structures should have $R < 0.2$. However, one should not be tempted to reduce the *R*-factor at all cost, for instance by introducing model parameters that are not justified by the information content of the data (overfitting). A validation criterion to test this is R_{free} [17], which is calculated as the *R*-factor but for a small subset of randomly selected reflections which are never used for model refinement. The R_{free} asks the question: "how well does the model predict data it has never 'seen'?" Another quality-control test looks for the distribution of main-chain torsion angles (Ramachandran plot), which are seldom used as refined parameters and are, therefore, ideal for validation. Less independent but easy to calculate are r.m.s. (root-mean-square) deviations of model parameters from the stereochemical standards used as refinement restraints. Well refined medium-to-high resolution protein models should be characterized by r.m.s. deviations values for bond distances of about $0.01\text{--}0.02 \text{ \AA}$ [18].

8. Recent advancement in macromolecular crystallography

Protein crystallography is a young science, born with the publication of the first macromolecular structures by John Kendrew (myoglobin) [19] and Max Perutz (hemoglobin) [20]. In the early nineties of the previous century, it appeared that protein crystallography had

already said its last word. However, since then an unprecedented surge of new data has been taking place, marking a rebirth and a new era in protein crystallography. Rapid advancements are seen in protein crystallization, in development of cryocrystallographic techniques (protein crystals are now routinely suspended in small nylon loops cooled to 100 K , Fig. 3), in the application of powerful synchrotron sources of X-ray radiation, in development of faster and more sensitive detectors, faster computers and better algorithms.



Figure 3. A protein crystal (measuring about $100 \mu\text{m}$ across) suspended in a tiny loop, prepared for an X-ray diffraction experiment. The loop is used to fish out the crystal from the crystallization drop, and then to place it immediately in a stream of nitrogen gas at 100 K . In this way, the water inside and around the crystal is vitrified (i.e., becomes amorphous and does not interfere with the protein diffraction). By the same trick, the crystal is protected from drying and its structure is "stabilized" because with a lowered temperature, the thermal motions of its atoms (expressed by the *B*-factors) are much reduced. Most importantly, however, the solidified water component of the crystal will drastically slow down the diffusion of free radicals, which are always created on exposure to ionizing radiation, thus improving the longevity of the crystal. *Courtesy of Dr. Zbigniew Dauter.*

There have been several factors contributing to the renaissance of protein crystallography, but as the most important, structural genomics initiatives should be mentioned. The need for a massive generation of structural information was a consequence of the success of genome sequencing projects (including the sequencing of the human genome), which have been generating astronomical volumes of genetic data with almost no obvious interpretation. The aim of structural genomics is then to determine in a high-throughput automated approach the three-dimensional structure of all the proteins encoded in the genome of a given organism, in order to understand their function. Contrary to classical biochemistry, the structure is studied before biochemical characterization of the target. A number of human pathogens are studied in this way, in search of new therapeutic agents.

Protein crystallography has also re-defined modern approach to drug discovery by providing precise molecular targets for accelerated, structure-guided design of new pharmaceuticals. The best known example is illustrated by the structure of HIV protease, which immediately after its elucidation [21] has become the most studied target for drug discovery. As a result, the HIV infection has been converted, within less than a decade, from a global health threat, and for an individual patient – an irrevocable death sentence, into a disease that can be treated. Today, there are eleven HIV protease inhibitors approved for the treatment of HIV infection [22] and other proteins of the virus are being targeted as well.

Methodological advancements stimulated by structural genomics projects are also benefiting other areas of protein crystallography. For example, with improved experimental tools, there is a steady increase of the number of structures determined at atomic resolution. First atomic-resolution protein structures appeared in the PDB in mid 1980's. Today, there are over 1 000 structures in this category. These accurate data provide us with an entirely new chemical perspective on the structure and functioning of the molecules of life.

In addition to looking into macromolecular structures with a more penetrating eye, protein crystallography is also attacking problems of ever increasing complexity. Viruses are among the largest molecular systems whose atomic details have been deciphered by protein crystallography. The first crystal structures of viruses (both helical and icosahedral) were solved in 1978 [23, 24], and even then the resolution was better than 3 Å. Currently, there is a large number of virus structures in the PDB. Recently, the biggest triumph of macromolecular crystallography is the mapping of the atomic structure of the ribosomal subunits (2.4–3.0 Å) [25–27] and of the entire ribosome (2.8 Å) [28], in complex with mRNA and tRNA molecules. The scale of this achievement is illustrated by the mass of this huge macromolecular machine, used by all living cells to synthesize proteins, which is measured in megadaltons, corresponding to about two hundred thousand non-H atoms. The ribosome is composed of both proteins and ribonucleic acid molecules (Fig. 4). One of the most unexpected secrets revealed by the structure of the ribosome was that its catalytic activity is associated with the ribonucleic acid component, and not with the proteins.

9. Conclusions

Crystallography, through the study of this special solid state of matter – crystalline protein, was historically the first method to reveal for us, almost 50 years ago, the secrets of protein structure. Today, we have accumulated in the PDB an enormous amount of structural information about proteins. Crystallography is now assisted in this effort by other methods: nuclear magnetic resonance (NMR) spectroscopy, electron microscopy, and bioinformatics. But crystallography still remains the

main source of information about the structure of proteins, especially in the context of structural genomics. Numerous breathtaking examples illustrate how, through unraveling macromolecular structures with increasing accuracy and at increasing level of complexity, the discipline of protein crystallography helps us to better understand the secrets of biological macromolecules, and in consequence – the secret of life.

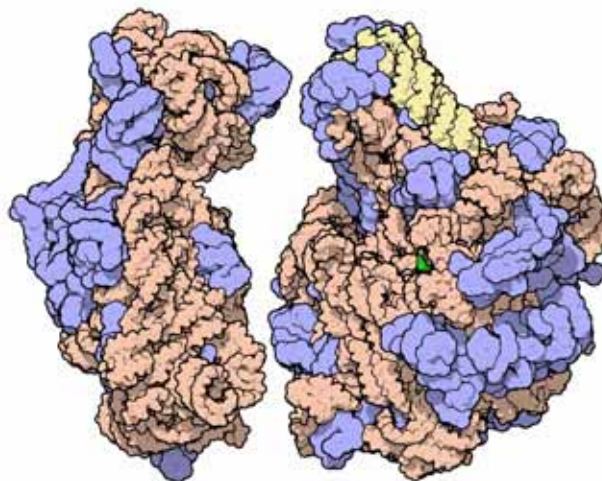


Figure 4. Crystallographic studies of the ribosome have revealed the position of each of the 200 000 atoms in the three-dimensional structure of this huge molecular factory, responsible for the synthesis of all proteins in a living cell according to the genetic information. The ribosome is composed of two subunits, here separated in a computer manipulation to reveal the complementary surfaces of the interface, where the biochemical synthesis of peptide bonds takes place. Both subunits are composed of proteins (blue) and of ribonucleic acid molecules (orange and yellow). It was a total surprise, when crystal structures clearly showed that the catalytic center (green) of the ribosome is not associated with the proteins, but that it resides within the nucleic acid component. *Courtesy of Dr. David Goodsell.*

References

- [1] B. Rupp, *Biomolecular Crystallography*, Garland Science, New York 2009.
- [2] M. Jaskolski, *Introduction to protein crystallography for physicists*, www.man.poznan.pl/CBB/PRESENTATIONS/Jaskolski-APP.pdf, 2009.
- [3] A.L. Patterson, *Z. Kristallogr. A* **90** (1935) 517.
- [4] M.G. Rossmann, D.M. Blow, *Acta Crystallogr.* **15** (1962) 24.
- [5] D.W. Green, V.M. Ingram, M.F. Perutz, *Proc. Roy. Soc. A* **225** (1954) 287.
- [6] Z. Dauter, M. Dauter, K.R. Rajashankar, *Acta Crystallogr.* **D56** (2000) 232.
- [7] W.A. Hendrickson, *Science* **254** (1991) 51.
- [8] Z. Dauter, M. Dauter, E.J. Dodson, *Acta Crystallogr.* **D58** (2002) 494.
- [9] G.N. Murshudov, A.A. Vagin, E.J. Dodson, *Acta Crystallogr.* **D53** (1997) 240.

- [10] A.T. Brünger, J. Kuriyan, M. Karplus, *Science* **235** (1987) 458.
- [11] R. Engh, R. Huber, *Acta Crystallogr.* **A47** (1991) 392.
- [12] F.H. Allen, *Acta Crystallogr.* **B58** (2002) 380.
- [13] G.M. Sheldrick, *Acta Crystallogr.* **D46** (1990) 467.
- [14] C. Jelsch, M.M. Teeter, V. Lamzin, V. Pichon-Pesme, R.H. Blessing, C. Lecomte, *Proc. Natl. Acad. Sci. USA* **97** (2000) 3171.
- [15] H.M. Berman, J. Westbrook, Z. Feng, G. Gilliland, T.N. Bhat, H. Weissig, I.N. Shindyalov, P.E. Bourne, *Nucleic Acids Res.* **28** (2000) 235.
- [16] A. Wlodawer, W. Minor, Z. Dauter, M. Jaskolski, *FEBS J.* **275** (2008) 1.
- [17] A.T. Brunger, *Nature* **355** (1992) 472.
- [18] M. Jaskolski, M. Gilski, Z. Dauter, A. Wlodawer, *Acta Crystallogr.* **D63** (2007) 611.
- [19] J.C. Kendrew, G. Bodo, H.M. Dintzis, R.G. Parrish, H. Wyckoff, D.C. Phillips, *Nature* **181** (1958) 662.
- [20] M.F. Perutz, M.G. Rossmann, A.F. Cullis, H. Muirhead, G. Will, A.C.T. North, *Nature* **185** (1960) 416.
- [21] A. Wlodawer, M. Miller, M. Jaskolski, B.K. Sathyanarayana, E. Baldwin, I.T. Weber, L.M. Selk, L. Clawson, J. Schneider, S.B.H. Kent, *Science* **245** (1989) 616.
- [22] M. Jaskolski, *Postepy Biochemii* **55** (2009) 15.
- [23] A.C. Bloomer, J.A. Champness, G. Bricogne, R. Staden, A. Klug, *Nature* **276** (1978) 362.
- [24] S.C. Harrison, A.J. Olson, C.E. Schutt, F.K. Winkler, G. Bricogne, *Nature* **276** (1978) 368.
- [25] F. Schluentzen, A. Tocilj, R. Zarivach, J. Harms, M. Gluehmann, D. Janell, A. Bashan, H. Bartels, I. Agmon, F. Franceschi, A. Yonath, *Cell* **102** (2000) 615.
- [26] B.T. Wimberly, D.E. Broderson, W.M. Clemons, A.P. Carter, R.J. Morgan-Warren, C. Vonnrhein, T. Hartsch, V. Ramakrishnan, *Nature* **407** (2000) 327.
- [27] N. Ban, P. Nissen, J. Hansen, P.B. Moore, T.A. Steitz, *Science* **289** (2000) 905.
- [28] M. Selmer, C.M. Dunham, F.V. Murphy, A. Weixlbaumer, S. Petry, A.C. Kelley, J.R. Weir, V. Ramakrishnan, *Science* **313** (2006) 1935.

ADVANCED METAHEURISTIC ALGORITHMS FOR LASER OPTIMIZATION

Hiromitsu Tomizawa *

Japan Synchrotron Radiation Research Institute (JASRI), XFEL Joint Project/SPring8,
1-1-1 Kouto, Sayo-cho, Sayo-gun, Hyogo, Japan

A laser is one of the most important experimental tools. In synchrotron radiation field, lasers are widely used for experiments with Pump-Probe techniques. Especially for X-ray-FELs, a laser has important roles as a seed light source or photo-cathode-illuminating light source to generate a high brightness electron bunch. The controls of laser pulse characteristics are required for many kinds of experiments. However, the laser should be tuned and customized for each requirement by laser experts. The automatic tuning of laser is required to realize with some sophisticated algorithms. The metaheuristic algorithm is one of the useful candidates to find one of the best solutions as acceptable as possible. The metaheuristic laser tuning system is expected to save our human resources and time for the laser preparations. I have shown successful results on a metaheuristic algorithm based on a genetic algorithm to optimize spatial (transverse) laser profiles and a hill climbing method extended with a fuzzy set theory to choose one of the best laser alignments automatically for each experimental requirement.

Keywords: XFEL, ERL, synchrotron radiation, photo-cathode, EO-sampling, genetic algorithms, metaheuristics, laser shaping, laser alignment

**) e-mail: hiro@spring8.or.jp*

1. Introduction

A laser pulse is characterized in its pulse energy, pulse chirp, spectral distributions (both of intensity and phase), 3D-profile (both of spatial and temporal), wavefront distortion, M^2 -value, pointing stability, timing jitter, etc. When we use a laser on our own purposes, we have to optimize some of these laser characteristics at the same time. However, these laser pulse characteristics are not perfectly independent of each other. In this case, it is almost impossible to determine the best solution uniquely by mathematical formulae. The metaheuristic algorithm is powerful methodology to find some of the acceptable and the most preferable solutions with searching better parameters. Many kinds of metaheuristic algorithms have been proposed and applied widely. I utilized a genetic algorithm [1] and a simulated annealing method [2] to optimize 3D laser pulse shape, and a hill climbing method with a fuzzy set theory [3] to align a laser to reliable path for each experiment at advanced photoinjector test facility in SPring-8.

Applying any kind of metaheuristic algorithm, a great number of system's parameter must be introduced. Making the probability higher to find some solutions as good as possible, it is necessary to increase freedom of its searching space. For instance, optimizing laser shape, I introduced adaptive optics to increase the parameters of laser system as shown in Fig. 1 (Deformable Mirror (DM) [1] for spatial (transverse) shaping & glass (fused silica)- plate-based Spatial Light Modulator (SLM) [4] for temporal (longitudinal) shaping).

In this paper, I review mainly adaptive optical system developed with metaheuristic algorithms for controlling 3D laser pulse shape and laser alignment. I completed system to manipulate 3D laser pulse shape as an illuminating light source for a photo-cathode RF gun [5]. In low-emittance electron beam generation, the experimental requirements for laser spot size on the

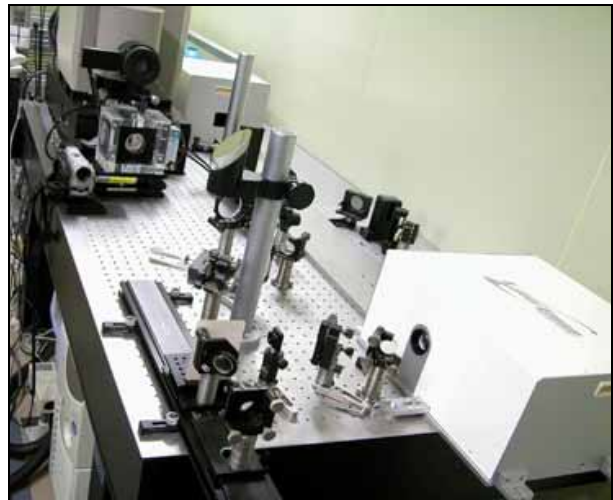


Figure 1. Adaptive-optic complex [4] for shaping both spatial and temporal laser profiles in Photo-cathode test facility at SPring-8 (Spatial shaping: DM as an adaptive actuator & UV-CCD camera (laser profiler) as a monitor; Temporal shaping: SLM with a grating pair as an adaptive actuator & Streak Camera (Fesca-200; Hamamatsu Photonics K.K.) as a monitor).

cathode should be optimized for all bunch charge densities. Therefore, I decided to develop an adaptive shaping system in spatial shaping. Note that the latest 3D UV-laser pulse shaping system was completed with a DM (transverse: 2D) assisted by a genetic algorithm and a chirped pulse stacker (longitudinal: 1D) [5]. The shape and pulse duration of the original micro chirped pulse of this pulse stacker is precisely optimized with DAZZLER (acousto-optic programmable dispersive filter (AOPDF)) in our present 3D pulse shaping system. On the other hand, a simulated annealing method was developed to optimize square laser pulses with the glass (fused silica)-

plate-based SLM [5]. However, our development of this SLM for adaptive square shaping (up to 20 ps) in high energy (\sim mJ) UV-pulse was discontinued in 2005. It could be operated as a square pulse shaper even for the cw-mode. The operation with high repetition rate is attractive for X-ray Free Electron Laser (XFEL) [6-8] and Energy Recovery Linac (ERL) [9]. However, long-term drifts and uncertain individual plate-twisting motions were not negligible to keep the phase masks of the intended square pulses.

2. Developments of genetic Algorithms for Deformable Mirror

The laser spatial profile was adaptively optimized with a genetic algorithm for a DM that consists of an aluminium-coated, multilayer silicon nitride membrane and 59 small mirror actuators behind the reflective membrane with a center-to-center distance of 1.75 mm between the actuators (left in Fig. 2). The reflective membrane is protected with MgF₂ coating to maintain reflectivity at about 80% in the UV region. Adjusting voltages between the control electrodes on the boundary actuators results in fine adjustment of each mirror actuator; the adjustable region of the control voltages is between 0 and 250 V in steps of 1 V, making it possible to shape the arbitrary spatial profiles for a total of 250⁵⁹ ($\sim 10^{141}$) deforming possibilities. However, since such high adjustability makes manual as well as simple algorithm adjustment impossible, this spatial shaping method with adaptive optics needs a sophisticated algorithm. Under the collaboration with F. Matsui (Industrial Technology Centre of Fukui Prefecture), we developed software based on a genetic algorithm to adaptively optimize DM deformation.

The set of the voltages of all DM-electrodes is treated as chromosomes in this software. A closed loop system is essential for a DM to adaptively optimize the laser's spatial profile. I used a PC to control the electrode voltage of the DM and to measure the spatial profile with a laser profile monitor (LBA300-PC, Spiricon Inc.).

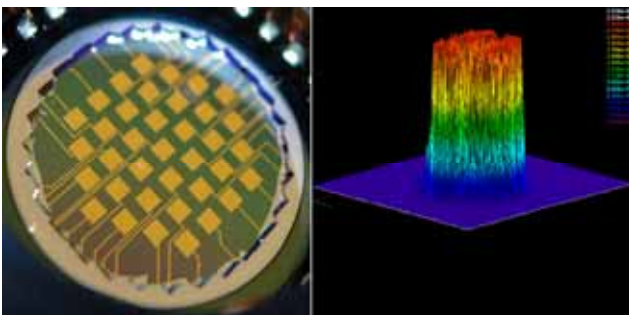


Figure 2. Result of spatial profile optimized to flattop (right) with a 59-ch DM: Mirror actuators behind the reflective membrane of a 37-ch type DM is shown in left as an example. Maximizing the fitting function consisted of laser profiling data analyzed with LBA300-PC, one of the best voltage sets applying to DM-actuators are searched by means of a metaheuristic method based on a genetic algorithm.

Laser light is reflected with deformation by the DM and monitored with a laser profile monitor, whose analyzing program can provide many parameters to evaluate the beam profile characteristics. I chose useful parameters to evaluate the flattop profiles and made a fitting function for the developed a genetic algorithm to optimize the profile toward an ideal flattop. The fitting function is a linear combination of flattop shaping parameters with certain optimal weights for fast convergence (see ref [2] for details). The value of this fitting function is returned as feedback to control the deformable mirror with the genetic algorithm. As a result, the laser profile on the cathode surface was spatially shaped as a quasi-flattop profile (right in Fig. 2). The laser spatial profile was remarkably improved by this shaping technique.

3.1. Square Temporal Shaping (Chirped UV Pulse Stacking)

Low-emittance generation experiments require keeping cathode laser spot sizes and bunch charge densities with varying longitudinal (temporal) square bunch lengths. Therefore, I developed several pulse stacking systems to provide several different total bunch lengths of stacked square pulses. To avoid the interference caused by stacking, orthogonally polarized chirped pulses are alternatively stacked with an optical delay. The optical delay period should be 1.2~1.3 times longer than the micro chirped Gaussian pulse duration to generate a precisely homogeneous electron bunch at the cathode. This method, which introduces additional chirp to avoid interference is referred to as "chirped pulse stacking." In 2007, we installed a new UV pulse stacking system [5] that consisted of four birefringent Alpha-BBO crystal rods (Fig.3 (B)) to fix the optical delays between neighboring micro chirped pulses in the previously developed mechanical pulse stacker (Fig.3 (A)) [2]. The angle of rotation of each crystal axis against incident polarization is 45° to make twin pulses. Then a pulse train with equivalent intervals is connected smoothly with pulse stretching controlled in chirping. These Alpha-BBO crystal rods can be used as a pulse stacker in the super broadband wavelength region (189–3500 nm).

3.2. Homogeneous connection at the cathode with adaptive AO-modulator

To generate a long square pulse without any timing gap or overlap, optical delays in each birefringent crystal, which are $\sim 20\%$ shorter than the micro Gaussian pulse duration, are applied to generate a precisely homogeneous electron bunch at the cathode. Micro pulse lengths T [fs] at the cathode stretched by the dispersion of the transparent materials for UV-laser in pulse stackers and transportation are estimated by the following formula, where no nonlinear process is assumed to occur in the optical elements:

$$T = t_0 \sqrt{1 + \left(4 \cdot \ln 2 \cdot GDD / t_0^2\right)^2} \text{ [fs]},$$

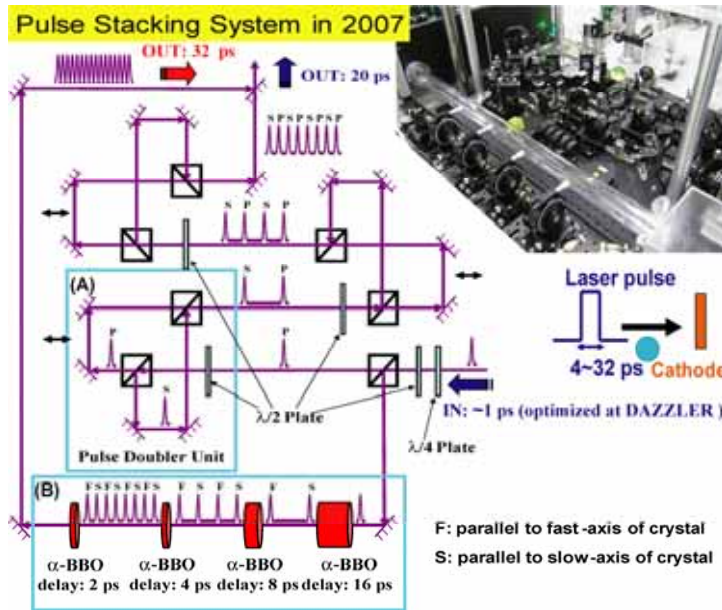


Figure 3. Drawing of UV-laser pulse stacking system [10]: (A) mechanical pulse stacker; (B) pulse stacking rods made of birefringent Alpha-BBO crystals. Initial UV-laser pulse interval is set to 2.5 ps for generating 5-, 10-, or 20-ps combined macro square pulses for three stages (pairs of polarizing UV-laser beam splitter cubes) of mechanical pulse stacker, while pulse stacking rods provide 4-, 8-, 16-, or 32-ps square UV-laser pulses.

where T and t_0 are the chirped pulse width and the pulse width of a Fourier-transform limited pulse, respectively. The UV-laser pulse intervals, which are usually set to 2.5 ps for the mechanical pulse stacker, were designed for a delay of 2.0 ps for the pulse stacking rods. To obtain smoothly squared combined macro pulses, micro pulse durations of 3.0 ± 0.1 ps for the stacker and 2.5 ± 0.1 ps for the birefringent rods should be prepared. We optimized a group delay dispersion (GDD) to roughly stretch the micro pulses with DAZZLER (HR-800, FASTLITE) and then additionally micro pulse shape for fine tuning with the depth and position of the dip in the spectra and the higher order dispersions up to the 7th.

I checked the electron bunch's homogeneity by measuring the electron energy spectra. The initial RF phase of the electron bunch was set near the zero-cross region to give quasi-linear energy chirp to the bunch generated at the cathode. The electron beam's energy is measured on the basis of the beam positions on a fluorescence profile monitor after they pass through a bending magnet downstream of the RF gun cavity. After introducing a second dispersion with DAZZLER, the micro chirped pulse duration is optimized so that the electron beam profile is homogeneous (lower right in Fig. 4) at the dispersion section [5].

By precisely optimizing the laser pulse's 3D shape, I strive to generate a beam with as high a brightness and as low an emittance as possible. Farther perfect homogeneity of temporal stacking is planning with a feedback routine between an AOPDF UV-pulse real-time measurement using a UV-DAZZLER [spectral phase interferometry [11] for THG (264 nm)] and a high-resolution DAZZLER (HR-800, FASTLITE) as a micro laser pulse adaptive shaper in IR. Directly monitoring a generated electron bunch structure with an electro-optic sampling (EO sampling) [12-13] in real time, it can be possible to optimized pulse stacking perfectly at the electron bunch generation with a metaheuristic feedback routine.

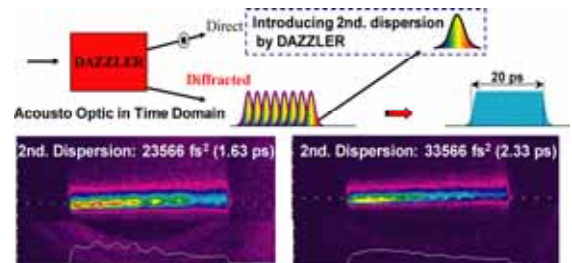


Figure 4. Generating a homogeneous electron bunch: Chirped pulse stacking made the connections between neighboring micro pulses smooth.

4. Auto-aligner with Fuzzy set theory

I have developed an auto-aligner for a large laser system together with Photo-Physics Laboratory Inc. since 2007. It is named Advanced Tactical Aligner (ATA), based on fuzzy set theory to find a better solution smoothly. It is principally one kind of hill climbing method. The fuzzy sets give certain step sizes according to their membership functions. The membership function is defined for each movement set. There are four movement sets classified by the achievement levels evaluated with a fitting function. They are a super fine-tuning set, a fine-tuning set, a rough-tuning set, and an out-of-target set, in the order of user-defined step size of movements to search. The membership functions can realize smooth movements to reach the most probable area implies the required solutions with a smoothly connected step size on the ambiguous "Fussy" boundaries between the classified sets.

I introduced several pairs of wedge plates (0.1 or 0.5 degrees of the wedge angles) mounted in remote-controlled rotary stages on the optical path of laser system. In the simple case, an analog signal of power meters or photodiodes are utilized as a fitting function to maximize with ATA system. To generate and keep laser profile, the fitting function is a linear combination of spatial laser shape parameters with certain optimal

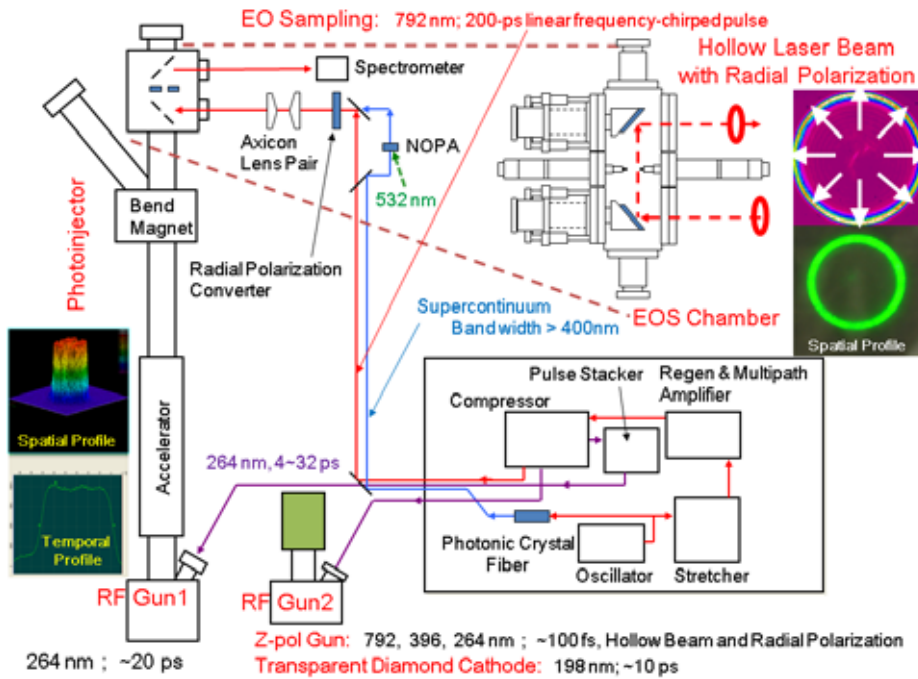


Figure 5. The present laser light distributions with swiching ATA system in the accelerator shird room at advanced photoinjector test facility in SPring-8 (Photo-cathode illumination at the test photoinjector: 3D- cylindrically shaped 4-32 ps pulse with DM and pulse stacker @264 nm; Photo-cathode illumination at the RF gun 2: radial or athmuthal polarization @264, 396, 792 nm; Probe laser for 3D-EOS: linear frequency-chirped 200-ps pulse and radial polarization @ 792 nm).

weights. As the target laser profiles, flattop profile for photo-cathode illumination, and hollow beam profile of a probe laser for single-shot 3D EO-sampling (EOS) monitor [12-13]. The present laser distributions are shown in Fig. 5. ATA has been successful to tune the laser automatically to each experimental station downstream.

5. Summary

The metaheuristic algorithm is useful to find one of the best solutions as acceptable as possible on each occasion. Tuning laser is one of the effective cases to apply such a sophisticated algorithm. The metaheuristic laser tuning system is expected to save our human resources and time for the laser maintenance and preparation in user's experiments. I have shown successful results on a genetic algorithm to optimize spatial (transverse) laser profiles and a hill climbing method extended with a fuzzy set theory to choose one of the best laser alignments automatically for each requirement at the experimental points downstream.

References

[1] H. Tomizawa, H. Dewa, H. Hanaki, "Development of automatically optimizing system of both spatial and temporal beam shaping for UV-laser pulse," Proc. of LO'03, St. Petersburg, Russia, 30 June -04 July 2003, (2004) 47-55.
 [2] H. Tomizawa, H. Dewa, H. Hanaki, F. Matsui, "Development of yearlong maintenance-free terawatt Ti:Sa laser system with 3-D UV-pulse shaping system for THG," *Russ. J. Quant. Electron.* (2007) 697-705.
 [3] H. Tomizawa, "Advanced laser pulse shaping," Plenary Talk at ICFA Advanced Accelerator and Beam Dynamics Workshop, HBEB'09, Maui, Hawaii, 17 November 2009.
 [4] H. Tomizawa, T. Asaka, H. Dewa, H. Hanaki, T.

Kobayashi, A. Mizuno, S. Suzuki, T. Taniuchi, K. Yanagida, F. Matsui, "Development of adaptive feedback control system of both spatial and temporal beam shaping for UV-Laser light source for RF gun," Proc. of LINAC'04, Luebeck, Germany, 16-20 August 2004, (2004) 207-209.
 [5] H. Tomizawa, "Adaptive 3-D UV-laser pulse shaping system to minimize emittance for photo-cathode RF gun," Invited talk at FEL'07, Novosibirsk, Russia, 26-31 August 2007; *Proc. of FEL'07*, (2008) 298-305.
 [6] *TESLA Technical Design Report, PART V, The X-Ray Free Electron Laser*, ed. G. Materlik, Th. Tschentscher, March 2001.
 [7] *Linac Coherent Light Source (LCLS) Conceptual Design Report*, SLAC-R-593, April 2002.
 [8] *SCSS X-FEL Conceptual Design Report*, RIKEN, May 2005.
 [9] I. Ben-Zvi, I.V. Bazarov, "Summary, Working Group 1: Electron guns and injector designs," Workshop on ERL 2005, Newport News, VA, USA, March 2005, *Nucl. Instrum. Meth. Phys. Res. A* **557**, (2006) 337-344.
 [10] H. Tomizawa, "Review of advanced laser technologies for photo-cathode high-brightness guns," Invited talk at LINAC'08, Victoria, British Columbia, Canada, 29 September - 3 October 2008; Proc. of LINAC'08, (2009) 1090-1094.
 [11] E. Cormier, L. Corner, E.M. Kosik, I.A. Walmsley, A.S. Wyatt, "Spectral phase interferometry for complete reconstruction of attosecond pulses," *Laser Phys.* **15**, No. 6, (2005) 1-7.
 [12] H. Tomizawa, H. Hanaki, and T. Ishikawa, "Non-destructive single-shot 3-D electron bunch monitor with femtosecond-timing all-optical system for pump &probe experiments," Proc. of FEL'07, Novosibirsk, Russia, 26-31 August 2007, (2008) 472-475.
 [13] H. Tomizawa, A. Maekawa, M. Uesaka, "Novel single-shot EO-based 3D bunch charge distribution monitor with femtosecond resolution," ICFA Advanced Accelerator and Beam Dynamics Workshop, HBEB'09, Maui, Hawaii, 18 November 2009.



(photo M. Mlekicki)

Dr. Zbigniew Dauter receives the highest science award from the Polish Academy of Sciences

On March 9, 2010, Dr. Zbigniew Dauter, a Principal Investigator working at the most powerful synchrotron source in the United States (Advanced Photon Source, APS), received from Prof. Michał Kleiber, the President of the Polish Academy of Sciences, the Nicolaus Copernicus Medal, which is the highest distinction awarded by the Polish Academy of Sciences. The ceremony took place in the Staszic Palace in Warsaw. The award recognizes Dr. Dauter's contribution to the development of protein crystallographic methodology involving synchrotron radiation, in particular in the areas of phasing methods and macromolecular structure at ultimate resolution [1]. The name of Dr. Dauter is already permanently associated with the technique of quick halide soaks [2] ("dauterization" of protein crystals), with the exploitation of weak anomalous signal [3] (for example, of phosphorus in nucleic acid structures), and with the use of SAD (Single-wavelength Anomalous Diffraction) [4] and RIP (Radiation-damage-Induced Phasing) [5] for macromolecular phasing. Dr. Dauter is an expert experimenter, widely known for his skills in getting the best possible diffraction data from macromolecular crystals. A graduate of the Gdansk University of Technology, he obtained his PhD degree for crystallographic work on small-molecule drugs (with Prof. Zofia Kosturkiewicz) and later his habilitation (DSc) for work in macromolecular crystallography (A. Mickiewicz University, Poznan). He spent a number of years at several synchrotron centers (EMBL c/o DESY, Hamburg; NSLS, Brookhaven; APS, Argonne) conducting structural biological research and helping external users of macromolecular crystallography beamlines. The stations that he has supervised are among the most successful protein crystallography beamlines. Dr. Dauter is a Principal Investigator in the Macromolecular Crystallography Laboratory of the National Cancer Institute at Frederick, and facilitator for

the National Institutes of Health beamline operating at the APS synchrotron in Argonne (Argonne National Laboratory). Dr. Zbigniew Dauter, or just Zbyszek to very many of us, has numerous collaborations with colleagues in Poland, mostly in the area of synchrotron macromolecular crystallography. He is famous for his commitment to teaching and for his didactic talents. He has taught at a number of schools, workshops and courses in Poland, including those organized by our Society. Currently, Dr. Dauter serves as the Editor of *Acta Crystallographica Section D* (Biological Crystallography). As a community, we are very proud of his achievements and distinction, and express our sincere congratulations.

References

- [1] J. Wang, M. Dauter, R. Alkire, A. Joachimiak, Z. Dauter, "Triclinic lysozyme at 0.65 Å resolution", *Acta Crystallogr. D***63** (2007) 1254–1268.
- [2] Z. Dauter, M. Dauter, K.R. Rajashankar, "Novel approach to phasing proteins: derivatization by short cryo-soaking with halides", *Acta Crystallogr. D***56** (2000) 232–237.
- [3] J. Wang, M. Dauter, Z. Dauter, "What can be done with a good crystal and an accurate beamline?", *Acta Crystallogr. D***62** (2006) 1475–1483.
- [4] Z. Dauter, M. Dauter, E.J. Dodson, "Jolly SAD", *Acta Crystallogr. D***58** (2002) 494–506.
- [5] S. Banumathi, P.H. Zwart, U.A. Ramagopal, M. Dauter, Z. Dauter, "Structural effects of radiation damage and its potential for phasing", *Acta Crystallogr. D***60** (2004) 1085–1093.

Mariusz Jaskolski
Department of Crystallography, Faculty of Chemistry,
A. Mickiewicz University
Poznan
mariuszj@amu.edu.pl

THE JUBILEE OF OUR CONFERENCES

Time is running quickly. This year we participate at the 10th International School and Symposium on Synchrotron Radiation in Natural Science thus we can celebrate the jubilee of our international synchrotron conferences in Poland organised by the Polish Synchrotron Radiation Society (PSRS) in co-operation with Polish universities and scientific institutions.

The PSRS was founded in May 1991 and as early as in May next year the first international meeting was organised because one of the main goals was and still is to propagate knowledge on synchrotron radiation and the newest results obtained by means of it by members of the Society and researches in all over the world. The other our aims are: an exchange and dissemination of information on measurements capabilities and current status of synchrotron beam lines over the world, building links and bridges between Polish scientific institutions and synchrotron facilities abroad.

In order to integrate the scientists working using synchrotron radiation in various fields of science, from physics and chemistry to biology and medicine, the members of our Society decided to meet every year. The PSRS organises the *International School and Symposium on Synchrotron Radiation in Natural Science (ISSRNS)* in even-numbered years and *National Symposium of Synchrotron Radiation Users (Krajowe Sympozjum Użytkowników Promieniowania Synchrotronowego – KSUPS)* in odd-numbered years.

A compact characterisation of all conferences is compiled in the Table in the next page. About 80 – 120 participants attended each of them. The programme of each conference contains 20 – 30 lectures, 10 – 20 oral presentations and 40 – 75 posters.



Figure 1. The 1st ISSRNS (1992) – a chat between lectures. In front from the left: I. Sosnowska, K. Jabłońska, B. Orłowski, E. Sobczak, J. Auleytner (co-chairman of the conference), G. Margaritondo (Lausanne) and T. Wroblewski (DESY).

The first ISSRNS was held in 1992 at Ustroń-Jaszowiec at the Gwarek hotel. This place, located in a picturesque part of the Beskidy mountains, was well known as a place very suitable for conferences of this number of participants, so we met there for the whole decade till 2002 (the first six conferences). The conferences were organised alternately by the PSRS scientific communities of Warsaw and Cracow under the direction of the president of the Society, Prof. Andrzej Kisiel, and vice-president, Prof. Julian Auleytner. Next two conferences (the 7th and 8th ISSRNS) were transferred to Zakopane to comfortable "Geovita Center". The 7th one was organised by colleagues of



Figure 2. The 1st ISSRNS (1992) – all participants gathered in front of the Gwarek at Ustroń-Jaszowiec.

TABLE - International ISSRNS conferences organised by the Polish Synchrotron Radiation Society¹

<i>Number of conference</i>	<i>Location and date</i>	<i>Chairpersons</i>	<i>Co-organizer</i>	<i>Proceedings</i>	<i>Editors</i>
1	Ustroń-Jaszowiec 13–21 May, 1992	J. Auleytner A. Kisiel	Institute of Physics of the PAS, Warsaw	Acta Physica Polonica A 82 (1992) Nos. 1 and 2	K. Jabłońska G. Kowalski
2	Ustroń-Jaszowiec 18–26 May, 1994	J. Auleytner A. Kisiel	Institute of Physics of the PAS, Warsaw	Acta Physica Polonica A 86 (1994) Nos. 4 and 5	K. Jabłońska R. Iwanowski
3	Ustroń-Jaszowiec 31 May – 8 June, 1996	J. Auleytner A. Kisiel	Jagellonian University, Cracow	Acta Physica Polonica A 91 (1997) Nos. 4 and 5	J. Konior
4	Ustroń-Jaszowiec 15–20 June, 1998	J. Auleytner (Honorary) A. Kisiel K. Jabłońska	Institute of Physics of the PAS, Warsaw	J. Alloys and Compounds 286 (1999) No 1-2	W. Paszkowicz E. Sobczak
5	Ustroń-Jaszowiec 12–17 June, 2000	J. Auleytner (Honorary) A. Kisiel	Jagellonian University, Cracow	J. Alloys and Compounds 328 (2001) No 1-2	Cz. Kapusta W.M. Kwiatek J. Konior M. Stankiewicz
6	Ustroń-Jaszowiec 17–22 June, 2002	J. Auleytner (Honorary) B. Orłowski K. Jabłońska	Institute of Physics of the PAS, Warsaw	J. Alloys and Compounds 362 (2004) No 1-2	W. Paszkowicz J. Gronkowski B. J. Kowalski A. Burian
7	Zakopane 8–13 June, 2004	J. Auleytner (Honorary) A. Burian	University of Silesia, Katowice	J. Alloys and Compounds 401 (2005) No 1-2	W. Paszkowicz B.J. Kowalski E.A. Görllich Z. Kaszukur
8	Zakopane 12–17 June, 2006	M. Szymoński	Jagellonian University, Cracow	Synchrotron Radiation in Natural Science 5 (2006) No 3	W. Paszkowicz
9	Ameliówka (Mąchoćcie Kapitulne) 15–20 June, 2008	B. Kowalski	Institute of Physics of the PAS, Warsaw	Radiation Physics and Chemistry 78 (2009) Suppl. 10	W. Paszkowicz J.B. Kowalski E.A. Görllich
10	Szklarska Poręba 6–11 June, 2010	M. Kozak	A. Mickiewicz University, Poznań	Radiation Physics and Chemistry (agreed)	M. Kozak, P. Piszora, Z. Kaszukur, W. Paszkowicz



Figure 3. The 4th ISSRNS (1998) - organizers and foreign participants after lectures. Sitting from the left J. Bąk-Misiuk and K. Jabłońska (chairperson); standing from the left: D. Nagy (Hungary), J. Auleytner (honorary chairperson), L. Datsenko (Ukraine), M. Lefeld-Sosnowska, behind her J. Grochowski, A. Kisiel (chairperson), D. Żymierska and B.V. Robouch (Italy).

Katowice and the 8th one by colleagues of Cracow. The 9th conference was located at Małocice Kapitulne near Kielce at the Ameliówka hotel at the Holy Cross Mountains. The present, jubilee 10th international conference takes part at Szklarska Poręba at the LAS Piechowice hotel in the Karkonosze mountains. All our meetings were located in selected interesting picturesque areas of Polish mountains. The participants had opportunity to come to the Beskidy district (conferences at Ustron-Jaszowiec), to the highest in Poland mountains, of Alpine character, the Tatry (conferences at Zakopane), and the oldest one the Holy Cross (conference at Ameliówka). This year during the 10th one we will hike at the Karkonosze.

After taking a breath of fresh air and nice impressions from the view of mountains we were ready to participate actively in interesting lectures, panel discussions and posters sessions during the conferences.

The tradition of these meetings is that poster sessions are organised in the evenings (beer and juice is usually served) what stimulate the discussion which is continued far into the night. Many friendships and collaborations were established during these sessions.

The invited lectures were delivered by well known scientists from many countries all over the world. Their names and lecture presentations remain deep in our memory. This way we have got very good friends. With company of them an interesting and effective scientific co-operation leads to valuable results and common publications. Due to them Polish scientists have got possibility to create common research with applications

of modern experimental facilities. The scientific community formed during these conferences reach the maturity and finally was able to formulate the project for construction of a Polish synchrotron. The project was approved in April 2010 and is under construction in new campus of the Jagellonian University in Cracow.

The proceedings of three first schools were published in *Acta Physica Polonica A*, next four, from the 4th one held in 1998 till the 7th one at Zakopane in 2004, in *Journal of Alloys and Compounds*. Since the 9th ISSRNS in 2008 we collaborate with *Radiation Physics and Chemistry*.

Since 2002 the Bulletin of the PSRS entitled like our international conferences "*Synchrotron Radiation in Natural Science*" has been published. For every conference the Editor, Wojciech Paszkowicz, prepares an issue with programme and abstracts of invited lectures, oral presentations and posters. Also, each issue contains interesting papers and information.

We wish all participants of the jubilee conference to have a good time at Szklarska Poręba and to enjoy interesting lectures, fruitful discussions during panels and poster sessions as well as to find proper solutions of their actual scientific problems and to create new ideas for future scientific research.

Danuta Żymierska
Secretary of the PSRS since 2002

Bronisław Orłowski
President of the PSRS in 1999-2005

NEWS FROM THE POLISH SYNCHROTRON RADIATION SOCIETY

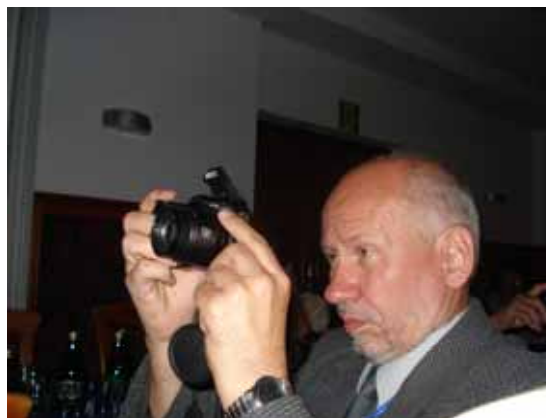
The 8th National Symposium of Synchrotron Radiation Users (8th KSUPS) was held at Podlesice on 24th – 26th September 2009. It was organised by the Polish Synchrotron Radiation Society in co-operation with the University of Silesia.

The Symposium gathered 74 participants, among them many students and young scientists. The programme contained 10 plenary lectures, 7 oral contributions, and 42 posters. The meeting was dedicated to young people, that is why the lectures were delivered in Polish, except two ones by lecturers affiliated in the USA, Tomasz Durakiewicz and Lee Chow. During the lectures and oral presentations the room was full, alike during poster sessions the hall of the hotel.

A special panel session concerned the project of a Polish synchrotron and experimental beam lines was carried on by Edward A. Görlich and Krzysztof Tomala.

The Symposium proceedings including 20 selected presentations were published in a regular issue of *Acta*

Physica Polonica A (vol. 117 (2010), No 2) prepared by Wojciech Paszkowicz, Marcin Sikora and Wojciech Szuszkiewicz as the guest editors.



Chairman of 8th KSUPS, Andrzej Burian, made records of all events.

(Photo: W. Paszkowicz)



Participants of the 8th National Symposium of Synchrotron Radiation Users at Podlesice.

In the first row from the left: A. Kisiel (Honorary Member of the PSRS, President of the PSRS in the period of 1991-1999), K. Jabłońska (President since 2005), B. Orłowski (President in the period of 1999-2005), A. Burian (Chairman of the Symposium), M. Walczak.

(Photo: Ł. Hawelek)



During an oral session.

(Photo: W. Paszkowicz)



Poster session at the hall of the hotel.

(Photo: W. Paszkowicz)

The last Annual General Meeting of the Polish Synchrotron Radiation Society was held at Podlesice on the 25th of September 2009. The first item of the agenda was connected with the membership of the Society. The Secretary, Danuta Żymierska, informed that the six new members were registered and that of long standing member, Jerzy Gronkowski (the University of Warsaw) passed away; thus the total membership reached 146 members: 1 honorary member, 124 full members, and 21 associate members (among them 10 foreigners).

From September 2009 till June 2010, three meetings of the Council of the PSRS were held, for cutting down the expenses, as internet conferences.

The reports for the period of June 2008 – September 2009 were the next point of the agenda. The President, Krystyna Jabłońska, presented the report from the PSRS activity. The Head of the Auditing Commission, Wojciech Wierzchowski, read the financial report prepared by the Treasurer, Wojciech Kwiatek, that was absent, as well as the minutes from the meeting of the Auditing Commission with the conclusion that the Commission approves the financial and activity reports of the Council. After a discussion, all reports were accepted by the General Assembly.

Then, the President presented the Council proposal to start efforts for organisation in Poland in 2015 the international conference on X-Ray Absorption Fine Structure (XAFS16) (about 600 participants are expected). The Council suggests the former capital of Poland, Cracow, as a place of this meeting and Wojciech Kwiatek as the chairman of the Organising Committee. The Assembly authorized the Council for preparing of Polish proposal which should be ready before the 1st of September 2011 and sent to the International Society of the X-Ray Absorption (see: <http://www.ixasportal.net/ixas/>). An international scientific community will decide on this matter during the XAFS15 in Beijing in 2012.

Next, Maciej Kozak of the Adam Mickiewicz University presented status of arrangements for the 10th International School and Symposium on Synchrotron Radiation in Natural Science at Szklarska Poręba in June 2010. Before closing the meeting, the Assembly accepted a project of an information leaflet about the Society prepared and presented by Paweł Piszora as well as a proposal of organising during the 10th ISSRNS a photographic competition “Our Beamtime” submitted by Wojciech Paszkowicz.

The last year was very successful for our community. The Polish membership in the European Synchrotron Radiation Facility (ESRF) in Grenoble has been continued. A special grant of Polish Ministry of Science and Higher Education coordinated by Prof. Jabłońska ensures funds till July 2011.

The PSRS actively participates in two (European and Polish) free electron laser (FEL) projects. In March 2010, the Parliament of Poland ratified the Constitution of the European X-ray Free Electron Laser (X-FEL) project. This opens for Poland the way to participate in the project as a full-rights member country. Prof. Jabłońska has been elected to its Scientific Advisory Committee for the three-year term. She took part in the first meeting of this Committee in Hamburg. The activity concerning the Polish Free Electron Laser (POLFEL) at the Andrzej Sołtan Institute for Nuclear Studies at Świerk is presented separately in this issue.

In my opinion the best news for our Society is that after more than ten years of hard efforts of the Polish synchrotron user community, especially colleagues from Cracow, the project of the Polish Synchrotron becomes reality. On 9th April 2010, the Minister of Science and Higher Education, Prof. Barbara Kudrycka, and the Rector of the Jagellonian University, Prof. Karol Musioł, signed the contract for realization of the project entitled “National Centre of Electromagnetic Radiation for research aims (the stage I)”.

All of us congratulate the team of Edward A. Görlich, Krzysztof Królas, and Krzysztof Tomala on having achieved this success.

Danuta Żymierska /Secretary of the PSRS/

On FEL in Ryn

The International Workshop on X-ray Diagnostics and Scientific Application of the European XFEL was held in Ryn in the Eastern North of Poland on 14th – 17th February 2010. It was the sixth in a series of workshops for the instrumentation and applications of the upcoming European X-ray Free Electron Laser (XFEL). This workshop was dedicated to the photon pulse diagnostics: coherence, energy spectrum, duration and arrival time measurements. Main challenges were defined during the introduction lectures on the FEL's light generation and its properties. The most emphasized ones were: single shot measurements, high intensity of the pulses, and the necessity to preserve the main pulse properties. Although the discussion was focused on specific case of the XFEL diagnostics, many of the proposed solutions will be valid for other short wave FELs. As a result of the workshop list of applicable techniques was established. Most of them will require further work, for which scientific collaborations have already been set up.

The operant topics were completed with lectures on the scientific applications of x-ray coherent beam. (The detailed programme can be found at the webpage http://www.xfel.eu/events/workshops/2010/x_ray_diagnostics_and_scientific_application_workshop/). It was a way to popularize short-wavelength FELs – the world's leading X-ray lasers – in the Polish scientific community

and, further to join the scientific collaboration in the very interesting field of x-ray laser light interactions with matter. It is especially important in the perspective of the Polish membership in the European X-ray Free Electron Laser. It was announced that in April 2010 Polish Parliament approved the Convention concerning the Construction and Operation of a European X-ray Free-Electron Laser Facility, signed by government in November 2009. It formally enables the participation of Poland in the XFEL company and the participation of Polish technicians and scientists in international team carrying this intriguing project out.

The Workshop was accompanied with a parallel seminar on the scientific program, users needs, accelerator and undulator options for planned Polish free electron laser, POLFEL. This first meeting open for a broad Polish scientific community, demonstrated, in particular, an interest in using short pulses in visible range to study de-excitation processes in luminofors, scintillators and biological molecules. An initiative has been taken to establish a consortium dedicated to POLFEL construction.

*Krystyna Lawniczak-Jablonska,
Robert Nietubyć,
Ryszard Sobierajski*

XFEL Workshop.

photo by Dominik Rybka.





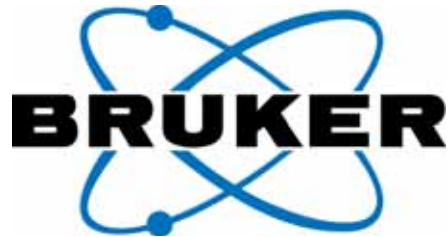
POLFEL Semina.

Photo by Dominik Rybka.



Zapowiedzi wydawnicze

Wydawnictwo Naukowe UAM planuje w najbliższym czasie wydanie podręcznika „Krystalografia dla biologów” pióra prof. Mariusz Jaskólskiego. Książka, która jest serią wykładów przedstawiających zarówno zagadnienia metodyczne krystalografii białek jak i zarys biologii strukturalnej, powinna wypełnić dotkliwą lukę w polskojęzycznej bibliografii tych zagadnień.



Bruker was founded in 1960 with nuclear magnetic resonance (NMR) products. Advances in scientific computing technology used for the Bruker NMRs, along with the pioneer work of Professor Ludwig Genzel (1922-2003), director of the Max Planck Institute in Stuttgart, Germany, led Bruker in a new direction: Fourier Transform Infrared Spectroscopy. Bruker launched its first-ever FT-IR spectrometer, the IFS series, and entered the field of vibrational spectroscopy in 1974. The 'Genzel' interferometer and many other unique options available on IFS series have instantly set standards in FT-IR spectroscopy. Since then, Bruker's Vibrational Spectroscopy product line has been continuously expanding with instruments suitable for both analytical and research applications. Today, Bruker Optics is a part of the Bruker Corporation and offers FT-IR, NIR, Raman, TD-NMR, TeraHertz spectrometers and imaging spectrographs for various markets and applications. Bruker Optics has R&D and manufacturing centers in Ettlingen, Germany, and The Woodlands, USA, supporting technical centers and offices throughout Europe, North and South America and Asia.

Whether it's a high-end research system, a life sciences tool, a routine quality control instrument or a process analyzer, Bruker Optics offers a wide variety of innovative analytical tools for all your demanding needs. The countless innovations found on our products, delivering unmatched analytical power, represent our philosophy of think forward.

Bruker Optics Branch office Poland
ul. Wołczyńska 18
60-003 Poznan
POLAND

Tel.: +48 (61) 6390256
Fax: +48 (61) 6390429
email: [info\(at\)brukeroptics.de](mailto:info(at)brukeroptics.de)

Bruker Optik GmbH
Rudolf-Plank-Str. 27
76275 Ettlingen
GERMANY

Tel.: +49 7243 504-2000
Fax: +49 7243 504-2050
email: [info\(at\)brukeroptics.de](mailto:info(at)brukeroptics.de)

**10th International School and Symposium
on Synchrotron Radiation in Natural Science
June 6-11, 2010
Szklarska Poręba, Poland**



Organized by Polish Synchrotron Radiation Society
in cooperation with Adam Mickiewicz University, Poznań, Poland

INTERNATIONAL ADVISORY BOARD

Francesco d'Acapito - European Synchrotron Radiation Facility, Grenoble, France

Edward Goerlich - Jagiellonian University, Kraków, Poland

Jürgen Härtwig - European Synchrotron Radiation Facility, Grenoble, France

Mariusz Jaskólski - Center for Biocrystallographic Research, Polish Academy of Sciences, Poznan, Poland

Andrzej Kisiel - Jagiellonian University, Kraków, Poland

Peter Laggner - Institute of Biophysics and Nanosystems Research, Graz, Austria

Andrea Lausi - Sincrotrone Trieste, Trieste, Italy

Jarosław Majewski - Los Alamos National Laboratory, USA

Giorgio Margaritondo - Ecole Polytechnique Federale de Lausanne, Switzerland

Gerhard Materlik - Diamond Light Source, Didcot, United Kingdom

Bronisław Orłowski - Institute of Physics, Polish Academy of Sciences Warszawa; Polish Synchrotron Radiation Society, Poland

Adam Patkowski - A. Mickiewicz University, Poznań, Poland

Christian Riekell - European Synchrotron Radiation Facility, Grenoble, France

Leonid Rivkin - LPAP Swiss Federal Institute of Technology Lausanne, Paul Scherrer Institute Villigen, Switzerland

Masaki Taniguchi - Hiroshima Synchrotron Radiation Center, Hiroshima University, Japan

Ernst Wehreter - Helmholtz-Zentrum Berlin, Elektronenspeicherring BESSY II, Germany

Alexander Wlodawer - Macromolecular Crystallography Laboratory NCI-Frederick, Frederick, USA

Dmitri I. Svergun - EMBL-Outstation c/o DESY Hamburg, Germany

Wojciech Paszkowicz (Proceedings Editor) - Institute of Physics, Polish Academy of Sciences, Warsaw, Poland

Paweł Piszora - A. Mickiewicz University, Poznań, Poland

Krystyna Jabłońska-Ławniczak - Institute of Physics, Polish Academy of Sciences, Warsaw, Poland

Radosław Przeniosło - University of Warsaw, Warsaw, Poland

Aleksandra Wypych - A. Mickiewicz University, Poznań, Poland

Kamil Szpotkowski - A. Mickiewicz University, Poznań, Poland

Michał Taube - A. Mickiewicz University, Poznań, Poland

Zuzanna Pietralik - A. Mickiewicz University, Poznań, Poland

Sebastian Wołoszczuk (www) - A. Mickiewicz University, Poznań, Poland

SPONSORS:

Ministry of Science and High Education

Rector of A. Mickiewicz University

Dean of Faculty of Physics, A. Mickiewicz University

Oxford Diffraction Sp z o.o.  Oxford Diffraction
Now a part of Varian, Inc.

BRUKER Polska Sp. z o.o.  BRUKER
Bruker Optics Branch office Poland, Bruker Optik GmbH

ORGANIZING COMMITTEE

Maciej Kozak (Chairman) - A. Mickiewicz University, Poznań, Poland

Wojciech Kwiatek (Treasurer) - Institute of Nuclear Physics, Polish Academy of Sciences, Kraków, Poland

TESTCHEM

Rigaku



SUNDAY, 6th June 2010

17:30 – 17:40	Opening		
17:40 – 18:20	Wladek Minor, Univ. of Virginia, Charlottesville, USA <i>Impact of 3rd generation synchrotron sources on structural biology</i>	L01	42
18:20 – 19:00	Augusto Marcelli, Laboratori Nazionali di Frascati, Frascati (Rome), Italy <i>Biological applications of synchrotron radiation infrared spectromicroscopy</i>	L02	43
19:00 – 20:00	Dinner		

MONDAY, 7th June 2010

9:00 – 9:40	Paolo Ghigna, Univ. of Pavia, Italy <i>Synchrotron radiation in solid state chemistry</i>	L03	44
9:40 – 10:20	Ullrich Pietsch, Univ. of Siegen, Siegen, Germany <i>X-ray strain evaluation at individual semiconductor nanowires</i>	L04	45
10:20 – 10:40	Christian Pettenkofer, Helmholtz Zentrum, Berlin, Germany <i>Chemical nature of N-ions incorporated into epitaxial ZnO films</i>	O01	46
10:40 – 11:00	Coffee break		
11:00 – 11:40	Udo Heinemann, Max Delbrueck Center for Molecular Medicine, Berlin, Germany <i>Use of synchrotron radiation in studies of protein structure and nucleic acid binding</i>	L05	47
11:40 – 12:20	Kenya Shimada, Hiroshima Synchrotron Radiation Center, Hiroshima Univ., Higashi-Hiroshima, Japan <i>Many-body interactions in solids studied by high-resolution ARPES using synchrotron radiation</i>	L06	48
12:20 – 13:00	Andrzej Kuczmow, The John Paul II Catholic Univ. of Lublin, Poland <i>Microchemical and structural regular variability of apatites in "overbuilt" enamel and dentin of human molar teeth</i>	L15	64
13:00 – 14:30	Lunch		
14:30 – 17:30	Excursion 1		
17:40 – 18:20	Yngve Cerenius, MaxLab, Lund Univ., Lund, Sweden <i>First phase beamlines on MAX IV</i>	L08	50
18:20 – 19:00	Dieter Einfeld, ALBA, Barcelona, Spain <i>Trends in state of the art storage ring based SR sources</i>	L09	51
19:00 – 20:00	Dinner		
20:00 – 22:00	Poster session 1		

TUESDAY, 8th June 2010

9:00 – 9:40	Victor Lamzin, EMBL-Outstation c/o DESY Hamburg, Germany <i>Mapping the protein world: Over 1500 biomolecular structures solved on-line at EMBL-Hamburg</i>	L10	52
9:40 – 10:20	Sebastian Thiess, Hasylab at DESY, Hamburg, Germany <i>Site specific XPS: Structural and electronic properties investigated by X-ray standing waves</i>	L11	54
10:20 – 10:40	Krystyna Ławniczak-Jabłońska, Institute of Physics PAS, Warsaw, Poland <i>The shape anisotropy of the MnSb inclusions formed in GaSb matrix as probed by XMCD</i>	O02	56
10:40 – 11:00	Coffee break		
	Session A		
11:00 – 11:40	Heinz Amenitsch, Elettra, Trieste, Italy <i>SAXS & GISAXS in bionanotechnology</i>	L12	58
11:40 – 12:20	Manfred Roessle, EMBL-Outstation c/o DESY Hamburg, Germany <i>Structural studies of biological macromolecules in solution using synchrotron small-angle X-ray scattering</i>	L13	59

12:20 – 12:40	Massimo Reconditi , Univ. of Florence, Italy SAXS studies of the muscle cell to identify the force-generating myosin molecules	O03	60
12:40 – 13:00	Henryk Drozdowski , A. Mickiewicz Univ., Poznań, Poland Determination of electron radial distribution function for liquid cyclohexylamine by X-ray diffraction	O04	61
	Session B		
11:00 – 11:40	Kristina Kvashnina , ESRF, Grenoble, France X-ray absorption and emission spectroscopy of rare-earth materials	L14	62
11:40 – 12:20	Bogdan Kowalski , Institute of Physics, PAS, Warsaw, Poland Photoelectron spectroscopy in studies of the band structure of IV-VI spintronic materials	L07	157
12:20 – 12:40	Jan Ivanco , Institute of Physics, Slovak Acad. of Sci., Bratislava, Slovak Republic Top metal contact on an organic film: Indium on copper phthalocyanine	O05	65
12:40 – 13:00	Abdul Ghaffar , Univ. of Vienna, Austria Confinement-induced structural changes of lithium and sodium in nano-porous silica glass	O06	66
13:00 – 14:30	Lunch		
14:30 – 16:30	Time for mountain activities		
16:30 – 17:00	Coffee break		
17:00 – 19:00	Poster session 2		
19:00 – 20:00	Dinner		
20:00 – 22:00	JANA Workshop – “Solution for difficult structures”		

WEDNESDAY, 9th June 2010

9:00 – 9:40	Vaclav Petricek , Institute of Physics of the AS CR, Praha, Czech Republic Jana2006 as a tool for solution and refinement of non-standard crystal structures	L16	67
9:40 – 10:20	Jacek Gapiński , A. Mickiewicz Univ., Poznań, Poland Application of X-ray scattering and diffraction techniques to studies of highly charged colloid suspensions in the vicinity of the crystallization point	L17	68
10:20 – 10:40	Marek Żbik , Queensland Univ. of Technology, Brisbane, Australia Synchrotron based transmission X-ray microscopy reveals smectite fine structure in an aqueous environment	O07	69
10:40 – 11:00	Coffee break		
11:00 - 11:40	Vincenzo Lombardi , Univ. of Florence, Italy X-ray interference measurements of the molecular motor of muscle with nanometer-microsecond resolution	L18	70
11:40 – 12:20	Marian Cholewa , Monash Univ., Monash Centre for Synchrotron Science, Australia High resolution X-ray microprobes and their applications	L19	71
12:20 – 12:40	Tomasz Ślęzak , AGH Univ. of Science and Technology, Kraków, Poland Depth-resolved magnetization structure at the spin reorientation transition in Fe/W(110) ultrathin films studied by the nuclear resonant scattering of synchrotron radiation	O08	72
12:40 – 13:00	Robert Nietubyc , Institute for Nuclear Studies, Otwock-Świerk, Poland Growth of niobium film on sapphire(001)	O10	78
13:00 – 14:30	Lunch		
14:30 – 19:00	Excursion 2		
19:00 – 20:00	Dinner		
20:00 – 22:00	JANA Workshop – “Solution for difficult structures”		

THURSDAY, 10th June 2010

9:00 – 9:40	Marek Stankiewicz, Jagiellonian Univ., Kraków, Poland Polish Synchrotron – present status	L20	74
9:40 – 10:20	Mikael Eriksson, MaxLab, Lund Univ., Lund, Sweden The accelerators for the Polish Light Source and MAX IV	L21	75
10:20 – 11:00	Jacek Szade, August Chelkowski Institute of Physics, Univ. of Silesia, Katowice, Poland Soft X-ray Spectroscopy - first beamline at Polish synchrotron	L22	76
11:00 – 13:00	Annual General Meeting of the Polish Synchrotron Radiation Society		
13:00 – 14:30	Lunch		
14:30 – 15:10	Burkhard Kaulich, ELETTRA, Trieste, Italy Transmission and emission soft X-ray spectromicroscopies for life and nanosciences at Elettra	L23	77
15:10 – 15:30	Wojciech Wierzchowski, Institute of Electronic Materials Technology, Warsaw, Poland X-ray topographic investigation of the deformation field around spots irradiated by flash single pulses	O09	73
15:30 – 15:50	Jakub Szlachetko, ESRF, Grenoble, France Application of wavelength-dispersive spectroscopy at ID21 X-ray Microscopy beamline of ESRF: new possibilities for micro-fluorescence and micro-XANES analysis	O11	79
15:50 – 16:10	Wojciech Paszkowicz, Institute of Physics PAS, Warsaw, Poland Properties of rare earth orthovanadates under high pressure	O12	80
16:10 – 16:30	Lukasz Walczak, Universidad Autónoma de Madrid, Spain Electronic structure and crystalline structure of vicinal Beryllium surfaces	O13	81
16:30 – 16:55	Coffee break		
	Special session "Numerical optimization methods: Applications in synchrotron science"		
16:55 – 17:00	Wojciech Paszkowicz, Institute of Physics PAS, Warsaw, Poland Introduction		
17:00 – 17:40	Cristian V. Ciobanu, Colorado School of Mines, Golden, Colorado, USA Genetic algorithms for structural optimization problems at the nanoscale	L24	82
17:40 – 18:20	Enrique Garcia Michel, Universidad Autónoma de Madrid, Spain Application of genetic algorithms to surface x-ray diffraction analysis	L25	83
18:20 – 19:00	Hiroimitsu Tomizawa, Japan Synchrotron Radiation Research Institute (JASRI), XFEL Joint Project/SPring8, Hyogo, Japan Strategy of metaheuristics algorithms for laser optimization	L26	84
19:00 – 22:00	Conference dinner		

FRIDAY, 11th June 2010

9:00 – 9:40	Jürgen Härtwig, ESRF, Grenoble, France Challenges in X-ray optics for modern X-ray sources	L27	158
9:40 – 10:00	Wojciech Sławiński, University of Warsaw, Poland Magnetoelastic coupling in CaMn₇O₁₂	O14	85
10:00 – 10:20	Marcin Zając, ESRF, Grenoble, France In situ high temperature magnetic and dynamic properties of Fe(110) nanostructures studied with nuclear resonant scattering techniques	O15	86
10:20 – 10:40	Matteo Amati, Sincrotrone Trieste SCpA, Trieste, Italy Recent achievement in characterization of micro- and nano-materials by scanning photoemission imaging and spectromicroscopy	O16	87
10:40 – 11:00	Coffee break		
11:00 – 11:40	Closing ceremony		

WELCOME to the Jubilee 10th ISSRNS

On behalf of the Organizing Committee and Scientific Advisory Board we would like to welcome you to the Jubilee 10th International School and Symposium on Synchrotron Radiation in Natural Science organized by the Polish Synchrotron Radiation Society (PTPS) in cooperation with the A. Mickiewicz University in Poznań.

Since the first meeting, in 1992, the ISSRNS has been organized as a biennial event. ISSRNS is a traditional forum for discussing fundamental issues of application of the synchrotron radiation and related methods in natural sciences. The aim of this interdisciplinary meeting is to bring together scientists working with synchrotron radiation and new comers interested in using SR based techniques. The Symposium is focusing on novel applications of synchrotron radiation in physics, chemistry, material and live sciences.

This year meeting is the 10th Jubilee Meeting and moreover is the first meeting after approving of the constriction of Polish synchrotron. The Polish National Synchrotron Radiation Source (NCPS) in Krakow is expected to meet the needs of Polish and Central-East-European users in the years to come. Therefore, now it is very important to educate young people (M.Sc. and Ph.D. students) in different fields that are necessary to develop, build and operate the synchrotron radiation source.

This year we meet in the “LAS” hotel located in Szklarska Poreba. This beautiful town is situated in the south-western part of Poland in Karkonosze and Izery mountain range and is an important regional and national centre for mountain hiking, cycling and skiing. Szklarska Poreba region is place know of occurrence of precious ores. There have been classified over 50 minerals, which commonly occur in Karkonosze and Izery mountains. Many of them present properties of such gemstone as: amethyst, aventurine, topaz, olivine, tourmaline, aquamarine, hyacinth, beryl, moonstone, agate, mountain crystal and smoky quartz. Therefore this beautiful town is known as the Mineralogical Capital of Poland.

However, not only the beautiful neighbourhood is interesting. We made an effort to ascertain a large variety of subjects to be presented at the meeting. The lecturers come from the best synchrotron laboratories in Europe, Asia and America as well as from university laboratories using the intense radiation sources.

We would like to thank all lecturers for accepting our invitations to show the results of their exciting research. We also thank all the participants for preparing oral and poster presentations. We hope that the participation in the conference will be fruitful and stimulating for all of you. We wish you good time with excellent science amid nature's splendor.

The Organizers

IMPACT OF 3RD GENERATION SYNCHROTRON SOURCES ON STRUCTURAL BIOLOGY

W. Minor

University of Virginia, Charlottesville, VA, 22908-0736, USA

Keywords: synchrotron, beamline productivity, structural biology, protein

The three-dimensional structures determined by X-ray crystallography play a central role in understanding protein-small molecule and protein-protein interactions at the molecular level. Accurate details of such interactions have direct implications for drug design and development of other biomedical treatments. Consequently, during the past 15 years the rate of protein structure determination by X-ray crystallography has increased about 8-fold. The use of synchrotron radiation was critical for this growth, as the fraction of macromolecular structures reporting the use of synchrotron radiation increased from 30% in 1990 to 88% in 2009. The superiority of the results obtained with the use of synchrotron radiation increases the pressure to build more stations dedicated for protein crystallography. Thus, the number of protein-crystallography-dedicated synchrotron stations has risen from 8 in 1985 to more than 120 worldwide, and there

are more than 20 stations either under construction or planned to be built in the near future. While this increase in the number of stations was important, other advancements in technology and procedures were even more critical for the rapid growth of protein crystallography. These advancements include increases of beam intensity and improvements of beam tunability, better detectors, increased computational capacity and better software, and most importantly, improved data collection/processing protocols. An experimental protocol is a result of a compromise between the ideal experiment possible and the various practical limitations encountered at the beamline. The difficulty implementing the best experimental protocols can be illustrated by the sharp differences in productivity of technologically similar synchrotron beamlines. In this talk I will discuss all factors influencing synchrotron beamline productivity.

BIOLOGICAL APPLICATIONS OF SYNCHROTRON RADIATION INFRARED SPECTROMICROSCOPY

A. Marcelli *

INFN – Laboratori Nazionali di Frascati, Via E. Fermi, 40 - 00044 Frascati (Rome), Italy

Keywords: infrared, synchrotron radiation, microscopy, imaging

*) e-mail: marcelli@lnf.infn.it

The field of infrared biological imaging covers a wide range of fundamental issues and applied researches such as cell imaging or tissue imaging. It continuously offers new opportunities to better understand cell interactions, cell micro-environment, tissue formation and diagnostic.

A synchrotron source (SR) has the capability of providing IR light through a 10 μm pinhole that is 2–3 orders of magnitude brighter than a conventional Globar such as those available in commercial FTIR instrumentation. This superior signal-to-noise ratio (SNR) allows collecting imaging with a spatial resolution down to the diffraction limit, or to allow analysis of thicker samples while maintaining good spatial resolution.

The availability of the infrared FPA detector and its recent installation at ultra-brilliance SR facilities around the world promises to extend the performance and overcome the existing limitations [1]. As an example FTIR microscopy with a FPA detector allows routine chemical imaging on individual cells in a few minutes only. The brilliance of SR IR sources may enhance the molecular signal obtained from such small biosamples containing reduced amount of organic matter. Molecular structure and function are strongly correlated. This aspect is particularly relevant in the case of proteins, which play important roles in cells biochemistry. Changes of structure may be easily detected in an IR spectrum and a cellular molecular marker may in fact be used to address a pathological status of tissues [2].

FPA detectors couple to SR sources may reduce data acquisition time from hours to minutes, improving the spectral quality and overcoming instability contributions sometime experienced at SR facilities [3].

Combining SR and array detectors we investigated individual cells obtained from a cell culture specifically developed for transmission FTIR imaging using either a Globar or a SR source. SR-IR source focalization was optimized time by time to control the energy distribution on the array detector.

I will show that access to IR absorption distribution from all organic contents of cells at $1 \times 1 \mu\text{m}$ pixel resolution is possible only with high circulating current and, illuminating a limited number of pixels of a FPA's detectors to increase the signal-to-noise ratio of IR images [4].

High current SR rings are mandatory to collect FTIR images of biosamples with a high contrast in minutes. Within this framework there is really a brilliant future for SR IR microscopy and imaging, and important results in biological and biomedical applications are expected in the next years.

References

- [1] C. Petibois, M. Piccinini, M. Cestelli Guidi, A. Marcelli, "Facing the challenge of biosample imaging by FTIR with a synchrotron radiation source", *J. Synchrotron Rad.* **17** (2010) 1-11.
- [2] W.M. Kwiatek, C. Paluszkiwicz, A. Banas, A. Kisiel, M. Podgórczyk, A. Marcelli, M. Cestelli Guidi, M. Piccinini, "Application of μ -FTIR-SR spectroscopy to prostate tissue analysis", *Acta Phys. Polon. A* **115** (2009) 602-605.
- [3] C. Petibois, M. Piccinini, M.A. Cestelli-Guidi, G. Délérís, "A bright future for synchrotron imaging", A. Marcelli, *Nature Photonics* **3** (2009) 177-236.
- [4] C. Petibois *et al.*, submitted (2010)

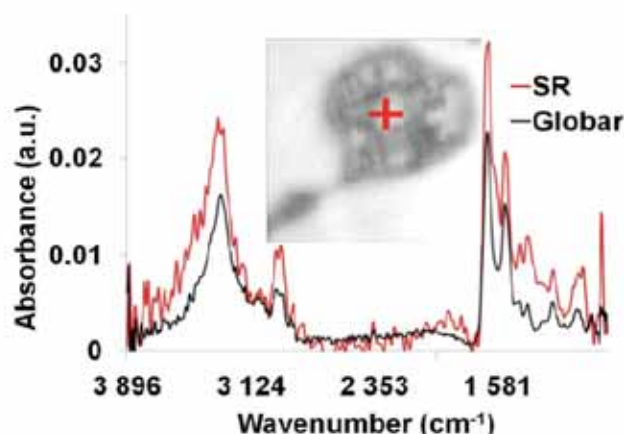


Figure 1. Comparison between FTIR spectra of individual cells collected with SR-IR at DAΦNE and a Globar source. Acquisitions were performed at 8 cm^{-1} spectral resolution with the 36X objective in the region indicated by a red cross on the visible image.

SYNCHROTRON RADIATION IN SOLID STATE CHEMISTRY

P. Ghigna*, S. Pin, and G. Spinolo

Dipartimento di Chimica Fisica "M. Rolla", Università di Pavia, 16, Viale Taramelli, 27100 Pavia, Italy

Keywords: solid state chemistry, reactivity, reaction mechanisms, XAS

*) e-mail: paolo.ghigna@unipv.it

Solid state reactivity in its various aspects plays a significant role in many different areas of science, such as Crystallography, Mineral Physics and Earth Sciences, Physical Metallurgy, Ceramic Science, Semiconductor Physics, Solid State Chemistry, but the basic knowledge and the main results (not to speak of the language itself) are not always well shared among the disciplines. Surface Science and Catalysis provide an ample background of knowledge on the transformations and reactions occurring at a free interface, while the processes occurring at the boundary between two condensed phases are an important topic in many of the scientific areas above quoted, for instance in the investigation of phase transformations or growth of thin films. All this knowledge provides important starting points but does not directly face the processes occurring when a *single* interface between two grains of the reagent phases is progressively turned into *two* different interfaces between each reagent and the newly formed product. So, for an extremely ample set of heterogeneous reactions, *i.e.* the reactions involving two condensed phases as reagents and producing a different crystalline phase, the present state of art is that thermodynamics gives tools to predict whether or not the formation of a particular product can occur, and the assessed kinetic theory gives tools to predict the growth rate of this product when diffusion is the rate determining step. However, we do not really understand the mechanism through which this product is formed. This means that we have no general knowledge of the very basic aspects of the chemical reactivity in the solid state; for instance we ignore how and why a reaction actually goes towards one or another polymorph, a compound or a broad range solid solution, a stable or metastable product.

Quite impressively, the scientific community still needs an assessed agreement concerning the procedures and the aforementioned experimental probes required to investigate this topic, as well as a sound common

background connecting the different areas that can seemingly provide important contributions to the advancement of knowledge, and that conversely can profit from that advancement.

As a matter of fact, in quite recent series of papers by our group, it has been demonstrated that some insight into the mechanisms and the kinetics of solid state reactions in the early stages can be obtained by: i) performing the reaction using at least one of the reactants in form of a very thin film (of the order of 10 nm), ii) using a local probe for the local chemical environment of one of the constituents such as XAS (X-Ray Absorption Spectroscopy) [1-4].

Aim of this lecture is to show how important insights into the mechanisms of a solid state reaction in its early stages can be retrieved. The use of different Synchrotron Radiation based techniques is of fundamental importance in this respect.

References

- [1] P. Ghigna, G. Spinolo, I. Alessandri, I. Davoli, F. D'Acapito, "Do we have a probe for the initial stages of solid state reactions? Complex oxide: defect chemistry, transport and chemical reaction", *Phys. Chem. Chem. Phys.* **5** (2003) 2244–2247.
- [2] F. D'Acapito, P. Ghigna, I. Alessandri, A. Cardelli, I. Davoli, "Probing the initial stages of solid-state reactions by total reflection EXAFS (refLEXAFS)", *Nucl. Instr. And Meth. in Phys. Res. B* **200** (2003) 421–424.
- [3] S. Pin, P. Ghigna, G. Spinolo, E. Quartarone, P. Mustarelli, F. D'Acapito, A. Migliori, G. Calestani, "Nanoscale formation of new solid-state compounds by topochemical effects: The interfacial reactions ZnO with Al₂O₃ as a model system", *J. Solid State Chem.* 2009, **182**, 1291–1296.
- [4] P. Ghigna, S. Pin, G. Spinolo, M.A. Newton, M. Zema, S.C. Tarantino, G. Capitani, F. Tatti, "μ-XANES mapping of buried interfaces: pushing microbeam techniques to the nanoscale", *Phys. Chem. Chem. Phys.*, (2010), in press.

X-RAY STRAIN EVALUATION AT INDIVIDUAL SEMICONDUCTOR NANOWIRES

U. Pietsch^{1*}, A. Davydok¹, S. Breuer², A. Biermanns¹, and L. Geelhaar²

¹ University of Siegen, Festkoerperphysik, Walter-Flex Str. 3, 57068 Siegen, Germany

² Paul Drude Institut fuer Festkoerperelektronik, Hausvogteiplatz 5-7, 10117 Berlin, Germany

Keywords: nanowires, GaAs, x-ray diffraction

*) e-mail: pietsch@physik.uni-siegen.de

Semiconductor nanowires (NW's) are of particular interest due to the ability to synthesize single-crystalline 1D epitaxial structures and heterostructures in the nanometer range. One of the most common methods for NW growth is the Vapour-Liquid-Solid mechanism[1]. Using x-ray diffraction we have investigated GaAs NW's on Si[111] substrate where the lattice mismatch is about 4%. Using synchrotron radiation and considering our experience in NW's structure analysis [2,3] we have performed X-ray reciprocal space mapping in vicinity of selected Bragg reflections to analyze the strain release between NW and substrate. For the investigation of strain at the NW to substrate interface we selected samples of different growth time corresponding to different phases of growth: after 60s – the whole surface of the sample is covered by islands; after 150 s – first wires appear; after 300 s – number of NW's is increase and after 1800 s – 3 μm -height NW's cover the whole substrate (Fig. 1).

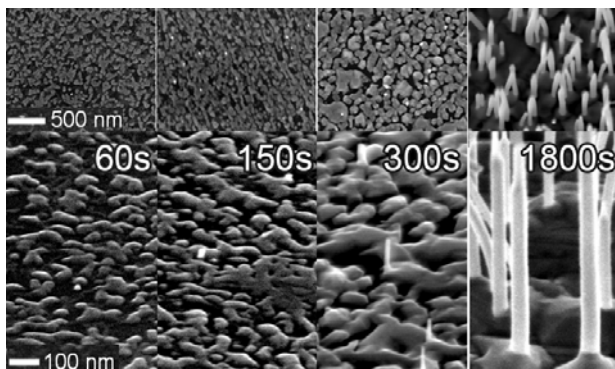


Figure 1. SEM – images of the early stage of GaAs nanowire growth on Si: During the initial stage (60 s to 300 s), the surface is covered with GaAs islands. After 300 s, nanowire growth starts and several micron long wires form (1800 s).

Using symmetric coplanar x-ray diffraction and subsequent rocking curve analysis based on the Tagaki-Taupin approach we could associate the different features seen in SEM to different structure elements appearing during crystal growth. The islands found after 60s are

grown in zincblende (ZB) type structure, gradually releasing the lattice mismatch between GaAs and Si. Contrary, the NWs appearing after 150s of growth are of wurtzite (WZ) type structure. Measuring structure type sensitive Bragg reflections, the evolution of the WZ content within the samples could be determined quantitatively from intensity ratio of (331)ZB/(10i5)WZ. Due to the different structure of wires and islands, single wires could be resolved and characterized using a nanometer sized x-ray beam.

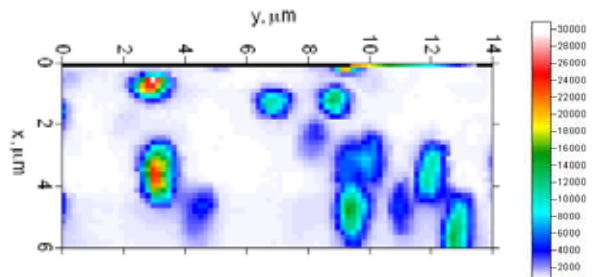


Figure 2. Spatially resolved intensity distribution of the GaAs (10i5) wurtzite reflection. The individual spots represent single nanowires grown in the wurtzite structure.

References

- [1] S.-G. Ihn, J.-In Song, T.-W. Kim, D.-S. Leem, T. Lee, S.-G. Lee, E.K. Koh, K. Song, "Morphology- and orientation-controlled gallium arsenide nanowires on silicon substrates", *Nano Lett.* **7** (2007) 39–44.
- [2] A. Biermanns, A. Davydok, H. Paetzelt, A. Diaz, V. Gottschalch, T.H. Metzger, U. Pietsch, "Individual GaAs nanorods imaged by coherent X-ray diffraction", *J. Synchrotron Rad.* **16** (2009) 796–802.
- [3] A. Davydok, A. Biermanns, U. Pietsch, J. Grenzer, H. Paetzelt, V. Gottschalch, "X-Ray diffraction from periodically patterned GaAs nanorods grown onto GaAs[111]B", *Metallurg. Mater. Trans. A* **41** (2010) 1191–1195.

CHEMICAL NATURE OF N-IONS INCORPORATED INTO EPITAXIAL ZnO FILMS

P. Hoffmann and C. Pettenkofer*

Helmholtz Zentrum Berlin, Albert Einstein Str 15, 12189 Berlin, Germany

Keywords: ZnO, p-doping, spectroscopy

*) e-mail: pettenkofer@helmholtz-berlin.de

Efficient p-type doping of zinc oxide (ZnO) is hindered on the one hand by the strong native n-type doping of the ZnO, on the other hand, compensation effects (defect generation due to p-doping) tend to preserve the n-type doping. Incorporation of nitrogen is proposed as a promising method to achieve p-type ZnO, because the ionic radii of nitrogen and oxygen are comparable. Therefore, nitrogen atoms can replace oxygen. Nevertheless, a reliable and stable p-doping is still an unmatched challenge.

This work will focus on the chemical nature of nitrogen implanted by ion irradiation into MO-MBE grown ZnO layers on sapphire substrate. The

incorporated nitrogen was investigated by photoelectron spectroscopy using synchrotron radiation (PES) and monochromatized Al-K α (mXPS), and X-ray absorption spectroscopy (NEXAFS). The preparation conditions were varied for preferential incorporation of the different nitrogen species. The three main N1s-PES components were assigned to different nitrogen compounds (molecular N₂, N-O-bonds, and N-Zn-bonds) with the help of NEXAFS data. In addition, the thermal stability of the nitrogen compounds was investigated. These results may lead to an optimization of the nitrogen implantation process for a better doping efficiency.

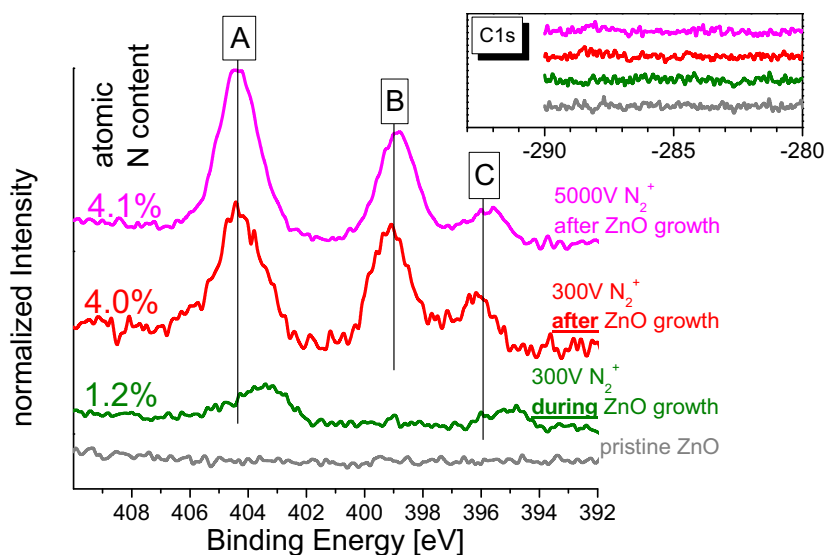


Figure 1. N1s spectra of nitrogen doped ZnO, grown by metal-organic MBE (MO-MBE), taken with monochromatized Al-K α excitation. The nitrogen was implanted (15 minutes for each sample) from a plasma ion source with a kinetic energy of 300 eV while (lower spectrum), and after (middle spectrum) the MO-MBE growth of the ZnO. At higher kinetic energy of the nitrogen ions, the nitrogen content is not significantly increased, but the crystalline quality of the layer (checked by LEED) is nearly lost. Additionally, the corresponding C1s spectra are given on the upper right corner.

USE OF SYNCHROTRON RADIATION IN STUDIES OF PROTEIN STRUCTURE AND NUCLEIC ACID BINDING

U. Heinemann^{1,2*}, **B. König**¹, **E. Lanka**³, **A. Schütz**¹, **D. Carstanjen**⁴, and **K.E.A. Max**¹

¹ Crystallography, Max-Delbrück-Center for Molecular Medicine, Robert-Rössle-Str. 10, 13125 Berlin, Germany

² Institute of Chemistry and Biochemistry, Free University of Berlin, Takustr. 6, 14195 Berlin, Germany

³ Max-Planck-Institute of Molecular Genetics, Ihnestr. 73, 14195 Berlin, Germany

⁴ Leibniz-Institute for Molecular Pharmacology, Kraehmerstr. 6, 12207 Berlin, Germany

Keywords: protein, DNA, RNA, transcription regulation, crystallography

*) e-mail: heinemann@mdc-berlin.de

Interactions between proteins and DNA or RNA are not governed by simple lock-and-key mechanisms. Instead, the conformation of both the protein and the nucleic acid may be altered upon binding. In some cases, a defined three-dimensional structure non-existent in the apo state may be brought about by protein-nucleic-acid complex formation. In addition, a thermodynamic stabilization of the folded state may be observed. High-resolution crystal structures, accessible through synchrotron-based diffraction experiments, are indispensable for elucidating these structural principles which will be illustrated with three examples.

(i) Binding of Krueppel-like factor 4 (Klf4) to double-stranded (ds) DNA carrying the Klf4 target sequence leads to an induction of tertiary structure in the protein's zinc-finger domain. The spatial disposition of the three C2H2 zinc fingers of Klf4 is determined by a rigid dsDNA scaffold.

(ii) The plasmid RP4-encoded repressor KorB [1, 2] displays structural flexibility which facilitates the protein's functional cooperation with co-repressor KorA on RP4 promoters [3]. Flexible linkers between folded domains of KorB are important for its interaction with KorA over a fixed distance, but with variable geometry.

(iii) Cold shock domains interact with single-stranded (ss) DNA or RNA. The bacterial major cold shock proteins Bs-CspB [4, 5] and Bc-Csp [6, 7] bind ssDNA and ssRNA sequence-specifically and with high affinity to a conserved surface [8, 9]. The nucleic-acid single strands acquire a defined 3D structure upon protein binding. The same protein surface is used for ssDNA and ssRNA binding to the homologous cold-shock domain of the human transcription factor YB-1. YB-1 assumes spectral characteristics of a folded protein and is conformationally stabilized upon binding to a single-stranded nucleic acid.

References

- [1] H. Delbrück, G. Ziegelin, E. Lanka. U. Heinemann, "An Src homology 3-like domain is responsible for dimerization of the repressor protein KorB encoded by the promiscuous IncP plasmid RP4", *J. Biol. Chem.* **277** (2002) 4191–4198.
- [2] D. Khare, G. Ziegelin, E. Lanka. U. Heinemann, "Sequence-specific DNA binding determined by contacts outside the helix-turn-helix motif of the ParB homolog KorB", *Nature Struct. Mol. Biol.* **11** (2004) 656–663.
- [3] B. König, J. Müller, E. Lanka. U. Heinemann, "Crystal structure of KorA bound to operator DNA: insight into repressor cooperation in RP4 gene regulation", *Nucleic Acids Res.* **37** (2009) 1915–1924.
- [4] H. Schindelin, M. Herrler, G. Willimsky, M.A. Marahiel, U. Heinemann, "Overproduction, crystallization, and preliminary X-ray diffraction studies of the major cold shock protein from *Bacillus subtilis*, CspB", *Proteins Struct. Funct. Genet.* **14** (1992) 120–124.
- [5] H. Schindelin, M.A. Marahiel, U. Heinemann, "Universal nucleic acid-binding domain revealed by crystal structure of the *B. subtilis* major cold-shock protein", *Nature* **364** (1993) 164–168.
- [6] U. Mueller, D. Perl, F.X. Schmid, U. Heinemann, "Thermal stability and atomic-resolution crystal structure of the *Bacillus caldolyticus* cold shock protein", *J. Mol. Biol.* **297** (2000) 975–988.
- [7] D. Perl, U. Mueller, U. Heinemann, F.X. Schmid, "Two exposed amino acid residues confer thermostability on a cold shock protein", *Nature Struct. Biol.* **7** (2000) 380–383.
- [8] K.E.A. Max, M. Zeeb, R. Bienert, J. Balbach, U. Heinemann, "T-rich DNA single strands bind to a preformed site on the bacterial cold shock protein Bs-CspB", *J. Mol. Biol.* **360** (2006) 702–714.
- [9] K.E.A. Max, M. Zeeb, R. Bienert, J. Balbach, U. Heinemann, "Common mode of DNA binding to cold shock domains. Crystal structure of hexathymidine bound to the domain-swapped form of a major cold shock protein from *Bacillus caldolyticus*", *FEBS J.* **274** (2007) 1265–1279.

MANY-BODY INTERACTIONS IN SOLIDS STUDIED BY HIGH-RESOLUTION ARPES USING SYNCHROTRON RADIATION

Kenya Shimada *

HSRC, Hiroshima University, Kagamiyama 2-313, Higashi-Hiroshima 739-0046, Japan

Keywords: high-resolution ARPES, many-body interactions in solids

*) e-mail: kshimada@hiroshima-u.ac.jp

Angle-resolved photoelectron spectroscopy (ARPES) reveals energy-band dispersions and Fermi surfaces of solids. Recently, energy and angular (momentum) resolutions of ARPES have been improved drastically, and now one can directly observe superconducting gaps or renormalization effect (or "kink") in the energy band dispersion. It is important to evaluate magnitudes of manybody interactions such as the electron-electron and electron-phonon interactions, to understand physical properties of solids.

In this talk, based on the quantitative lineshape analyses of high-resolution ARPES spectra, we discuss coupling parameters of the electron-phonon and electron-electron interactions in the surface and bulk-derived electronic states in metals (Fe, Ni, Cu, and Al) [1-4]. We also report our new ARPES measurement system to utilize linear polarization of undulator radiation. It is very effective to selectively observe the electronic states of solids depending on the symmetry with respect to the mirror planes.

High-resolution ARPES experiments with VUV and soft X-ray range ($h\nu = 5\text{-}30$ eV and $25\text{-}300$ eV) were performed on the undulator beamlines (BL-1 and BL-9A) of a compact electron-storage ring (HiSOR) at Hiroshima University [5-7]. Clean surfaces of single crystals were obtained by repeated cycles of sputtering and annealing

for metal samples (Fe, Ni, Cu, Pd and Al) and by cleaving *in situ* for layered compounds. Samples were mounted on the 5 or 6 axes manipulator. Temperature was controlled from 300 K down to 8 K, using liquid He. Typical energy and momentum resolutions were $\Delta E = 4$ meV, $\Delta k = 0.0006 \text{ \AA}^{-1}$ at $h\nu \sim 10$ eV, $\Delta E = 15$ meV, $\Delta k = 0.01 \text{ \AA}^{-1}$ at $h\nu \sim 40$ eV.

For most of the single crystalline metals we examined (Fe, Ni, Cu, and Al), the kink structure in the energy-band dispersions was observed at the binding energy corresponding to the energy scale of the Debye temperature. We have experimentally obtained the imaginary and real parts of the self-energy due to the electron-phonon interaction. As for the magnitude of the electron-electron interaction, we have evaluated the reduction of the band width or the group velocity with respect to the theoretical one given by the band-structure calculation.

Figure 1 shows the evaluated electron-phonon and electron-electron coupling parameters (λ_{ep} and λ_{ee}). The Fermi velocity is reduced due to the many-body interactions by the renormalization factor of $Z = 1/(1 + \lambda_{ep} + \lambda_{ee})$, and the effective mass is enhanced by the factor of $Z^{-1} = 1 + \lambda_{ep} + \lambda_{ee}$. These coupling parameters are also related to the superconducting transition temperatures of solids.

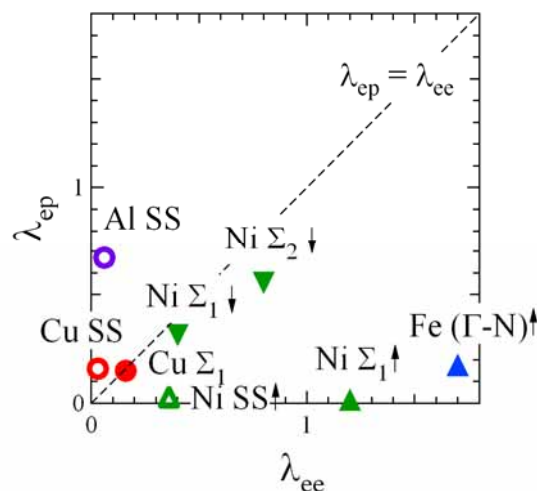


Figure 1. Evaluated coupling parameters for the electron-phonon (λ_{ep}) and electron-electron (λ_{ee}) interactions. Al SS, Cu SS and Ni SS are determined for the surface state. In the case of Fe, we determined coupling parameters along the Γ -N direction. Arrows indicate the spin direction of magnetic materials.

If several Fermi surfaces exist (multi-band systems), it is not always easy to perform detailed lineshape analyses. In order to selectively observe the Fermi surfaces or energy-band dispersions, one can utilize the dipole selection rule with a linearly polarized incident light. We have constructed new ARPES measurement system at HiSOR BL-1 which can be rotated around the light axes of linearly polarized undulator radiation. By changing the *s*- or *p*-polarization geometries, we could selectively observe the Fermi surfaces and energy-band dispersions of multi-band systems such as Pd(100), Sr₂RuO₄ and iron-based superconductors.

With tunable photon energy and tunable polarization geometries, we have more chance to quantitatively evaluate electronic structures of multi-band systems, which is very helpful to understand physical properties of novel materials.

Acknowledgments: This works have been done in collaboration with Dr. Higashiguchi, Dr. Cui, Dr. Iwasawa, Dr. Aiura, Dr. Ino, Mr. Arita, Mr. Miura, Mr. Jiang, Mr. Hayashi, Mr. Tanaka, Mr. Nakashima, Prof. Sakisaka, Prof. Kato, Prof. Oguchi, Prof. Namatame, and Prof. Taniguchi.

References

- [1] X.Y. Cui *et al.*, to be published.
- [2] M. Higashiguchi, K. Shimada, K. Nishiura, X. Cui, H. Namatame, M. Taniguchi, "Energy band and spin-dependent many-body interactions in ferromagnetic Ni (110): A high-resolution angle-resolved photoemission study", *Phys. Rev. B* **72** (2005) 214438.
- [3] M. Higashiguchi, K. Shimada, M. Arita, Y. Miura, N. Tobitaa, X. Cui, Y. Aiura, H. Namatame, M. Taniguchi, "High-resolution angle-resolved photoemission study of Ni(1 1 1) surface state", *Surf. Sci.* **601** (2007) 4005–4009.
- [4] J. Jiang, M. Higashiguchi, N. Tobida, K. Tanaka, S. Fukuda, H. Hayashi, K. Shimada, H. Namatame, M. Taniguchi, "High-resolution angle-resolved photoemission study of the Al(100) single crystal", *e-J. Surf. Sci. Nanotech.* **7** (2009) 57–60.
- [5] K. Shimada, M. Arita, Y. Takeda,; H. Fujino, K. Kobayashi, T. Narimura, H. Namatame, M. Taniguchi, "High-resolution, low-temperature photoemission spectroscopy at the hisor linear undulator beamline", *Surf. Rev. Lett.* **9**, (2002) 529–534.
- [6] M. Arita, K. Shimada, H. Namatame, M. Taniguchi, "High-resolution and low-temperature photoemission spectroscopy at the Hisor helical-undulator beamline", *Surf. Rev. Lett.* **9** (2002) 535–539.
- [7] K. Shimada, in: *Very High Resolution Photoelectron Spectroscopy*, Edited by S. Hüfner (Springer-Verlag, Berlin-Heidelberg, 2007) *Lect. Notes Phys.* **715**, Chapter. 4.

FIRST PHASE BEAMLINES AT MAX-IV

Y. Cerenious *

¹ MAX-laboratory, Lund University, Sweden

Keywords: beamline, synchrotron

*) e-mail: namer@zzz.edu.fr

The construction of the next Swedish synchrotron light source, the MAX IV, is scheduled to begin during 2010. MAX IV will be succeeding the present MAX I, II & III storage rings and it will consist of two state-of-the-art storage rings, one larger (528 m in circumference) operating at an energy of 3 GeV and one smaller (96 m in circumference) 1.5 GeV ring optimized primarily for lower photon energies. The first user activity is, however, expected to take place on the short pulse facility (SPF) which is situated on the extension of the linear accelerator. This linac is then providing both storage rings with electrons in topping up mode as well as serves as electron source for the SPF. At the SPF are the electron bunches from the linac utilized to produce short (femtoseconds) spontaneous X-ray pulses. It is expected that this facility will be in operation at a very early stage of the project. At a much later stage it also foreseen that the linac will be used as a source for a Free Electron Laser (FEL) in the UV and X-ray spectral range. Fully equipped, the new facility will be accommodating about 30 beamlines for research in a wide range of disciplines. The main radiation source of MAX IV, the 3 GeV ring [1], will be an ultra-low emittance ring for the generation of high brilliance soft- and hard X-rays. The storage ring is designed to meet the requirements of state-of-the-art insertion devices which will be installed on the nineteen available 5 m long dispersion-free straight sections. Several of the preliminary beamline studies have been based on 3.8 m long in-vacuum undulators with a peak field of 1.2 T. These will deliver an outstanding brilliance up to energies of about 30 keV.

At present (April 2010) funding is secured for a start version of MAX IV which includes the accelerators and a first beamline. In addition, a proposal has been submitted to the Knut and Alice Wallenberg (KAW) Foundation for

the financing of 5-6 additional beamlines. The beamline prioritization process has been ongoing since 2004 and first set of beamlines where proposed in the Conceptual Design Report [2] from 2006. For the KAW proposal this procedure culminated during the spring 2010 and resulted in a list of 5 beamline with the highest priority and second set of 5 beamline with only slightly lower priority. From this second group it is foreseen that one or two additional beamlines will be selected during the autumn. The prioritization process has been delicate due to the large number of considerations and the broad range of involved scientific areas. These first high profile beamlines have been selected since they among other things do take advantage of the unique performance of the MAX IV. However, they can only be considered to be a subset of the portfolio of the required beamlines for the mature MAX IV project and many important experimental techniques are missing. This includes also techniques that have a large and active user community on the existing MAX-lab and therefore should be granted the possibility for a continuation on MAX IV.

At the 10th ISSRNS meeting there will be a brief overview of the first selected high profile beamlines as well as an attempt to foresee the future process to identify the next generation of MAX IV beamlines.

References

- [1] S.C. Leemann, Å. Andersson, M. Eriksson, L.-J. Lindgren, E. Wallen, J. Bengtsson, A. Streun, Beam dynamics and expected performance of Sweden's new storage-ring light source: MAX IV, *Phys. Rev. ST Accel. Beams* **12** (2009) 200171:1–15.
- [2] Detailed Design Report on the MAX IV Facility: http://www.maxlab.lu.se/local/maxiv_ddr/MXAIV_DDR_Master_Subs/DDR_pdf_documents_100406.html.

TRENDS IN THE STATE OF THE ART STORAGE RING BASED SR SOURCES

D. Einfeld

¹ CELLS-ALBA, E-08290 Cerdanyola del Valles, Spain

Keywords: storage rings, emittance, stability

The storage ring based Synchrotron Light Sources have to deliver to the experiments and users a high quality beam, with high brilliances and small flux densities. Furthermore, the beam has to be stable in the position as well in the current. To get a high brilliance and a high flux density a small cross section of the beam is required, which is determined by a small emittance of the beam as well small beta functions in the storage ring. Both are determined by the lattice, which is given by the arrangements of magnets around the storage ring. Within

this seminar it will be explained how this is achieved in modern synchrotron light sources. Furthermore the functionality of all components used in a synchrotron light source, like bending magnets, quadrupoles, sextupoles, rf-system, vacuum system, *etc.* will be described too. A special issue is the stability of the beam, which is given by the impedance of the accelerator and the rf-system. Within the seminar it will be explained too, how modern light sources are getting a stable beam up to 500 mA.

PHOTOELECTRON SPECTROSCOPY IN STUDIES OF THE BAND STRUCTURE OF IV-VI SPINTRONIC MATERIALS

B.J. Kowalski^{1*}, **M.A. Pietrzyk**¹, **W. Knoff**¹, **R. Nietubyć**², **K. Nowakowska-Langier**²,
J. Sadowski^{1,3}, **A. Łusakowski**¹, and **T. Story**¹

¹ Institute of Physics, Polish Academy of Sciences, Al. Lotników 32/46, 02-668 Warsaw, Poland

² The Andrzej Soltan Institute for Nuclear Studies, 05-400 Swierk/Otwock, Poland

³ MAX-lab, Lund University, Box 118, SE-22100 Lund, Sweden

Keywords: IV-VI semiconductors, band structure, photoelectron spectroscopy

*) e-mail: kowab@ifpan.edu.pl

Among several groups of chemical compounds exploited in the quest for materials suitable for spintronic application diluted magnetic semiconductors have particular set of properties. Although the ferromagnetic transition temperatures observed in such systems are still markedly below the room temperature, their electronic characteristics, similar to those of the host semiconducting system, and the compatibility with electronic device technology are obvious advantages. $\text{Ge}_{1-x}\text{Mn}_x\text{Te}$, a member of the IV-VI semiconductor family, attracts considerable interest due to the relatively high Curie temperature-it can be as high as 190 K [1]. This inspired extensive investigations of this solid solution and development of technological methods in view of increase of the ferromagnetic transition temperature. The magnetic properties of systems based on IV-VI semiconductors depend on the interaction between the magnetic ions mediated by charge carriers of the host semiconductor. The interaction is successfully described by the RKKY model. As a consequence, knowledge of electronic band structure of such materials is important for understanding their transport, optical, and also magnetic properties. We present a set of experimental results, acquired by photoelectron spectroscopy, showing the electronic structure of $\text{Ge}_{1-x}\text{Mn}_x\text{Te}$ in comparison with GeTe and results of ab initio pseudopotential calculations.

Photoelectron spectroscopy with use of synchrotron radiation is the experimental technique particularly suitable for studying electronic structure of semiconductors. We used an angle-resolved photoemission spectroscopy to investigate samples of GeTe and $\text{Ge}_{0.85}\text{Mn}_{0.15}\text{Te}$. The epilayers of these two systems were grown by MBE on BaF_2 substrates. The rhombohedral structure of the layers was determined by X-ray diffraction measurements. The clean and ordered sample surface was prepared for photoemission experiments by cycles of Ar^+ ion sputtering and annealing under UHV conditions. The surface quality was assessed by LEED. In the experiments performed with use of the photoelectron spectrometer at the beamline 41 in the MAXlab synchrotron radiation laboratory of Lund University (Sweden) we acquired the data revealing the valence band structure of GeTe and

$\text{Ge}_{0.85}\text{Mn}_{0.15}\text{Te}$ along the Γ -L (in the normal-emission mode) and T-W-L (under off-normal emission conditions) (Fig. 1) directions in the Brillouin zone. The Mn related features could be identified by comparison of the results acquired for these two systems.

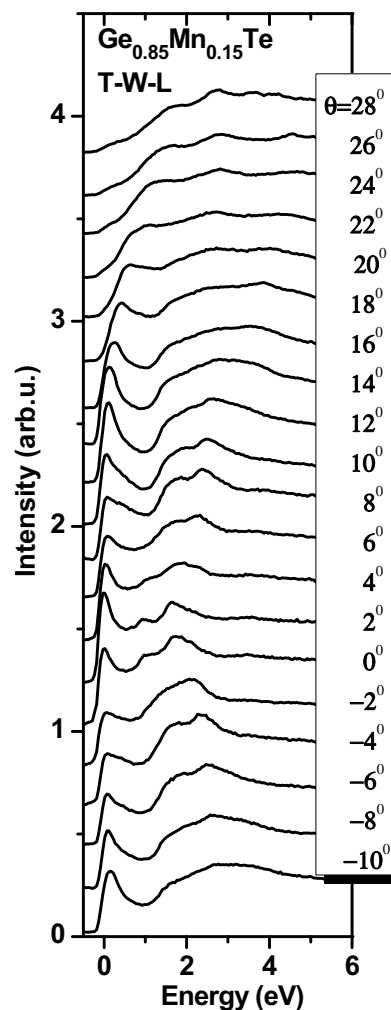


Figure 1. The set of photoemission spectra taken for $\text{Ge}_{0.85}\text{Mn}_{0.15}\text{Te}$ and corresponding to the scan of the valence band along the T-W-L direction in the Brillouin zone. The spectrum taken for normal emission corresponds to the T point.

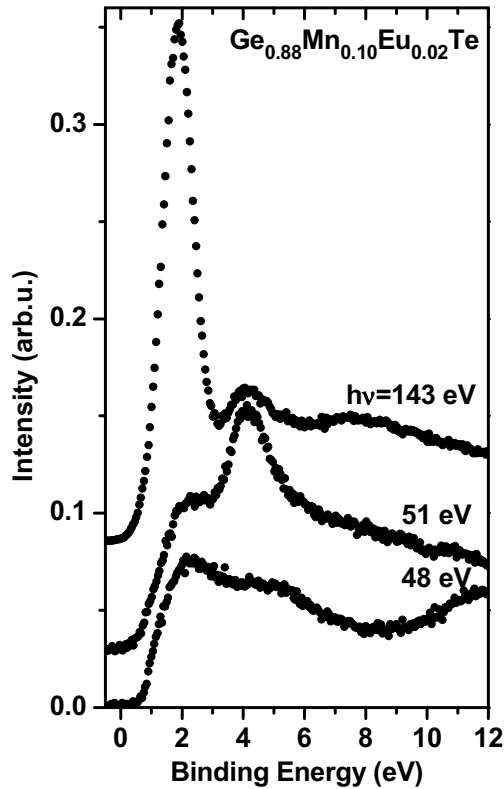


Figure 2. The resonant photoemission spectra of $\text{Ge}_{0.88}\text{Mn}_{0.10}\text{Eu}_{0.02}\text{Te}$ taken for photon energies of 48, 51, and 143 eV.

The experimental data were also compared with the results of fully relativistic LDA pseudopotential calculations of the band structure of GeTe. The primitive cell of GeTe was characterized by experimental values [2] of three parameters: lattice constant, a_0 , angle between neighbouring bonds, α , and the position of Ge atom on the diagonal of the cell, τ . Best agreement between experimental $E(k)$ diagrams and the results of calculation was obtained for the highest valence band. Additional calculations for several different sets of the parameters a_0 , α , τ showed that the shape of highest valence band depended mainly on α . The agreement between the calculations and the experiment was achieved for $\alpha <$

90° . This proved that rhombohedral distortion of the layers corresponded to that expected for bulk GeTe. Thus, we concluded that the $1\mu\text{m}$ GeTe/BaF₂ layer was relaxed and could be treated as a bulk crystal.

The electronic structure of $\text{Ge}_{1-x-y}\text{Mn}_x\text{Eu}_y\text{Te}$ was investigated by resonant photoemission spectroscopy (Fig. 2). This system is supposed to exhibit particular magnetic properties, with increased T_C , due to co-doping with Mn and Eu [3]. The spectra were taken for an epitaxial layer (grown on BaF₂ by MBE) of $\text{Ge}_{0.88}\text{Mn}_{0.10}\text{Eu}_{0.02}\text{Te}$ for the photon energies close to the intra-ion transitions Mn 3*p*-3*d* and Eu 4*d*-4*f*. Thus, the Fano resonances and enhancement of emission from Mn 3*d* and Eu 4*f* states were observed at photon energies 51 and 143 eV, respectively. A comparison of the spectra taken at the resonances and anti-resonances allowed us to reveal the Mn 3*d* and Eu 4*f* contributions to the emission from the valence band of the system. The advantages of photoelectron spectroscopy with application of synchrotron radiation are emphasized with an example of investigation of $\text{Ge}_{1-x-y}\text{Mn}_x\text{Eu}_y\text{Te}$ - a system containing both a transition metal and a rare earth element.

Acknowledgements: The authors acknowledge support by MSHE (Poland) grants N202 101 31/0749 (2006-2009), 0992/T02/2007/32 (2007-2010). The research leading to these results has also received funding from the European Community's Seventh Framework Programme (FP7/2007-2013) under grant agreement n° 226716.

References

- [1] Y. Fukuma, H. Asada, S. Miyawaki, T. Koyanagi, S. Senba, K. Goto, H. Sato, "Carrier-induced ferromagnetism in $\text{Ge}_{0.92}\text{Mn}_{0.08}\text{Te}$ epilayers with a Curie temperature up to 190 K", *Appl. Phys. Lett.* **93** (2008) 252502.
- [2] N.R. Serebryanaya, V.D. Blank, V.A. Ivdenko, "GeTe-phases under shear deformation and high pressure up to 56 GPa", *Phys. Lett. A* **197** (1995) 63–66.
- [3] W. Dobrowolski, M. Arciszewska, B. Brodowska, V. Domukhovski, V.K. Dugaev, A. Grzęda, I. Kurylyszyn-Kudelska, M. Wójcik, E.I. Slynko, "IV-VI ferromagnetic semiconductors recent studies", *Sci. Sintering* **38** (2006) 109–116.

SITE SPECIFIC XPS: STRUCTURAL AND ELECTRONIC PROPERTIES INVESTIGATED BY X-RAY STANDING WAVES

S. Thiess^{1*}, **T.-L. Lee**², **F. Bottin**³, **A. Gloskovskii**⁴, **W. Drube**¹, and **J. Zegenhagen**⁵

¹ *Hasylab, DESY, Notkestr. 85, 22607 Hamburg, Germany*

² *Diamond Light Source Ltd., Didcot, Oxfordshire, OX11 0DE, United Kingdom*

³ *CEA, DAM, DIF, 91297 Arpajon, France*

⁴ *Inst. f. Anorg. u. Analyt. Chemie, Universität Mainz, 55099 Mainz, Germany*

⁵ *European Synchrotron Radiation Facility (ESRF), 6 rue Horowitz, 38043 Grenoble, France*

Keywords: X-ray standing waves, X-ray photoelectron spectroscopy, valence band structure, XSW imaging

**) email: sebastian.thiess@desy.de*

One of the powerful tools for surface science available at synchrotron light sources is the X-ray standing wave (XSW) method [1]. Its strength is the very high spatial resolution of the order of 0.01 Å, which the technique adds to common spectroscopic methods, like fluorescence, Auger, or photoelectron spectroscopy. The XSW technique is applicable if the wavelength of the X-rays is of the order of unit cell dimensions, which corresponds to an X-ray photon energy of typically few keV.

The X-ray standing wave method utilizes the spatial intensity modulation of an X-ray interference field, which can be generated by interference via Bragg reflecting an X-ray plane wave from a single crystal. By scanning the photon energy or the angle of the incident beam through the range of Bragg reflection, the intensity maxima of the wavefield are moved by half the wavefield period over the distribution of atoms in the unit cell. The X-ray absorption profile for specific elements, indirectly detected by the fluorescence, Auger, or photoelectron signal, exhibits a shape characteristic of the elemental distribution in the unit cell. Selecting the photon energy or the incident angle of the beam within the Bragg range allows positioning the wavefield to preferentially excite atoms at specific lattice sites.

This presentation will mainly focus on two recently established applications of the XSW method:

(1) XSW valence electronic structure analysis

X-ray photoelectron spectroscopy (XPS) is an important tool for investigating the density of occupied electronic states. Combined with the XSW technique, we can obtain electronic information spatially resolved on the atomic scale: It is possible to reveal how structure and chemical composition are related to the electronic structure of a solid.

We used the XSW method to exactly identify the site within the unit cell of the wide gap (3.2 eV) semiconductor SrTiO₃ from which the electrons from a specific region of the valence band arise [2].

XSW interference fields were established in the surface region of a SrTiO₃ single crystal for the (111) and (112) Bragg reflections. The period of these interference fields reflects the spacing of the diffracting planes, which for a (111) reflection are indicated with respect to the

SrTiO₃ unit cell in Fig. 1. We can shift this wavefield by varying the X-ray energy within the range of the Bragg reflection, which occurs over a few 100 meV. In this way we can scan the planes of the interference field in a controlled way across the atomic positions. A maximum number of photoelectrons with a characteristic energy will be emitted when the maxima of the wavefield coincide with the centre of the atoms of a specific element in the unit cell, here Sr, Ti, and O. The emission will be strongly localised even for the largely delocalized valence electrons, since the dipole approximation applies, meaning that photoelectron emission occurs from the centre of the atoms exclusively.

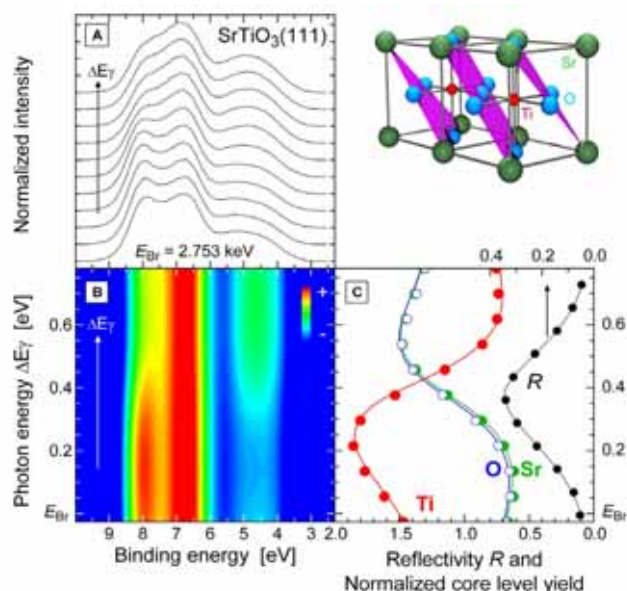


Figure 1. Two SrTiO₃ unit cells with the (111) diffraction planes indicated (top right). a) SrTiO₃ valence band for different standing wave positions while crossing the (111) reflection b) 2D colour rendering of a). c) SrTiO₃(111) reflectivity curve and simultaneously recorded Ti, O, and Sr XPS core levels emission.

For the SrTiO₃(111) reflection at around 2.753 keV, the valence band recorded for different positions of the standing wave within the unit cell exhibits a pronounced

variation in line shape, as Figs. 1a and 1b show. The simultaneously recorded reflectivity curve shown in Fig. 1c allows unambiguously determining the position of the wavefield within the unit cell of the SrTiO₃ crystal. Maxima in the O, Sr, and Ti XPS core level intensities are observed when the maxima of the wavefield are located at the position of the corresponding atoms.

Just by visible inspection of Figs. 1a and 1b and comparison with Fig. 1c one can conclude that the valence band at about 4.5 eV binding energy is dominated by emission from Sr and O sites, whereas at 8 eV binding energy the photoelectrons mainly arise from Ti sites. With respect to the (111) reflection, Sr and O are located on a common plane. However, utilising the (112) reflection, the contributions from the Sr and O sites can be disentangled.

The result of a quantitative XSW analysis is shown in Fig. 2 compared with the results of *ab initio* density functional theory (DFT) calculations in the local density approximation (LDA). The agreement is excellent. It should be noted that the density of states, which is determined by theory, must be weighted for comparison with experiment with the X-ray cross sections. This must be done for the individual elements and angular momentum states. As *a priori* unknown values for the solid state, valence band cross sections are a further important result of this study.

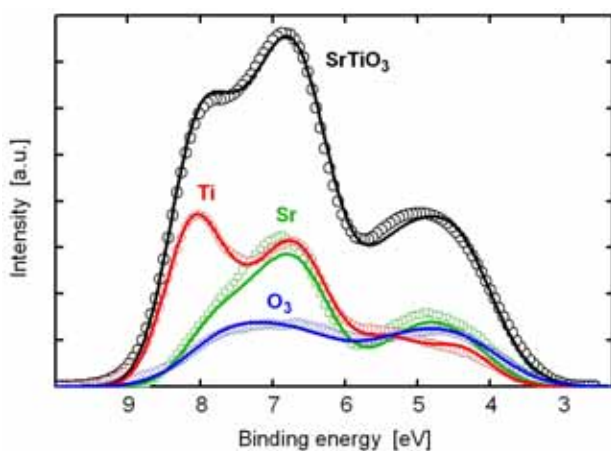


Figure 2. SrTiO₃ valence band spectrum and the determined partial contributions arising from the Ti, Sr, and O sites. Symbols: experimental results, lines: DFT/LDA calculations, weighted with cross sections.

(2) XSW real space imaging

The early stages of epitaxial growth processes can comprise complicated nucleation mechanisms. This can in particular be the case for multi-elemental compounds with a complex unit cell, such as high-temperature superconductors.

We employed XSW real space imaging for studying the atomic structure of 0.5 layers of YBa₂Cu₃O_{7-δ} deposited on the (001) surface of a SrTiO₃ single crystal by pulsed laser deposition. XSW core level photoelectron yield was recorded for all 6 elements present in film and substrate for 7 different Bragg reflections, each providing

amplitude *and* phase of one Fourier coefficient of the elemental atomic distribution function. Assuming a 4-fold in-plane symmetry of the film yielded 29 Fourier coefficients. By direct Fourier inversion, a three-dimensional real space image of the atomic distribution for each of the elements was reconstructed, as shown in Fig. 3.

The study has contributed towards the understanding of the nucleation mechanism of a heteroepitaxially grown complex material: The images confirmed the formation of a (Y/Ba)CuO₃ mixed perovskite precursor phase prior to the formation of the YBa₂Cu₃O_{7-δ} phase during the growth of the first monolayer of the film.

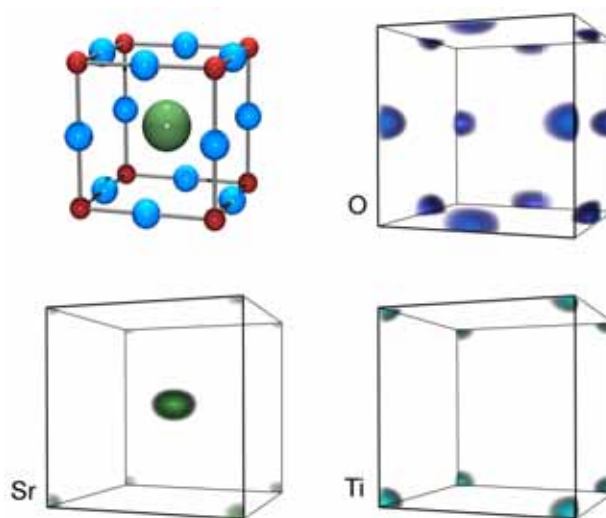


Figure 3. Sketch of the unit cell of SrTiO₃ (top left) and 3-dimensional images of the Sr, Ti, and O atomic distributions reconstructed from XSW data recorded from a SrTiO₃ single crystal covered with 0.5 monolayers YBa₂Cu₃O_{7-δ}.

A hard X-ray XPS (HAXPES) instrument suitable for XSW studies is currently under commissioning at undulator beamline P09 at the new 6 GeV storage ring PETRA III at DESY in Hamburg, Germany. Two sets of focussing mirrors (the second yet to be installed) will allow beam spot sizes of about 2 × 2 microns on the sample surface. A SPECS Phoibos 225 spectrometer with an operational range of photoelectron energies up to 15 keV allows XSW experiments for high Bragg reflection orders of the sample.

References

- [1] J. Zegenhagen, "Surface structure determination with X-ray standing waves", *Surf. Sci. Rep.* **18** (1993) 199.
- [2] S. Thiess, T.-L. Lee, F. Bottin, J. Zegenhagen, "Valence band photoelectron emission of SrTiO₃ analyzed with X-ray standing waves", *Solid State Commun.* **150** (2010) 553.
- [3] J. Zegenhagen, B. Detlefs, T.-L. Lee, S. Thiess, H. Isern, L. Petit, L. André, J. Roy, Y. Mi, I. Joumard, "X-ray standing waves and hard X-ray photoelectron spectroscopy at the insertion device beamline ID32", *J. Electron Spectrosc. Relat. Phenom.* **178-179** (2010) 258.

THE SHAPE ANISOTROPY OF THE MnSb INCLUSIONS FORMED IN GaSb MATRIX AS PROBED BY XMCD

K. Lawniczak-Jablonska^{1*}, **A. Wolska**¹, **M.T. Klepka**¹, **J. Gosk**^{2,3}, **A. Twardowski**²,
D. Wasik², **A. Kwiatkowski**², and **J. Sadowski**^{1,4}

¹*Institute of Physics PAS, al. Lotnikow 32/46, 02-668 Warsaw, Poland*

²*Institute of Experimental Physics, University of Warsaw, Hoza 69, 00-681 Warsaw, Poland*

³*Faculty of Physics, Warsaw University of Technology, Koszykowa 75, 00-662 Warsaw, Poland*

⁴*Lund University, MAX-Lab, Lund, SE-221 00, Sweden*

Keywords: XMCD, MnSb inclusions, shape anisotropy,

**) e-mail: jablo@ifpan.edu.pl*

The formation of the inclusions inside of the matrix leads to the breaking of the symmetry and bonding at the interface between the matrix and inclusions. Magnetized grains produce magnetic charges or poles at the surface. This surface charge distribution, is itself another source of a magnetic field, which acts in opposition to the magnetization and is called the demagnetizing field. The resulted magnetization depends on the inclusions shape and exhibits the shape anisotropy. *E.g.* in the case of inclusions with the shape of a long thin needle the demagnetizing field is smaller if the magnetization is along the long axis than if it is along one of the short axes. This can produce an easy axis of magnetization along the long axis. A sphere, on the other hand, has no shape anisotropy. For the grain, smaller than about 20 microns, shape anisotropy is the dominant form of magnetic anisotropy. In larger sized particles, shape anisotropy is less important than magnetocrystalline anisotropy which is an intrinsic property of a ferrimagnet and is independent of grain size and shape. The anisotropy effects can be studied by X-ray magnetic circular dichroism (XMCD) technique [1]. The XMCD possess several advantages over the traditional magnetic techniques. The most important is the element specific, quantitative separation and determination of spin and orbital magnetic moment. Moreover, in the well oriented samples by changing the angle between magnetic field, circularly polarized X-ray and sample the anisotropy of spin and orbital magnetic moments can be studied. This possibility was first suggested by Bruno [2] in the case of transition metal thin films.

Usually it is implicitly assumed that the dichroism intensities do not depend on the sample orientation relative to the X-ray wave vector or polarization. This is rather good approximation for material which have high symmetry lattices (fcc, bcc or hcp) and hence the bonding and charge distribution is rather isotropic. Nevertheless, this assumption does not hold for the thin l

ayers or nanostructures with the different dimensions in the in-plane and out-of-plane axis.

In the presented paper we demonstrate the first attempt to measure the anisotropy effects in the samples with MnSb hexagonal inclusions formed inside the GaSb matrix and in MnSb thick layers grown on GaAs substrates oriented into two crystallographic directions (111)B and (100).

The samples were characterized by several methods. The morphology of surface was studied by AFM and MFM and it was shown that inclusions ferromagnetic at the room temperature with in plain dimensions from 200 to 500 nm and height up to 70 nm were formed. The example of the surface morphology in the studied samples is shown in Fig. 1. The SQUID measurement showed the ferromagnetic behavior of the investigated samples starting from the helium temperatures till the RT, see Fig. 2.

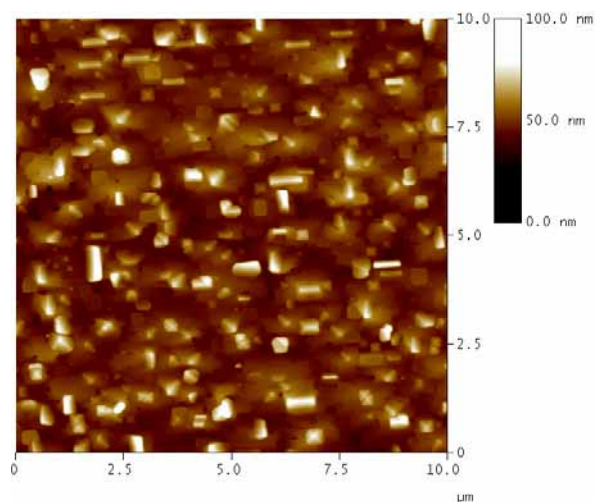


Figure 1. The example of surface morphology measured by AFM for HT5 sample.

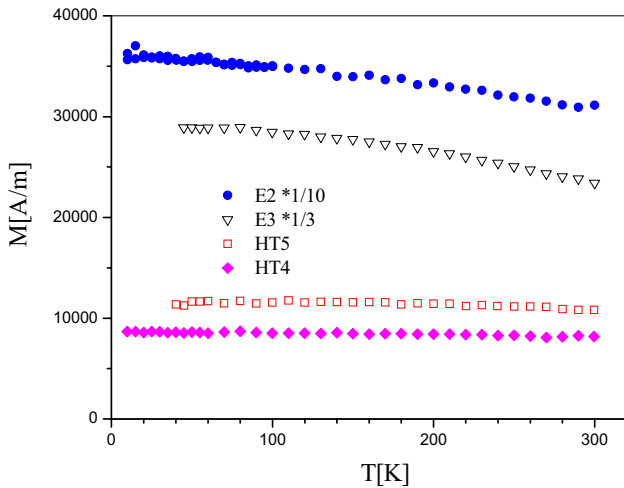


Figure 2. The temperature dependence of the magnetisation in the samples E2 and E3 grown on the GaAs(111) substrate and HT4 and HT5 grown on GaSb substrate. The magnetic field was in plane of samples. E2, E3 and HT4 were measured under the field of 0.33 T and HT5 under 0.05 T.

The EXAFS studies confirmed that all Mn atoms in these samples are located in the MnSb hexagonal inclusions. The XMCD of the samples was measured at the MAXLAB, Lund University at the D1011 and I1011 stations. The XMCD spectra were recorded in remanence after pulse magnetization by 0.035 T external magnetic field, oriented parallel to the X-ray propagation in the total electron yield mode and at liquid nitrogen temperature.

The measurements were performed at several angles with respect to the surface normal of the sample. The example of the XMCD signal for thick MnSb layer as measured at 45 and 10 degree in respect to the sample surface is shown in Fig. 3.

The XMCD was strongly dependent on the angle of measurement in thick MnSb layers as well as in the case of MnSb inclusions. Moreover, it depends on the morphology of formed inclusions which in turn depends on the substrate and growth conditions.

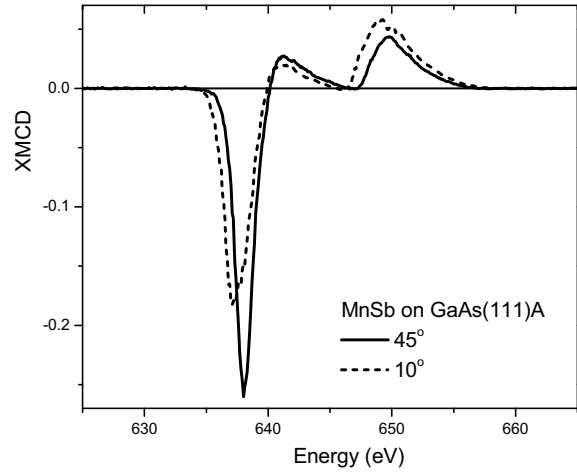


Figure 3. The XMCD signal for MnSb thick layer measured at LN for 45 and 10 degree in respect to the sample surface.

Acknowledgments: This work was supported by national grant of Ministry of Science and High Education N202-052-32/1189. The research leading to these results has received funding from the European Community's Seventh Framework Programme (FP7/2007-2013) under grant agreement n° 226716.

References

- [1] J. Stoehr, "Exploring the microscopic origin of magnetic anisotropy with x-ray magnetic circular dichroism (XMCD) spectroscopy", *J. Magn. Magn. Mater.* **200** (1999) 470–497.
- [2] P. Bruno, "Tight-binding approach to the orbital magnetic moment and magnetocrystalline anisotropy of transition metal monolayers", *Phys. Rev. B* **39** (1989) 865–868.

APPLICATIONS OF SAXS AND GISAXS IN BIONANOTECHNOLOGY

H. Amenitsch *

Institute of Biophysics and Nanosystems Research, Schmiedlstr. 6, A-8042 Graz, Austria

Keywords: small angle scattering, grazing incidence, self-assembly, fast chemical reactions

**) e-mail: amenitsch@elettra.trieste.it*

Small Angle X-ray Scattering (SAXS) has developed as a powerful working horse in almost all synchrotrons in the world. Its fundamental strength is the capability of *in situ* investigations for all states of matter - gas, liquid and solid – as well as probing materials in bulk, surface sensitive (grazing incidence SAXS) or with high local spatial resolution (scanning SAXS).

This presentation should summarize the current state of the art investigating self-assembly processes *i.e.* watching molecules *in situ* to form nano(bio)materials or the *in-situ* response of supramolecular structures to physical/chemical parameter changes as temperature, stretch *etc.* Some highlights of the current research covering the fields of life sciences till nanomaterials will be discussed and will include the above mentioned application areas of the SAXS and GISAXS technique. The examples will range – to name just a few – from self-assembly of nanotubes in form of helical ribbons [1], *in-situ* study of the formation of mesoporous materials on surfaces as well as in solution [2], to self-assembly of nanoparticles [3].

At the same time, for advanced studies on nanomaterials, the integration of *in-situ* chemical and physical perturbation techniques into the experimental set-up is a prerequisite. Some sophisticated instrumental developments like ultrafast mixers with μ s-resolution

[4,5], *in situ* aerosol reactors [6], or optical tweezers [7] are presented with adequate examples.

References

- [1] C.V. Teixeira, *et al.*, "Formfactor of a N-layered helical tape and its application to nanotubeformation of Hexa-peri-hexabenzocoronene based molecules", *J. Appl. Crystallogr.* (2010), accepted.
- [2] D. Grosso, *et al.*, "Periodically ordered nanoscale islands and mesoporous films composed of nanocrystalline multimetallic oxides", *Nature Mater.* **3** (2004) 787.
- [3] R. Viswanatha, *et al.*, "Growth mechanism of cadmium sulfide nanocrystals", *J. Phys. Chem. Lett.* **1** (2010) 308.
- [4] B. Marmioli, *et al.*, "Free jet micromixer to study fast chemical reactions by small angle X-ray scattering", *Lab on Chip* **9** (2009) 2063.
- [5] W. Schmidt, *et al.*, "Accessing ultrashort reaction times in particle formation with SAXS experiments: ZnS precipitation on the microsecond time scale", *JACS* (2010) 10.1021/ja101519z.
- [6] I. Shyjumon, *et al.*, "Novel in situ setup to study the formation of nanoparticles in the gas phase by small angle x-ray scattering", *Rev. Sci. Instrum.* **79** (2008) 43905.
- [7] D.Cojoc, *et al.*, "Scanning x-ray microdiffraction of optically manipulated liposomes", *Appl. Phys. Lett.* **91** (2008) 234107.

STRUCTURAL STUDIES OF BIOLOGICAL MACROMOLECULES IN SOLUTION USING SYNCHROTRON SMALL-ANGLE X-RAY SCATTERING

M. Roessle^{*} and D.I. Svergun

European Molecular Biology Laboratory, Hamburg Outstation c/o DESY, Notkestr. 85, D22603 Hamburg, Germany

Keywords: x-ray scattering, quaternary structure, remote experiments

**) e-mail: svergun@embl-hamburg.de*

Small-angle X-ray scattering (SAXS) experiences a renaissance in the studies of solutions of biological macromolecules. SAXS is a low resolution (1-2 nm) structural method, which is applicable to native states of macromolecules in solution providing information about the overall structure and structural transitions. The method covers a broad range of sizes, from individual macromolecules to multi-domain proteins and large macromolecular assemblies. High brilliance synchrotron sources and novel data analysis methods [1] significantly enhanced resolution and reliability of structural models provided by the technique. Emerging automation of the synchrotron SAXS experiment, data processing and interpretation make solution SAXS a streamline tool for large scale structural studies in molecular biology. The method provides low resolution macromolecular shapes *ab initio* and is readily combined with other structural and biochemical techniques in multidisciplinary studies. In particular, rapid validation of predicted or experimentally obtained high resolution models in solution, identification of biologically active oligomers and addition of missing fragments to high resolution models are possible. For macromolecular complexes,

quaternary structure is analyzed by rigid body movements/rotations of individual subunits. Recent developments made it possible also to quantitatively characterize flexible macromolecular systems, including intrinsically unfolded proteins. The novel methods will be illustrated by advanced applications of synchrotron SAXS to solutions of biological macromolecules. Possibilities of remote and high throughput operation using synchrotron radiation combined with automated sample changers and data analysis pipelines [2] will be presented.

References

- [1] M.V. Petoukhov, D.I. Svergun, "Analysis of X-ray and neutron scattering from biomacromolecular solutions," *Curr. Opin. Struct. Biol.* **17** (2007) 562–571.
- [2] A.R. Round, D. Franke, S. Moritz, R. Huchler, M. Fritsche, D. Malthan, R. Klaering, D.I. Svergun and M. Roessle, "Automated sample-changing robot for solution scattering experiments at the EMBL Hamburg SAXS station X33", *J. Appl. Crystallogr.* **41** (2008) 913–917..

SAXS STUDIES OF THE MUSCLE CELL TO IDENTIFY THE FORCE-GENERATING MYOSIN MOLECULES

M. Reconditi^{1*}, **G. Piazzesi**¹, **M. Irving**², and **V. Lombardi**¹

¹ *Laboratory of Physiology, Department of Evolutionary Biology, University of Florence, 50019 Sesto Fiorentino, Italy*

² *Randall Division of Cell and Molecular Biophysics, King's College London, London, U.K.*

Keywords: myosin, muscle

**) e-mail: massimo.reconditi@unifi.it*

In the X-ray diffraction pattern from skeletal muscle the third order myosin-based meridional reflection, M3, originates from the axial repeat of myosin heads along the thick filament. Changes in the intensity (I_{M3}), spacing (S_{M3}), and fine structure (R_{M3}) of the M3 reflection in contracting skeletal muscle at full filament overlap (~2.1 μm sarcomere length) have been measured in many different protocols [1-7]. These studies showed the presence of a fixed periodic mass that is insensitive to filament sliding and attributed to detached myosin heads, with their center of mass axially displaced from the center of mass of attached heads by ca 1 – 2 nm toward the center of the sarcomere. The estimates of the contribution of the detached heads to I_{M3} relative to that of the attached heads ranged between 37% [6] and 100% [7]. Here we have used the dependence of the number of attached and detached heads on the degree of overlap between the actin and myosin filaments during isometric contractions at different sarcomere length (sl) to modulate the M3 reflection parameters [8] and to constrain the relative contribution to I_{M3} of detached heads. Final refinement in the selection of the model is provided by the constraint represented by the I_{M3} and R_{M3} response to a shortening step of 1 – 2 nm that shifts the center of mass of the attached heads with respect to that of the detached heads [1,6,9]. We conclude that in isometric contraction at full filament overlap the contribution to I_{M3} of detached myosin heads is no more than 40% of that of the attached heads and is mostly provided by the detached (partner) heads of the myosin dimers with one head attached to actin.

Acknowledgements: This work was supported by MiUR Italy, MRC UK, ESRF, EMBL.

References

- [1] G. Piazzesi *et al.*, "Mechanism of force generation by myosin heads in skeletal muscle", *Nature* **415** (2002) 659–662.
- [2] M. Reconditi *et al.*, "The myosin motor in muscle generates a smaller and slower working stroke at higher load", *Nature* **428** (2004) 578–581.
- [3] M. Linari *et al.*, "The structural basis of the increase in isometric force production with temperature in frog skeletal muscle", *J. Physiol.* **567** (2005) 459–469.
- [4] H. Huxley *et al.*, "X-ray interference studies of crossbridge action in muscle contraction: evidence from quick releases", *J. Mol. Biol.* **363** (2006) 743–761.
- [5] H. Huxley *et al.*, "X-ray interference studies of crossbridge action in muscle contraction: evidence from muscles during steady shortening", *J. Mol. Biol.* **363** (2006):762–772.
- [6] E. Brunello *et al.*, "Skeletal muscle resists stretch by rapid binding of the second motor domain of myosin to actin", *PNAS* **104** (2007) 20114–20119.
- [7] G. Piazzesi *et al.*, "Skeletal muscle performance determined by modulation of number of myosin motors rather than motor force or stroke size", *Cell* **131** (2007) 784–795.
- [8] M. Linari *et al.*, "Interference fine structure and sarcomere length dependence of the axial x-ray pattern from active single muscle fibers", *PNAS* **97** (2000) 7226–7231.
- [9] G. Piazzesi *et al.*, "Changes in the x-ray diffraction pattern from single, intact muscle fibers produced by rapid shortening and stretch", *Biophys. J.* **68** (1995) 92s–96s.

DETERMINATION OF ELECTRON RADIAL DISTRIBUTION FUNCTION FOR LIQUID CYCLOHEXYLAMINE BY X-RAY DIFFRACTION

H. Drozdowski^{*}, K. Nowakowski, and Z. Błaszczak

Department of Optics, Faculty of Physics A, Mickiewicz University, ul. Umultowska 85, 61-614 Poznań, Poland

Keywords: electron-density radial-distribution function, liquid state

**) e-mail: riemann@amu.edu.pl*

An angular distribution of X-ray radiation scattered in liquid cyclohexylamine $C_6H_{11}-NH_2$ was measured. The electron-density radial-distribution function was calculated. Structural parameters, the mean distances between the neighbouring molecules as well as the coordination numbers were found.

X-ray scattering in liquid cyclohexylamine (melting point 256 K, boiling point 406 K), at a temperature of 293 K, was measured by applying MoK_{α} radiation, $\lambda = 0.71069 \text{ \AA}$, monochromatized by a graphite crystal. The scattered intensity distribution was measured by a goniometer HZG-3 for the angles $3^{\circ} < \theta < 60^{\circ}$, where 2θ is the scattering angle. Small-angle scattering ($0 < \theta < 3^{\circ}$) results were extrapolated to the origin of the coordinate system using a second-order function.

Shapes of the scattered intensity were analyzed subsequent to correction for polarization of the monochromatic radiation and absorption in plane samples and after normalization to electron units (Fig. 1).

The method of Warren *et al.* [1] was applied to obtain the electron density radial distribution function. The most probable intermolecular distances were found from the positions of the maxima of the radial distribution function (Fig. 2), whereas the corresponding coordination numbers were obtained from the area delimited by these maxima.

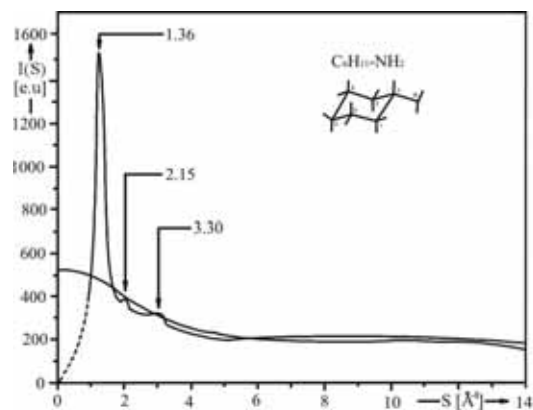


Figure 1. Normalized, experimental curve of angular distribution of X-ray scattered intensity of liquid cyclohexylamine.

The mean distance calculated for two molecules of cyclohexylamine in the antiparallel arrangement between the nitrogen atoms of the functional groups (NH_2) is 7.30 \AA (Fig. 3).

References

- [1] H. Drozdowski, "Local structure and molecular correlations in liquid 1-methylnaphthalene at 293 K", *Chem. Phys. Lett.* **351** (2002) 53–60.

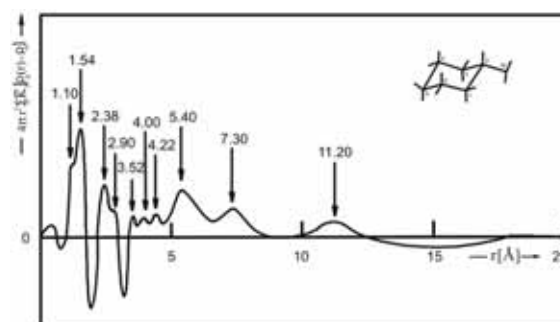


Figure 2. Electron density radial distribution function of liquid cyclohexylamine.

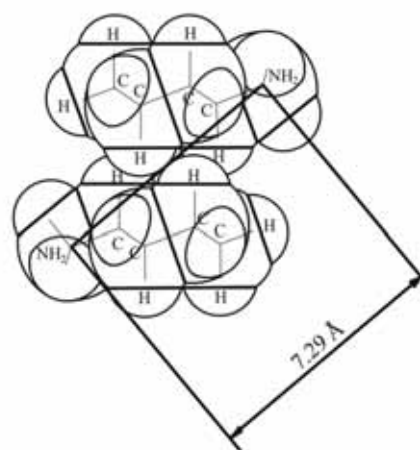


Figure 3. Model of probable conformation of molecules in liquid cyclohexylamine. The antiparallel arrangement of molecules.

X-RAY ABSORPTION AND EMISSION SPECTROSCOPY OF RARE-EARTH MATERIALS

K.O. Kvashnina^{1*}, **S.M. Butorin**², **A. Kotani**^{3,4}, and **P. Glatzel**¹

¹ European Synchrotron Radiation Facility (ESRF), BP22, 6 rue Jules Horowitz, 38043 Grenoble, France

² Department of Physics and Astronomy, Uppsala University, Box 516, S-751 20 Uppsala, Sweden

³ Photon Factory, High Energy Accelerator Research Organization, 1-1 Oho, Tsukuba, Ibaraki 305-0801, Japan

⁴ RIKEN SPring-8 Center, 1-1-1 Kouto, Sayo, Hyogo 679-5148, Japan

Keywords: XAS, RLXS, rare-earths, spectroscopy

*) e-mail: kristina.kvashnina@esrf.fr

Hard X-ray absorption spectroscopy (XAS) is a widely used technique at synchrotron radiation sources for analyses of the electronic structure of materials. There are several methods for measuring the variation of the absorption coefficient as a function of photon energy. Figure 1a shows schematically the experimental setup for XAS in transmission mode and medium energy

resolution fluorescence mode (using an energy dispersive X-ray detector). In conventional XAS experiments the large core-hole lifetime broadening, which is around 4 eV for rare earths L₃ edges give rise to broad spectral features. A spectral narrowing below the natural core-hole lifetime width can be achieved by employing an X-ray emission spectrometer [1] (cf. Fig. 1b).

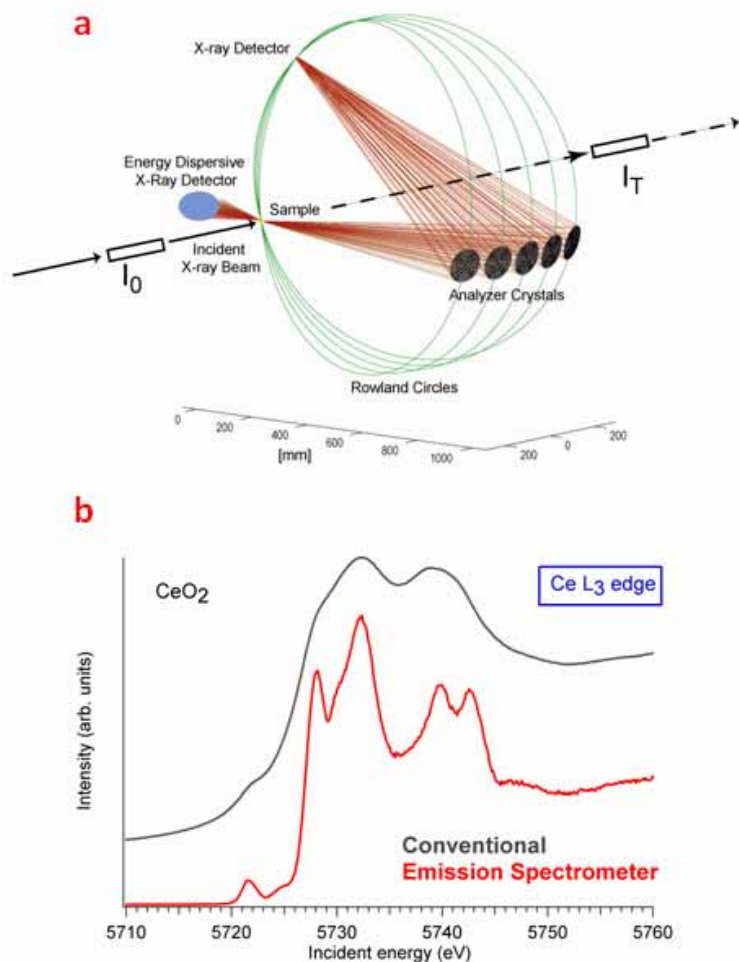


Figure 1. a) Schematic experimental setup for XAS in transmission (I_T), medium (energy dispersive X-ray detector) and high energy resolution fluorescence detection mode; b) standard (grey) and high energy resolution XAS (red) of CeO₂ at the Ce L₃ edge.

Figure 1a shows a schematic drawing of the X-ray emission spectrometer with five spherically bent crystal analyzers installed at beamline ID26 of the European Synchrotron Radiation Facilities (ESRF) in Grenoble. This contribution will provide an overview of the possible spectroscopic techniques, such as resonant inelastic X-ray scattering (RIXS) and high-energy-resolution fluorescence detected (HERFD) absorption spectroscopy [2] that become available using such an experimental setup.

We have studied the electronic structure of cerium, ytterbium and uranium systems in different oxidation states by means of HERFD and RIXS. In case of the latter we observed transitions between core levels as well as valence band excitations. The experimental spectral features were characterised using a variety of theoretical codes including the LDA+*U* approximation within DFT [3], atomic multiplet theory [4] and full multiple scattering FEFF [5]. We found that the experimental results for valence band RIXS in some cases can be modelled using a surprisingly simple theoretical model that uses the ground state electron density. We furthermore show how valence band RIXS can be used to

assess the effect of the core hole in inner-shell spectroscopy. We demonstrate that RIXS can provide important information for applied, environmental and fundamental science.

References

- [1] K. Hämäläinen, D.P. Siddons, J.B. Hastings, L.E. Berman, "Elimination of the inner-shell lifetime broadening in x-ray-absorption spectroscopy", *Phys. Rev. Lett.* **67** (1991) 2850–2853.
- [2] P. Glatzel, U. Bergmann, "High resolution 1s core hole X-ray spectroscopy in 3d transition metal complexes - electronic and structural information", *Coord. Chem. Rev.* **249** (2005) 65–95.
- [3] V.I. Anisimov, J. Zaanen, O.K. Andersen, "Band theory and Mott insulators - Hubbard-U instead of Stoner-I," *Phys. Rev. B* **44** (1991) 943–954.
- [4] R.D. Cowan, *The theory of atomic structure and spectra*. (University of California Press, Berkeley, 1981).
- [5] A.L. Ankudinov, B. Ravel, J.J. Rehr, S.D. Conradson, "Real-space multiple-scattering calculation and interpretation of x-ray-absorption near-edge structure", *Phys. Rev. B* **58** (1998) 7565–7576.

MICROCHEMICAL AND STRUCTURAL REGULAR VARIABILITY OF APATITES IN "OVERBUILT" ENAMEL AND DENTIN OF HUMAN MOLAR TEETH

A. Kuczumow^{1*}, J. Nowak¹, and R. Chalas²

¹ Department of Chemistry, Lublin Catholic University, 20-718 Lublin, Poland

² Department of Conservative Medicine, Lublin Medical University, 20-081 Lublin, Poland

Keywords: apatite, X-ray fluorescence, Raman microscopy, crystallographic unit cells

* e-mail: kuczon@kul.lublin.pl

The vast program of making linear elemental profiles along the cross sections of molar teeth was undertaken. The aim was to recognize the structural changes in apatites forming both the enamel and dentin of human tooth. All the trends in linear profiles were strictly determined, in the enamel zone being the increasing or decreasing curves of exponential character if one starts from the tooth surface towards the dentin-enamel junction (DEJ). The results were exaggerated if the detected material was divided in arbitrary way on the prevailing "core" enamel (~93.5% of the total mass) and remaining "overbuilt" enamel. The material in "core" enamel was fully stable and with clearly determined chemical and mechanical features. Totally different and dynamic situation was in the "overbuilt enamel". Here, Ca, P, Cl and F profiles present the decaying while Mg, Na, K and CO₃²⁻ the growing distribution curves. Close to the surface of the tooth, the mixture of hydroxy-, chlor- and fluorapatite is formed, much more resistant than the rest of the enamel. On passing towards the DEJ, the apatite is enriched in Na, Mg and CO₃²⁻. 3 of 6 phosphate groups were substituted with carbonate groups in this location. In parallel, the Mg is associated with the hydroxyl groups around hexad axes. The mechanisms of exchange reactions were established. The crystallographic structures of new phases located close to DEJ were proposed (Fig.1).

In dentin zone, the variability of elemental profiles is different, with most characteristic changes in Mg and Na concentrations. The Mg content increases even more on passing deeper in dentin, while Na contents decreases along this route. Na concentration reaches maximum very close to DEJ zone. It testifies that the dentin deeply inside the tooth involves more and more hydroxyl groups in pair with decreasing contents of carbonates.

In reality, this evolution of the apatite material in maturing tooth occurs from the deep regions of dentin through DEJ up to internal and finally external layers of enamel.

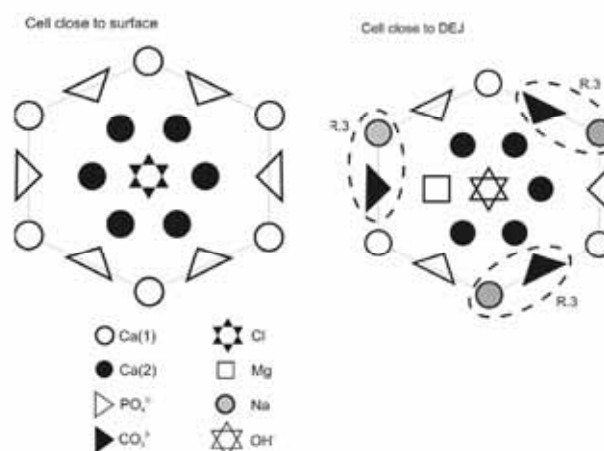


Figure 1. Proposed structures of tooth apatite unit cells: a) close to surface; b) close to DEJ, plane a×a.

References

- [1] J.L. Cuy, A.B. Mann, K.J. Livi, M.F. Teaford, T.P. Weihs, "Nanoindentation mapping of the mechanical properties of human molar tooth enamel", *Archs. Oral Biol.* **47** (2002) 281–291.
- [2] J.C. Elliott, R.M. Wilson, S.E.P. Dowker, "Apatite structures", *Adv. X-ray Anal.* **45** (2002) 172–181.
- [3] J.A. Weatherell, C. Robinson, A.S. Hallsworth, "Variations in the chemical composition of human enamel", *J. Dent. Res.* **53** (1974) 180–192.
- [4] B. Jälevik, H. Odelius, W. Dietz, J.G. Norén, "Secondary ion mass spectrometry and X-ray microanalysis of hypomineralized enamel in human permanent first molars", *Archs Oral Biol.* **46** (2001) 239–247.

TOP METAL CONTACT ON AN ORGANIC FILM: INDIUM ON COPPER PHTHALOCYANINE

J. Ivančo^{1,2*}, **D. Karnaushenko**², **P. Schäfer**², **D.R.T. Zahn**², **W. Braun**³, and **E. Majková**¹

¹ Institute of Physics, Slovak Academy of Sciences, SK-845 11 Bratislava, Slovak Republic

² Institute of Physics, Chemnitz University of Technology, D-09107 Chemnitz, Germany

³ Helmholtz-Zentrum Berlin für Materialien und Energie GmbH, D-12489 Berlin, Germany

Keywords: photoemission spectroscopy, organic thin films, metal clusters

*) e-mail: jan.ivanco@savba.sk

Properties of organic-based electronic devices are in a large extent affected by their metal-organic contacts. Thus, understanding the fundamental processes which occur at metal-organic interfaces is of great importance.

We have studied *in situ* the chemical and electronic structure of indium contact to copper phthalocyanine (CuPc) thin films by photoemission. Both core levels photoemission spectra (In 4*d*, C 1*s*, N 1*s*, O 1*s*) and valence band spectra were probed during the initial stages of the contact formation. The In 4*d* core level revealed a high-binding energy shifted component (Fig. 1, left panel) emerging at the lowest indium coverage. With the increased indium nominal thickness, the component diminishes, while the later emerging metallic component dominates. Such behaviour suggests a formation of a reactive layer at the indium-CuPc interface buried below a metallic indium [1].

However, the would-be reactive component is less pronounced if the system is probed with the higher photon energy of 335 eV (right panel), *i.e.* resulting in the larger probing depth. This suggests that the reactive component is not associated with the buried indium-CuPc interface, but with the surface of the probed system. The inconsistency is explained by the formation of inert indium nanoclusters residing on the CuPc surface [2]. Metal nanoclusters may display non-metallic behaviour in the photoemission process, *i.e.* their spectra may shift toward high binding energy due to the positive charge left on the cluster in the photoemission final state (*e.g.* Ref. [3]). The effect is tantamount to the chemical shift induced by chemical bonding.

New orbitals formed upon the indium deposition below the Fermi level – *i.e.* in the gap of the organic semiconductor (Fig. 2), and therefore commonly referred to as gap states – are supposed to reflect the reacted interface as well [1]. We show that the newly formed orbitals also come out from indium nanoclusters residing at the CuPc surface and lacking metallicity; their photoemission signal is simply superposed to the photoemission signal of the CuPc.

Acknowledgements: We acknowledge the support of HZB staff at the electron storage ring BESSY II and the financial support from the BMBF (project No. 05ES7BYA) and the SAV (project No. FM-EHP-2008-01-01).

References

[1] V.Y. Aristov, O.V. Molodtsova, V.M. Zhilin, D.V. Vyalikh, M. Knupfer, "Chemistry and electronic properties of a

metal-organic semiconductor interface: In on CuPc", *Phys. Rev. B* **72** (2005) 165318.

[2] J. Ivanco, T. Toader, A. Firsov, M. Brzhezinskaya, M. Sperling, W. Braun, D.R.T. Zahn, "Indium on copper phthalocyanine thin film: not a reactive system", *Phys. Rev. B* **81** (2005) 115325.

[3] G.K. Wertheim, S.B. DiCenzo, S.E. Youngquist, "Unit charge on supported gold clusters in photoemission final state", *Phys. Rev. Lett.* **51** (1983) 2310-2313.

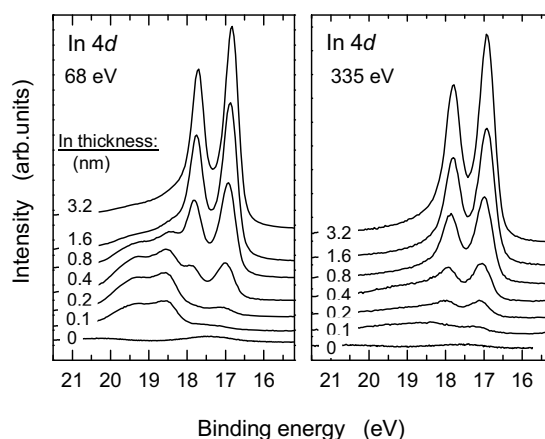


Figure 1. Evolution of the In 4*d* core level photoemission spectra recorded at photon energy of 68 eV and 335 eV upon step-like indium growth on the CuPc layer. The nominal indium thicknesses are given next to the spectra.

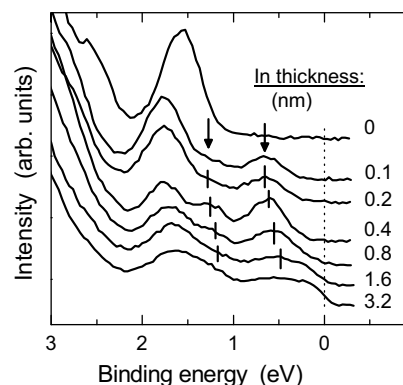


Figure 2. Evolution of the upper region of the valence band photoemission spectra recorded at a photon energy of 55 eV upon stepwise increased indium coverage. The ticks indicate new orbitals.

CONFINEMENT-INDUCED STRUCTURAL CHANGES OF LITHIUM AND SODIUM IN NANO-POROUS SILICA GLASS

A. Ghaffar^{1*}, W. Pichl¹, G. Krexner¹, and I. Zizak²

¹ University of Vienna, Faculty of Physics, Boltzmannng.5, A-1090 Vienna, Austria

² Helmholtz-Zentrum Berlin für Materialien und Energie, Albert-Einstein Strasse 15, D-12489 Berlin, Germany

Keywords: Alkali metals, geometrical confinement, nanoporous glass, synchrotron x-ray diffraction, close-packed structures

*) e-mail: abdul.ghaffar@univie.ac.at

At ambient conditions, all alkali metals have body-centered cubic structure. At low temperatures, lithium and sodium undergo martensitic transitions to closed-packed phases at 78 K and 35 K, respectively. Their structures are highly faulted but predominantly 9R for Li while in Na also a substantial fraction of HCP develops. At high pressure, Li and Na exhibit structural transitions to FCC at 6.9 GPa and at 65 GPa, respectively [1, 2].

Nanoporous systems increasingly serve as confining matrices to study the behaviour of constrained gases and liquids, since new physical phenomena arise due to the strong interaction at the interface and as a consequence of geometrical constraints. Concerning metals, only few low-melting elements in nanoporous environments were studied so far and, generally, a moderate decrease of the melting point (< 10 K) was observed in these systems.

Zero temperature calculations of the energies of Li and Na show that the differences between the BCC and close-packed structures are very small, *i.e.* of the order of 10^{-4} eV [3]. This strongly suggests that significant structural changes due to slight variations in the energy may occur. The possibility to introduce such changes by the way of geometrical confinement provides a motivation to investigate whether such changes may indeed be observed. In the present investigation, the structures of geometrically confined metallic Li and Na have been studied as a function of temperature.

Nanoporous silica glasses (Vycor and Gelsil) with an average pore size of 9.2 nm, 7.5 nm, 5.0 nm and 2.6 nm were charged with Na and Li by vaporization and melting techniques. The filling fractions in different samples varied depending on sample dimensions and experimental conditions.

Synchrotron radiation of 12 keV was used for powder diffraction measurements at the beamline KMC-2 at BESSY (Berlin). The sample surface was adjusted at the fixed angle of $\sim 10^\circ$ to the incident X-ray beam which had a cross section of $100 \mu\text{m} \times 500 \mu\text{m}$. The measurements were done in a furnace with Be-windows evacuated to 10^{-6} mbar and covered a temperature range from ambient temperature up to 700°C .

Contrary to the bulk behaviour, at room temperature, both lithium and sodium were found to crystallize in close-packed structures (FCC, HCP, dHCP and 9R) inside the nanopores while the bulk BCC phase is completely absent. These results indicate an upward shift of the martensitic phase transition temperatures (see above) by more than 200 K due to geometrical confinement.

Very surprisingly, on heating, no melting was observed near the bulk melting temperatures ($\sim 98^\circ\text{C}$ for Na, $\sim 180^\circ\text{C}$ for Li). Instead, well defined powder diffraction patterns indicating a fully crystalline structure was observed up to the highest temperatures investigated. It should be noted that no chemical reaction between the metals and the silica glass took place. The results provide strong evidence that the reduction of the geometrical dimensions in metallic systems may indeed have profound implications for the thermodynamic equilibrium structure.

The diffraction patterns mostly reveal the simultaneous presence of several close-packed structures. A strong diffuse background indicates the presence of a large concentration of stacking faults which is also reflected in variations of peak intensities and distorted peak shapes as compared to the bulk. Figure 1 shows a spectrum of Li at ambient temperature as an example.

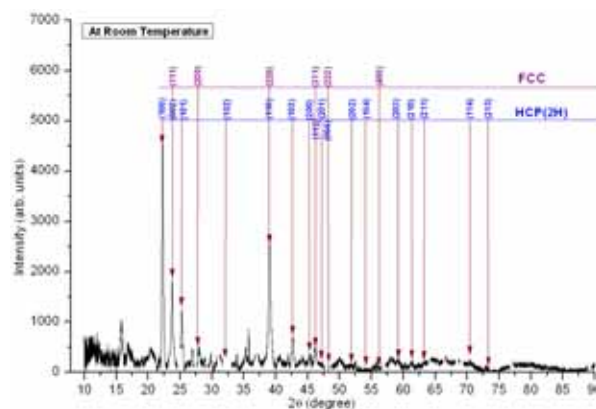


Figure 1. Powder diffraction pattern of Li in Vycor glass pores with an average size of 9.2 nm. The diffuse background has been subtracted and the Be peaks due to the furnace removed. The pattern is indexed with HCP and FCC peaks.

References

- [1] R. Berliner, H.G. Smith, J.R.D. Copley, J. Trivisonno, "Structures of sodium metal", *Phys. Rev. B* **46** (1992) 14436–14447.
- [2] W. Schwarz, O. Blaschko, I. Gorgas, "Diffuse neutron scattering investigation of the low-temperature phases of sodium", *Phys. Rev. B* **46** (1992) 14448–14452.
- [3] V.G. Vaks, M.I. Katsnelson, V.G. Koreshkov, A.I. Likhtenstein, O.E. Parfenov, V.F. Skok, V.A. Sukhoparov, A.V. Trefilov, A.A. Chernyshov, "An experimental and theoretical study of martensitic phase transitions in Li and Na under pressure", *J. Phys.:Cond. Matt.* **1** (1989) 5319–5335.

JANA2006 AS A TOOL FOR SOLUTION AND REFINEMENT OF NON-STANDARD CRYSTAL STRUCTURES

V. Petříček* and M. Dušek

Institute of Physics AS CR, v.v.i., Na Slovance 2, 18040 Praha 8, Czech Republic

Keywords: crystal structure analysis, modulated crystal

**) e-mail: petricek@fzu.cz*

The experimental techniques used in a standard diffraction experiment allow nowadays much deeper insight into crystal structure details than in the past. CCD cameras are able to scan in reasonably short time a large portion of the reciprocal space. Thus the problem how to collect sufficient number of systematically weak reflections such as satellites for modulated crystals is considerably reduced. This opens possibility to study difficult modulated structures at very reasonable resolution and redundancy.

Modulation in crystals can substantially affect crystal properties and they are very often connected with phase transitions. As it has been shown in pioneer's works of de Wolff, Janner and Janssen [1] modulated crystals, which have not anymore classical three dimensional translation symmetry, can be described in higher dimensional space - superspace - as generalized crystal with translation symmetry relocated in the higher dimension. Since this discovery in eighties of the last century the classical techniques available for solution and refinement of regular structures have been eventually generalized to aperiodic ones making structure analysis of modulated structures almost a routine task. An important progress in the last years is connected with new solution technique, charge flipping algorithm, which has been also generalized to aperiodic crystals and implemented to the program Superflip [2].

The program system Jana2006 [3] contains all tools necessary for refinement and interpretation of modulated structures. For solution the above mentioned method of charge flipping has been used and the program Superflip was directly connected with Jana2006. Its power will be demonstrated with already published structure of $\text{KAsF}_4(\text{OH})_2$ [4].

The modulation functions describing periodic perturbation of the basic structural parameters (atomic occupancies, positions and ADP's) can often exhibit discontinuities. For this reason discontinuous functions called crenel and saw-tooth function have been introduced [5]. They are used to model discontinuity in the crystal and they can be combined with additional continuous modulation. Their usage has been recently facilitated by introducing of Legendre polynomials for positional and ADP modulation. This approach overcomes the tricky problem of missing orthogonalism due to discontinuity which complicated combination of discontinuous and harmonic functions. With Legendre polynomials seamless switching between continuous and

discontinuous functions is possible as well as between crenel and sawtooth function.

Another problem complicating structure determination and refinement is twinning. The computing system Jana2006 allows refinement of structures having complete overlap (*i.e.* meroedric twins and pseudo-meroedric twins with negligible oblique) or partial overlaps of diffraction spots. The number of twin domains is arbitrary, the program uses either twinning matrices or HKLF5 format. The method has been recently generalized for multiphase single-crystal samples composed from related, but generally different, phases. It can be used even in cases when one of phases in modulated and the second one not [6]. Such an option is especially important for samples of natural minerals and in analysis of phase transitions.

The newest version of the system Jana2006 can also use and combine several data sets from different sources, for instance powder and single crystal data either from X-ray diffraction with different wave lengths or from neutrons. This approach makes possible to refine structural details with different contribution to structure factors, for instance anharmonic ADPs and charge densities, against joint data sets based on X-ray and neutron diffraction.

References

- [1] P.M. de Wolff, T. Janssen, A. Janner, "The superspace groups for incommensurate crystal structures with a one-dimensional modulation", *Acta Cryst. A* **37** (1981) 625–636.
- [2] L. Palatinus, G. Chapuis, "SUPERFLIP – a computer program for the solution of crystal structures by charge flipping in arbitrary dimensions", *J. Appl. Cryst.* **40** (2007) 786–790.
- [3] V. Petříček, M. Dušek, L. Palatinus, *Jana2006-the crystallographic computing system*, (Praha, Czech Republic, 2006).
- [4] J. Peterková, M. Dušek, V. Petříček, J. Loub, "Structures of fluoroarsenates ($\text{KAsF}_{6-n}(\text{OH})_n$, $n=0,1,2$). Application of heavy atom method for modulated structures", *Acta Cryst. B* **54** (1998) 809–818.
- [5] V. Petříček, A. van der Lee, M. Evain, "On the use of crenel functions for occupationally modulated structures", *Acta Cryst. A* **51** (1995) 529–535.
- [6] H. Krüger, V. Kahlenberg, V. Petříček, F. Phillipp, W. Wertl, "High-temperature phase transition in $\text{Ca}_2\text{Fe}_2\text{O}_5$ studied by *in-situ* X-ray diffraction and transmission electron microscopy", *J. Solid State Chem.* **182** (2009) 1515–1523.

APPLICATION OF X-RAY SCATTERING AND DIFFRACTION TECHNIQUES TO STUDIES OF HIGHLY CHARGED COLLOID SUSPENSIONS IN THE VICINITY OF THE CRYSTALLIZATION POINT

J. Gapiński* and A. Patkowski

Faculty of Physics, A. Mickiewicz University, Umultowska 85, 61-614 Poznań, Poland

Keywords: colloid crystal, collective diffusion, freezing criterion, DLVO potential

**) e-mail: gapinski@amu.edu.pl*

Colloidal suspensions of monodisperse silica particles (diameter 164 nm) in dimethylformamide (DMF) have been studied by means of small angle X-ray scattering (SAXS) and X-ray photon correlation spectroscopy (XPCS) near and above the crystallization conditions. The SAXS measurements performed at low volume fractions ϕ and relatively high added salt (LiCl) concentrations C_s revealed multiple (above twenty) minima in the form factor $P(q)$, confirming low polydispersity of the colloidal particles (below 2%).

This and similar colloidal systems have been studied by means of SAXS and XPCS in the liquid phase [1-3].

Static properties of the colloidal suspension (its structure) is usually described in terms of the structure factor $S(q)$ which can be relatively easily extracted from the SAXS results and calculated theoretically using appropriate models. Fitting the models to the experimental data allowed estimation of the particle effective charge value Z_{eff} , the only free parameter in the model. The colloid and added salt concentrations were adjusted such that the freezing criteria (Hansen-Verlet) could be met for relatively dilute samples ($\phi < 0.1$) and the samples often crystallized. In such cases the scattering spectrum turned into diffraction pattern which could be best seen using the CCD detector (Pilatus).

The diffraction patterns from crystalline samples sometimes resembled those characteristic for single monocrystals, suggesting large dimensions of ordered regions even for those samples which looked like a system of coexisting liquid and crystal (Fig. 1).

The XPCS measurements performed close to the crystallization conditions revealed a mild transition from short-time to long-time diffusive behaviour with the ratio of the respective diffusion coefficient taking values between 2 and 3.

The most interesting finding in our study was the effect of colloidal crystal melting in the X-ray beam. We discovered that in some samples the diffraction pattern slowly changed into the liquid-like scattering profile. Moreover, after the beam was blocked, the diffraction pattern was recreated in an identical shape (Fig. 2).

At the end of the presentation an attempt to explain the observed effects will be made.

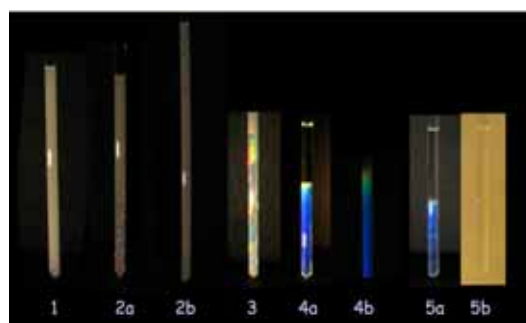


Figure 1. Colloidal samples in capillaries. For these pictures the samples were illuminated with white light directed from the left except the last picture, where only ambient light was present. 1 – liquid phase, 2 – liquid-crystal coexistence, 3 – polycrystal (or glass-crystal coex.), 4 – variable monocrystal, 5 – variable monocrystal in ambient light conditions.

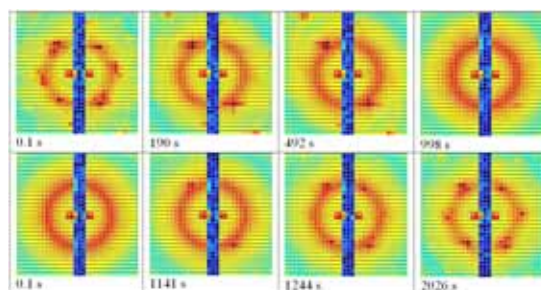


Figure 2. Structure melting (upper row) and recovery (lower row) observed using Pilatus detector.

References

- [1] A.J. Banchio, J. Gapiński, A. Patkowski, W. Haeußler, A. Fluerasu, S. Saccana, P. Holmqvist, G. Meier, M.P. Lettinga, G. Nägele, "Many-body hydrodynamic interactions in charge-stabilized suspensions", *Phys. Rev. Lett.* **96** (2006) 138303.
- [2] J. Gapiński, A. Patkowski, A. Banchio, P. Holmqvist, G. Meier, M.P. Lettinga and G. Nägele, "Collective diffusion in charge-stabilized suspensions: concentration and salt effects", *J. Chem. Phys.* **126** (2007) 104905.
- [3] J. Gapiński, A. Patkowski, A.J. Banchio, J. Buitenhuis, P. Holmqvist, M.P. Lettinga, G. Meier, G. Nägele, "Structure and short-time dynamics in suspensions of charged silica spheres in the entire fluid regime", *J. Chem. Phys.* **130** (2009) 084503.

SYNCHROTRON BASED TRANSMISSION X-RAY MICROSCOPY REVEALS SMECTITE FINE STRUCTURE IN AN AQUEOUS ENVIRONMENT

Marek S. Żbik^{*} and Ray L. Frost

*Faculty of Science and Technology, Queensland University of Technology,
2 George Street, GPO Box 2434, Brisbane Qld 4001 Australia*

Keywords: X-ray microscopy, smectite

**) e-mail: namer@zzz.edu.fr*

A transmission X-ray microscope with 60 nm tomographic resolution has been used at beamline BL01B of NSRRC in Taiwan. This device has a superconducting wavelength shifter source, which provides a photon flux of 5×10^{12} photons/s/0.1% bw in the energy range 5–20 keV. The TXM observations of smectites in aqueous suspension shows network of connected nano-size platelets which form a gel where highly flexible sheets are interacting with each other by a combination of edge attraction and basal plane repulsion. These build an expanded and extremely voluminous cellular network, composed of chain-like sheet assemblies. In such an extended cellular network, flexible smectite sheets may encapsulate water within cellular voids of dimensions up to 0.5 – 2 μm . This flocculated cellular structure can span all volume of clay slurry. In such a case the suspension is gelled; there is no free settling in the system and further compacting may proceed slowly only by structural re-arrangement of the entire network. In a 3-D structure and in the absence of shear, smectite sheets are not oriented in any particular direction and therefore, their most probable orientation in the volume of suspension is random. In 2-D, TXM micrographs reveal the Na-smectite gel structure in water. In this finding, elongated smectite sheets form a cellular network, 0.6 to 1.5 μm in diameter (average 940 nm).

The smectite sample was size fractionated and sodium exchanged as described elsewhere. Solutions of aluminium and gallium 13 Keggin ions were prepared. To an aliquot of the Keggin ion solution, the sodium exchanged smectite was added in an amount which ensured the Keggin ion remained four times the CEC. The clay in Keggin ion solution was mixed overnight using a magnetic stirrer before collection, washing and drying via vacuum filtration. The Keggin ion exchanged smectite was subjected to x-ray diffraction to ensure complete exchange. A 10% w/v suspension of the Keggin exchanged smectite was prepared in filtered water. To this suspension an aliquot (3 $\mu\text{l/ml}$ of suspension) of 1 mg/L gold nanoparticles (0.8–0.5 μm) was added.

Observed structural effects of smectite modified nano-clay may be explained by hydration of the exchangeable counter ions, allowing these ions to then

set up an electric field double layer. It is also possible that AFM measured long-distance forces, similar to electrostatic repulsion, have a steric origin and reflect the flexibility of smectite flakes. In dense suspension hindrance of neighbour platelets would be unavoidable. The scale of squeezing of the smectite gelled structure by the AFM cantilever spring is consistent with microscopy observations as well as force measurements.

Significant differences between smectite with Na^+ and Ca^{2+} exchangeable cations may be due to the differences in the rigidity of the smectite flakes. In the case of the presented results it may suggest that thicker and more rigid flakes made with Ca^{2+} exchangeable cations will build much smaller cellular structures than the thinner, more flexible smectite flakes made with Na^+ exchangeable cations. A 3-D space reconstruction, allowed in TXM tomography reconstruction reveals, for the first time, the cellular orientation of associated mineral sheets within aqueous based electrolyte. The reconstruction also allowed for observation of the difference in sheet thickness between single smectite flakes. Individual colloidal size particles are well visible in the presented still picture and the distinctive spongy and cellular structure can be carefully studied in this reconstruction when rotating this image. The cellular network of Na-smectite consists of highly bent elastic flakes of diameter in excess of 1 μm assembled in a continuous structure pattern. This pattern is similar to a typical honeycomb structure. The thickness of sheets assembled cells walls are below the resolution of TXM but well visible when rotating this image. A much denser gel assembled of 20 – 50 nm thick flakes was reported to build a cellular network in Ca-smectite with a cell diameter around 0.5 μm . Such flakes are stiffer and do not bend to the degree observed in Na smectite gel.

Much smaller voids of ~ 200 nm diameter were observed between mostly randomly oriented Keggin intercalated smectite flakes when gelled as an effect of keggin addition to the smectite suspension. These flakes form compact aggregates randomly positioned in space and mostly EF orientation spanning network.

X-RAY INTERFERENCE MEASUREMENTS OF THE MOTION OF THE MOLECULAR MOTOR IN MUSCLE WITH NANOMETER-MICROSECOND RESOLUTION

V. Lombardi^{1*}, **M. Linari**¹, **M. Reconditi**¹, **E. Brunello**², **L. Fusi**¹,
T.C. Irving³, **T. Narayanan**⁴, **G. Piazzesi**¹, and **M. Irving**²

¹ *Laboratory of Physiology, Department of Evolutionary Biology, University of Florence, 50019 Sesto Fiorentino, Italy*

² *Randall Division of Cell and Molecular Biophysics, King's College London, London, UK*

³ *BioCAT, Advanced Photon Source Argonne, IL, USA*

⁴ *European Synchrotron Radiation Facility, Grenoble, France*

Keywords: X-ray diffraction, muscle, myosin motor

*) *e-mail: vincenzo.lombardi@unifi.it*

In a contracting muscle, arrays of the dimeric motor protein myosin II pull the actin filament towards the centre of the sarcomere (the structural unit of the striated muscle) during cyclical ATP driven interactions. When the external load is smaller than the array force, the sarcomere works as a motor, converting metabolic energy into mechanical work; when the external load is larger than the array force, the sarcomere acts as a brake resisting the load with reduced metabolic cost. Due to the regular arrangement of molecular motors in striated muscle, X-ray diffraction is the best structural technique for imaging muscle contraction at molecular level. The high spacial resolution of the third generation synchrotrons (European Synchrotron Radiation Facility, ESRF, Grenoble, France and Advanced Photon Source, APS, Argonne, IL, USA) allows to record the fine structure of the meridional reflection originating from the 14.5 nm axial repeat of myosin motors, showing that the reflection is split in two peaks by the X-ray interference between the two arrays of myosin motors in each sarcomere [1]. Using the interference effect, the motion of myosin motors can be directly measured with subnanometer precision [2, 3].

Here we use sarcomere-level mechanics and X-ray interferometry in intact single cells from the skeletal muscle of the frog (*Rana temporaria*), to investigate the molecular basis of the work production and the braking action of muscle. During isometric contraction, each motor bears a force of about 6 pN. During shortening against high and moderate loads, the number of myosin motors reduces in proportion to the external load, while individual motors maintain a force of 6 pN pulling the actin filament through a 6 nm stroke [4].

Rapid stretches of 1-5 nm between each overlapping set of myosin and actin filaments in a muscle sarcomere cause the stiffness of the array of myosin motors to double within 2 ms [5]. Simultaneous X-ray interference changes indicate a rapid attachment to actin of the

second motor domain of the myosin molecules with the first domain already attached to actin [6]. This mechanism explains the ability of active muscle to efficiently resist a sudden increase in load.

Acknowledgements: The study was supported by MiUR and Ente CRF (Italy), NIH (USA), MRC (UK), EMBL, ESRF.

References

- [1] M. Linari, G. Piazzesi, I. Dobbie, N. Koubassova, M. Reconditi, T. Narayanan, O. Diat, M. Irving, V. Lombardi, "Interference fine structure and sarcomere length dependence of the axial X-ray pattern from active single muscle fibres", *Proc. Natl. Acad. Sci. USA* **97** (2000) 7226-7231.
- [2] G. Piazzesi, M. Reconditi, M. Linari, L. Lucii, Y.-B. Sun, T. Narayanan, P. Boesecke, V. Lombardi, M. Irving, "The mechanism of force generation by myosin heads in skeletal muscle", *Nature* **415** (2002) 659-662.
- [3] M. Reconditi, M. Linari, L. Lucii, A. Stewart, Y.-B. Sun, P. Boesecke, T. Narayanan, R.F. Fischetti, T. Irving, G. Piazzesi, M. Irving, V. Lombardi, "The myosin motor in muscle generates a smaller and slower working stroke at higher loads", *Nature* **428** (2004) 578-581.
- [4] G. Piazzesi, M. Reconditi, M. Linari, L. Lucii, P. Bianco, E. Brunello, V. Decostre, A. Stewart, D. Gore, T. Irving, G. Piazzesi, M. Irving, V. Lombardi, "Skeletal muscle performance determined by modulation of number of myosin motors rather than motor force or stroke size", *Cell* **131** (2007) 784-795.
- [5] L. Fusi, M. Reconditi, M. Linari, E. Brunello, R. Elangovan, V. Lombardi, G. Piazzesi, "The mechanism of the increase in resistance to stretch of isometrically contracting single muscle fibres", *J. Physiol.* **588** (2010) 495-510.
- [6] E. Brunello, M. Reconditi, R. Elangovan, M. Linari, Y.-B. Sun, T. Narayanan, P. Panine, G. Piazzesi, M. Irving, V. Lombardi, "Skeletal muscle resists stretch by rapid binding of the second motor domain of myosin to actin", *Proc. Natl. Acad. Sci. USA* **104** (2007) 20114-20119.

HIGH RESOLUTION X-RAY MICROPROBES AND THEIR APPLICATIONS

M. Cholewa *

Monash Centre for Synchrotron Science, Monash University, Clayton, VIC, Australia

Keywords: synchrotron, beamline, microprobe

**) e-mail: Marian.Cholewa@sync.monash.edu.au*

Australian Synchrotron is in the routine operation since 2007. Eight beamlines are already in operation and one is in the construction phase. The speaker has been involved in several new projects, such as:

(a) High resolution imaging. Recent results achieved at the existing laboratory topographic systems in Australia allowed obtaining a resolution down to 1 μm for 2-dimensional (2D) and 3-dimensional (3D) imaging. There is a growing demand in Australia for a synchrotron based imaging system with spatial resolution below 50nm. And several groups from Monash University have been using Transmission X-ray Microscopy (TXM) systems at ALS in USA and BESSY II in Germany. The speaker has been also involved in development of a unique high resolution imaging beamline that will involve Transmission X-ray Microscopy (TXM),

Infrared Microscopy (IRM) and Confocal Microscopy (CM).

(b) Single cell irradiation. Targeted irradiation to sub-cellular components enables the investigation of the radiation response contribution from organelles and cellular compartments such as the nucleus and the cytoplasm. We used a microbeam for single cell and microbeam radiotherapy (MRT) investigations at the Photon Factory in Japan. We targeted nuclei or cytoplasm with a $10 \times 10 \mu\text{m}^2$ X-ray microbeam with 5.35 keV to investigate the DNA damage response. While in Australia he has been also involved in the development and applications of high resolution live cell irradiation facilities with X-rays which also will be discussed. Experimental data from Photon Factory in Japan and Australian Synchrotron in Melbourne will be presented.

DEPTH-RESOLVED MAGNETIZATION STRUCTURE AT THE SPIN REORIENTATION TRANSITION IN Fe/W(110) ULTRATHIN FILMS STUDIED BY THE NUCLEAR RESONANT SCATTERING OF SYNCHROTRON RADIATION

T. Ślęzak^{1*}, **M. Zając**¹, **M. Ślęzak**¹, **K. Matlak**¹, **N. Spiridis**², **K. Freindl**²,
D. Wilgocka-Ślęzak², **R. Ruffer**³, and **J. Korecki**^{1,2}

¹ Faculty of Physics and Applied Computer Science, AGH University of Science and Technology, Al. Mickiewicza 30, 30-059 Kraków, Poland

² Institute of Catalysis and Surface Chemistry, Polish Academy of Sciences, ul. Niezapominajek 8, 30-239 Kraków, Poland

³ European Synchrotron Radiation Facility, BP220, F-38043 Grenoble, France

Keywords: magnetism, Fe nanostructures, nuclear resonant scattering of synchrotron radiation

**) e-mail: slszak@agh.edu.pl*

For almost two decades different Fe nanostructures deposited on W(110) have been one of the most intensely studied model systems in surface science. An in-plane spin reorientation transition (SRT) belongs to the most fascinating magnetic phenomena observed for Fe/W(110) ultrathin films [1]. During the film growth, when approaching the critical Fe film thickness, the magnetization switches from $[1\bar{1}0]$ to $[001]$ in-plane direction. While the driving source of this transition, namely magnetic surface anisotropy, is well recognized its scenario is not fully understood. It is usually considered either as continuous magnetization rotation from $[1\bar{1}0]$ to $[001]$ or as coexistence of the $[1\bar{1}0]$ and $[001]$ oriented magnetic domains with different occupation. We used in-situ, Grazing Incidence Nuclear Resonant Scattering (NRS) of synchrotron radiation to monitor under ultrahigh vacuum conditions the thickness induced evolution of the spin structure of Fe(110)/W system. The measurements were done at the beamline ID18 at European Synchrotron Radiation Facility (ESRF) in Grenoble. NRS is a synchrotron analogue of Mössbauer spectroscopy (MS), in the sense that recoilless excitation (induced by the resonant x-rays with energy 14.4 keV for ^{57}Fe) of the nuclear energy levels, split due to the hyperfine interactions, is involved. In this method, the hyperfine parameters can be obtained from a characteristic beat pattern seen in the time evolution of the intensity of nuclear resonant scattering (the so called time spectrum) [2].

The present GI-NRS experiment allowed us to get insight into the mechanism of the in plane SRT. In a single experimental run, multiple transition steps induced by the film thickness could be studied. The ^{57}Fe was evaporated on the W(110) crystal held at 330 K with the rate of 0.3 ML/min to the final thickness of 30 ML. During the preparation, a set of NRS time spectra were collected (acquisition time per spectrum was only several seconds), thus probing the hyperfine parameters in 0.3 ML thickness steps.

NRS time spectra and corresponding theoretical fits at about 10 ML of Fe film thickness indicate domination

of the film interior with $B_{\text{hf}} = 33$ T, uniformly magnetized along $[1\bar{1}0]$. Such a magnetization state persists up to above 20 ML. Around 25 ML, the beat pattern changes essentially and corresponds to a unique $B_{\text{hf}} = 33$ T along $[001]$. Assuming a homogeneous magnetization depth profile across the Fe(110) films, the following models were considered for the magnetization transition from $[1\bar{1}0]$ to $[001]$: (i) coherent rotation and (ii) decay to $[001]$ oriented domains. Both models showed distinctly different spectra but, unfortunately, any combination of the magnetization configuration resulting from the models could give a satisfactory description of the NRS time spectra series in the thickness induced spin reorientation transition. Interestingly, when the depth dependent magnetization structure was assumed the perfect fits could be obtained indicating a more complex nature of the transition [3]. The non-collinear, exotic magnetic phase of epitaxial Fe films was found in the vicinity of a critical SRT thickness. Such a magnetic structure resembles a planar domain wall with its center propagating towards the surface as the thickness increases.

Acknowledgments: This work was supported in part by the Polish Ministry of Science and Higher Education and in part by the European Community under the project NMP4-CT-2003-001516 (DYNASYNC), as well as by the Team Program of the Foundation for Polish Science co-financed by the European Regional Development Fund.

References

- [1] H.J. Elmers, U. Gradmann, "Magnetic Anisotropies in Fe(110) Films on W(110)", *Appl. Phys. A* **51** (1990) 255.
- [2] R. Rohlsberger, *Nuclear Condensed Matter Physics with Synchrotron Radiation*, STMP 208, (Springer-Verlag, Berlin 2004).
- [3] T. Ślęzak, S. Stankov, M. Zając, M. Ślęzak, K. Matlak, N. Spiridis, B. Laenens, N. Planckaert, M. Rennhofer, K. Freindl, D. Wilgocka-Ślęzak, R. Ruffer, J. Korecki, "Magnetism of ultra-thin iron films seen by the nuclear resonant scattering of synchrotron radiation", *Mater. Sci. (Poland)* **26** (2008) 885.

X-RAY TOPOGRAPHIC INVESTIGATION OF THE DEFORMATION FIELD AROUND SPOTS IRRADIATED BY FLASH SINGLE PULSES

W. Wierzchowski^{1*}, **K. Wieteska**², **D. Klinger**³, **R. Sobierajski**³, **J. Pelka**³, and **T. Balcer**¹

¹ Institute of Electronic Materials Technology, 133, Wólczyńska Str, 01-919 Warsaw, Poland

² Institute of Atomic Energy, 05-400 Świerk-Otwock, Poland

³ Institute of Physics, PAS, 32/46, Al. Lotników, 02-668 Warsaw, Poland

Keywords: silicon, gallium arsenide, FLASH irradiation, X-ray diffraction, deformation fields

*) e-mail: wierzc_w@itme.edu.pl

The important problem in the experiment performed with the intense fourth generation X-ray sources are the damages of the examined samples caused by the high energy impact. The effect introduced by the beam from the FLASH source in crystalline silicon and gallium arsenide samples was studied with synchrotron white beam projection and section topography enabling the evaluation of the strain field associated with the damages.

The silicon and GaAs crystal wafer samples were irradiated in an UHV chamber at a beamline BL2 of the FLASH facility by single pulses at wavelength of $\lambda = 32.5 \pm 0.5$ nm with pulse duration of $\tau = 25 \pm 0.5$ fs. The pulse energy was up to 10 mJ. The beam was focused surface-normal onto the sample using a grazing-incidence carbon-coated ellipsoidal mirror, external to the chamber. Some structural properties of analogous spots were studied with the synchrotron microdiffraction method [1,2].

The samples were studied in back-reflection geometry by means of white beam projection topograph at F1 experimental station of DORIS III in HASYLAB. A relatively small glancing angle of 4° , and in case of section topographs a $5 \mu\text{m}$ narrow slit was used. The topographs were taken for the azimuths differing through 90° , and in the case of section topographs also for slightly altered positions of the incident beam.

Both the section and projection experimental topographs revealed significant extinction contrast coming from the vicinity of the irradiated spot. It was confirmed that the contrast around each of the spots is practically not changing for various azimuths. Apart from the extinction contrast the section topographs exposed along the longer side of the silicon sample revealed the interference fringes characteristic for the elastically bent samples.

It was possible to obtain a reasonable similarity of the presently recorded section images of some spots to the numerically simulated images of the rod-like defects using recently developed numerical procedure described in [3] (see Figs. 1 and 2).

References

- [1] J. B. Pelka, A. Andrejczuk, H. Reniewicz, N. Schell, J. Krzywinski, R. Sobierajski, A. Wawro, Z. Zytkeiwicz, D. Klinger, L. Juha: "Structure modifications in silicon

irradiated by ultra-short pulses of XUV free electron laser", *J. Alloys Compds* **382** (2004) 264–270.

- [2] J.B. Pelka, R. Sobierajski, D. Klinger, W. Paszkowicz, J. Krzywinski, M. Jurek, D. Zymierska, A. Wawro, A. Petrouchik, L. Juha, V. Hajkova, J. Cihelka, J. Chalupsky, T. Burian, L. Vysin, S. Toleikis, K. Sokolowski-Tinten, N. Stojanovic, U. Zastra, R. London, S. Hau-Riege, C. Riekel, R. Davies, M. Burghammer, E. Dynowska, W. Szuszkiewicz, W. Caliebe, R. Nietubyc, "Damage in solids irradiated by a singleshot of XUV free-electron laser: Irreversible changes investigated using X-ray microdiffraction, atomicforce microscopy and Nomarski optical microscopy", *Rad. Phys. Chem.* **78** (2009) S46–S52.
- [3] T. Balcer, W. Wierzchowski, K. Wieteska, "Simulation of Bragg-Case Section Images of Dislocations and Inclusions in aspect of identification of defects in SiC crystals", *Acta Phys. Polon. A* **117** (2010) 333-340.

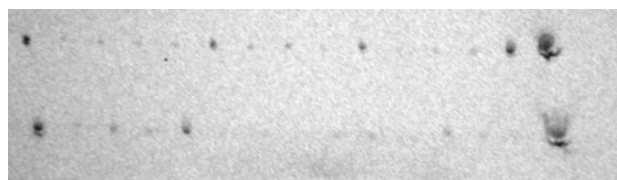


Figure 1. The fragment of Bragg-case white-beam diffraction topograph of the spots irradiated in silicon sample by FLASH single pulses.



Figure 2. The simulated Bragg-case section image of the rod-like inclusion in silicon.

POLISH SYNCHROTRON – THE PRESENT STATUS

M.J. Stankiewicz^{*}, E.A. Görlich, and K. Królas

¹*Institute of Physics, Jagiellonian University, ul. Reymonta 4, 30-059 Kraków, Poland*

Keywords: synchrotron design, beamline

**) e-mail: m.j.stankiewicz@uj.edu.pl*

The current status, timetable of actions for the next four years and the plans for the future development of the recently granted Polish Synchrotron source located in Kraków will be presented. The layout and basic design parameters of the planned machine are going to be discussed.

The Polish synchrotron radiation source installation will contain:

- Electron injection system including electron source and 400-700 eV linear accelerator
- 96 m circumference, 1.5 GeV, 500 mA storage ring with 12 bending magnets separated by 3.5 m long straight sections
- 1 undulator based experimental beamline with a multi-grating monochromator and VUV - Soft X-ray electron spectroscopy end-station.

Innovative design concepts have been applied to the linear accelerator and the storage ring, based on the new linac design and integrated bending magnets technology

developed by the accelerator team at MAX-lab in Lund (Sweden). Critical energy of the storage ring is calculated at ~ 1 keV. Insertion devices, including superconducting wigglers will allow for shifting the critical energy up by few keV enabling crystallography and material science research to be performed. At the low energy region the THz operation of the source is foreseen.

Although the granted project includes only one experimental beamline it is assumed that the search for funds for the range of new beamlines and endstations will start immediately. These can be either bending magnet, undulator or wiggler (superconducting) based facilities.

The synchrotron building complex, apart of the synchrotron components will also accommodate all the necessary auxiliary facilities *e.g.* workshops, preparatory laboratories, staff and administration offices.

The Centre with the budget of 143 740 000 PLN is scheduled to be commissioned in September 2014.

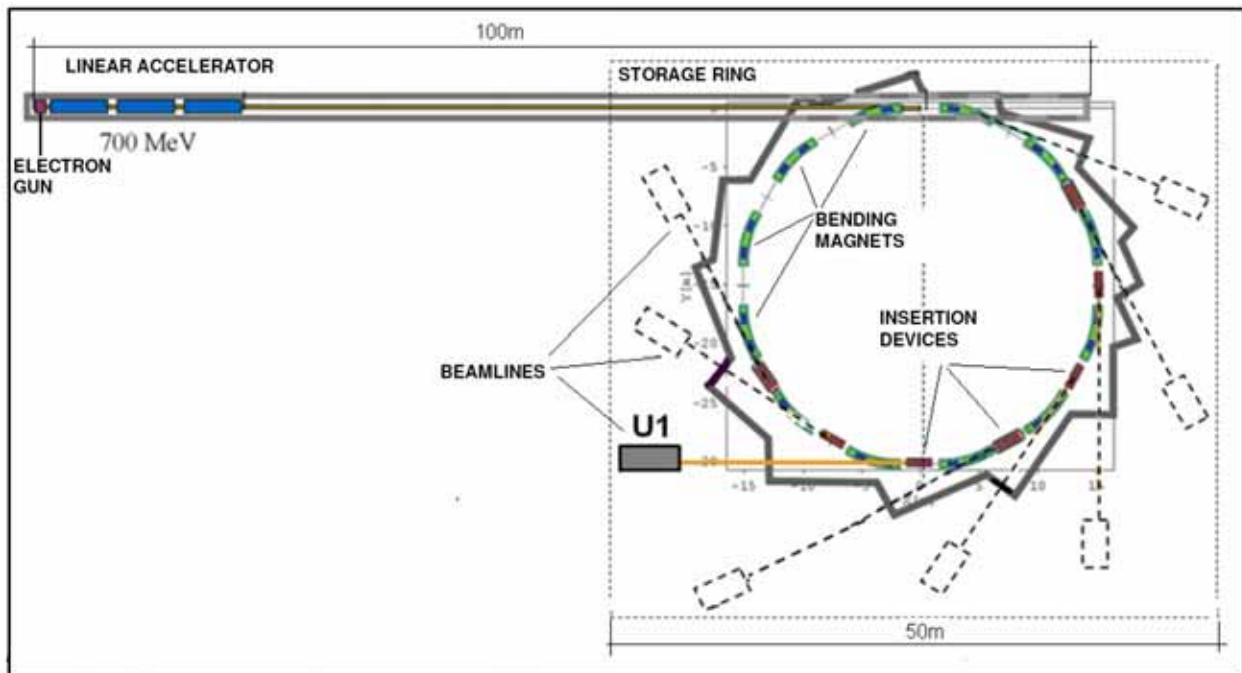


Figure 1. The layout of the Polish Synchrotron.

THE ACCELERATORS FOR THE POLISH LIGHT SOURCE AND MAX IV

Mikael Eriksson^{1*}, **Adriana Wawrzyniak**^{1,2}, and **Piotr Goryl**^{1,2}

¹ *MAX-lab Lund University, P.O. Box 118, SE-221 00 Lund, Sweden*

² *Institute of Physics, Jagiellonian University, PL 30-059 Krakow Poland*

Keywords: synchrotron, Polish Light Source, insertion device

Two light source facilities are planned to be built up in parallel. The Polish Light Source (PLS) to be raised in Krakow and the MAX IV facility in Lund, Sweden.

The MAX IV facility will consist of one 3 GeV injector linac and two storage rings operated at 1.5 GeV and 3 GeV respectively. The 1.5 GeV ring is planned to be produced in two examples, one for PLS and one for MAX IV. As an injector for PLS, a 400 MeV

recirculated linac system, similar to the MAX-lab injector, is planned to be used.

Both the MAX IV as well the PLS facility will be presented with the emphasis put on the PLS facility. The accelerator design philosophy as well as the design itself will be discussed. The synchrotron radiation properties for different types of insertion devices will also be presented.

SOFT X-RAY SPECTROSCOPY - FIRST BEAMLINE AT POLISH SYNCHROTRON

J. Szade^{1*}, B.A. Orłowski², B.J. Kowalski², E. Görlich³, K. Tomala³, and P. Starowicz³

¹ *A. Chelkowski Institute of Physics, University of Silesia, ul. Uniwersytecka 4, 40-007 Katowice, Poland*

² *Institute of Physics PAS, Al. Lotników 32/46; 02-668 Warsaw, Poland*

³ *Institute of Physics, Jagiellonian University, ul. Reymonta 4, 30-059 Kraków, Poland*

Keywords: synchrotron, beamlines, spectroscopy

*) *e-mail: jacek.szade@us.edu.pl*

First beamline at Polish synchrotron should start in 2014. The concept of this line emerged since the beginning of the attempts to create in Poland a source of synchrotron radiation. Soft x-ray spectroscopy was present in all early projects.

The beamline is designed to perform possibly polarization dependent spectroscopic studies of solids using photons within a relatively large energy range, provided by an undulator and a grating monochromator. The main technique is photoelectron spectroscopy, including angle resolved version. The layout of the beamline and endstation allows to use the light from the same source also for additional techniques - X-ray absorption (XAS) and x-ray emission spectroscopy (XES, RIXS) – in the next stage of beamline development. This solution enables complex analysis of the electronic structure of various materials including strongly correlated electron systems. Depending on the budget the project will be realized in one or two steps. First step – the basic photoelectron spectrometer, the second step: spin detector, x-ray emission spectrometer, MBE in the attached chamber.

Source:

circular (elliptical) polarization undulator,

- energy 30 – 1500 eV, variable polarization
- grating monochromator; resolving power $E/\Delta E \sim 10^4$
- beamsize at sample $\sim 100 \times 100 \mu\text{m}^2$
- intensity $\sim 10^{12} - 10^{13}$ phot/s/0.1%BW

Endstation

1. Photoelectron spectroscopy – resonant photoemission, spin resolved photoemission – hemispherical high resolution analyser, resolution ~ 1 meV, multichannel detector and micro-Mott detector for spin resolution (switchable),
- 6-axis manipulator with sample heating and cooling, temperature range at least 20-800 K,
2. Angle Resolved Photoemission – realised with the same analyser or with use of a spectrometer dedicated for angle resolved measurements,
3. X-ray Absorption Spectroscopy – sample current detector (TEY), fluorescence detector (TFY) – in the main chamber,

4. X-ray Emission Spectroscopy – Soft x-ray fluorescence spectrometer, (RIXS – Resonant Inelastic X-ray Scattering).

The available photon energy range includes the absorption edges of all elements important for new materials research. Both bulk materials and thin films can be studied with use of several techniques. Complex information about their electronic structure will be obtained in a large temperature range, using one main analysis chamber and due to in-situ sample preparation. Fast switching between the techniques will be an important advantage of this multitechnique solution.

Resonant photoemission gives information about localization of partial densities of states in valence band. In connection with the spin resolved photoemission, the beamline enables complex studies of materials designed for spintronics. Photon energies below 100 eV and an 6-axes manipulator enable angle resolved photoemission spectroscopy studies – the basic method used for electron band mapping of single crystalline bulk solids and thin films. Electron band structure of the new materials, including thin epitaxial films can be investigated. This knowledge is of great importance especially for materials with special electronic properties which are crucial for modern electronics. Strongly correlated electron systems are important in spintronics, magnetoelectronics and superconductivity.. One of the techniques which enables studies of electron correlations is Resonant Inelastic X-ray Scattering (RIXS). X-ray emission spectroscopy can give complementary information to x-ray absorption and photoemission.

Additionally, switchable circular polarization of x-ray which can be used for all techniques available at the endstation enables exploring the local magnetic moments and all electronic states sensitive to light polarization.

The beamline will be used to study:

- new materials for spintronics and magnetoelectronics,
- thin films and nanostructure multilayer systems, obtained in-situ (MBE is planned to be attached to the analysis chamber),
- surface of bulk compounds, cleaned and doped in-situ,
- surface magnetism,
- chemical reactions taking place at the surface.

TRANSMISSION AND EMISSION SOFT X-RAY SPECTROMICROSCOPIES FOR LIFE AND NANOSCIENCES AT ELETTRA

B. Kaulich *, A. Gianoncelli, and M. Kiskinova

¹ ELETTRA – Sincrotrone Trieste, S.S. 14, km 163.5 in Area Science Park, I-34149 Trieste-Basovizza, Italy

Keywords: X-ray microscopy, X-ray spectromicroscopies, X-ray microfluorescence

**) e-mail: burkhard.kaulich@elettra.trieste.it*

Exploring the biochemistry and functionality of complex biological systems at sub-cellular length scales continues to be a challenge. It requires interdisciplinary approaches for discriminating qualitatively and quantitatively the constituent elements and correlating them to the sub-cellular morphology. In this respect high resolution X-ray imaging combined with its chemical sensitivity and complemented by other microanalytical techniques is attractive since it provides specific information not achievable by a single method. The contribution will present the most recent achievements demonstrating the capabilities of the TwinMic soft X-ray spectromicroscope [1] (see Fig. 1) at the Elettra synchrotron radiation facility (Trieste, Italy) in tissue, cellular or subcellular analysis based on imaging with low-energy X-ray fluorescence spectroscopy and micro-spot X-ray absorption spectroscopy [2]. Selected results will represent research fields including biotechnology, biomaterials, food science and nanotoxicology, neuroscience and clinical medicine. They will illustrate

new insights into the morphology and compositional enrichment, distribution and correlation of the elements resulting from growth of plants under altered environmental or toxic conditions, concentration dependence of penetration of engineered nanoparticles in different cell organelles and changes in the nanoparticle chemistry inside the cells, chemical reaction of lung tissue in the presence of inhaled asbestos species, among others. The importance of complementing the X-ray imaging and spectromicroscopy by other microscopies and conventional lab-based techniques as well as future developments will be outlined.

References

- [1] <http://www.elettra.trieste.it/twinmic>
- [2] B. Kaulich *et al.*, "Simultaneous Soft X-ray Transmission and Emission Microscopy", *J. Roy. Soc. Interf.* **6** (2009) 641–647.



Figure 1. The TwinMic X-ray transmission and emission microscopy station at Elettra, Trieste, Italy.

GROWTH OF NIOBIUM FILM ON SAPPHIRE(001)

**R. Nietubyc^{1*}, E. Dynowska², R. Mirowski¹, K. Nowakowska-Langier¹, J. Pelka²,
P. Romanowski², and J. Witkowski¹**

¹ Institute for Nuclear Studies, 05 400 Otwock-Świerk, Poland

² Institute of Physics PAS, Aleja Lotników 32/46, 02 668 Warsaw, Poland

Keywords: thin film, crystalline structure

*) e-mail: r.nietubyc@ipj.gov.pl

A structure of deposited film is determined by an interaction of arriving atoms with these of substrate and with those already stacked on. In case of ions having the kinetic energy in the range of tens electronvolts and falling into hot target, the interaction is dominated by an inelastic scattering with the stacked atoms, which happen during the subplantation few tens of angstroms inwards the film. Continuous ions influx to the near-surface part of the film accompanied by an enhanced vibration and mobility of constituent atoms and followed by a gradual cooling and crystallisation occurring when the new material accumulates above, facilitates the growth of compact and dense material composed of large crystallites.

Ultra High Vacuum Cathodic Arc (UHVCA) deposition method utilises the ions produced in explosive spots on the cathode, gaining there an energy about 100 eV and subsequently transported in the discharge channel towards the substrate to form pure films of regular and dense morphology. One of the most demanding application of such deposited films is particle accelerator technology where the Nb films have been proposed to coat inner walls of copper RF cavities. Such obtained superconducting cavities may, in some applications, replace the bulk niobium ones.

The aim of these studies is to describe the growth of the Nb film on the single crystal sapphire. It was accomplished by complementary measurements of X-ray Diffraction patterns (XRD) and Extended X-ray Absorption Fine Structure (EXAFS) performed for a series of Nb/sapphire(001) samples having various thicknesses ranging from about 3 nm up to more than 500 nm. These two methods, enabled the structural analysis of samples showing long or short range of crystalline order, respectively.

Diffraction patterns measured in $\omega/2\theta$ coupling for the films thinner than 15 nm, showed only single, broad maximum corresponding to Nb(110) planes (Fig. 1), which is the strongest among all of that crystal. It indicated small out-of-plane extent of diffracting crystallites.

For the films thicker than 15 nm a narrow component was observed on the background of broaden maximum. The pattern did not show peaks form any other planes. That indicated the presence of large crystallites of the same orientation such that Nb(110) planes were parallel to sapphire(001) face layers.

The films thicker than 400 nm showed diffraction patterns containing further reflections characteristic for the Nb crystal, which is typical for polycrystalline metallic film.

The shorter range of crystalline order in the early grown part of film as compared to the part stacked on it during the further deposition, was verified with the Nb K-edge EXAFS measurements performed in fluorescence yield mode. Absorption fine structures for films having the thickness less than or equal to 5 nm differ from that obtained for thicker films by a specific spectral feature observed at $k = 4 \text{ \AA}^{-1}$ (Fig. 1). Model multiple scattering calculations performed for Nb bcc crystal showed that the distinctive feature originates from the scattering paths involving fifth and sixth coordination shells. The lack of that feature for thin films was interpreted as a result of crystalline order range shorter than five coordination shells.

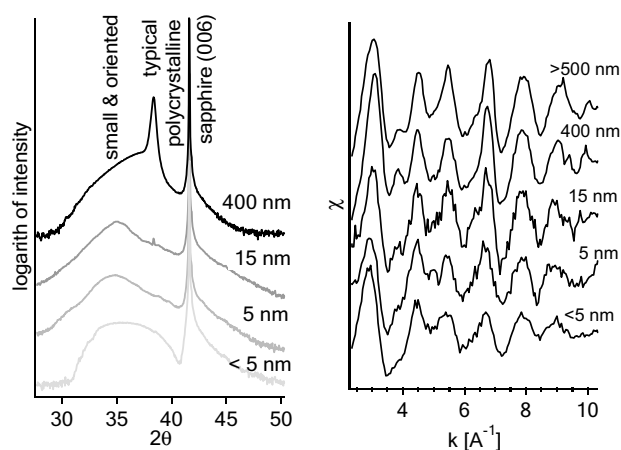


Figure 1. XRD $\omega/2\theta$ patterns and EXAFS measured Nb/sapphire(001) films of various thicknesses

The obtained results show that polycrystalline niobium does not grow directly on the sapphire substrate. Its growth follows the formation of the layer containing extremely small crystallites and subsequently the layer of larger and oriented crystallites. As a result, the film of the thickness larger than 400 nm contains three pronouncedly different phases of niobium.

Acknowledgements: The work has been supported by the EC 7th Framework Programme under the grant agreement n° 226716.

APPLICATION OF WAVELENGTH-DISPERSIVE SPECTROSCOPY AT ID21 X-RAY MICROSCOPY BEAMLINE OF ESRF: NEW POSSIBILITIES FOR MICRO-FLUORESCENCE AND MICRO-XANES ANALYSIS

J. Szlachetko^{1,2*}, **M. Cotte**^{1,3}, **J. Morse**¹, **M. Salomé**¹, **M. Pajek**¹, **P. Jagodzinski**⁴,
J.-Cl. Dousse⁵, **J. Hoszowska**⁵, **Y. Kayser**⁵, and **J. Susini**¹

¹ European Synchrotron Radiation Facility, Grenoble, France

² Institute of Physics, Jan Kochanowski University, Kielce, Poland

³ Centre of Research and Restoration of French Museums, UMR171, Paris, France

⁴ University of Technology, Kielce Poland

⁵ Department of Physics, University of Fribourg, Switzerland

Keywords: wavelength-dispersive spectroscopy, micro-fluorescence, x-ray imaging

*) jakub.szlachetko@esrf.fr

The ESRF ID21 beamline relies on a submicrometer X-ray probe in the energy range between 2 keV and 7.2 keV and is mainly oriented to micro-X-ray fluorescence and micro-XANES analysis. Increasing demands for developing new and complementary x-ray techniques to be used in different applications (e.g. semiconductor nano-technology, biology, geology, archaeology) are presently focused on high-resolution and sensitivity x-ray fluorescence techniques combined with a narrow, down to the sub-micrometer range, x-ray beam excitation. Until now, the ID21 beamline relied on several solid-state detectors, which are complementary in terms of count-rate throughput and solid-angle collection efficiency. However, the attainable energy resolution (120–180 eV) of such energy-dispersive detectors is often inadequate to permit unequivocal elemental and chemical speciation. To improve the energy resolution of fluorescence detection of the X-ray microscope, a new x-ray wavelength dispersive spectrometer (WDS) have been developed for the micro-fluorescence analysis [1].

The spectrometer employs a polycapillary optics that gives a large (20°) collection solid angle for X-ray fluorescence. Such collimating polycapillary optics outputs a quasi-parallel beam which is directed onto plane crystal analyzer and recorded by a gas-proportional counter. In order to record the x-rays in energy range between 0.5 keV to 7 keV four different crystals are employed. The simple design results in a compact spectrometer, which fits a limited space available around immediate sample environment of the X-ray Microscope.

We present the construction details, operational characteristics, and the performance achieved with the new spectrometer. In particular, the spectral energy resolution, line shapes and throughput are compared with results from Monte Carlo simulations.

The examples of application of the spectrometer in the measurements combining two-dimensional imaging with a high spectral resolution will be discussed. The advantages of using WDS micro-fluorescence and micro-

XANES for analysis of the cultural heritage and geological samples (see Fig. 1) will be demonstrated. Further possibilities for improving the energy resolution, down to the ~1 eV level, will be discussed and preliminary results from tests made using a double-crystal geometry will be given. The latter provides the measurements of absorption spectra which are free of the lifetime-broadening.

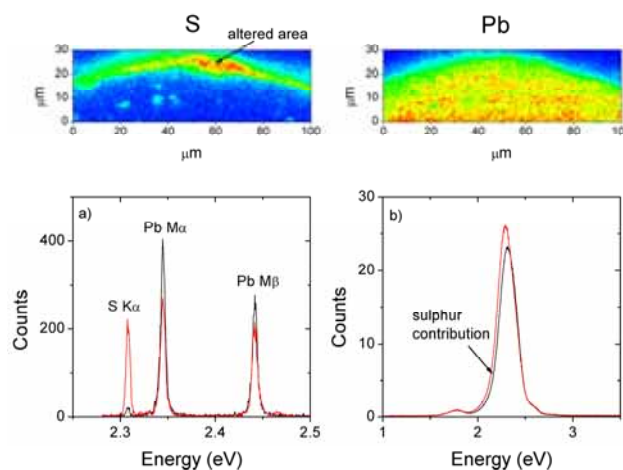


Figure 1. Top panels: X-ray fluorescence maps of S and Pb in the painting cross section containing the altered area. (a) The polycapillary-based WDS X-ray fluorescence spectrum recorded in the altered (red) and safe (black) areas. (b) The same as (a) but acquired using a Si drift diode detector.

References

- [1] J. Szlachetko, M. Cotte, J. Morse, M. Salomé, P. Jagodzinski, J.-C. Dousse, J. Hoszowska, Y. Kayser, J. Susini, "Wavelength-dispersive spectrometer for X-ray microfluorescence analysis at the X-ray microscopy beamline ID21 (ESRF)", *J. Synchrotr. Rad.* **17** (2010) 400.

PROPERTIES OF RARE-EARTH ORTHOVANADATES UNDER HIGH PRESSURE

W. Paszkowicz *

Institute of Physics, Polish Academy of Sciences, Al. Lotników 32/46, 02-668 Warsaw, Poland, e-mail: paszk@ifpan.edu.pl

Keywords: high pressure, phase transition, bulk modulus orthovanadate, rare earth

**) e-mail: paszk@ifpan.edu.pl*

RVO_4 , ($R = Y, Sc, Pr - Lu$) orthovanadates, crystallizing in $I4_1/amd$ space group (zircon type structure), exhibit physical properties that may lead to various applications. One of well known examples is the Nd doped YVO_4 , a laser material. Some of compounds of this family are considered as being suitable for birefringent lasers, optical waveguides and polarizers, they can be used for remote thermometry, as catalysts for oxidative dehydrogenation, and are candidates for advanced bio-imaging phosphors and as components of toughened ceramic composites. For example, $EuVO_4$, is considered as both, a potential phosphor (the metastable scheelite phase) [1,2] and a potential ionic conductor (the stable zircon phase) [2].

RVO_4 compounds belong to a large family of AXO_4 compounds that most frequently adopt the structures of zircon, scheelite, fergusonite, monazite, wolframite, $CrVO_4$, $ZnSO_4$ and rutile types [3-5]. Phase relationships in this family observed as a function of pressure have been systematized in Refs. [4,6] (for all possible AXO_4 compounds), and in Refs. [5] for RXO_4 compounds ($X = P, As, V$). For RVO_4 , $R = Ce$ to Lu , the most stable ambient pressure structure is of zircon type, space group $I4_1/amd$, this structure can be also obtained for $R = La$ using special preparation methods.

A number of studies have been performed by means of various experimental techniques and theoretical approaches, yielding the limited information on the equations of state and on zircon-scheelite pressure transitions. For the given compound, the discrepancies in bulk modulus between different experimental and theoretical datasets attain 20 GPa. Moreover, the phase-transition point and the range of pressures where both

phases coexist, show a considerable scatter. Understanding of these discrepancies may be useful for further studies of these or similar compounds.

In this talk, existing data for compressibility and zircon-scheelite phase transition in RVO_4 is reviewed. The importance of using hydrostatic-compression conditions is emphasised. Systematic trends for the bulk modulus and phase transition pressure are revealed within the RVO_4 family and connected with the lanthanide contraction effect. Differences between the elastic properties reported by various author for the given compound will be discussed.

References

- [1] U. Rambabu, D.P. Amalnerkar, B.B. Kale, S. Buddhudu, "Fluorescence spectra of Eu^{3+} -doped $LnVO_4$ ($Ln = La$ and Y) powder phosphors", *Mater. Res. Bull.* **35** (2000) 929–936.
- [2] L.-P. Li, G.-S. Li, Y.-F. Xue, H. Inomata, "Structure, luminescence, and transport properties of $EuVO_4$ ", *J. Electrochem. Soc.* **148** (2001) J45–J49.
- [3] O. Muller, R. Roy, "Phase transitions among ABO_4 compounds", *Z. Kristallogr.* **198** (1973) 237–253. FULL
- [4] O. Fukunaga, S. Yamaoka, "Phase transformations in ABO_4 type compounds under high pressure", *Phys. Chem. Miner.* **5** (1979) 167–177.
- [5] U. Kolitsch, D. Holtstam, "Crystal chemistry of $REEXO_4$ compounds ($X = P, As, V$). II. Review of $REEXO_4$ compounds and their stability fields", *Eur. J. Miner.* **16** (2004) 117–126.
- [6] D. Errandonea, F.J. Manjón, "Pressure effects on the structural and electronic properties of ABX_4 scintillating crystals", *Prog. Mater. Sci.* **53** (2008) 711–773.

ELECTRONIC STRUCTURE AND CRYSTALLINE STRUCTURE OF VICINAL BERYLLIUM SURFACES

L. Walczak¹, **V. Joco**², **G. Goryl**³, **M.A. Valbuena**⁴, **T. Balasubramanian**⁵,
P. Segovia¹, **M. Szymonski**³, and **E.G. Michel**¹

¹*Departamento de Física de la Materia Condensada, Universidad Autónoma de Madrid, 28049 Madrid, Spain.*

²*Centro de Microanálisis de Materiales, Universidad Autónoma de Madrid, 28049 Madrid, Spain.*

³*Faculty of Physics, Astronomy and Applied Computer Science, Jagiellonian University in Krakow, Poland.*

⁴*Ecole Polytechnique Fédérale de Lausanne, Inst. de Physique de la Matière Condensée, Lausanne, Switzerland.*

⁵*MAX-Lab, Lund University, Lund S 22100, Sweden*

Keywords: vicinal surface, beryllium, angle resolved photoemission spectroscopy

*) *e-mail: lukasz.walczak@uam.es*

A surface vicinal to a high-symmetry crystalline orientation is an interesting example of a one-dimensional nanostructured system. The case of noble metal surfaces vicinal to the (111) direction has been studied in detail in recent years [1,2]. It was found that the surface states are confined by the periodic step superlattice. Under adequate conditions, quantum well states are observed. Group II metals (like Be and Mg) exhibit several prominent surface states with a high density of states [3]. In the case of the (10-10) surface, there are different surface states, both for normal and off-normal emission (surface A point) [4].

The main objective of the present work is an investigation on the electronic properties of beryllium surfaces vicinal to the (10-10) direction using a low energy electron diffraction (LEED), Scanning Tunneling Microscope (STM), Angle Resolved Photoemission Spectroscopy (ARPES) with synchrotron radiation from I4 beamline at Maxlab. Lund. The sample long range order was confirmed by LEED, which showed superstructure spot splitting. The step superlattice was optimized by STM, that shows regular steps along [0001] direction. The electronic structure along steps (Gamma M surface direction) and perpendicular to steps (Gamma A surface direction) for several photon energies and for a range of different miscut angles was characterized. We identified several surface state bands, for both normal

and off-normal emission (surface A point). The binding energy of the surface state at the surface A point depends on the crystal miscut angle, so that the surface state becomes slightly shallower than for a flat surface, as expected assuming a partial lateral confinement by the step superlattice. Concerning the surface state observed at normal emission, we find the appearance of additional subbands whose dispersion is compatible with lateral confinement induced by the step superlattice. The results for different miscut angles will be discussed and interpreted within this model.

References

- [1] J.E. Ortega, S. Speller, A.R. Bachmann, A. Mascaraque, E. G. Michel, A. Närmann, A. Mugarza, A. Rubio, F.J. Himpsel, "Electron wave function at a vicinal surface: switch from terrace to step modulation", *Phys. Rev. Lett.* **84** (2000) 6110-6113.
- [2] A. Mugarza, J.E. Ortega, "Electronic states at vicinal surfaces", *J. Phys. Cond. Matt.* **15** (2003) S3281.
- [3] E.W. Plummer, J. B. Hannon, "The surface of beryllium", *Prog. Surf. Sci.* **46** (1994) 149.
- [4] T. Balasubramanian, L.I. Johansson, P.-A. Glans, C. Virojanadara, V.M. Silkin, E.V. Chulkov, P.M. Echenique, "Surface electronic band structure and \bar{A} surface state lifetimes at the Be(1010) surface: Experiment and theory", *Phys. Rev. B* **64** (2001) 205401.

GENETIC ALGORITHMS FOR STRUCTURAL OPTIMIZATION PROBLEMS AT THE NANOSCALE

Cristian V. Ciobanu *

Division of Engineering, Colorado, School of Mines, Golden, Colorado 80401, USA

Keywords: global optimization, genetic algorithm, nanoscale, scanning tunneling microscopy, cluster, semiconductor surface, nanowire

**) e-mail: cciobanu@mines.edu*

In the cluster structure community, global optimization methods are common tools for seeking the structure of molecular and atomic clusters. The large number of local minima of the potential energy surface (PES) of these clusters, and the fact that these local minima proliferate exponentially with the number of atoms in the cluster simply demands the use of fast stochastic methods to find the optimum atomic configuration. Therefore, most of the development work has come from (and mostly stayed within) the cluster structure community. Partly due to wide availability and landmark successes of scanning tunneling microscopy (STM) and other high resolution microscopy techniques, finding the structure of periodically reconstructed semiconductor surfaces was not generally posed as a problem of stochastic optimization until recently, when we have shown that high-index semiconductor surfaces can have a rather large number of local minima with such low surface energies that the identification of the global

minimum becomes problematic. We have therefore set out to develop global optimization methods for systems other than clusters, focusing on periodic systems in one- and two- dimensions as such systems currently occupy a central place in the field of nanoscience.

In this talk, we review some of our recent work on global optimization methods (the parallel-tempering Monte Carlo method and the genetic algorithm) and show examples/results from two main problem categories: (a) the two-dimensional problem of determining the atomic configuration of clean semiconductor surfaces, and (b) finding the structure of freestanding nanowires. While focused on mainly on atomic structure, our account will show examples of how these development efforts contributed to elucidating several physical problems and we will attempt to make a case for widespread use of these methods for structural problems in one and two dimensions.

APPLICATION OF GENETIC ALGORITHMS TO SURFACE X-RAY DIFFRACTION ANALYSIS

J. Martinez-Blanco ¹, V. Joco ¹, C. Quiros ², P. Segovia ¹, and E.G. Michel ^{1*}

¹ *Departamento de Física de la Materia Condensada and Instituto Universitario de Ciencia de Materiales 'Nicolas Cabrera', Universidad Autonoma de Madrid, 28049 Madrid, Spain*

² *Departamento de Física, Universidad de Oviedo–CINN, c/ Calvo Sotelo s/n, 33007 Oviedo, Spain*

Keywords: genetic algorithm, surface x-ray diffraction, surface phase transitions

**) e-mail: enrique.garcia.michel@uam.es*

A precise knowledge of the crystalline structure of a surface is one of the most important aspects required to understand its properties [1]. SXRD is one of the most powerful techniques sensitive to long-range order. A generalized use of SXRD as a standard technique has been hindered by several difficulties, one of them being the fact that if the surface structure is complex, with several different adsorption sites and a large unit cell, the process of fitting an SXRD dataset can be long and tedious. In this contribution we introduce the use of genetic algorithms [2] for the analysis of SXRD data, taking into account its specificities, and compare their features with other methods commonly used, like simulated annealing or Levenberg–Marquardt algorithms. We also present the analysis of the surface structure of Sn/Cu(100)-(3√2×√2)R45° using these methods. This structure has been analyzed in detail using dynamic LEED, so that the results of the use of a genetic algorithm can be compared easily to previous structural data. We find a good agreement between dynamic LEED results, and sometimes an almost exact coincidence, with most of the distances obtained in this work from SXRD and using the differential evolution algorithm for the optimization of the fit.

As there are no precedents in the use of this algorithm for the crystallographic analysis using SXRD, these findings support the validity of the method, which is found to be a promising and powerful tool in the analysis of this kind of problem [4]. It is able to extract crystallographic information in a fast and reliable way, in

spite of the large size of the unit cell and the significant number of parameters fitted. A general comparison with other methods is difficult, as only the Levenberg–Marquardt and the *simulated annealing* method are actually implemented in a fitting code of widespread use. While these methods are useful for the refinement of a model, the genetic algorithm appears as a much powerful and fast method to discriminate between possible models and to find the best structure for a certain model, *i.e.* in what concerns the uniqueness and reliability of the model found, mainly due to the much broader range of structures probed in a systematic way.

References

- [1] R. Feidenhans'l, "Surface structure determination by X-ray diffraction", *Surf. Sci. Rep.* **10** (1989) 105–188.
- [2] J.H. Holland, *Adaptation in Natural and Artificial Systems, an Introductory Analysis with Application to Biology, Control and Artificial Intelligence* (Ann Arbor, MI: The University of Michigan Press, 1975).
- [3] K. Pussi, E. AlShamaileh, E. McLoughlin, A.A. Cafolla, M. Lindroos, "Determination of the structure of Cu{100}-p(3√2×√2)R45°–Sn by dynamical LEED", *Surf. Sci.* **549** (2004) 24–30.
- [4] J. Martinez-Blanco, V. Joco, C. Quiros, P. Segovia, E.G. Michel, "Surface x-ray diffraction analysis using a genetic algorithm: the case of Sn/Cu(100)-(3√2×√2)R45°", *J. Phys. Cond. Mat.* **21** (2009) 134011.

STRATEGY OF METAHEURISTIC ALGORITHMS FOR LASER OPTIMIZATION

Hiromitsu Tomizawa *

Japan Synchrotron Radiation Research Institute (JASRI), XFEL Joint Project/SPring8,
1-1-1 Kouto, Sayo-cho, Sayo-gun, Hyogo, Japan

Keywords: XFEL, ERL, synchrotron radiation, photocathode, EO-sampling, genetic algorithms, metaheuristics, laser shaping, laser alignment

*) e-mail: hiro@spring8.or.jp

A laser is one of the most important experimental tool. In synchrotron radiation field, a laser widely used for experiments with Pump-Probe techniques and so on. Especially for the future X-ray-FELs, a laser has important roles as a seed light source, or photocathode-illuminating light source to generate a high brightness electron bunch. The controls of laser pulse characteristics are required for many kinds of experiments. A laser pulse is characterized in its pulse energy, pulse chirp, spectral distributions (both of intensity and phase), 3D-profile (both of spatial and temporal), wavefront distortion, M^2 -value, pointing stability, timing jitter, *etc.* However, the laser should be tuned and customized for each requirement by laser experts. The automatic tuning of laser is required to realize with some sophisticated algorithms. The metaheuristic algorithm is one of the useful candidates to find one of the best solutions as acceptable as possible. The metaheuristic laser tuning system is expected to save our human resources and time for the laser preparations.

However, these laser pulse characteristics are not perfectly independent of each other. In this case, it is almost impossible to determine the best solution uniquely by mathematical formulae. The metaheuristic algorithm is powerful methodology to find some of the acceptable and the most preferable solutions with searching better parameters. Many kinds of metaheuristic algorithms have been proposed and applied widely. I utilized a genetic algorithm (GA) [1] and a simulated annealing method [2] to optimize 3D laser pulse shape, and a hill climbing method with a fuzzy set theory [3] to align a laser to reliable path for each experiment at advanced photoinjector test facility in SPring-8. Applying any kind of metaheuristic algorithm, a great number of system's parameter must be introduced. Making the probability higher to find some solutions as good as possible, it is necessary to increase freedom of its searching space. For instance, optimizing laser shape, I introduced adaptive optics to increase the parameters of laser system. I have planned to use a deformable mirror (DM) [1] for spatial (transverse) shaping, and a glass (fused silica)-plate-based spatial light modulator (SLM) [4] for temporal (longitudinal) shaping. In 2005, I completed system to manipulate 3D laser pulse shape as an illuminating light source for a photocathode RF gun [5]. The laser spatial profile was adaptively optimized with a metaheuristic method designed for a DM that consists of an

aluminium-coated membrane and 59 small mirror actuators behind the reflective membrane. Adjusting voltages between the control electrodes on the boundary actuators results in fine adjustment of each mirror actuator; the adjustable region of the control voltages is between 0 and 250 V in steps of 1 V, making it possible to shape the arbitrary spatial profiles for a total of 250^{59} ($\sim 10^{141}$) deforming possibilities. Because of such high adjustability, the spatial shaping with the DM needs a sophisticated algorithm. Software based on a GA was developed to adaptively optimize DM deformation.

The set of the voltages of all DM-electrodes is treated as chromosomes in this software. A closed loop system is essential for a DM to adaptively optimize the laser's spatial profile. I used a PC to control the electrode voltage of the DM and to measure the spatial profile with a laser profile monitor (LBA300-PC, Spiricon Inc.). Laser light is reflected with deformation by the DM and monitored with the laser profile monitor, whose analyzing program can provide many parameters to evaluate the beam profile characteristics. I chose useful parameters to evaluate the flattop profiles and made a fitting function for the developed the GA software to optimize the profile toward an ideal flattop. The fitting function is a linear combination of flattop shaping parameters with certain optimal weights for fast convergence. The fitting function is returned as feedback to control the DM with the GA. As a result, the laser profile on the cathode surface was spatially shaped as a quasi-flattop profile [2].

I review mainly adaptive optical system developed with metaheuristic algorithms for controlling 3D laser pulse shape and laser alignment.

References

- [1] H. Tomizawa, *et al.*, Proc. of LO'03, St. Petersburg, Russia, 30 June -04 July 2003, (2004) 47–55.
- [2] H. Tomizawa, *et al.*, *Russian Journal of Quantum Electronics*, (2007) 697–705.
- [3] H. Tomizawa, "Advanced laser pulse shaping", Plenary Talk at ICFA Advanced Accelerator and Beam Dynamics Workshop, HBEB'09, Maui, Hawaii, 17 November 2009.
- [4] H. Tomizawa, *et al.*, Proc. of LINAC'04, Luebeck, Germany, 16-20 August 2004, (2004) 207–209.
- [5] H. Tomizawa, *et al.*, Invited talk at Proc. of tFEL'07, Novosibirsk, Russia, 26-31 August 2007, (2007) 298–305.

MAGNETOELASTIC COUPLING IN $\text{CaMn}_7\text{O}_{12}$

W. Sławiński^{1*}, **R. Przeniosło**¹, **I. Sosnowska**¹, and **M. Bieringer**²

¹ *Institute of Experimental Physics, University of Warsaw, 69 Hoża Str., 00-681 Warsaw, Poland*

² *Department of Chemistry, University of Manitoba, Winnipeg, R3T 2N2, Canada*

Keywords: perovskites, manganites, atomic position modulation, magnetic moments modulation, magnetoelastic coupling

**) e-mail: wojciech.slawinski@fuw.edu.pl*

The mixed manganese oxide $\text{CaMn}_7\text{O}_{12}$ is a multiferroic material [1] with a distorted perovskite structure [2]. The crystal structure [3] and the magnetic ordering [4] of $\text{CaMn}_7\text{O}_{12}$ have been studied by using high resolution SR diffraction and high resolution neutron diffraction. These diffraction studies show a modulation of the atomic positions in $\text{CaMn}_7\text{O}_{12}$ at temperatures below 250 K and magnetic structure modulation below $T_N = 90$ K [5,6].

The modulation of atomic positions has been described by using a quantitative model with a propagation vector $(0,0,q_p)$ [5] which gives good agreement with the results of both SR and neutron diffraction studies [6]. The neutron diffraction studies of $\text{CaMn}_7\text{O}_{12}$ show a modulated magnetic ordering below the Néel temperature $T_N = 90$ K. The modulation of the magnetic structure is described with a propagation vector $(0,0,q_m)$. Both magnetic and positional modulations are coupled together. The modulation length of the atomic positions (L_p) and of the magnetic moment modulation length (L_m) fulfill the relation $L_m = 2L_p$ at temperatures between 50 K and the Néel temperature T_N . The relation between modulation lengths L_p and L_m as well as minimum and maximum of the lattice constant c clearly show the magnetoelastic coupling in $\text{CaMn}_7\text{O}_{12}$ [1]. Below 50 K, there is a magnetic phase transition which is associated with important changes of the magnetic

modulation length and also with the increase of magnetoelastic coupling [1].

References

- [1] M. Sánchez-Andújar, S. Yáñez-Vilar, N. Biskup, S. Castro-García, J. Mira, J. Rivas, M. Señarís-Rodríguez, "Magnetolectric behaviour in the complex $\text{CaMn}_7\text{O}_{12}$ perovskite", *J. Magn. Magn. Mater.* **321** (2009) 1739–1742.
- [2] B. Bochu, J.L. Buevoz, "Bond lengths in $[\text{CaMn}_3][\text{Mn}_4]\text{O}_{12}$ "A new Jahn–Teller distortion of Mn^{3+} octahedral", *Solid State Commun.* **36**(2) (1980) 133–138.
- [3] W. Sławiński, R. Przeniosło, I. Sosnowska, M. Bieringer, I. Margiolaki, A.N. Fitch, E. Suard, "Phase coexistence in $\text{CaCu}_x\text{Mn}_{7-x}\text{O}_{12}$ solid solutions", *J. Solid State Chem.* **179**(8) (2006) 2443–2451.
- [4] R. Przeniosło, I. Sosnowska, D. Hohlwein, T. Hauß, I.O. Troyanchuk, "Magnetic ordering in the manganese perovskite $\text{CaMn}_7\text{O}_{12}$ ", *Solid State Commun.* **111**(12) (1999) 687–692.
- [5] W. Sławiński, R. Przeniosło, I. Sosnowska, M. Bieringer, I. Margiolaki, E. Suard, "Modulation of atomic positions in $\text{CaCu}_x\text{Mn}_{7-x}\text{O}_{12}$ ($x \leq 0.1$)", *Acta Crystallogr. B* **65** (2009) 535–542.
- [6] W. Sławiński, R. Przeniosło, I. Sosnowska, M. Bieringer, "Structural and magnetic modulations in $\text{CaCu}_x\text{Mn}_{7-x}\text{O}_{12}$ " *J. Phys.: Condens. Matt.* **22** (2010) 186001–6.

IN SITU HIGH TEMPERATURE MAGNETIC AND DYNAMIC PROPERTIES OF Fe(110) NANOSTRUCTURES STUDIED WITH NUCLEAR RESONANT SCATTERING TECHNIQUES

M. Zając^{1,2*}, **T. Ślęzak**¹, **M. Ślęzak**¹, **K. Freindl**^{1,3}, **P. Cierniak**¹,
E. Partyka-Jankowska⁴, and **J. Korecki**^{1,3}

¹ Faculty of Physics and Applied Computer Science, AGH University of Science and Technology,
Al. Mickiewicza 30, 30-059 Kraków, Poland

² European Synchrotron Radiation Facility, 6 rue Jules Horowitz, 38043 Grenoble, France

³ Institute of Catalysis and Surface Chemistry, Polish Academy of Sciences,
ul. Niezapominajek 8, 30-239 Kraków, Poland

⁴ Faculty of Physics University of Vienna Dynamics of Condensed Systems, Strudlhofgasse 4, A-1090 Vienna, Austria

Keywords: magnetism, nuclear resonance scattering, nuclear inelastic scattering, Fe(110)/W(110)

*) e-mail: zajac@esrf.fr

The developments of the third-generation synchrotron radiation sources during the last decades resulted in an enormous brilliance of the delivered x-ray beams, which has opened new possibilities in characterizing nanoscale objects. In particular, nuclear resonance scattering (NRS) of synchrotron radiation was brought to a stage, which allows one to systematically investigate electronic, magnetic, and dynamic properties of low-dimensional systems. In order to study well-defined nanostructures, one needs to prepare, characterize, and maintain the samples during experiments under controlled, preferably ultrahigh vacuum (UHV) conditions, which requires a dedicated sample environment. This is nowadays possible at the NRS beamline ID18 [1] of the ESRF using recently constructed UHV system [2], which combines the standard surface preparation and characterization techniques with the modern NRS-based spectroscopies. The capabilities of such methodology has been recently demonstrated in studies of epitaxial Fe/W(110) ultrathin films. The evolution of the spin structure was determined during the growth of Fe on W(110) single crystal with use of Nuclear Resonant Scattering of X-rays [3]. Analysis of the measured time spectra allowed for resolving the complex magnetic structure occurring in the 1 - 2 Fe monolayer coverages. For thicker Fe films the scenario of in-plane spin reorientation transition was determined indicating that during the transition an exotic non-collinear magnetization structure is formed.

In parallel, the dynamical properties of Fe nanostructures and surfaces were investigated by Nuclear Inelastic Scattering technique. The systematical investigation of the evolution of the thermo-elastic properties of Fe from the bulk to a single atomic layer (ML) by measuring the density of phonon states (DOS) were performed [4].

In this contribution we report on further progress in that field connected with the unusual structural and magnetic properties of epitaxial iron monolayers and nanostructures on W(110) observed at high temperatures.

Thermodynamic stability of Fe films on W(110) crucially depends on their thickness. The monolayer is believed to be stable at least to 1000 K [5], while thicker

films (beyond 2 ML) break into islands already at 600 K as we have observed for 2.5 ML [6]. The morphology of islands depends strongly on the deposition/annealing temperature, but also on the morphology of the tungsten substrate. Using NRS we have observed entirely unexpected magnetic properties of Fe nanostructures formed from the 1.5 ML of iron after annealing. It will be shown that magnetic order persisting in such system up to approximately Curie temperature of bulk Fe diminishes during cooling from high temperature and disappears around room temperature. Moreover, this "inverse" magnetic transition seems to be reversible, i.e. magnetic order re-appear at subsequent heating to 500°C.

As the second result a high temperature phonon density of states for Fe(110) monolayer measured with Nuclear Inelastic Scattering will be discussed.

Acknowledgments: This work was supported in part by the Polish Ministry of Science and Higher Education and in part by the European Community under the project NMP4-CT-2003-001516 (DYNASYNC), as well as by the Team Program of the Foundation for Polish Science co-financed by the European Regional Development Fund.

References

- [1] R. Rüffer, A.I. Chumakov, "Nuclear Resonance Beamline at ESRF", *Hyperfine Interact.* **97-98** (1995) 589.
- [2] S. Stankov, R. Rüffer, M. Sladeczek, M. Rennhofer, B. Sepiol, G. Vogl, T. Ślęzak, J. Korecki, "An ultrahigh vacuum system for *in situ* studies of thin films and nanostructures by nuclear resonance scattering of synchrotron radiation", *Rev. Sci. Instrum.* **79** (2008) 045108.
- [3] T. Ślęzak, M. Ślęzak, N. Spiridis, K. Freindl, M. Zając, S. Stankov, R. Rüffer, J. Korecki, "Magnetism of ultrathin iron films seen by the Nuclear Resonance Scattering of Synchrotron Radiation", *ICAME Conference*, Vienna, 2010.
- [4] S. Stankov, R. Röhlberger, T. Ślęzak, M. Sladeczek, B. Sepiol, G. Vogl, A.I. Chumakov, R. Rüffer, N. Spiridis, J. Łażewski, K. Parliński, J. Korecki, "Phonons in Iron: From the Bulk to an Epitaxial Monolayer", *Phys. Rev. Lett.* **99** (2007) 185501.
- [5] P.J. Berlowitz, J.-W. He, D.W. Goodman, "Overlayer growth and chemisorptive properties of ultra-thin Fe films on W(110) and W(100)", *Surf. Sci.* **231** (1990) 315.
- [6] K.V. Bergmann, PhD Thesis, available at <http://www.physnet.uni-hamburg.de/services/fachinfo.htm>

RECENT ACHIEVEMENT IN CHARACTERIZATION OF MICRO- AND NANO-MATERIALS BY SCANNING PHOTOEMISSION IMAGING AND SPECTROMICROSCOPY

Matteo Amati ^{*}, **Majid Kazemian Abyaneh**, **Matteo Maria Dalmiglio**,
Luca Gregoratti, and **Maya Kiskinova**

Sincrotrone Trieste SCpA, SS14 Km163.5 in Area Science Park, 34149 Trieste, Italy

Keywords: electron spectroscopy, microscopy

**) e-mail: matteo.amati@elettra.trieste.it*

The Scanning PhotoEmission Microscope (SPEM) uses a direct approach to characterize chemically surfaces and interfaces at the submicron scale *i.e.* the use of a small focused x-ray photon probe to illuminate the sample. The focusing of the x-ray beam is performed by using a Zone Plate (ZP), which is a Fresnel type lens. The SPEM at the Elettra synchrotron light source, hosted at the ESCAmicroscopy beamline, can operate in two modes: imaging and spectroscopy. In the first mode the sample surface is mapped by synchronized-scanning the sample with respect to the focused photon beam and collecting photoelectrons with a selected kinetic energy. The second mode is an XPS from a microspot. The x-ray beam can be downsized to a diameter of 120 nm which allows imaging resolution of less than 50 nm. The overall energy resolution is better than 200 meV. Samples can be heated and biased during the measurements.

The beamline is open to the public and private research community; two call for proposals of experiment are available per year together with the possibility of dedicated collaborations on specific projects. Some recent achievements in the chemical, physical and electronic characterization of nano- and micro-structured materials will be presented providing an overview of the capabilities of this powerful technique. Metallic adsorbate interaction, oxidation and supporting properties of multiwall carbon, semiconducting and metal-based nanotubes will be presented, showing how even dynamic phenomena such as mass transport along the nanotube surface can be monitored by the SPEM [1,2]. A special design of the samples allows for the investigation of single nanotubes with diameter down to 50nm (see Fig. 1). The study of compositional and electronic properties of morphological complex 3D semiconducting structures will be presented as well.

Important industrial collaborations with international companies have been established in last years. A first example will report on the study of the degradation processes occurring on Organic Light Emitting Devices (OLEDs) [3]. Results on both OLEDs operated in ambient atmosphere and grown and operated in ultra-high-vacuum will be compared. Another example will illustrate the chemical characterization of the cathode surfaces of Solid Oxide Fuel Cells under working conditions [4]; the elemental distribution and its change

under biasing and the observation and explanation of the cathode electrochemical activation have been addressed.

Finally an overview of the limits in the applications of the x-ray photoelectron microscopes imposed by the operation principles will be given together with the future developments allowing the investigation of materials at mbar and even ambient pressure.

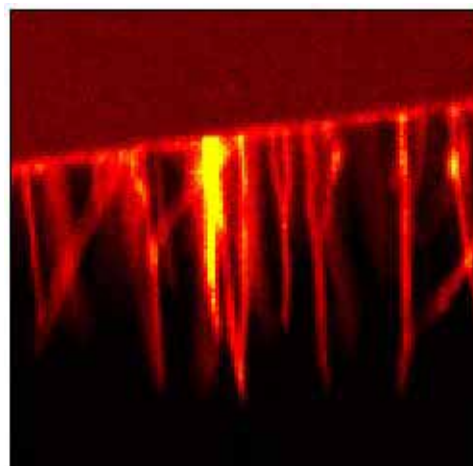


Figure 1. C1s photoemission map of aligned multiwall carbon nanotubes. Single separated tubes can be analysed.

References

- [1] A. Barinov, L. Gregoratti, P. Dudin, S. La Rosa, M. Kiskinova, "Imaging and spectroscopy of multiwalled carbon nanotubes during oxidation: Defects and oxygen bonding", *Adv. Mater.* **21** (2009) 1916–1920.
- [2] A. Barinov, H. Üstünel, S. Fabris, L. Gregoratti, L. Aballe, P. Dudin, S. Baroni, M. Kiskinova. "Defect-Controlled Transport properties of metallic atoms along carbon nanotube surfaces", *Phys. Rev. Lett.* **99** (2007) 046803.
- [3] P. Melpignano, A. Baron-Toaldo, V. Biondo, S. Priante, R. Zamboni, M. Murgia, S. Caria, L. Gregoratti, A. Barinov, M. Kiskinova, "Mechanism of dark-spot degradation of organic light-emitting devices", *Appl. Phys. Lett.* **86** (2005) 041105.
- [4] M. Backhaus-Ricoulta, K. Adib, T. St. Clair, B. Luerssen, L. Gregoratti, A. Barinov, "In-situ study of operating SOFC LSM/YSZ cathodes under polarization by photoelectron microscopy", *Solid State Ionics* **179** (2008) 891–895.

STRUCTURAL AND MAGNETIC PROPERTIES OF Si SINGLE CRYSTALS IMPLANTED WITH Mn

P. Romanowski^{1*}, **A. Shalimov**^{1,2}, **J. Bak-Misiuk**¹, **A. Misiuk**³, and **W. Caliebe**⁴

¹*Institute of Physics, Polish Academy of Sciences, al. Lotnikow 32/46, PL-02668 Warsaw, Poland*

²*Forschungszentrum Dresden-Rossendorf, Bautzner Landstr. 400, D-01328 Dresden, Germany*

³*Institute of Electron Technology, al. Lotnikow 46, PL-02668 Warsaw, Poland*

⁴*HASYLAB at DESY, Notkestr. 85, D-22603 Hamburg, Germany*

Keywords: silicon, manganese, implantation, annealing, ferromagnetism, synchrotron, diffraction, X-ray, SQUID, Si:Mn

**) e-mail: Przemyslaw.Romanowski@ifpan.edu.pl*

Ferromagnetic ordering in silicon implanted with Mn⁺ ions is of wide interest recently. This ordering is related to the structure of Mn-enriched near-surface layer in the implanted material (see, e.g., Refs. [1-4]). Silicon-based diluted magnetic semiconductors would be the preferred spintronic materials due to existing technology used in Si-based microelectronics and wide availability of high quality Si single crystals. The aim of present work is to study an influence of the ferromagnetic phase Mn₄Si₇ created during annealing on ferromagnetic properties of Si:Mn.

Si(001) samples were implanted with 160 keV Mn⁺ ions, to a dose, $D = 1 \times 10^{16}$ cm⁻². Si:Mn samples were processed for $t_A = 1-10$ h at up to $T_A = 1070$ K (HT) under ambient or enhanced hydrostatic pressures (HP), up to $p_A = 1.1$ GPa (see Table 1). To investigate the phase composition of thin polycrystalline layers created at processing, X-ray measurements were performed using coplanar 2θ scans in the glancing incidence geometry at W1 beamline of HASYLAB at DESY. The sample was fixed with the angle between monochromatic X-ray beam (wavelength $\lambda = 1.54056$ Å) and the sample surface equal to 1°. The detector moved parallel to the diffraction plane. Magnetic properties were studied by superconducting quantum interference device (SQUID) magnetometry using a Quantum Design MPMS XL. Two types of measurements, magnetization (M) vs. temperature (T) and M vs. field (H) were performed. The $M(T)$ curves were obtained using zero-field-cooling/field-cooling (ZFC/FC) protocol at the constant field of 100 Oe.

Si:Mn sample	T_A [K]	t_A [h]	p_A [Pa]
1	920	10	1.1×10^9
2	720	10	1.1×10^9
3	1070	5	1×10^5
4	610	1	1×10^5

Table 1. Annealing conditions of Si:Mn samples.

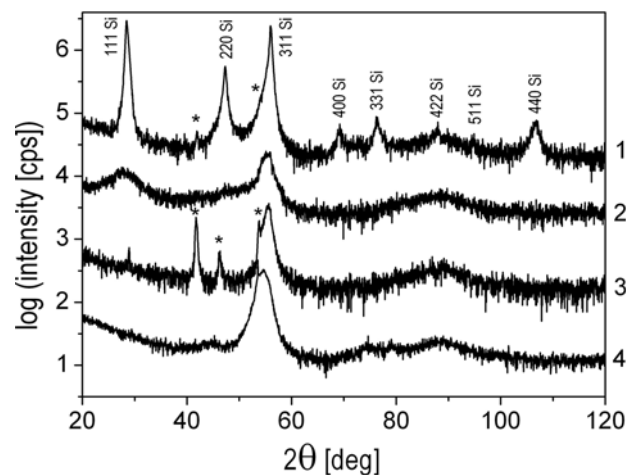


Figure 1. Coplanar 2θ scans measured using glancing incidence geometry for Si:Mn 1-4 samples (see Table 1). Diffraction peaks coming from Mn₄Si₇ phase are indicated by stars.

As shown in Fig. 1, the X-ray diffraction peaks from the ferromagnetic Mn₄Si₇ phase were detected mainly for the samples 1 and 3. The $M(H)$ curves were recorded at 4 K, 150 K and 300 K (Fig. 2). Magnetic field was applied parallel to the sample surface for the both experimental procedures. Experimental curves have been modeled using the Preisach approach of magnetic response described by T. Song *et al.* [5].

Experimental magnetic curves, $M(H)$ and $M(T)$, possess diamagnetic background at the temperature range of 4–300 K caused by silicon host crystal. The diamagnetic background was approximated by a straight line for both experimental protocols and has been extracted from the original data in order to investigate magnetic response of pure magnetic component of SiMn. From these experiments, we can conclude that after annealing at temperature range of 570–1070 K under atmospheric pressure no significant magnetic response was observed in Si crystals implanted with Mn. However, HT-HP annealing affects in generation of

magnetic particles (domains, clusters) with relatively high spontaneous magnetization of $(3-4)\times 10^{-16}$ emu/particle and absolute concentration of $(5.8-8.3)\times 10^8$ particles/mg. Surprisingly, average spontaneous magnetization and density of magnetic particles values decrease with the increasing of temperature during HT-HP annealing.

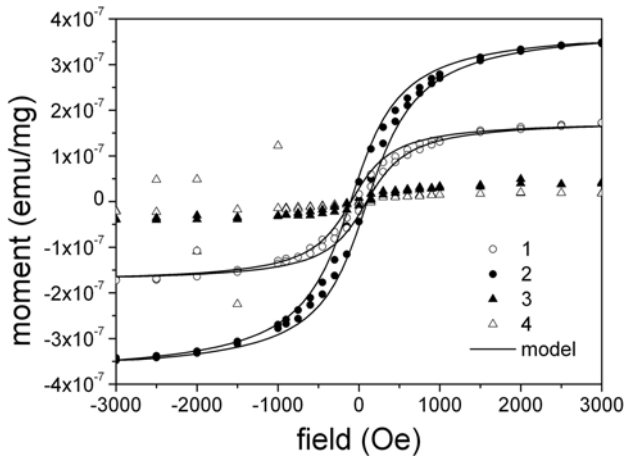


Figure 2. $M(H)$ curves measured at 300 K for Si:Mn 1–4 samples (see Table 1).

From our experiments it follows that magnetic properties of samples are not directly related to formation of the Mn_4Si_7 phase. Probably some other defects created during processing are responsible for observed magnetic properties of samples.

References

- [1] M. Bolduc, C. Awo-Affouda, A. Stollenwerk, M.B. Huang, F.G. Ramos, G. Agnello, V.P. LaBella, "Above room temperature ferromagnetism in Mn-ion implanted Si", *Phys. Rev. B* **71** (2005) 033302-(1–4).
- [2] J. Bak-Misiuk, E. Dynowska, P. Romanowski, J.Z. Domagala, A. Misiuk, W. Caliebe, "Structure of Si implanted with Mn", *HASYLAB Annual Report 2007* (2008) 821–822.
- [3] J. Bak-Misiuk, A. Misiuk, P. Romanowski, A. Barcz, R. Jakiela, E. Dynowska, J.Z. Domagala, W. Caliebe, "Effect of processing on microstructure of Si:Mn", *Mater. Sci. Eng. B* **159-160** (2009) 99–102.
- [4] J. Bak-Misiuk, E. Dynowska, P. Romanowski, A. Shalimov, A. Misiuk, S. Kret, P. Dłuzewski, J.Z. Domagala, W. Caliebe, J. Dabrowski, M. Prujarczyk, "Structure of magnetically ordered Si:Mn", *Sol. State Phen.* **131-133** (2008) 327–332.
- [5] T. Song, R.M. Roshko, E. Dan Dahlberg, "Modelling the irreversible response of magnetically ordered materials: a Preisach-based approach", *J. Phys.: Condens. Matt.* **13** (2001) 3443–3460.

HRXRD AND RBS/CHANNELING DETERMINATION OF THE CORRELATION BETWEEN RADIATION DAMAGE AND INTERPLANAR SPACING IN GaN EPILAYERS

M. Wojcik^{1*}, J. Gaca¹, A. Turos^{1,2}, P. Caban¹, W. Strupiński¹, and K. Pałowska²

¹ Institute of Electronic Materials Technology 01 919 Warsaw, Wolczynska 133, Poland

² Soltan Institute for Nuclear Studies, 05-400 Świerk /Otwock, Poland

Keywords: radiation damage, GaN, lattice misfit, HRXRD, RBS, MOCVD, epilayer

*e-mail:wojcik-m@itme.edu.pl

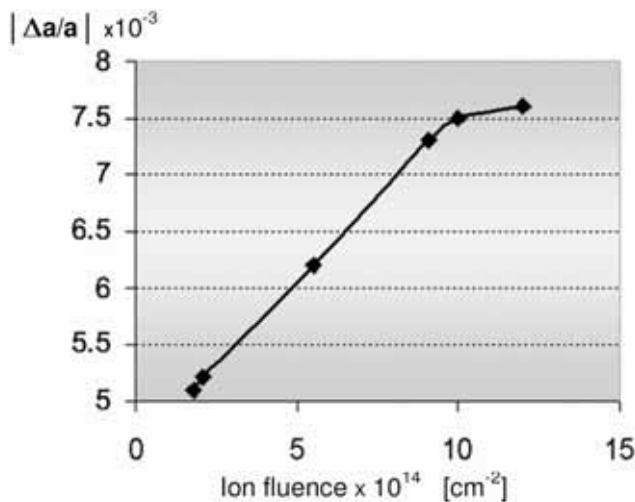


Figure 1. The lattice misfit $|\Delta a/a|$ between the ion-implantation damaged and non-damaged GaN layers as a function of the ions fluence.

Modification of the interplanar spacing profile (ISP) along the [1000] direction produced by Ar-ion irradiation of $1\mu\text{m}$ thick GaN epitaxial layers have been investigated by means of HRXRD and RBS techniques. GaN layers were grown on [1000] sapphire substrates in an AIX200/4RF-S metalorganic vapor phase epitaxy low-pressure reactor (LP MOVPE). Ar ions of 320 keV energy produce radiation defects in the surface layer extending over first 400 nm. The applied ion fluences ranged from $7 \cdot 10^{13} \text{ cm}^{-2}$ to $1.2 \cdot 10^{15} \text{ cm}^{-2}$ are well below the

amorphization threshold. ISP for each sample has been determined by simulation of the x-ray rocking curve using defect depth distributions provided by the RBS/channeling method as starting input data. The whole procedure consists of the following steps:

- determination of the defect density profile by the RBS technique,
- measurement of the rocking curve using synchrotron radiation with the wavelength $\lambda = 0.13993 \text{ nm}$,
- evaluation of the interplanar spacing and planar scattering power profiles using the RBS data as a first approximation of the crystal model for rocking curve calculation,
- variation of the shape of the interplanar spacing and planar scattering power profiles until the best fit between the experimental and calculated rocking curves has been obtained.

For all investigated samples the interplanar spacing increased as a result of ion bombardment. This change proved to be a linear function of the ion fluence (see Fig. 1) for ion fluences lower than $1.0 \cdot 10^{15} \text{ cm}^{-2}$. This effect can also be closely correlated with the concentration of structural defects in the irradiated volume.

Acknowledgments: The authors would like to thank the European Commission for the financial support of part of this experiment at ROBL (experiment SI-1261 at BM20 line, ESRF).

LOCAL STRUCTURE IN Te DOPED GaAs

R. Bacewicz^{1*}, **A. Pietnoczka**¹, **W. Zalewski**¹, **A. Antonowicz**¹, and **T. Słupiński**²

¹Faculty of Physics, Warsaw University of Technology, ul. Koszykowa 75, 00-662 Warsaw, Poland

²Institute of Experimental Physics, Warsaw University of Technology, ul. Hoża 69, 00-681 Warsaw, Poland

Keywords: EXAFS, gallium arsenide, tellurium, dopant

*) e-mail: bacewicz@if.pw.edu.pl

Tellurium doping of GaAs is used to provide n-type conductivity. Tetrahedrally coordinated Te substituting As is a shallow donor, and the electron concentration is usually close to the concentration of Te atoms. However, in heavily doped GaAs:Te reversible changes of the free electron concentration with the high temperature annealings were observed since early sixties of 20th century [1]. Various hypotheses were proposed to explain a deactivation mechanism in GaAs:Te. Fuller and Wolfstirn [1] suggested creation of "impurity molecules" which trap electrons. Gebauer *et al.* [2] identified $V_{\text{Ga}}\text{-Te}_{\text{As}}$ complexes as responsible for the compensation effect. However, the latter hypothesis does not explain recovery of the electron concentration by the high temperature annealing. Using the X-ray diffuse scattering technique, the reversible changes of the concentration were attributed in [3] to the creation of the impurity pairs. In this contribution, we report the results of XAFS measurements in an attempt to determine local changes around Te atoms for different states of GaAs:Te crystals corresponding to different electron concentrations.

GaAs:Te crystal has been grown by Czochralski method with the tellurium concentration $(1.7\text{-}1.8)\times 10^{19}\text{ cm}^{-3}$. Three samples were cut from that crystal and annealed at 1185°C for 4 h (sample J1), at 1050°C for 39 h (sample BA), and at 800°C for 288 h (sample J3). For the J1 sample free electron concentration is approximately equal to Te atoms concentration. For the samples BA and J3 free carrier concentration is $1.5\times 10^{19}\text{ cm}^{-3}$ and $3.5\times 10^{18}\text{ cm}^{-3}$ respectively. EXAFS measurements at the Te K edge have been carried out at the X1 beamline in the HASYLAB at room temperature and at 80 K. Due to the dilution of Te in our crystals ($[\text{Te}] < 0.1\%$) multiple-scans were recorded in the fluorescence mode with a Si:Li detector. Fig. 1 shows the Fourier transforms of the EXAFS oscillations for three samples.

For the J1 and BA samples the substitutional Te_{As} model fits perfectly the EXAFS data with dilatation of the nearest-neighbour distance due to the difference in atomic radii of Te and As (from 2.43 Å for the As–Ga distance to 2.65 Å for the Te–Ga bond length). For the J3 sample the EXAFS from the first coordination shell is very similar to that of other two samples. Thus in a low electron concentration state, the close environment of Te atoms remains unchanged as compared to the high concentration state (J1). So, we have to reject those of DX models of Te impurity in GaAs which assume large

lattice relaxation in the first-neighbour shell of Te impurity.

Following the authors of the paper [3] we assumed that in the low concentration state (J3 sample) electrons are trapped by clusters of the Te pairs. We allowed a relaxation of two Te atoms towards each other in the $\langle 110 \rangle$ direction. We found that a model combining the substitutional Te_{As} with the Te pairs model in a proportion resulting from the electron concentration ratio provides a good fit to the EXAFS data with a Te relaxation of 0.8 Å. However, it has to be noted that the EXAFS itself is not able to provide a univocal evidence for the Te pairs model. We await a theoretical justification to support such a hypothesis.

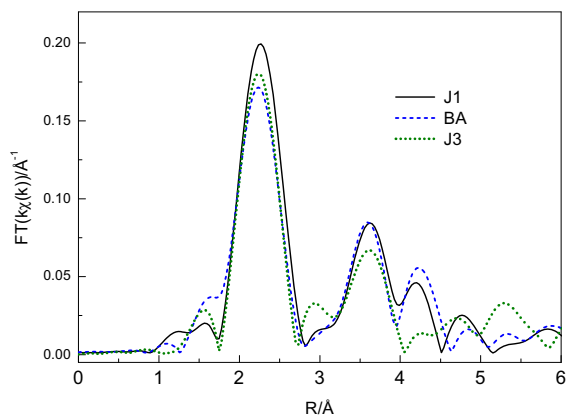


Figure 1. Fourier transforms of the EXAFS oscillations for 3 samples of GaAs:Te with $[\text{Te}] = 1.7\times 10^{19}\text{ cm}^{-3}$ subject to different thermal treatments.

References

- [1] C.S. Fuller, K.B. Wolfstirn, "Changes in electron concentration of donor-doped GaAs crystals", *J. Appl. Phys.* **34** (1963) 2287–2289.
- [2] J. Gebauer, E.R. Weber, N.D. Jaeger, K. Urban, Ph. Ebert, "Determination of the charge carrier compensation mechanism in Te-doped GaAs by scanning tunnelling microscopy", *Appl. Phys. Lett.* **82** (2003) 2059–2061
- [3] T. Słupiński, E. Zielińska-Rohozińska, "Local order of Te Impurity atoms in heavily doped GaAs:Te and accompanying electron localization effect", *MRS Symp. Proc.* **583** (2000) 261–266

HIGH ENERGY PHOTOEMISSION FROM COVERED LAYER

B.A. Orlowski^{1*}, **P. Dziawa**¹, **K. Gas**¹, **S. Mickievicius**², **M. Szot**¹, **J.B. Pelka**¹,
M.A. Pietrzyk¹, **B.J. Kowalski**¹, **S. Thies**³, and **W. Drube**³

¹*Institute of Physics, Polish Academy of Sciences, Al. Lotnikow 32/46, 02-668 Warsaw, Poland*

²*Semiconductor Physics Institute, A. Gostauto 11, 2600 Vilnius, Lithuania*

³*Hamburger Synchrotronstrahlungslabor HASYLAB am Deutschen Elektronen-Synchrotron DESY, Notkestr. 85, D-22603 Hamburg, Germany*

Keywords: photoemission spectroscopy, synchrotron radiation, IV-VI semiconductors

**) orbro@ifpan.edu.pl*

The experiment was performed using the Tunable High Energy X-ray Photoemission Spectrometer (THE-XPS) at wiggler beam line station BW2 of the HASYLAB, DESY, Hamburg, Doris III storage Ring. Double crystal monochromator (Si(111)) covers an energy range from 2.4 to 10 keV with a monochromatic photon flux of about 5×10^{12} photons/s and with total energy resolution power of 0.5 eV for radiation energy around 3000 eV was used.

The nanostructure was grown by MBE deposition method in the Institute of Physics, Polish Academy of Sciences in Warsaw [1]. The CdTe buffer layer (45 nm) was evaporated on GaAs (100) wafer and $\text{Pb}_{0.95}\text{Eu}_{0.05}\text{Te}$ layer of 6 nm thickness was evaporated on it. The layer of $\text{Pb}_{0.95}\text{Eu}_{0.05}\text{Te}$ was covered by CdTe layer of thickness 22 nm.

The energy $h\nu = 3510$ eV was found as an optimal for measurements where the kinetic energy of the $\text{Eu}3d$ electrons is not overlapping of Pb Auger electrons from the $\text{Pb}_{0.95}\text{Eu}_{0.05}\text{Te}$ layer. The set of spectra containing: valence band, Cd $3d$ and $4d$, Pb $4f$ and $5d$, Eu $3d$, was measured. The big thickness of CdTe layer (22 nm) covering $\text{Pb}_{0.95}\text{Eu}_{0.05}\text{Te}$ layer was strongly damping the electrons emitted from Pb and Eu atoms. After Ar ion sputtering of CdTe top layer, down to about 7nm, the photoemission signal belonging to the electrons of covered layer atoms, Pb $5d$, Pb $4f$ and Eu $3d$, remarkably increases. The increase of the signal of photoemitted electrons from Pb $5d$ and Eu $3d$ of buried layer appears when the angle of light incidence approaches the region of the value located close to the critical angle. The change of relative height of Pb $5d$ peak relatively to the height of Cd $4d$ ($\text{Pb}5d/\text{Cd}4d$) versus the angle incident of light were determined.

The interference of incidence and reflected part of X-ray beam leads to the creation of standing waves in the crystal. It leads to the creation of electric field structure in the region of sample surface. The remarkable change of the value of electric field occurs for the angle of X-ray incidence in the region of critical angle (value around 89 degree relatively to the perpendicular to the plane of crystal surface). The intensity of excited photoelectrons from particular depth of the sample surface region is proportional to the value of electric field corresponding to the depth of the region from the surface. The electric field distribution in the samples CdTe/PbEuTe/CdTe studied by X-ray photoemission, have been calculated with a program based on Parrat algorithm implementing the Fresnel recursive approach [2]. The calculated results helps to interpret measured results.

Acknowledgments: The authors acknowledge support by MSHE of Poland research Projects DESY/68/2007 and by the European Community via the Research Infrastructure Action under the FP6 Structuring the European Research Area, Programme through the Integrated Infrastructure Initiative "Integrating Activity on Synchrotron and Free Electron Laser Science" at DESY as well the research was partially supported by the European Union within European Regional Development Fund, through grant Innovative Economy (POIG.01.01.02-00-008/08).

References

1. M. Szot, L. Kowalczyk, E. Smajek, V. Domukhovski, J. Domagała, E. Łusakowska, B. Taliashvili, P. Dziawa, W. Knoff, W. Wiater, T. Wojtowicz, T. Story, *Acta Phys. Polon.* **114** (2009) 1397.
2. L.G. Parratt, *Phys. Rev.* **95** (1954) 359.

ELECTRONIC STRUCTURE OF TERNARY $\text{Pb}_{1-x}\text{Cd}_x\text{Te}$ CRYSTAL BY MEANS OF PHOTOEMISSION SPECTROSCOPY

B.A. Orlowski¹, A. Szczerbakow¹, B.J. Kowalski¹, M.A. Pietrzyk^{1*}, K. Gas¹,
M. Szot¹, W. Szuszkiewicz¹, V. Domukhovski¹, S. Mickevicius²,
R.L. Johnson³, S. Thiess³, and W. Drube³

¹*Institute of Physics, Polish Academy of Sciences, Al. Lotnikow 32/46, 02-668 Warsaw, Poland*

²*Semiconductor Physics Institute, A. Gostauto 11, 2600 Vilnius, Lithuania*

³*Hamburger Synchrotronstrahlungslabor HASYLAB am Deutschen Elektronen-Synchrotron DESY, Notkestr. 85, D-22603 Hamburg, Germany*

Keywords: photoemission spectroscopy, IV-VI crystals

**) pietrzyk@ifpan.edu.pl*

The nanostructures with a quantum dots are of great interest of application as well in electronics (high electric conductivity and low thermo-conductivity) as in optoelectronics (infrared detectors). Highly promising case is represented by the quantum dots of PbTe created in between the layers of CdTe as well as quantum dots of CdTe created in between the layers of PbTe [1]. The both crystals PbTe and CdTe are of different crystalline structure and their relative solubility is remarkably low. The PbTe belongs to the group of IV-VI narrow gap (0.23 eV) semiconductor compounds and crystallizes in the six fold coordinated lattice of rock salt while the CdTe belongs to the group of II-VI middle gap (1.45 eV) semiconductor compounds and crystallizes in four fold coordinated zinc blend lattice.

The bulk single crystals of $\text{Pb}_{1-x}\text{Cd}_x\text{Te}$, were grown in the Institute of Physics, Polish Academy of Sciences in Warsaw by physical vapor transport (PVT) method with proper quenching [2]. The frozen rock salt crystals of $\text{Pb}_{1-x}\text{Cd}_x\text{Te}$ ($x = 0.06, 0.08, 0.15$) about 1 cm with (001) oriented natural facets were obtained. The X-ray diffraction studies of the crystals showed the reflections of a very good crystals.

The experiment was performed using the Tunable High Energy X-ray Photoemission Spectrometer (THE-XPS) at wiggler beam line station BW2 of the HASYLAB, DESY, Hamburg, Doris III storage Ring. Double crystal monochromator (Si(111)) covers an energy range from 2.4 to 10 keV with a monochromatic photon flux of about 5×10^{12} photons/s and with total energy resolution power of 0.5 eV for radiation energy around 3000 eV. The station is adopted to perform the experiment with High-Energy X-ray Photoelectron Spectroscopy. The station E1 with the FLIPPER II monochromator was used to obtain

ultraviolet PES spectra. Tunable High Energy PES and Ultraviolet PES were applied to study the crystals spectra containing: valence band, Cd 3d and 4d, Pb 4f and 5d and Te 3d and 4d. The valence band density of states distribution spectra remarkably changes with the crystal composition. In most cases obtained valence band spectra of ternary crystal can be in first approximation treated as a sum of the components spectra. In the case of measured $\text{Pb}_{1-x}\text{Cd}_x\text{Te}$ ternary crystal this first order approximation does not follow the rule and inclination of ternary crystal spectra possesses some differences from the sum of spectra measured for crystal PbTe and CdTe. The core levels chemical shifts and appearance of shoulders of the core peaks were studied to illustrate the interaction with different nearest neighbors. X-ray diffraction studies recognized kind of defects suggesting the preference to create the dots of PbTe while the other defects can be correlated to the preference of CdTe dots creation.

Acknowledgements: The authors acknowledge support by MSHE of Poland research Projects DESY/68/2007 and by the European Community via the Research Infrastructure Action under the FP6 Structuring the European Research Area" Programme (through the Integrated Infrastructure Initiative "Integrating Activity on Synchrotron and Free Electron Laser Science") at DESY as well the research was partially supported by the European Union within European Regional Development Fund, through grant Innovative Economy (POIG.01.01.02-00-008/08).

References

- [1] M. Szot, A. Szczerbakow, K. Dybko, L. Kowalczyk, E. Smajek, V. Domukhovski, E. Lusakowska, P. Dziawa, A. Mycielski, T. Story, M. Bukala, M. Galicka, P. Sankowski, R. Buczek, P. Kacman, *Acta Phys. Pol.* **116** (2009) 959.
- [2] A. Szczerbakow, K. Durose, *Prog. Cryst. Growth Charact. Mater.* **51**, (2005) 81.

INFLUENCE OF IONIZING RADIATION ON DISULFIRAM IN THE SOLID STATE

B. Marciniak¹, **M. Kozak**^{2*}, **K. Dettlaff**¹, and **M. Naskrent**³

¹ Poznan University of Medical Sciences, Department of Pharmaceutical Chemistry,
Grunwaldzka 6, 60-780 Poznań, Poland

² Department of Macromolecular Physics, Faculty of Physics, A. Mickiewicz University,
Umultowska 85, 60-614 Poznań, Poland

³ Faculty of Physics, Adam Mickiewicz University, Umultowska 85, 61-614 Poznań, Poland

Keywords: radiation sterilization, E-beam, disulfiram, solid state

**) e-mail: kozak@amu.edu.pl*

Disulfiram (Antabuse, Esperal, bisdiethylthio-carbamoyl disulphide) is a well-known drug administered in treatment of chronic alcohol disease as a substance producing many unpleasant side effects such as headaches, memory lapses, cardiac and circular system problems, alimentary system problems, allergies and others in response to alcohol consumption. These symptoms appear because disulfiram inhibits alcohol oxidation at the stage of acetate aldehyde, binds alcohol forming strongly toxic ammonium complexes and blocks synthesis of norepinefrine.

Disulfiram is applied in the form of tablets or hypodermal implants. According to the pharmacopoeia recommendations the latter as well as many other forms of drugs (injections, infusions or eye drops) should be sterile. In the 1980s and 1990s the first attempts were made at application of radiation sterilisation. According to literature [1], small doses of radiation < 1 kGy can be used without any risk of degradation of disulfiram.

Results of our recent study performed for the standard doses (10–25 kGy) recommended for radiation sterilisation by European Union Standards (EN 552) do not confirm the earlier reports. As a result of radiation sterilisation disulfiram emits specific unpleasant smell and changes its colour from white to grey-green. To recognise fully the character of these changes a thorough study of disulfiram sterilised *in substantia* has been performed in an extended range of radiation doses from

10 to 100 kGy. Sterilisation was carried out in solid state, at room temperature, and at normal air humidity with the electron beam of 9.96 MeV from an accelerator. The irradiation caused changes in the substance were analysed 2 days after the irradiation. All measurements were made simultaneous for the irradiated and non-irradiated substance.

The analyses were performed by a number of instrumental methods including: spectrophotometric (UV, IR, NMR, MS, EPR), chromatographic (TLC, HPLC), thermal (TG, DSC), and other (SEM, X-ray diffraction).

The results obtained were discussed against a background of literature data and the final conclusion was that disulfiram in solid state is characterised by a too low radiochemical stability to ensure no risk of its degradation on its radiation sterilisation with an electron beam.

References

- [1] M. Phillips, R.P. Agarwal, R.J. Brodeur, V.F. Garagusi, K.L. Mossan, "Stability of an injectable disulfiram formulation sterilized by gamma radiation", *Am. J. Hosp. Pharm.* **42** (1985) 343-345.

TOPOGRAPHIC X-RAY CHARACTERIZATION OF GGG HOMOEPITAXIAL LAYERS WITH INTRODUCED DIVALENT IONS OF TRANSITION-METALS

K. Mazur^{1*}, **J. Sarnecki**¹, **W. Wierzchowski**¹, **K. Wieteska**², and **A. Turos**^{1,3}

¹ *Institute of Electronic Materials Technology, 133, Wólczyńska Str, 01 919 Warsaw, Poland*

² *Institute of Atomic Energy, 05 400 Świerk-Otwock, Poland*

³ *Soltan Institute for Nuclear Studies, 05-400 Swierk/Otwock, Poland*

Keywords: GGG films, LPE, HRXRD, X-ray diffraction topography

*) *e-mail: Krystyna.Mazur@itme.edu.pl*

Optical properties of transition-metal (TM) doped materials have attracted significant attention for application in tunable mid-infrared lasers, for passive Q-switching of lasers operating in the near-infrared region and also as sensitizers for rare-earth ions up-conversion. Among transition metals activators the lasing potential of Cr and Ti ions are most widely used, nevertheless the others, like Co and Ni also exhibit promising optical properties, predestinating them for an application in solid laser systems.

In this paper, we report results of the study on structural perfection of epitaxial films of $Gd_3Ga_5O_{12}$ (GGG) doped with Co^{2+} and Ni^{2+} ions grown by liquid phase epitaxy (LPE). Our previous study on LPE growth of rare earth ions doped garnet waveguide films has indicated that LPE technique is a proper method to fabricate solid state laser structures. We have successfully prepared Cr^{4+} ions doped YAG and GGG layers as saturable absorbers in passively Q-switched epitaxial microchip laser structures [1]. The obtained micro laser performance has stimulated our research on epitaxial growth of Co^{2+} : YAG/YAG structures used as passive Q-switches for 1.54 μm Er: glass laser [2]. As a consequence, the results of Co^{2+} :YAG layers study have focused our attention on the possibility of using Ni^{2+} :GGG and Co^{2+} :GGG layers as passive Q-switches for solid state laser operating in 1.1 – 1.5 μm range. In order to obtain cobalt or nickel ions in the appropriate valence state it was necessary to compensate the electric charge by optically inert ion such as Ge^{4+} .

Epitaxial layers of Ni,Ge: GGG and Co,Ge: GGG films grown on GGG substrates by means of the LPE method have been studied by conventional high resolution X-ray diffraction (HRXRD), synchrotron X-ray topography and optical spectroscopy.

Synchrotron topographic studies were performed using both monochromatic (E2) and white beam (F1) topographic stations at Hasylab. In the case of monochromatic beam topographs were taken at different points of the rocking curve, providing alternative images of defects in the substrate and in the layer.

The most important defects revealed by topographs were the segregation fringes, faceted regions and threading dislocations continued in the epitaxial layers.

High structural perfection and good optical quality of epitaxial Ni,Ge: GGG and Co,Ge: GGG films grown by means of LPE method has been confirmed. The method of controlled incorporation of cobalt and nickel ions in combination with charge compensating germanium ions into garnet layers has been successfully tested, thus, opening good perspectives for its application in the solid state laser technology.

References

- [1] K. Kopczynski, J. Sarnecki, J. Mlynczak, Z. Mierczyk, J. Skwarcz, *Proc. SPIE* **5958** (2005) 5958E1–5958E8.
- [2] J. Sarnecki, K. Kopczynski, Z. Mierczyk, J. Skwarcz, J. Mlynczak, *Opt. Mat.* **27** (2004) 445–447.

STRUCTURAL CHARACTERIZATION OF Mn^+ ION-IMPLANTED GaSb

J. Bak-Misiuk^{1*}, **E. Dynowska**¹, **P. Romanowski**¹, **A. Kulik**², and **W. Caliebe**³

¹*Institute of Physics, PAS, al. Lotnikow 32/46, PL-02668 Warsaw, Poland*

²*Maria Curie-Skłodowska University, pl. M. Curie-Skłodowskiej 5, PL-20031 Lublin, Poland*

³*HASYLAB at DESY, Notkestr. 85, D-22603 Hamburg, Germany*

Keywords: GaSb, implantation, spintronics, X-ray, diffraction

**) e-mail: bakmi@ifpan.edu.pl*

Synthesis of ferromagnetic nanoclusters embedded in semiconductor matrix is of particular interest for potential application in spintronics. Due to high Curie temperature of MnSb (580 K), granular GaSb:MnSb may be interesting material for spintronic application.

The formation of Mn-based nanoclusters by ion implantation and subsequent annealing is a relatively simple technique if compared to the growth of diluted magnetic semiconductors by epitaxial method, with an advantage to control the relative Mn density. However, up to now, there are no papers concerning MnSb inclusions formed in GaSb by implantation.

Two sets of Mn^+ -implanted GaSb crystals prepared by implantation at energy $E = 150$ keV and dose $D = 9 \times 10^{14} \text{ cm}^{-2}$ were investigated.

For first set of samples implantation was performed at liquid nitrogen temperature. Before implantation, the samples were pre-implanted with He^+ , Ne^+ , or $He^+ + Sb^+$. The pre-implantation with above mentioned ions was carried out at such conditions, that their project ranges (R_p) were equal or near R_p for Mn^+ (94.7 nm). After implantation the samples were annealed face to face in Ar atmosphere for 5 min. at 620 K and next at 920 K for 10 min.

In the case of second set of samples, Mn^+ implantation was carried out at 340 K and 470 K. Next the samples were annealed at 620 K for 30 min. just in the implanter chamber.

Post-implanted structure investigation of the samples was carried out using synchrotron X-ray diffraction. The crystallographic orientation of inclusions in respect to the GaSb surface, as well as, the phase analysis of the near surface polycrystalline layers, were performed using the $2\theta-\omega$ and 2θ scans in glancing incidence geometry, respectively.

The diffraction patterns measured in these two modes are presented in Figs. 1 and 2. The high intensity peaks detected on the $2\theta-\omega$ scans, for both sets of samples, come from the GaSb bulk crystals. For all the samples, prepared by implantation at liquid nitrogen temperature, the diffraction peaks from polycrystalline Sb, MnO_2 and GaSb, as well as, single crystalline inclusions of MnSb, were detected (Fig. 1).

For the samples prepared by implantation at 340 K or 470 K, the polycrystalline phase from GaSb was detected only. An analysis of the $2\theta-\omega$ pattern suggests the

creation of hexagonal MnGaSb inclusions with well-defined orientation. This effect deserves further research.

Acknowledgements: This work was partially supported by national grant of Ministry of Science and High Education N202-052-32/1189 as well as by DESY/HASYLAB (EC support program: Transnational Access to Research Infrastructures) and by the European Community under Contract RII3-CT-2004-506008 (IA-SFS).

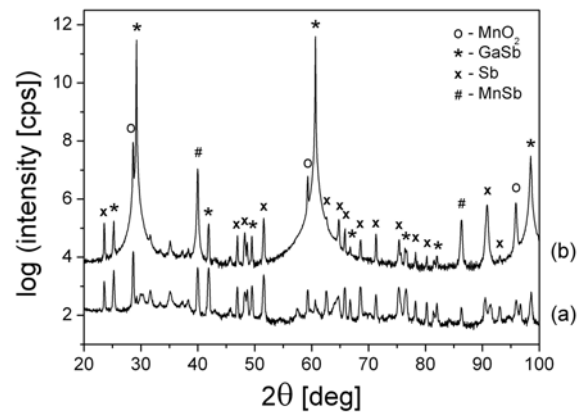


Figure 1. 2θ in glancing incidence geometry (a) and $2\theta-\omega$ (b) scans for GaSb sample implanted with He^+ and Mn^+ at liquid nitrogen temperature.

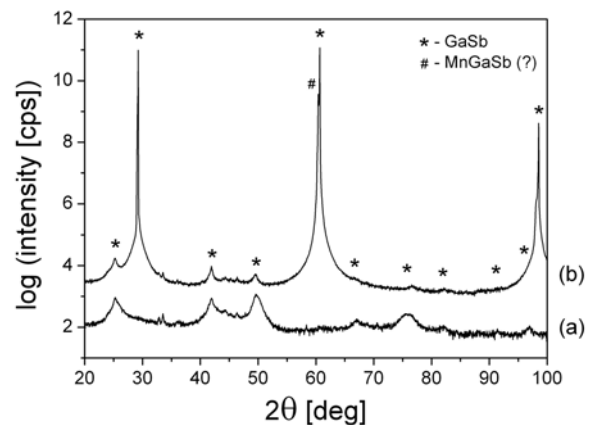


Figure 2. 2θ in glancing incidence geometry (a) and $2\theta-\omega$ (b) scans for GaSb sample implanted with Mn^+ at 470 K.

SYNCHROTRON AND X-RAY STUDIES OF SPONGY-LIKE BURIED LAYERS PRODUCED IN SILICON BY HELIUM IMPLANTATION

I. Capan ¹, J. Bak-Misiuk ^{2*}, A. Misiuk ³, P. Dubček ¹, S. Bernstorff ⁴, and P. Romanowski ²

¹ Ruder Basković Institute, P.O.Box 18010000 Zagreb, Croatia

² Institute of Physics, Polish Academy of Sciences, al. Lotnikow 32/46, PL-02668 Warsaw, Poland

³ Institute of Electron Technology al. Lotnikow 32/46, PL-02668 Warsaw, Poland

⁴ Sincrotone Trieste, SS14 Basovizza, Trieste, Italy

Keywords: silicon, implantation, synchrotron, GISAXS, X-ray scattering

*) e-mail: bakmi@ifpan.edu.pl

Helium implantation into silicon produced bubbles and other defects; in effect of heat treatment He out-diffusions partially creating spongy-like buried layer and leaving voids [1]. Such voids are of considerable interest as their properties find numerous applications in semiconductor devices. The formation and morphology of defects, induced by He⁺ implantation in silicon followed by temperature and pressure treatments, have been studied using X-ray reciprocal space mapping and grazing incidence small angle X-ray scattering (GISAXS). GISAXS is a powerful, non-destructive technique, useful for analysing structures with 1-150 nm dimensions. The goal of this work was to show how the high temperature and high pressure treatments influence the creation of voids (gas-empty cavities) formed from gas-filled cavities in Si:He.

The X-ray reciprocal space maps for the 004 reflection were recorded at room temperature on high resolution diffractometer using CuK α radiation. The GISAXS experiments were carried out on the SAXS beamline at synchrotron facility of Electra, Trieste, using radiation with wavelength $\lambda = 0.07$ nm and photon energy 16 keV. Two-dimensional CCD detector positioned perpendicularly to the incident beam was used to record the SAXS intensity.

Numerous interference fringes were observed on the X-ray 004 reciprocal space maps for the as-implanted sample confirming the layered structure, composed of the relatively perfect top Si layer of about 1 μ m thickness and of the disturbed buried layer containing implanted helium. After processing at 720 K, the X-ray diffuse scattering, related to the presence of point defects as well as the thickness fringes originating from the less disturbed top Si layer, remained to practically unchanged. Processing at 1270 K resulted in increasing diffuse scattering. However, the diffuse scattering intensity from Si:He treated under pressure at 1270 K was lower in comparison to that for the Si:He sample annealed under enhanced pressure.

The 2D GISAXS pattern representing map of the scattered intensity for the as-implanted Si:He sample is presented in Fig 1. The 2D GISAXS pattern exhibits isotropic scattering, whose iso-intensity contour plots are circles, showing a random distribution of spherical objects in average. To get quantitative information about

He bubbles created by ion implantation and subsequent processing, Guinier's approximation has been used. When Guinier's approximation is applied for the experimental results, the radius of gyration for the bubbles in as-implanted Si:He are estimated to be around 1 nm. That gives us the value for the average radius of the bubbles at around 1.3 nm. This value is the same as the value estimated for the sample annealed at 720 K. To get information about the transformation from bubbles to the voids, and about the structure of the voids, the samples were annealed under enhanced pressure. Most interesting results were obtained upon annealing of the Si:He sample at 1270 K under 0.6 GPa. It has been shown that enhanced pressure strongly affects the formation of voids and/or large cavities in the spongy-like buried Si layer. After high temperature and high-pressure treatments, the {111} facets on the cavities in spongy-like buried Si have been observed. It means that high-pressure treatment suppresses the creation of interstitial-related defects.

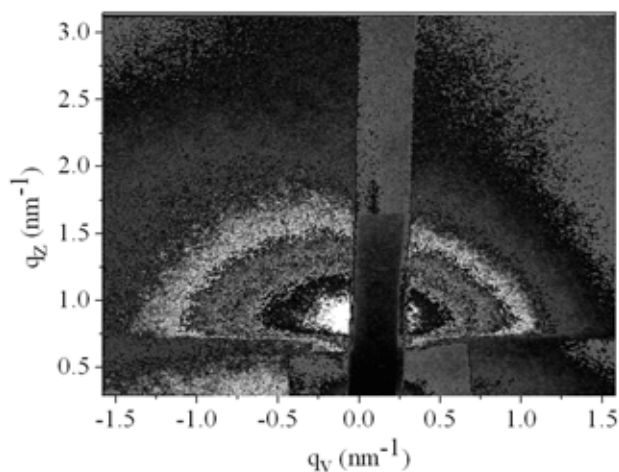


Figure 1. 2D GISAXS pattern for as implanted Si:He sample.

References

- [1] C.C. Griffioen, J.H. Evans, P.C. De Jong, A. Van Veen, "Helium desorption/permeation from bubbles in silicon: A novel method of void production", *Nucl. Instrum. Methods Phys. Res. B* **27** (1987) 417–420.

XAFS STUDY OF NOVEL TYPE OF METALLOCHELATES OF PHENYLAZODERIVATIVES OF SCHIFF BASES

V.G. Vlasenko^{1*}, **A.S. Burlov**², **Y.V. Zubavichus**³, **I.S. Vasilchenko**²,
A.I. Uraev², and **A.D. Garnovskii**²

¹ Institute of Physics, Southern University, Stachki ave. 194/2, Rostov-on-Don, 344090 Russian Federation

² Institute of Physical and Organic Chemistry, Southern Federal University, Stachki ave. 194/2, Rostov-on-Don, 344090 Russian Federation

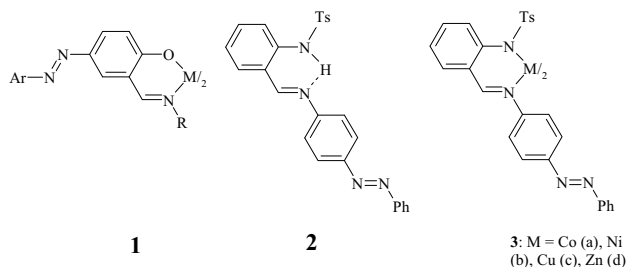
³ Kurchatov Center for Synchrotron Radiation and Nanotechnology, Russian Research Center "Kurchatov Institute", Academic Kurchatov sq. 1, Moscow, 123182 Russian Federation

Keywords: metalchelates, azomethine ligands, XAFS spectroscopy

*) e-mail: vlasenko@ip.rsu.ru

Acyclic and cyclic Schiff bases are the very important ligands of the modern coordination chemistry due to the possibility of creation on their basis novel polyfunctional materials: magnetics, luminophores, bioactive chelates, chemosensors and liquid crystals. Metallocomplexes of Schiff bases take an important place in supra- and nanochemistry [1,2].

Coordination compounds of Schiff bases with azogroup are represented by complexes of the ligands containing Ar-N=N- fragment in aldehyde moiety – chelates of azomethines of arylazosalicylaldehyde **1**. Schiff base derived from *o*-tosylaminobenzaldehyde and *p*-aminoazobenzene **2** and its metallochelates (Co²⁺, Ni²⁺, Cu²⁺) **3** were synthesized and investigated by XANES and EXAFS spectroscopy.



The NiK-, CoK- and CuK-edges EXAFS spectra for the complexes were obtained at the Station K1.3b "Structural Materials Science" of the Kurchatov Center for Synchrotron Radiation and Nanotechnology (KCSRNT, Moscow, Russia). EXAFS data were analyzed using the IFEFFIT 1.2.11 data analysis package. The structural parameters, including interatomic distances (R), coordination numbers (CN) and the distance mean-square deviation- Debye-Waller factors (σ^2), were found by the non-linear fit of theoretical spectra to experimental ones. Experimental data were simulated using theoretical EXAFS amplitude and phase functions, which were calculated using the program FEFF7. The modules of Fourier transforms (MFT) of the NiK-, CoK- and CuK-edges EXAFS data for the metallochelates **3** are shown in Fig. 1. From our EXAFS and XANES analysis, it is possible to propose a model of coordination environment of Cu, Ni and Co ions in metallochelates **3**.

All complexes possess distorted tetrahedral (due to additional coordination of oxygen atoms of Ts-tosylamino group) donor environment. The obtained distances M...O(Ts) are dependent on the metal atom type so that Cu...O(Ts) < Ni...O(Ts) < Co...O(Ts).

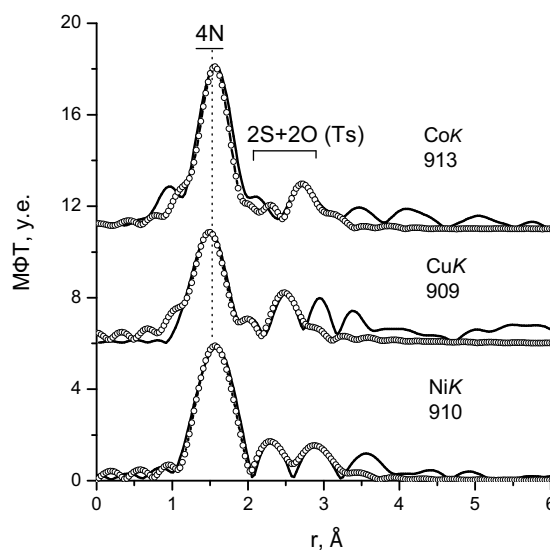


Figure 1. MFT of the Co, Cu and NiK-edge EXAFS spectra for the metallochelates studied: experiment (solid lines) and best-fits (open circles).

Acknowledgments: This work has been made due to the financial support of the grant of Russian Foundation for Fundamental Investigation (RFFI, grants № 08-03-00154, 08-03-00223, 10-03-00434),

References

- [1] A.D. Garnovskii, B.I. Kyarissov, *Synthetic Coordination and Organometallic Chemistry* (Marcel Dekker, New York-Basel, 2003).
- [3] R. Hernandez Molina, A. Mederos, *Comprehensive Coordination Chemistry II*, A.B.P. Lever (Ed.), vol. 1, (Elsevier – Pergamon Press, Amsterdam-Oxford-New York, 2003), p. 411.

SYNCHROTRON PHOTOEMISSION STUDY OF (Zn,Co)O FILMS WITH UNIFORM Co DISTRIBUTION

E. Guzewicz^{1*}, **M. Lukasiewicz**¹, **L. Wachnicki**¹, **K. Kopalko**¹,
B.S. Witkowski¹, **J. Sadowski**², and **M. Godlewski**^{1,3}

¹ Institute of Physics, Polish Academy of Sciences, Al. Lotników 32/46, 02-668 Warsaw, Poland

² MAX-lab, Lund University, Box 118, SE-22100 Lund, Sweden

³ Department of Mathematics and Natural Sciences, College of Science, Cardinal Wyszyński University, ul. Dewajtis 5, 01-815 Warsaw, Poland

Keywords: zinc oxide, atomic layer deposition, resonant photoemission spectroscopy

*) e-mail: guzel@ifpan.edu.pl

Zinc oxide containing transition metal (TM) elements is intensively studied because of prospective application in spintronics [1,2]. Ferromagnetic ordering in (Zn,Co)O has been found and reported by several groups, but the origin of the ferromagnetism is still not clear. It is often related to formation of foreign phases and metal accumulations in the nm scale. The ferromagnetism of these composite systems strongly depend on the growth conditions and co-doping with shallow impurities [1].

In our previous studies on (Zn,Mn)O material we have demonstrated that low temperature growth, below 300°C, leads to paramagnetic films with the uniform manganese distribution. These (Zn,Mn)O layers are free of manganese accumulations and foreign phases [3-4].

The presented photoemission studies are focused on (Zn,Co)O material grown at low temperature. We have shown that in order to avoid the presence of foreign phases and metal accumulations (Zn,Co)O films should be grown at temperature below 200°C [5-6]. These films are paramagnetic and, as shown by SIMS and TEM studies, free of foreign phases and accumulations of metallic cobalt. The subject of the present study was to investigate the electronic structure of uniform (Zn,Co)O films with different cobalt content.

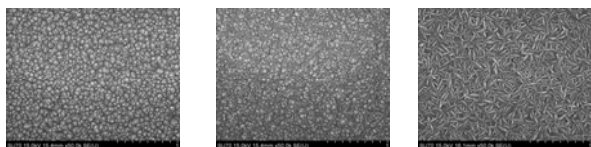


Figure 1. SEM images for (Zn,Co)O films grown by ALD at 160°C. The Co content is: 2% (left), 3.5% (middle) and 7% (right).

The investigated (Zn,Co)O films were grown by the Atomic Layer Deposition (ALD) method at the same temperature of 160°C and using the same zinc, cobalt and water precursors (dimethylzinc, Co(acac)₂ and water, respectively). The growth method as well as properties of obtained films are described elsewhere [7]. Different parameters of the ALD process (precursors' doses, purging time and proportion between zinc and cobalt precursors'

pulses) resulted in different Co content that varied between 0.1% and 7%. For photoemission studies we prepared three samples with Co content 2%, 3.5% and 7%. SEM images of the surface of these films are presented in Fig. 1.

We investigated the electronic structure of these films in the energy range between the Fermi level and 14 eV below. This binding energy region covers the (Zn,Co)O valence band together with the Zn3d core level. We used the resonant photoemission spectroscopy, which is as an effective tool for identification of the Co3d ion charge states in the valence band electronic structure of the (Zn,Co)O material.

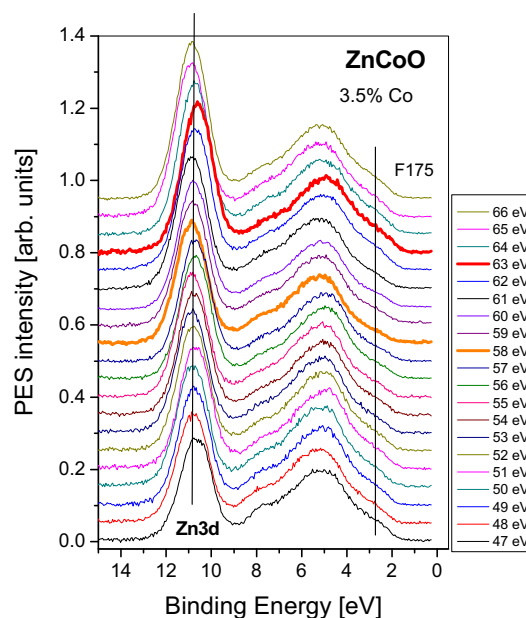
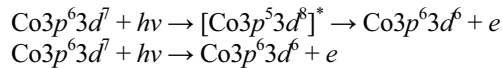


Figure 2. EDC spectra of the (Zn,Co)O film with 3.5% Co measured across the Co3p→Co3d resonance. Thicker lines shows resonant (63 eV, red on-line) and anti-resonant (58 eV, orange on-line) spectra.

The resonant photoemission process is the result of interference between two photoemission paths that, in the case of cobalt, can be described as follows:



As a result, we observe an increase of Co3d related features in photoemission spectra when photon energy is tuned to the Co3p→Co3d energy difference.

In Fig. 2, we show the set of Energy Distribution Curves (EDC's) for all measured (Zn,Co)O films. EDC's were taken for photon energies between 47 eV and 66 eV, e.g. across the Co3p→Co3d transition.

For all three investigated films the maximum of the Fano resonance was observed at photon energy 63 eV and the minimum at 58 eV. In Fig. 3, we present resonant and anti-resonant EDC spectra for films containing a) 2% Co, b) 3.5% Co, and c) 7% Co. We also show the difference spectra (Δ EDC) that is related to the Co3d contribution to the valence band of the (Zn,Co)O system.

We noticed that resonant enhancement of the photoemission intensity from the Co3d shell does not scale with the cobalt content. The strongest photoemission response from the Co3d electron shell was observed for (Zn,Co)O film with 3.5% of cobalt. The resonant photoemission signal from the Co3d states for (Zn,Co)O films with 7% of Co was similar to that which was obtained for (Zn,Co)O film with 2% of cobalt.

Moreover, we also noticed that films with different content of cobalt give different Co3d contributions to the valence band electronic structure. For films containing 3.5% of Co we observe only one Co3d contribution, which is located between 2 eV and 4 eV below the Fermi level with the maximum at 3 eV (see Fig. 3b). For two remaining (Zn,Co)O films the additional Co3d contribution at higher binding energy is also present. In case of film with 2% of Co it is located 9 eV below the Fermi level (see Fig. 3a), while for (Zn,Co)O film with 7% of Co it is observed at 7.4 eV below the Fermi level (see Fig. 3c).

We expect that photoemission investigation of the Co3p core level may shed some light on the Co states in the measured (Zn,Co)O films.

Acknowledgements: The work was supported by the FunDMS ERC Advanced Grant Research and the European Community – Research Infrastructure Action under the FP6 « Structuring the European Research Area » Program (through the Integrated Infrastructure Initiative "Integrating Activity on Synchrotron and Free Electron Laser Science").

References

- [1] A. Bonanni, T. Dietl, "A story of high-temperature ferromagnetism in semiconductors", *Chem. Soc. Rev.* **39** (2010) 526-539.
- [2] K. Ueda, H. Tabata, T. Kawai, "Magnetic and electric properties of transition-metal-doped ZnO films", *Appl. Phys. Lett.* **79**, 988-990 (2001).
- [3] A. Wójcik, K. Kopalko, M. Godlewski, E. Guziewicz, R. Jakiela, R. Minikayev, W. Paszkowicz, "Magnetic properties of ZnMnO films grown at low temperature by atomic layer deposition", *Appl. Phys. Lett.* **89**, 051907 (2006).
- [4] A. Wójcik, M. Godlewski, E. Guziewicz, K. Kopalko, R. Jakiela, M. Kiecana, M. Sawicki, M. Guziewicz, M. Putkonen, L. Niinistö, Y. Dumont, N. Kelner, "Low

temperature growth of ZnMnO: A way to avoid inclusions of foreign phases and spinodal decomposition", *Appl. Phys. Lett.* **90**, 082502 (2007).

- [5] M. Lukasiewicz, B. Witkowski, M. Godlewski, E. Guziewicz, M. Sawicki, W. Paszkowicz, E. Łusakowska, R. Jakiela, T. Krajewski, I.A. Kowalik, B.J. Kowalski, "ZnCoO films by atomic layer deposition—influence of a growth temperature on uniformity of cobalt distribution", *Acta Phys. Polon.* **A116** (2009) 921-923.
- [6] M.I. Łukasiewicz, B. Witkowski, M. Godlewski, E. Guziewicz, M. Sawicki, W. Paszkowicz, R. Jakiela, T.A. Krajewski, G. Łuka, *Phys. Stat. Solidi (b)*, in print.
- [7] E. Guziewicz, M. Godlewski, T. Krajewski, Ł. Wachnicki, A. Szczepanik, K. Kopalko, A. Wójcik-Głodowska, E. Przędziecka, W. Paszkowicz, E. Łusakowska, P. Kruszewski, N. Huby, G. Tallarida, S. Ferrari, "ZnO grown by atomic layer deposition: A material for transparent electronics and organic heterojunctions", *J. Appl. Phys.* **105** (2009) 122413.

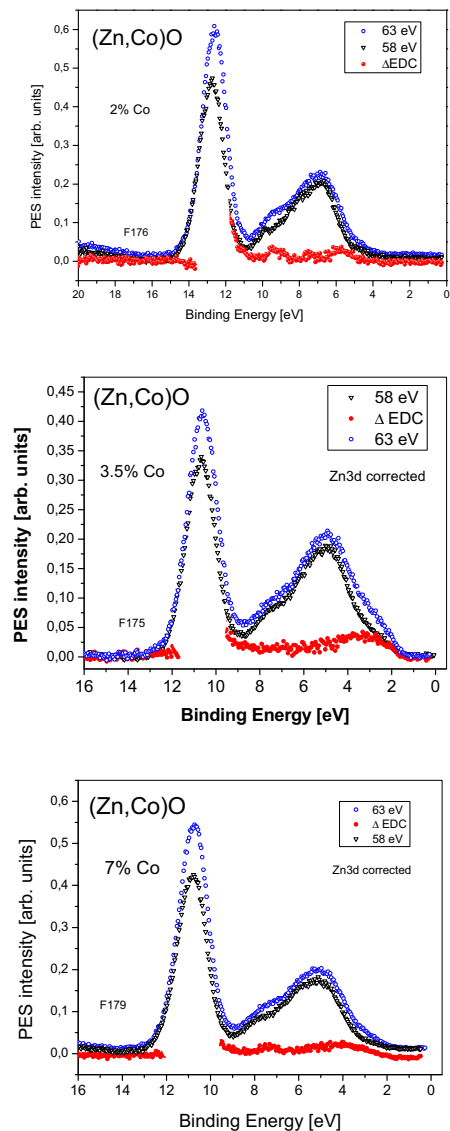


Figure 3. EDC spectra taken at resonance (63 eV, blue solid circles) and anti-resonance (58 eV, black open triangles) photon energy along with the calculate difference curve (Δ EDC, red open circles).

STRUCTURAL AND MAGNETIC PROPERTIES OF GaSb:MnSb GRANULAR LAYERS

E. Dynowska^{1*}, **J. Bak-Misiuk**¹, **P. Romanowski**¹, **J. Domagala**¹, **J. Sadowski**^{1,2},
T. Wojciechowski¹, **A. Kwiatkowski**³, and **W. Caliebe**⁴

¹Institute of Physics PAS, al. Lotnikow 32/46, PL-02668 Warsaw, Poland

²MAX-Lab, Lund University P.O. Box. 118, S-22100 Lund, Sweden

³Institute of Experimental Physics, Faculty of Physics, University of Warsaw,
ul. Hoza 69, PL-00681 Warsaw, Poland

⁴Hasylab at DESY, Notkestr. 85, D-22603 Hamburg, Germany

Keywords: GaMnSb, X ray diffraction, magnetic properties, synchrotron radiation

*) e-mail: dynow@ifpan.edu.pl

The Ga_{1-x}Mn_xSb layers were grown by molecular beam epitaxy method on two kinds of substrates: GaSb(100) and GaAs(111)A covered by thin GaSb buffer layer. The growth temperature of all layers was kept at 450°C. The nominal Mn contents ($x = 0.01, 0.03, 0.07$ and 0.08) were defined as a ratio of Mn to Ga flux during growth.

The structure of the layers was investigated by X-ray diffraction with the use of synchrotron radiation (XRD), scanning electron microscopy (SEM), as well as by atomic and magnetic force microscopy (AFM, MFM).

The results of XRD studies showed the presence of the hexagonal MnSb clusters embedded in a GaSb matrix formed during growth. The lattice parameters of these inclusions were determined on the base of $2\theta-\omega$ scans in the vicinity of 20.2 and 30.0 hexagonal reflections for the layers grown on (100)-oriented substrates and for 00.4 and 10.5 reflections in the case of layers grown on (111)-oriented ones. The different results were obtained for these two kinds of samples. For the first kind the lattice parameters of the inclusions, within the range of experimental errors, were the same as those for bulk MnSb, it means: $a = 4.128 \text{ \AA}$, $c = 5.789 \text{ \AA}$. On the other hand, the lattice parameters of the inclusions created in the layers grown on (111)-oriented substrates were significantly different from those for bulk MnSb. This result suggests that the MnSb clusters in these samples are strained on the contrary to the first kind of samples where the inclusions are relaxed. The spatial distribution of the clusters inside GaSb matrix depends also on the substrate orientation. In the case of GaSb:MnSb layers on GaSb/GaAs(111) substrates all clusters grow with their c -axis parallel to the $\langle 111 \rangle$ directions of the matrix, while in the case of layers grown on (100)-oriented substrates the MnSb clusters contain differently oriented blocks (see Fig. 1). According to the SEM studies (Fig. 2) the sizes of these clusters were ranging from ~ 50 nm to ~ 600 nm.

The AFM studies revealed the grains on the surfaces which were sources of strong magnetic contrasts. It suggests that the grains are ferromagnetic at room temperature.

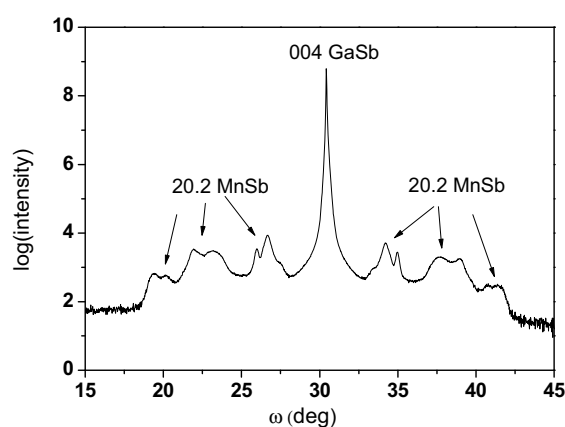


Figure 1. The 004 GaSb rocking curve in the wide range of ω angles – the small peaks on both sides of central peak are related to 20.2 peaks of different blocks of hexagonal MnSb clusters.

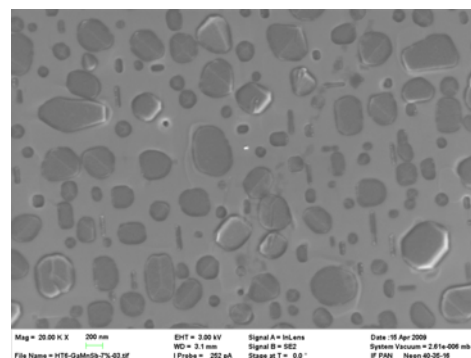


Figure 2. An example of the SEM picture of GaSb:MnSb granular layer grown on GaSb(100) substrate. The sizes of the clusters ranged from ~ 50 nm to ~ 600 nm.

Acknowledgements: This work was partially supported by national grant of Ministry of Science and Higher Education N202-052-32/1189 as well as by EC-RIA under the FP6 "Structuring the European Research Area" Programme, Contract RII3-CT-2004-506008.

CRYSTALLIZATION AND MELTING BEHAVIOR OF POLY(ETHYLENE OXIDE) AND ITS BLEND WITH STYRENE-BASED IONOMER USING TIME-RESOLVED SAXS/WAXS EXPERIMENTS

Cz. Ślusarczyk *

Institute of Textile Engineering and Polymer Materials, University of Bielsko-Biala, 2, Willowa Str, 43-309 Bielsko-Biala, Poland

Keywords: blends, PEO, ionomers, SAXS, WAXS

e-mail: cslusarczyk@ath.bielsko.pl

Polymer blends of a crystallizable polymer and a noncrystallizable polymer have gained significant interests because of the rich morphology offered by these systems [1]. When such blend is crystallized quiescently, the noncrystallizable component can be redistributed to any of the following places: between lamellae, between growth lamellar bundles, or between spherulites. These morphological patterns show the dispersion of an amorphous component from the nanoscopic scale to the micrometer scale. Different scales of dispersion may lead to different properties. The type of segregation is determined by the interplay between the diffusion coefficient of an amorphous component molecules and the crystal growth rate. Intermolecular interactions are well known to influence both of these factors and taking them into account is important to understanding the blend crystallization.

In the earlier works [2,3] we used "static" SAXS, WAXS experiments as well as differential scanning calorimetry (DSC) to determine the miscibility and morphology of blends of poly(ethylene-oxide) (PEO) and styrene-acrylic acid (S-AA) copolymers neutralized with alkali metals (Na^+ , Li^+). In these studies, we investigated the effects of blend composition and the content of ionic groups in amorphous ionomers on the segregation of amorphous component. It was found that PEO is partially miscible with styrene based ionomers due to ion-dipole interactions and that ionomers segregated interfibrillarly.

In the present study we focus on non-isothermal crystallization and melting (via time-resolved small- and wide-angle X-ray scattering experiments) of neat PEO and its 50/50 blend with ionomer containing 6.4 mol% of sodium acrylate (ANa). During crystallization of the blend we have observed a modest increase of the lamellar layer thickness at temperatures below 20°C, *i.e.* below the glass temperature of the ionomer (Fig. 1). This indicates on separation of the blend components

and crystallization of those PEO crystallizable segments which, due to strong interactions with the ionomer, remained amorphous.

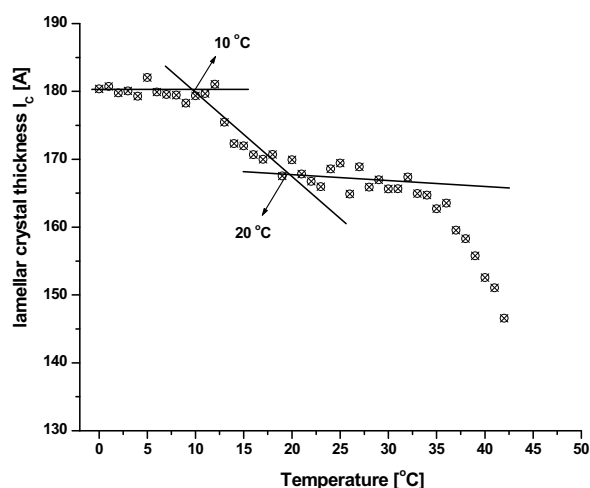


Figure 1. Temperature dependence of the lamellar crystal thickness during the crystallization process for 50/50 PEO/S-ANa(6.4) blend.

References

- [1] J.P. Runt, in: *Polymer Blends*, edited by D.R. Paul, C.B. Bucknall (Wiley, New York, 2000).
- [2] Cz. Ślusarczyk, K. Suchocka-Gałaś, J. Fabia, A. Włochowicz, "Small-angle X-ray scattering study of poly(ethylene-oxide) and styrene based ionomers blends", *J. Appl. Cryst.* **36** (2003) 698-701.
- [3] Cz. Ślusarczyk, K. Suchocka-Gałaś, "Poly(ethylene-oxide)/styrene ionomers blends: crystallization of poly(ethylene-oxide) component studied by wide-angle X-ray diffraction", *Solid State Phenom.* **130** (2007) 251-256.

GROWTH AND SPIN STRUCTURE OF ULTRATHIN Fe FILMS ON W(110)

M. Ślęzak^{1*}, **A. Koziol**¹, **K. Matlak**¹, **T. Ślęzak**¹, **M. Zajac**^{1,2}, **R. Rüffer**², and **J. Korecki**^{1,3}

¹ Faculty of Physics and Applied Computer Science, AGH, Kraków, Poland

² European Synchrotron Radiation Facility, BP 220, 38043 Grenoble Cedex, France

³ Institute of Catalysis and Surface Chemistry, PAN, ul. Niezapominajek 8, Kraków, Poland

Keywords: magnetism, ultrathin films, iron, NRS

*) e-mail: mislezak@agh.edu.pl

We investigated structure and magnetism of uncovered ultrathin epitaxial Fe films grown on W(110). In addition to standard surface sensitive techniques we applied *in-situ* Grazing Incidence Nuclear Resonant Scattering of X-rays (GI-NRS) [1]. The GI-NRS is a synchrotron analogue of the Mössbauer spectroscopy. Recoilless excitations of the nuclear energy levels, split due to the hyperfine interactions, are involved and the hyperfine parameters can be derived from a characteristic beat pattern seen in the time evolution of the nuclear resonant scattering (time spectrum) [1]. Due to the high brilliance of the third generation synchrotron sources the method provides unique possibilities to probe magnetic properties with submonolayer sensitivity allowing one to accumulate a high quality time spectrum for one monolayer of ⁵⁷Fe film in a few minutes.

The experiment was performed in a multi-chamber ultra high vacuum (UHV) system (base pressure 1×10^{-10} mbar) at ID18 at ESRF Grenoble [2]. A special NRS scattering chamber, equipped with a ⁵⁷Fe electron beam evaporator, was mounted on a Huber goniometer, so that the time spectra could be collected simultaneously with Fe deposition. On the atomically clean W(110)

single crystal ⁵⁷Fe films were grown at a rate of about ~ 0.12 Å/min, which was precisely calibrated using a quartz monitor and X-ray reflectivity. Two large diameter beryllium UHV windows allowed the incident and scattered X-ray beam to access the sample and an avalanche photodiode detector array, respectively. The grazing incidence angle (~ 3.8 mrad) was optimized for the maximum count rate of the delayed quanta.

First, 1.8 Å of ⁵⁷Fe, corresponding to 1.1 pseudomorphic monolayer (psML), was deposited at 500 K. Next, a series of room temperature deposition steps was performed, each one corresponding to evaporation of 0.4 Å, till 10 Å (~ 5 ML) of the total Fe thickness was reached. After each deposition step, a time-spectrum was collected at room temperature for *k* vector of the incident X-ray beam parallel to the [1-10] in-plane direction of W(110). The whole process of deposition and time-spectra accumulation took only 1.5 h, and therefore the residual gas adsorption effects were negligible. The GI-NRS data were fitted using the program CONUSS [3]. In Fig. 1, the measured time spectra are shown for selected Fe thickness. The spectrum of the 1.1 psML film shows no quantum beat

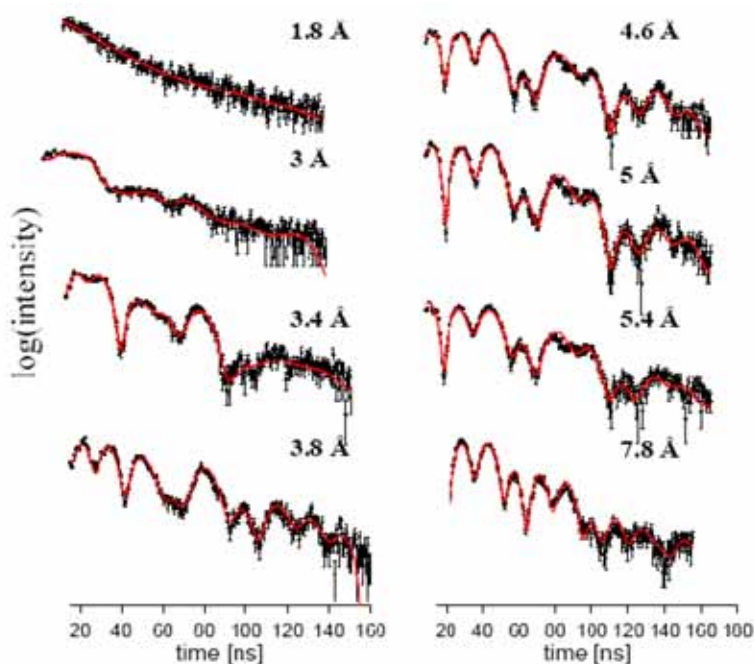


Figure 1. Fitted NRS time spectra for Fe/W(110) films of selected thicknesses.

pattern and could be fitted assuming a single paramagnetic site. The site is characterized by a distribution of the quadruple splitting due to the electric field gradient with the principal axis perpendicular to the surface. A quantum beat structure appeared in the time spectra when the nominal Fe thickness reached 3 Å, which corresponds to 1.8 psML. For coverage between 3 and 5.8 Å, analysis of the time spectra indicated a gradual transition from nearly perpendicular magnetization for 3 Å film to the in plane collinear magnetic order above 5.8 Å. For intermediate coverage a complex magnetic structure was derived from the numerical analysis. The magnetic structure is related to the film morphology characterized by a deviation from a layer-by-layer growth mode beyond the first monolayer. Competition of out-of-plane and in plane magnetic anisotropy for double layer Fe patches and for thicker Fe areas, respectively, leads to coexistence of non-collinear

spin structures at buried layers, which could not be solved using traditional methods.

Acknowledgements: This work was supported in part by the Polish Ministry of Science and Higher Education and by the Team Program of the Foundation for Polish Science co-financed by the EU European Regional Development Fund.

References

- [1] R. Röhlberger, *Nuclear Condensed Matter Physics with Synchrotron Radiation*, STMP 208, (Springer-Verlag, Berlin Heidelberg 2004).
- [2] S. Stankov, R. Rüffer, M. Sladeczek, M. Rennhofer, B. Sepiol, G. Vogl, N. Spiridis, T. Slezak, J. Korecki, "An ultra-high vacuum system for in-situ studies of thin films and nanostructures by nuclear resonance scattering of synchrotron radiation", *Rev. Sci. Instrum* **79** (2008) 045108
- [3] W. Sturhan, "CONUSS and PHOENIX: Evaluation of nuclear resonant scattering data", *Hyperfine Interact.* **125** (2000) 149–172.

STRUCTURAL STUDIES OF DISORDERED CARBONS - COMPARISON OF SIMULATIONS AND HIGH-ENERGY X-RAY DIFFRACTION DATA

L. Hawelek^{1*}, **A. Brodka**¹, **J.C. Dore**², **V. Honkimaki**³, and **A. Burian**¹

¹ *A. Chelkowski Institute of Physics, University of Silesia, ul. Uniwersytecka 4, 40-007 Katowice, Poland*

² *School of Physical Sciences, University of Kent, Canterbury, CT2 7NR, UK*

³ *European Synchrotron Radiation Facility, BP 220, 38043 Grenoble, France*

Keywords: X-ray diffraction, activated carbons, structure, molecular dynamic, density functional theory

**) e-mail: hawelek@us.edu.pl*

The X-ray diffraction measurement was carried out for sample of disordered, commercially produced carbon CXV on the ID15B beam-line at the European Synchrotron Radiation Facility (ESRF), Grenoble, France (Fig. 1).

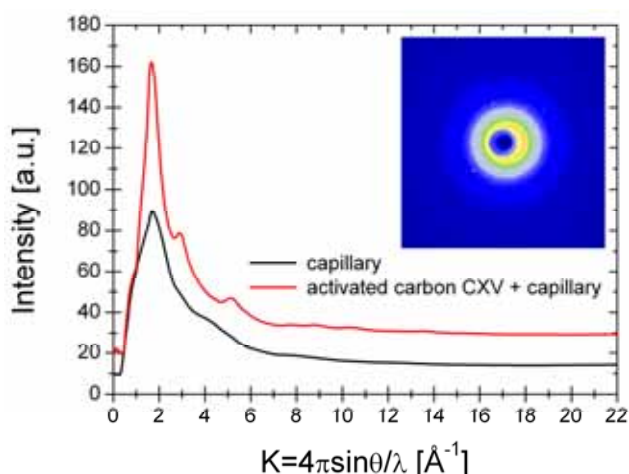


Figure 1. Comparison of the experimental intensities for the activated carbon CXV with capillary and the empty capillary. The 2D diffraction intensity for the CXV sample presented in the inset.

The obtained results show that the structure of the studied sample consists of two graphite like layers, stacked without spatial correlations. The size of the ordered region was described by the model of 4.5 Å in radius. The disordered structure was simulated by introducing the Stone-Wales defects (pair of two pentagons and two heptagons), randomly distributed in the network. The optimisation of those disordered carbon structure was performed by combining the classical molecular dynamic simulation using the REBO2 (the reactive bond order) potential [1] with the density functional theory using B3LYP functional method [2,3]. In Fig. 2 the relaxed atomic arrangement using the

REBO2 potential is displayed. The Grimme's empirical Van der Waals correction was used [4]. Finally, the HOMO-LUMO molecular orbitals calculated using the 6-31g* basis set for such carbon were compared.

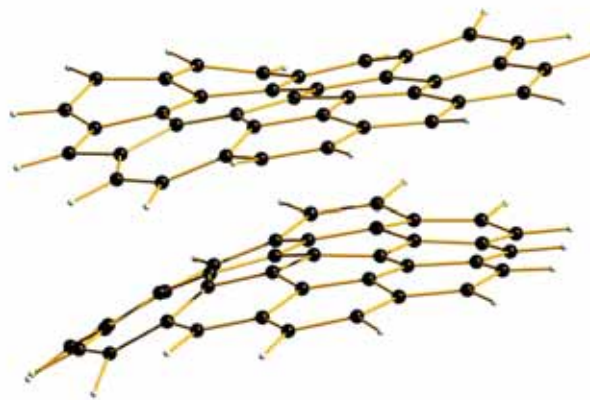


Figure 2. Arrangement of carbon (black) and hydrogen (grey) atoms for the model of the CXV after geometry optimisation using molecular dynamics simulation with REBO2 potential.

References

- [1] D.W. Brenner, O.A. Shenderova, J.A. Harrison, S.J. Stuart, N. Boris, S.B. Sinnott, "A second-generation reactive empirical bond order (REBO) potential energy expression for hydrocarbons", *J. Phys.: Condens. Matter* **14** (2002) 783–802.
- [2] A.D. Becke, "Density-functional thermochemistry. III. The role of exact exchange", *J. Chem. Phys.* **98** (1993) 5648–5652.
- [3] C. Lee, W. Yang, R.G. Parr, "Development of the Colle-Salvetti correlation-energy formula into a functional of the electron density", *Phys. Rev. B* **37** (1988) 785–789.
- [4] S. Grimme, "Semiempirical GGA-type density functional constructed with a long-range dispersion correction", *J. Comput. Chem.* **27** (2006) 1787–1799.

VALENCE BAND STUDY OF $\text{LaNiO}_{3-\delta}$ THIN FILMS

S. Grebinskij¹, M. Senulis¹, H. Tvardauskas¹, V. Bondarenka¹, V. Lisauskas¹, K. Sliuziene¹,
B. Vengalis¹, B.A. Orlowski², R.L. Johnson³, and S. Mickevicius^{1*}

¹ Institute of Semiconductor Physics, A. Gostauto 11, LT-01108 Vilnius, Lithuania

² Institute of Physics, Polish Academy of Sciences, Al. Lotnikow 32/46, 02-668 Warsaw, Poland

³ Hamburger Synchrotronstrahlungslabor HASYLAB am Deutschen Elektronen-Synchrotron DESY, Notkestr. 85, D-22603 Hamburg, Germany

Keywords: rare earth alloys and compounds, resonance photoemission, valence band electronic structure, oxide materials

*) e-mail: sigism@pfi.lt

LaNiO_3 is one of the few conductive oxides with a crystal structure suitable for integration in epitaxial heterostructures with perovskites of enormous technological potential such as colossal magnetoresistance materials, high-temperature superconductors and ferroelectrics. It is known that the considerable surface segregation of elements may place in LaNiO_{3-x} samples and is the tendency of rare earth and nickel oxides to absorb water vapor and carbon dioxide from air, so that any *ex situ* exposure of these films to air will result in an uncontrolled reaction and surface stoichiometry variation [1-2]. Thus the knowledge of the surface composition is extremely important because it is directly related to the heterostructures properties.

The initially hydrated $\text{LaNiO}_{3-\delta}$ surface may be restored by heating above dehydration temperature. Nickel hydroxide, in turn, decomposes at $T > 230^\circ\text{C}$ (melting point). When heated to decomposition it emits toxic fumes of metallic nickel, and one would expect a decrease of Ni-species relative concentration in the previously hydrated surface layer. The aim of this work is to investigate the valence band electronic structure and chemical composition of $\text{LaNiO}_{3-\delta}$ thin films after heating above dehydration temperature about 500°C .

Thin LaNiO_{3-x} films onto monocrystalline (100)-plane oriented NdGaO_3 substrate were deposited by using a reactive DC magnetron sputtering technique. To prevent the film bombardment by high energy ions during deposition, NdGaO_3 substrates were positioned in "off-axis" configuration at a distance of 15 mm from the symmetry axis of the discharge and 20 mm over the target plane. The substrate temperature was $\sim 750^\circ\text{C}$ and the resultant thickness of LaNiO_{3-x} film was about $0.1 \mu\text{m}$.

The resonant photoemission experiments were performed in the synchrotron radiation laboratory

HASYLAB, Hamburg (Germany). Synchrotron radiation obtained from the storage ring DORIS III was monochromatized with the FLIPPER II plane grating vacuum monochromator designed for the photon energy range of 15–200 eV. The spectrometer was equipped with a CMA electron energy analyzer. The total energy resolution was kept at 0.1 eV. The origin of the energy axis was set at the Fermi energy as measured for a reference metallic sample.

The giant resonance in La 5*p* and La 5*s* peaks intensity observed at excitation energy corresponding to a La[4*d* → 4*f*] threshold ($h\nu = 119.5 \text{ eV}$) is accompanied by a weak resonance of $\text{N}_{4,5}\text{O}_{2,3}\text{O}_{2,3}$ and $\text{N}_{4,5}\text{O}_{2,3}\text{V}$ Auger peaks. The obtained results are in an agreement with the model of an autoionization process after resonant excitation. The relatively weak enhancement of the intensity of valence band maxima (at about 6 eV) may be explained by the small mixing of the La 5*d* ionic character to the O 2*p* valence band. No resonant features were observed in the VB spectra under Ni[3*p* → 3*d*] excitation (escape depth $L \approx 2 \text{ ML}$), indicating that nickel species are not presented at the $\text{LaNiO}_{3-\delta}$ film surface after heat treatment.

References

- [1] J. Choisnet, N. Abadzhieva, P. Stefanov, D. Klissurski, J.M. Bassat, V. Rives, L. Minchev, "X-ray photoelectron spectroscopy, temperature-programmed desorption and temperature-programmed reduction study of LaNiO_3 and $\text{La}_2\text{NiO}_{4+\delta}$ catalysts for methanol oxidation", *J. Chem. Soc. Faraday Trans.* **90** (1994) 987–991.
- [2] Y. Li, N. Chen, J. Zhou, S. Song, L. Liu, Z. Yin, C. Cai, "Effect of the oxygen concentration on the properties of Gd_2O_3 thin films", *J. Cryst. Growth* **265** (2004) 548–552.

XANES STUDY OF THE SYNTHETIC EQUIVALENT OF HEMOZOIN DISSOLVED IN ORGANIC SOLVENTS BEFORE AND AFTER INTERACTION WITH CHLOROQUINE

M.S. Walczak^{1*}, **K. Ławniczak-Jablonska**¹, **A. Wolska**¹, **M. Sikora**^{2,3}, **A. Sienkiewicz**^{1,4},
L. Suárez⁵, **A. Kosar**⁵, **M.J. Bellemare**⁵, and **D.S. Bohle**⁵

¹ *Institute of Physics, PAS, Al. Lotników 32/46, PL-02-668 Warsaw, Poland*

² *Faculty of Physics and Applied Computer Science, AGH University of Science and Technology,
Al. Mickiewicza 30, PL-30-059 Krakow, Poland*

³ *European Synchrotron Radiation Facility, 6 rue Jules Horowitz, Boîte Postale 220, 38043 Grenoble, France*

⁴ *Institute of Condensed Matter Physics, Ecole Polytechnique Fédérale de Lausanne, Lausanne, CH-1015, Switzerland*

⁵ *Department of Chemistry, McGill University, 801 Sherbrooke Street West, Montreal QC H3A 2K6, Canada*

Keywords: malaria, malarial pigment, hemozoin, X-ray absorption spectroscopy

*) e-mail: mwalczak@ifpan.edu.pl

According to the World Health Organization half of the human population is at risk of malaria disease [1]. The same source also attributes one million fatalities and 247 million cases to malaria in 2006. The intraerythrocytic stage of parasite involves haemoglobin proteolysis as the primary nutrient source and haem detoxification into an inert crystalline material, called malarial pigment, or hemozoin [2]. The blood stage of parasite is responsible for the clinical manifestations of the disease. Currently an effective malaria vaccine does not exist and therapy is totally based on the use of drugs with the most effective treatment being a combination of artemisinin drugs. The crystal structure of hemozoin has been solved by X-ray powder diffraction [3] and revealed to be identical as β -hematin one. For the purpose to examine ferriprotoporphyrin IX – chloroquine complex into organic solvent solution the synthetic analogue of hemozoin was synthesized. Although many tribes of parasite are resistant to chloroquine understanding of all possible interactions and chemical structures related to malarial pigment become now critically important in respect that also artemisinin based drugs started to be less effective. The parasite is susceptible for to both drugs in its intraerythrocytic stage.

The X-ray absorption spectroscopy (XAS) method for solving the ferriprotoporphyrin IX – chloroquine complex structure in the local iron atomic neighborhood was applied. The EXAFS results were reported previously [4]. The synthetic soluble analog of hemozoin, mesohematin anhydride, was used as model compound. High resolution XANES spectra enabled us to reveal the differences before and after supplementing with drug in dimethyl sulfoxide solutions. Knowing that the pre-edge structure of the XANES spectrum results from p and d states hybridization and is sensitive to the symmetry change, an attempt was made to model near edge spectra also with reconstruction of the pre-edge structure using FEFF, MXAN and FDMNES multiple scattering codes.

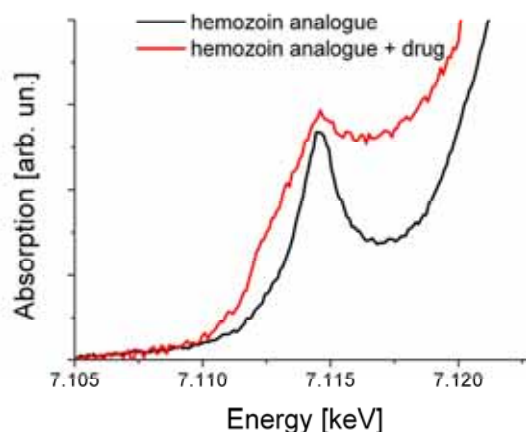


Figure 1. Comparison of pre-edge features in XANES spectra of hemozoin analogue before and after interaction with antimalarial drug in solution of dimethyl sulfoxide.

Acknowledgements: This work was supported by research grant nr.: N20205332/1197 and special project ESRF/73/2006 from the Ministry of Science and High Education. We acknowledge also the European Synchrotron Radiation Facility ESRF.

References

- [1] <http://www.who.int/topics/malaria/en/>
- [2] A. Dorn, R. Stoffel, H. Matile, A. Bubendorf, R.G. Ridley, "Malarial haemozoin/ β -haematin supports haem polymerization in the absence of protein", *Nature* **374** (1995) 269-271.
- [3] S. Pagola, P.W. Stephens, D.S. Bohle, A.D. Kosar, S.K. Madsen, "The structure of malaria pigment β -haematin", *Nature* **404** (2000) 307-310.
- [4] M.S. Walczak, K. Ławniczak-Jablonska, A. Wolska, M. Sikora, A. Sienkiewicz, L. Suárez, A.J. Kosar, M.J. Bellemare, D.S. Bohle, "Towards understanding the chloroquine action at the molecular level in antimalarial therapy - EXAFS studies", submitted to *J. Inorg. Biochem.* (2010).

XANES AND X-RAY PHOTOEMISSION OF THE $\text{La}_{0.67}(\text{Ca,Pb})_{0.33}(\text{Mn}_{1-x}\text{Fe}_x)\text{O}_3$ COMPOUNDS

M. Kowalik^{1,2*}, **M. Sikora**¹, **A. Kołodziejczyk**¹, and **Cz. Kapusta**¹

¹ Department of Solid State Physics, AGH University of Science and Technology, 30, Mickiewicza Str, 30-059 Cracow, Poland

² Department of Physics, Rzeszów University of Technology, 6, Powstańców Warszawy Str, 35-959 Rzeszów, Poland

Keywords: colossal magnetoresistive perovskites, XANES, photoemission

*) e-mail: mkowalik@prz.edu.pl

Polycrystalline compounds $\text{La}_{0.67}\text{Ca}_{0.33}(\text{Mn}_{1-x}\text{Fe}_x)\text{O}_3$ ($x = 0, 0.08$) and $\text{La}_{0.67}\text{Pb}_{0.33}(\text{Mn}_{1-x}\text{Fe}_x)\text{O}_3$ ($x = 0, 0.01, 0.03, 0.06, 0.10, 0.15$) were prepared by the sol-gel low-temperature method followed by heat treatment at 1273 K in air [1].

High resolution Mn *K*-edge XANES spectra of the samples and the reference oxides have been acquired in total *K* fluorescence yield using undulator fundamental mono-chromatized by a pair of Si (311) single crystals at the XAS-XES ID26 beamline of the ESRF, Grenoble. The spectra of all the samples reveal similar shape with a small, but significant gradual shift of the edge energy (Fig. 1), which is attributed to Mn charge disproportionation upon Fe substitution. A shift towards higher energy can be interpreted within the model of preferential Fe $3d^6$ configuration and gradual decrease of the average Mn $3d$ occupation upon substitution. **Conclusion:** the shift by $\sim 0.25\text{eV}$ from $x = 0.0$ to $x = 0.15$ agrees well with the expected average valence change from $\text{Mn}^{3.33+}$ to $\text{Mn}^{3.45+}$, assuming linear relationship between edge position and Mn oxidation [2].

Special attention was focused to the analysis of the Mn $2p$ core-level lines and the multiplet splitting (MS) of the lines was taken into account. It arises when, upon

ejection of core electron, the angular momenta of the partially filled core shell can couple with the angular momenta of open atomic valence shell to form several multiplets of different energies [3]. The MS is expected to be observed if the specimen possesses unpaired electrons in its outer valence shells, e.g. for the ground-state configuration $2p^53d^3$ for Mn^{+4} and $2p^53d^4$ for Mn^{+3} ions. To analyse the MS of the Mn $2p$ core-level line we have adopted the results of the MS calculations for Mn^{+3} and Mn^{+4} ions presented in [3,4] in order to fit the Mn $2p_{3/2}$ spectra. The selected spectra and the fittings are shown in Fig. 2.

Photoemission measurements were carried out by use of the angle resolved X-ray and ultraviolet XPS/ARUPS Omicron photoemission spectrometer. The XP spectra were measured for $x = 0, 0.08$ and 0.10 with the Al- K_α X-ray source with energy resolution about 1 eV at 300 K.

As the result of the fit the areas under the Mn^{3+} and Mn^{4+} lines were obtained and the ratio of $\text{Mn}^{3+}/\text{Mn}^{4+} = 1.9 \pm 0.2$ for $\text{La}_{0.67}\text{Ca}_{0.33}(\text{Mn}_{1-x}\text{Fe}_x)\text{O}_3$ ($x = 0.08$) and 1.6 ± 0.2 $\text{La}_{0.67}\text{Pb}_{0.33}(\text{Mn}_{1-x}\text{Fe}_x)\text{O}_3$ ($x = 0.10$) were obtained. **Conclusion:** the ratios are in fairly good agreement with the expected values and with assumption that for $x=0$ the ratio is equal to 2.0.

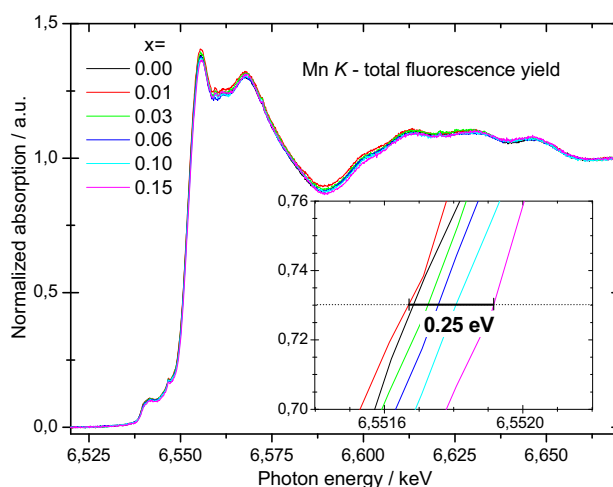


Figure 1. The normalized Mn *K*-edge XANES spectra of $\text{La}_{0.67}\text{Pb}_{0.33}(\text{Mn}_{1-x}\text{Fe}_x)\text{O}_3$. Insert: magnified part of the spectra at half of maximum to extract the edge shift vs the Fe content.

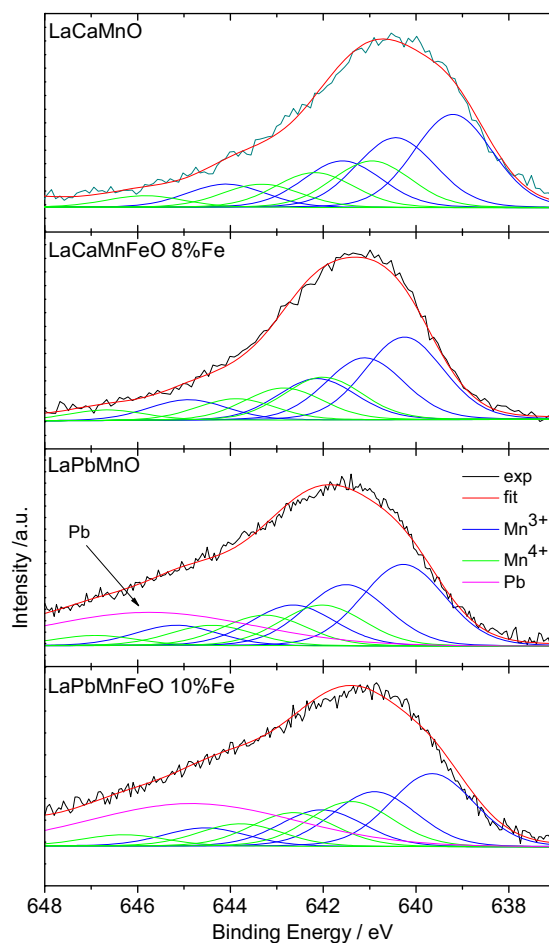


Figure 2. The Mn $2p_{3/2}$ spectra and the fitting of four multiplet for each $Mn^{3+} 2p_{3/2}$ and $Mn^{4+} 2p_{3/2}$ ions according to the analysis in [3,4], as well as with the Pb $4p_{3/2}$ line overlapping the Mn $2p_{3/2}$ lines. The XPS Peak program was used [5].

References

- [1] G. Gritzner, M. Koppe, K. Kellner, J. Przewoźnik, J. Chmista, A. Kołodziejczyk, K. Krop, "Preparation and properties of $La_{0.67}Pb_{0.33}(Mn_{1-x}Fe_x)O_3$ compounds", *Appl. Phys. A* **81** (2005) 1491-1495.
- [2] A.H. de Vries, L. Hozoi, R. Broer, "On the origin of the chemical shift in X-ray-absorption near-edge spectroscopy at the Mn K edge in manganese oxide compounds", *Int. J. Quantum Chem.* **91** (2003) 57-61.
- [3] R.P. Gupta, R.K. Sen, "Calculation of multiplet structure of core p -vacancy levels I", *Phys. Rev. B* **10** (1974) 71-77.
- [4] R.P. Gupta, R.K. Sen, "Calculation of multiplet structure of core p -vacancy levels II", *Phys. Rev. B* **12** (1975) 15-19.
- [5] R.W.M. Kwok, *XPS Peak Fitting Program Version 4.1*, Department of Chemistry, The Chinese University of Hong Kong, <http://www.phy.cuhk.edu.hk/~surface/XPSPEAK>

SYNCHROTRON-BASED X-RAY DIFFRACTION OF THE PYROMORPHITE-VANADINITE AND MIMETITE-VANADINITE SERIES

J. Klasa ¹, O. Borkiewicz ², J. Flis ^{1*}, and M. Manecki ¹

¹ Department of Mineralogy, Petrography and Geochemistry, AGH – University of Science and Technology, Al. Mickiewicza 30, 30 – 059 Kraków, Poland

² Department of Geology, Miami University, Oxford, OH 45056, USA

Keywords: lead apatites, solid solution, synchrotron radiation, Rietveld refinement

*) e-mail: flisjustyna@tlen.pl

Pyromorphite $Pb_5(PO_4)_3Cl$, mimetite $Pb_5(AsO_4)_3Cl$ and vanadinite $Pb_5(VO_4)_3Cl$ (commonly called: lead apatites) are minerals isostructural with apatite. In-situ chemically induced precipitation of pyromorphite and mimetite has recently gained a considerable attention as a cost effective reclamation method of soils and wastes contaminated with Pb(II) and As(V). The unique crystal structure and chemistry of these minerals, however, allow for numerous substitutions of both metal cations and anionic complexes [1]. Natural pyromorphites and mimetites usually contain substituted VO_4^{3-} , AsO_4^{3-} and PO_4^{3-} . This suggests that pyromorphite, mimetite and vanadinite tend to form solid solutions which are relatively stable in environment. [2]. There are several reports on the response of the lead apatites structure to cationic substitutions, however, the knowledge about anionic substitutions which strongly influences the environmental stability of these minerals is sparse. Detailed crystal-chemical study of pyromorphite – mimetite solid solution series has been recently reported by Flis *et al.*, 2010. The performed structural Rietveld refinement of the synchrotron-based data allowed for precise determination of structural parameter of the series including: cell dimensions, ionic bond lengths and angles as well as anionic site occupancies. To date, the only X-ray diffraction studies regarding vanadate substitutions in the lead apatite series is reported by Baker *et al.* [3]. He reports that pyromorphite-vanadinite and mimetite-vanadinite solid solution series are complete. His X-ray data, however, is not supported by the chemical analysis of synthesised solids. Furthermore pyromorphite-mimetite-vanadinite solid solution series are prone to serve peak overlapping and characterized by subtle structural changes among adjacent members. Thus, detailed crystal-chemical studies of these minerals demand high resolution X-ray radiation source.

In order to supplement existing data, a number of compounds covering a wide range of compositions between pyromorphite-vanadinite and mimetite-vanadinite end members were synthesized from aqueous solutions by drop-wise mixing of the respective chemical reagents. The syntheses were carried out at 90°C and pH = 3. Products were characterized by SEM coupled with EDS chemical microanalyser, as well as synchrotron-based X-ray diffraction. Diffraction experiments were carried on the dedicated high-resolution high-throughput powder diffractometer at Sector 11-BM B of the Advanced Photon Source, Argonne National Laboratory,

USA. Analyses were performed at room temperature using monochromatic radiation of the wavelength of 0.42 Å. Intensities of the diffracted X-rays were collected on a 12-element Analyzer/Detector System offering supreme resolution and greatly reduced data collecting time [4]. Raw data from each of the 12 detectors was calibrated, merged and reduced using in-house routine. The diffraction data was analyzed by Rietveld method using the computer program GSAS and EXPGUI. The background was modeled using Chebyshev polynomials of the first kind. Apatite starting atomic parameters came from the refinement based on neutron data in P63/m of Holly Springs hydroxylapatite.

The use of the dedicated high-resolution, high-throughput diffraction beamline 11-BM allowed for quick collection of data of a quality unavailable on any conventional radiation source. The results from Rietveld refinement confirm that the pyromorphite-vanadinite and mimetite-vanadinite solid solution series are continuous. Unit cell parameters vary linearly with anionic substitutions and they depend primarily on chemical properties of constituting anions. The refinement of the occupancies of the anionic position in the mineral structure of all synthesized compounds was in good agreement with the theoretical composition of the samples based on the chemistry of the starting solutions. The results supplement characteristics of environmentally important mineral series.

Acknowledgments: This work was supported by the MNiSW grant No. NN307101535.

References

- [1] Y. Pan, M.E. Fleet, *Phosphates: Geochemical, Geobiological, and Materials Importance, Reviews in Mineralogy and Geochemistry*, (Mineralogical Society of America, Washington, DC, 2002)
- [2] A. Nakamoto, Z. Urasima, S. Sugiura, H. Nakano, T. Yachi, K. Tadokoro, "Pyromorphite – mimetite minerals from the Otraru-Matasukra barite mine in Hokkaido", *Jpn. Miner. J.* **6** (1969) 85–101.
- [3] W.E. Baker, "An X-ray diffraction study of synthetic members of the pyromorphite series", *Am. Miner.* **51** (1996) 1712–1721
- [4] P.L. Lee, D. Shu, M. Ramanathan, C. Preissner, J. Wang, M.A. Beno, R.B. Von Dreele, L. Ribaud, C. Kurtz, S.M. Antao, X. Jiao, B.H. Toby, "A twelve-analyzer detector system for high-resolution powder diffraction", *J. Synchrotr. Rad.* **15** (2008) 427–432.

LOCAL ATOMIC ORDER IN Zr-Cu METALLIC GLASSES STUDIED BY X-RAY ABSORPTION FINE STRUCTURE METHOD

W. Zalewski*, A. Pietnoczka, J. Antonowicz, and R. Bacewicz

Faculty of Physics, Warsaw University of Technology, Koszykowa 75, 00-662 Warsaw, Poland

Keywords: EXAFS, amorphous materials, metallic glasses

*) e-mail: wojtekzal@gmail.com

Results of the Extended X-ray Absorption Fine Structure (EXAFS) measurements of Zr-Cu amorphous alloys are presented. The samples of investigated alloys were obtained by rapid quenching of liquid using the melt-spinning technique. The EXAFS experiments were carried out for K_{Zr} and K_{Cu} absorption edges in a transmission mode at liquid nitrogen temperature. The local environment of Zr and Cu atoms was studied in a wide composition range. From the experimental data the values of interatomic distance, mean square variation in bond length (Debye-Waller factor) and coordination number were calculated. The EXAFS spectra were used to evaluate the pair distribution functions (PDFs) [1]. The concept of ideal solution behaviour in Zr-Cu glasses [2] was applied to the resulting PDFs. The structural data are correlated with the thermal stability results derived from differential scanning calorimetry (DSC) experiments.

The effect of deformation and thermal annealing on the local environment of the atomic species is demonstrated. In the heavily deformed samples a clear decrease of the coordination number is observed indicating that additional free volume was introduced to the amorphous structure during deformation. The structural similarities between the local structure of the glassy phase and their crystalline equivalents are demonstrated.

References

- [1] J. Antonowicz, D.V. Louzguine-Luzgin, A.R. Yavari, K. Georgarakis, M. Stoica, G. Vaughan, E. Matsubara, A. Inoue, *J. Alloys Compds.* **471** (2009) 70.
- [2] K. Georgarakis, A. R. Yavari, D. V. Louzguine-Luzgin, J. Antonowicz, M. Stoica, Y. Li, M. Satta, A. LeMoulec, G. Vaughan, A. Inoue, *Appl. Phys. Lett.* **94** (2009) 191912; *ESRF Highlights* 2009, p.40.

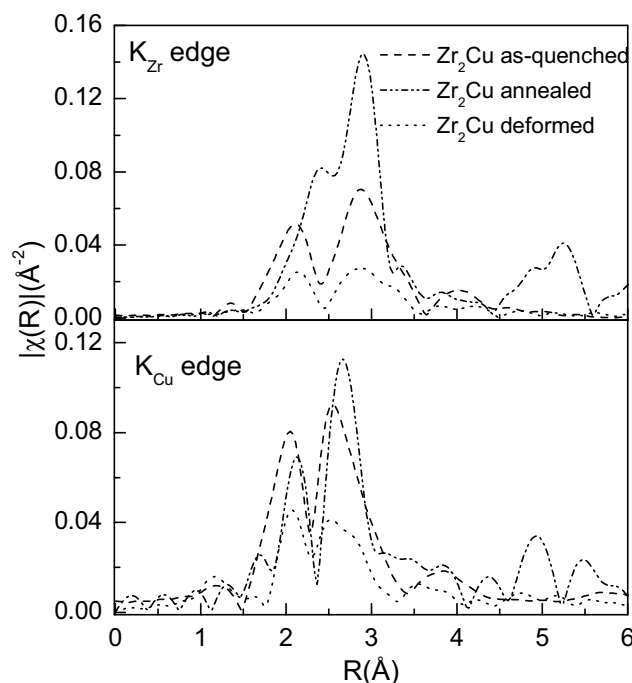


Figure 1. Fourier transformed K-edges of Zr and Cu for Zr_2Cu amorphous alloy in the as-quenched, deformed and annealed (crystalline) state.

THE DETERMINATION OF THE CHEMICAL COMPOSITION PROFILE OF THE GaAs/AlGaAs HETEROSTRUCTURES DESIGNED FOR QUANTUM CASCADE LASERS BY MEANS OF SYNCHROTRON RADIATION

Jarosław Gaca^{1*}, Marek Wójcik¹, Maciej Bugajski², and Kamil Kosiel²

¹ Institute of Electronic Materials Technology, ul. Wolczyńska 133, 01-919 Warsaw, Poland

² Institute of Electron Technology, Warsaw, Al. Lotnikow 32/46, 02-668 Warsaw, Poland

Keywords: QCL, HRXRD, heterostructure, chemical composition

*) e-mail: gaca-jr@itme.edu.pl

The determination of the chemical composition profile of GaAs/AlGaAs heterostructures designed for quantum cascade lasers is crucial for the development of the special procedures of their growth. The core of the heterostructure makes combined injector and active regions. These dual regions are repeated typically 25-70 times (fig. 1). Each region contains series of ultra-thin AlGaAs and GaAs layers. The thickness of each layer is in the range of a few nanometers. So high-resolution X-ray diffractometry and reflectometry using synchrotron radiation along with the computer simulation is an excellent tool for achieving this goal. Nonetheless, because of high degree of complication of the final structure, it is advisable, to start to investigate each part of the heterostructure separately, beginning with simple units such as injector and active region, and next moving on to the more complicated structures. To this end, samples containing: injector, active region, combined injector and active region, the later repeated 30 times and full quantum cascade laser structure had been grown by means of MBE device with reactor Riber Compact 21T at the Institute of Electron Technology, Warsaw, Poland [1]. As a next step, rocking curves were registered for each sample using synchrotron radiation with wavelength $\lambda = 0.154114$ nm at the ROBL-CRG beamline BM20 at the ESRF Grenoble (France). Collected rocking curves were analyzed by means of numerical analysis. Computer program designed for simulating rocking curves, based on Darwin dynamical theory of X-ray diffraction was employed [2]. For the purpose of simulation, a heterostructure was modeled as a stack of parallel atomic planes with different chemical composition. The analysis was performed so that, the chemical composition of each atomic plane had been varied until the best fit between experimental and simulated curves was achieved. The developed method has enabled: to optimize the process of epitaxy, to work out the chemical composition profile as well for the whole heterostructure of the quantum cascade laser as for its parts, to detect and identify the departures from designed structure. The great advantage of this method is the fact that it is nondestructive one, can be used as a method of verification of the quality of the heterostructures without any special prior arrangements and allows for the correction of errors made during the process of epitaxy.

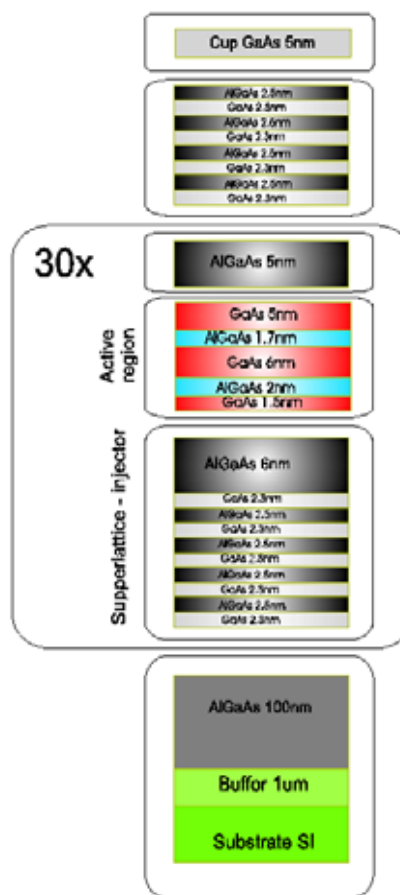


Figure 1. The sample heterostructure for AlGaAs/GaAs quantum cascade laser.

References

- [1] K. Kosiel, J. Kubacka-Traczyk, P. Karbownik, A. Szerling, J. Muszalski, M. Bugajski, P. Romanowski, J. Gaca, M. Wójcik, "Molecular-beam epitaxy growth and characterization of mid-infrared quantum cascade laser structures", *Microelectron. J.* **40** (2009) 565–569.
- [2] J. Gaca, M. Wójcik, A. Jasik, K. Pierscinski, M. Kosmala, A. Turowski, A.M. Abdul-Kader, "Effects of composition grading at heterointerfaces and layer thickness variations on Bragg mirror quality", *Opto-Electron. Rev.* **16** (1) (2008) 12–17.

XAFS ON CTAB-STABILIZED GOLD NANOPARTICLES

W. Szczerba^{1*}, **M. Radtke**¹, **U. Reinholz**¹, **H. Rieseemeier**¹, **A.F. Thünemann**¹,
R. Fenger², and **K. Rademann**²

¹ BAM Federal Institute for Materials Research and Testing, Richard-Willstätter-Straße 11, 12489 Berlin, Germany

² Department of Chemistry, Humboldt Universität zu Berlin, Brook-Taylor-Straße 2, 12489 Berlin, Germany

Keywords: gold, nanoparticles, x-ray absorption spectroscopy

*) e-mail: wojciech.szczerba@bam.de

The modifications of the electronic structure and the structural order with decreasing particles size are of great interest for the explanation of catalytic properties of gold nanoparticles. One of the issues is the predicted Au-Au bond contraction with particle size decrease. For the purpose of the study, x-ray absorption spectroscopy (XAFS) has been chosen as a probe, since it provides information about both, the local coordination and the electronic structure of the absorbing element. There were several studies on deposited gold nanoparticles employing XAFS [1,2]. However, reports on experiments on free gold nanoparticles are scarce.

The study presented has been carried out on free gold nanoparticles (AuNP) in liquid cetrimonium bromide (CTAB) solution, and on freeze-dried CTAB/AuNP solutions. The gold nanoparticles were prepared by seeding growth according to the method reported by N.R. Nikhil *et al.* [3]. Samples of 3.2, 9.0, 13.4 and 28.0 nm diameter were received with a gold concentration of 2.5×10^{-4} mol/L. The average particle sizes were determined on a different lot of samples in a small angle x-ray scattering (SAXS) experiment. One lot was freeze-dried overnight immediately after preparation in a FINN-AQUA LYOVAC GT2 freeze-dryer in order to obtain powder samples of higher Au concentration. However, during the freezing process a change of the color of the substance from red to violet occurred during the transition from the intermediate gel phase to solid. Such a change of color indicates usually a coagulation of gold nanoparticles. A behavior like this has not been observed on a control sample with colloidal gold nanoparticles produced by standard citrate synthesis. The other lot was measured as cast shortly after preparation. The XAFS measurements were conducted in the fluorescence mode at the BAMline and μ -Spot beamlines at BESSY II, Berlin. Together with the samples a gold leaf reference of 200 nm thickness has been measured, too.

The obtained XAFS spectra did not show any significant differences in the near absorption edge region (XANES) indicating that the gold nanoparticles maintained the electronic structure of bulk gold in all the cases. The EXAFS spectra of the nanoparticles and the gold reference were almost identical, showing that there was no change in the local order of the nanoparticles with decreasing size. In order to estimate the Au-Au bond length parameter, *ab-initio* calculations using FEFF

8.40 have been employed. A first shell theory fit was performed of the experimental data sets using IFFEFIT 1.2.11c software.

The Au-Au bond length of the coagulated particles due to freeze-drying was the almost same for all four samples as that of bulk gold, 2.889 Å compared to 2.883 Å. The free gold nanoparticles in liquid CTAB solution have a slightly larger Au-Au bond length than bulk gold, by 4.2 pm; and no size depended behavior has been observed. This stays in contrast to standard citrate synthesized gold nanoparticles, where an increasing Au-Au bond length contraction of the same order of magnitude with decreasing particle size has been observed by our group on standard NIST gold nanoparticles [4] and has also been reported for deposited nanoclusters [1,2].

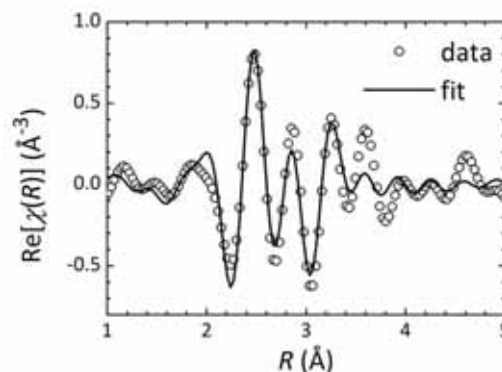


Figure 1. First shell fit of the FEFF generated model spectrum to the EXAFS spectrum of the smallest AuNP sample (3.2 nm) in liquid.

References

- [1] A. Belerna *et al.*, "Extended x-ray absorption fine-structure and near-edge-structure studies on evaporated small clusters of Au", *Phys. Rev. B* **31** (1985) 5058.
- [2] J.T. Miller *et al.*, "The effect of gold particle size on Au-Au bond length and reactivity toward oxygen in supported catalysts", *J. Catal.* **240** (2006) 222.
- [3] N.R. Jana *et al.*, "Seeding growth for size control of 5–40 nm diameter gold nanoparticles", *Langmuir* **17** (2001) 6782
- [4] W. Szczerba *et al.*, "EXAFS study of Au-Au bond length in gold nanoparticle standards", (2010) *to be published in Anal. Bioanal. Chem.*

DISTRIBUTION OF SELECTED ELEMENTS IN ATHEROSCLEROTIC PLAQUES OF APOE/LDLR-DOUBLE KNOCKOUT MICE SUBJECTED TO DIETARY AND PHARMACOLOGICAL TREATMENTS

M. Gajda^{1*}, **J. Kowalska**², **A. Banaś**³, **K. Banaś**³, **W.M. Kwiatek**²,
R. Kostogrys⁴, **Ł. Mateuszuk**⁵, **S. Chłopicki**⁵, **J.A. Litwin**¹, and **K. Appel**⁶

¹Department of Histology, Jagiellonian University Medical College, Kopernika 7, 31-034 Kraków, Poland

²Institute of Nuclear Physics, Radzikowskiego 152, 31-342 Kraków, Poland

³Singapore Synchrotron Light Source, National University of Singapore, 5 Research Link, 117603 Singapore

⁴Department of Human Nutrition, Agricultural University of Kraków, Balicka 122, 30-149, Kraków, Poland

⁵Department of Pharmacology, Jagiellonian University Medical College, Kopernika 7, 31-531 Kraków, Poland

⁶Hasylab, DESY, Notkestraße 85, D-22607, Hamburg, Germany

Keywords: atherosclerosis, iron, zinc, copper, phosphorus, calcium, mouse

*) e-mail: mmgajda@cyf-kr.edu.pl

Atherosclerosis is a multietiological inflammatory and degenerative vascular disease with growing incidence in westernized populations. Gene-targeted, apolipoprotein E and LDL receptor-double knockout (apoE/LDLR-DKO) mice represent a new animal model that displays severe hyperlipidemia and atherosclerosis. We have successively used apoE/LDLR-DKO mice to study biological effects of new antiatherosclerotic drugs and diets [1,2]. Furthermore, we applied synchrotron radiation microprobes to characterize elemental composition of atheromas in this animal model [3]. The aim of the present study was to show changes in the distribution of selected elements in atherosclerotic plaques of apoE/LDLR-DKO mice fed egg-rich proatherosclerotic diet supplemented or not with antiatherosclerotic drug perindoprilat (inhibitor of angiotensin converting enzyme). We have combined synchrotron radiation micro-XRF spectrometry with histological stainings to determine distribution and concentration of trace and essential elements in histologically defined areas of atherosclerotic lesions.

Fifteen female apoE/LDLR-DKO mice were used for the study. Up to the age of 4 months the mice were fed a commercial, cholesterol-free pelleted diet and then they were randomly assigned to one of three experimental groups fed for the following 2 months: *i.* AIN-93G diet ($n=5$; CHOW), *ii.* AIN-93 diet supplemented with 5% egg-yolk lyophilisate ($n = 5$; LIOPH), *iii.* AIN-93G diet supplemented with egg-yolk lyophilisate and perindoprilat (2 mg/kg b.w., $n = 5$; LIOPH/PERIND). Six-month-old animals were sacrificed; hearts with ascending aorta were dissected out and snap-frozen. Serial 10 μm -thick cryosections of the aortic root were cut and mounted either on routine slides (histology) or on 3 μm -thick Mylar foil (microprobes). Consecutive slides were stained with oil red O (ORO) for the demonstration of lipids, picosirius red for collagen fibers and double immunostained: CD68 for macrophages and smooth muscle actin (SMA) for smooth muscle cells.

All micro-XRF measurements were carried out at beamline L of the storage ring DORIS III (Hasylab, Hamburg). The primary photon energy was set to 17.5 keV by a multilayer double monochromator. A polycapillary half-lens was used for beam focusing, hence the final beam size on the sample was approximately 15 μm in diameter. Emitted elemental spectra were recorded with Vortex SDD detector. Two-dimensional maps were acquired from lesional areas of the aortic root with surrounding cardiac muscle (resolution 15 μm , time of acquisition 5 s from each point). From morphologically defined areas, precise point spectra were recorded (resolution 15 μm , time of acquisition 300 s).

Based on histological stainings, more advanced atherosclerosis expressed by total area occupied by lipids, number of macrophages and smooth muscle cells was observed in animals fed egg-rich diet. The perindoprilat treatment slightly attenuated these effects. In animals fed egg-rich diet, higher concentrations of Ca, P, K and lower concentrations of Cl, Cu, Fe, Se, Zn in atheromas were seen in comparison to chow diet-fed animals. After perindoprilat treatment, concentrations of Ca, Cl, Cu, K, Se and Zn showed the tendency to achieve levels like in chow diet-fed animals.

References

- [1] J. Jawien, M. Gajda, M. Rudling, Ł. Mateuszuk, R. Olszanecki, T. Guzik, T. Cichocki, S. Chłopicki, R. Korbut, *Eur. J. Clin. Invest.* **36** (2006)141-146.
- [2] M. Franczyk-Żarów, R.B. Kostogrys, B. Szymczyk, J. Jawień, M. Gajda, T. Cichocki, L. Wojnar, S. Chłopicki, P.M. Pisulewski, *Braz. J. Nutrition.* **99** (2008) 49-58.
- [3] M Gajda, K Banaś, A Banaś, J Jawień, Ł Mateuszuk, S Chłopicki, WM Kwiatek, T Cichocki, G Falkenberg, *X-Ray Spectrom.* **37** (2008) 495-502.

LATERAL DISTRIBUTION OF ELEMENTS IN THE MULTIELEMENTAL STANDARD SAMPLES STUDIED BY THE SYNCHROTRON RADIATION BASED MICRO X-RAY FLUORESCENCE

A. Kubala-Kukuś^{1*}, J. Szlachetko^{1,2}, M. Pajek¹, J. Susini², and M. Salome²

¹ *Institute of Physics, Jan Kochanowski University, Świętokrzyska 15, 25-406 Kielce, Poland*

² *European Synchrotron Radiation Facility (ESRF), Jules Horowitz 6, 38000 Grenoble, France*

Keywords: standard sample, micro x-ray fluorescence, TXRF, GEXRF

**) e-mail: aldon.kubala-kukus@ujk.kielce.pl*

Total-reflection X-ray fluorescence (TXRF) [1] is commonly employed in the semiconductor industry for determination of contaminants on silicon wafer surfaces. Similarly, the grazing emission X-ray fluorescence (GEXRF) [2] combined with synchrotron radiation and high-resolution detection of the fluorescence photons has proven to be successful to determine the concentration of low-level impurities on silicon [3, 4]. These techniques provide quantitative results and the calibration procedure normally used involves placing a micro-droplet (~ μ l) of the standard solution onto a silicon wafer. After evaporation of the solvent, the residual amount of elements on the wafer is used as a reference standard [1,3,4]. However, a distribution of residue material on the substrate surface is not known accurately and consequently, such calibration method is burdened with uncertainty as to whether the standard sample is of the pure particulate type, which is usually assumed for evaluation purposes, or whether forms a film-type layer.

In the present work the investigation of the lateral distribution of elements in the multielemental calibrating samples by using the synchrotron radiation based micro x-ray fluorescence is presented. The goal of this project was the investigation of a uniformity of the elemental distributions and determination of the droplet morphology. The studies have been performed at the European Synchrotron Radiation Facility (ESRF) at the ID21 X-ray microscopy beamline.

In the experiment the multielemental standard solution was deposited as a droplet (0.5 μ l) on the silicon wafers and dried in oven in temperatures ranging from 20°C to 200°C. After evaporation of the solvent, the residual amount of elements on the wafer were analysed by the micro-XRF. The photon beam (energy 7.2 keV, flux $\sim 10^9$ photons/s) was focused using Fresnel zone plate to the size 0.7 μ m \times 0.3 μ m. The full fluorescence spectrum was recorded (HpGe detector) for each pixel of the map. The X-ray 2D-images were next compared with the optical and the scanning electron microscope images (Fig. 1).

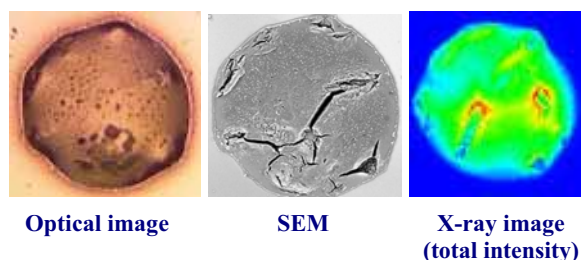


Figure 1. Comparison of optical, scanning electron microscope (SEM) and X-ray images for the multielemental standard solution deposited as a droplet on the silicon wafer and dried in 30°C. A size of the residue is about 380 μ m.

It was found that for high drying temperature a size of the residue corresponds to the size of a droplet, while for low temperature the residue shrinks to much smaller size of 300-400 μ m. Moreover, no losses of material was observed for low temperature and the correlations between elements were observed. The results are important for developing more accurate calibration procedures for surface sensitive x-ray techniques (e.g. TXRF, high-resolution GEXRF) used for determination of contaminants on semiconductor surfaces.

References

- [1] R. Klockenkämper, *Total Reflection X-ray Fluorescence Analysis* (Wiley, New York, 1997).
- [2] H. P. Urbach, P.K. de Bokx, "Calculations of intensities in grazing-emission x-ray fluorescence", *Phys. Rev. B* **53** (1996) 3752.
- [3] J. Szlachetko *et al.*, "Application of the high-resolution grazing-emission x-ray fluorescence method for impurities control in semiconductor nanotechnology", *J. Appl. Phys.* **105** (2009) 086101.
- [4] A. Kubala-Kukuś *et al.*, "Observation of ultralow-level Al impurities on a silicon surface by high-resolution grazing emission x-ray fluorescence excited by synchrotron radiation", *Phys. Rev. B* **80** (2009) 113305.

X-RAY DIFFRACTION INVESTIGATION OF CYCLOHEXANE DERIVATIVES AT 293 K

H. Drozdowski *, K. Nowakowski, and Z. Błaszczak

Department of Optics, Faculty of Physics A, Mickiewicz University, ul. Umultowska 85, 61-614 Poznań, Poland

Keywords: X-ray diffraction, cyclohexane derivatives, electron-density radial-distribution function

*) e-mail: riemann@amu.edu.pl

This paper reports results of X-ray diffraction study of three the cyclohexane derivatives: methylcyclohexane $C_6H_{11}-CH_3$ (Fig. 1a), cyclohexylamine $C_6H_{11}-NH_2$ (Fig. 1b) and cyclohexanol $C_6H_{11}-OH$ (Fig. 1c). The aim of the study was to establish the role of the cyclohexane ring and the functional groups ($-CH_3$, $-NH_2$, $-OH$) attached to it at the equatorial position in configurations of the molecules of the liquids studied.

The measurements of scattered radiation intensity were performed with molybdenum radiation (MoK_{α} , $\lambda = 0.71069 \text{ \AA}$) and graphite monochromator on the diffracted beam in a range 2θ of $6^\circ - 120^\circ$ by the step-scanning method [1] with a step of 0.2° and counting time of 15 s.

The most important results of the paper are listed below:

- 1) New experimental data on the structure of cyclohexane derivatives (Fig. 1) at 293 K.
- 2) New information on mutual arrangement, orientation and packing coefficient of the molecules studied.
- 3) Proposition of models if intermolecular binary radial correlations in the antiparallel orientation of dipole moments in the liquids studied.
- 4) The presence of short-range ordering reaching about 20 \AA has been proved [2].

References

- [1] H. Drozdowski, "Structural analysis of liquid 1,4-dimethylbenzene at 293 K", *J. Mol. Struct.* **783** (2006) 204–209.
- [2] H. Drozdowski, K. Nowakowski, "X-ray diffraction studies of liquid methylcyclohexane $C_6H_{11}-CH_3$ structure at 293 K", *Acta Phys. Polon. A* **114** (2008) 383–389.

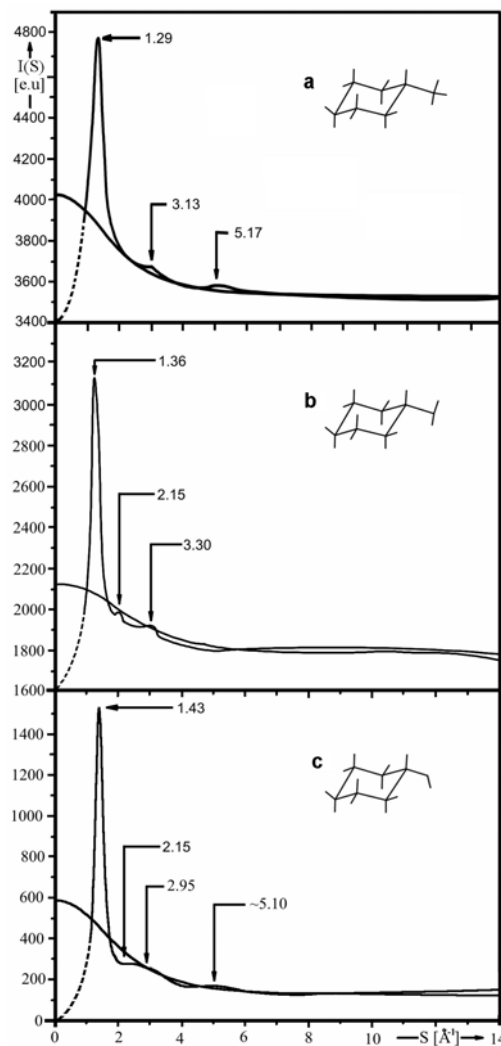


Figure 1. The experimental curves of angular distribution of X-ray scattered intensity in cyclohexane derivatives ($S = 4\pi \sin\theta / \lambda$).

SIMULATIONS OF POLYCAPILLARY-BASED WAVELENGTH DISPERSIVE X-RAY FLAT-CRYSTAL SPECTROMETER

P. Jagodziński^{1*}, **M. Pajek**², **J. Szlachetko**^{2,3}, **D. Banaś**², **A. Kubala-Kukuś**²,
J.-Cl. Dousse⁴, **J. Hoszowska**⁴, and **Y. Kayser**⁴

¹Department of Physics, Kielce University of Technology, 25-314 Kielce, Poland

²Institute of Physics, Jan Kochanowski University, 25-406 Kielce, Poland

³European Synchrotron Radiation Facility (ESRF), F-38043 Grenoble, France

⁴Department of Physics, University of Fribourg, CH-1700 Fribourg, Switzerland

Keywords: polycapillary, Monte-Carlo simulations, wavelength-dispersive x-ray spectroscopy

*) e-mail: jagodzin@tu.kielce.pl

The polycapillary x-ray optics is widely used in x-ray fluorescence applications. Polycapillary x-ray lenses can collect a radiation emitted from a small source into a large solid angle and therefore they have a strong impact on the development of x-ray fluorescence analysis by improving the detection limits. Increasing demands for developing new and complementary x-ray methods to be used for various applications are presently focused on high-resolution and high-sensitivity x-ray fluorescence techniques combined with a narrow, down to the sub-micrometer range, x-ray beam excitation. For this reason, a new polycapillary based flat-crystal x-ray wavelength dispersive spectrometer (WDS) [1] have been implemented for the x-ray micro-fluorescence analysis applications at the ESRF ID21 beamline.

The factors affecting transmission of x-rays through a polycapillary optics include its shape, size, surface roughness, x-ray source – polycapillary geometry and x-ray energy and polycapillary optical properties. In order to predict the focusing properties and energy resolution of the polycapillary-based wavelength dispersive x-ray spectrometer, the Monte-Carlo simulation software was created. The calculations of x-ray transmission through the polycapillary exploit the phenomenon of total external reflection of x-rays by a surface below a critical angle, including the multiple reflections. In this simulations the quasi-parallel x-ray beam formed by a polycapillary is directed onto a flat crystal at an angle θ , where the photons are diffracted according to the Bragg formula, and finally they are recorded by a detector placed at the angle 2θ . The simulation software has been written using C++ compiler, which gives a possibility to predict the transmission, spectrometer resolution and x-ray fluorescence spectrum.

The developed WDS spectrometer was applied to study the trace elements in speleothems (stalactite, cave pearl) from the Paradise Cave (central Poland) (see Fig. 1).

The Monte-Carlo simulations predict reasonable well the main characteristic of the polycapillary-based WDS spectrometer, which was tested experimentally (see Fig. 2). The developed high-resolution WDS spectrometer was found to be well suited for the measurements of trace elements in geological samples (speleothems).

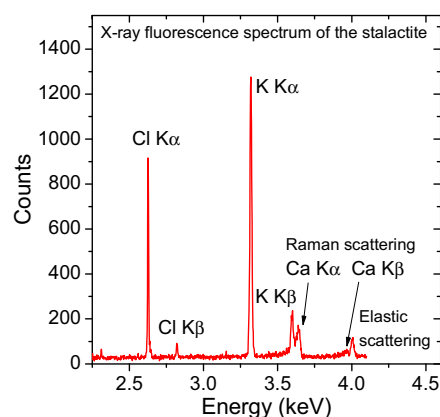


Figure 1. X-ray fluorescence spectrum recorded for stalactite sample measured with WDS spectrometer.

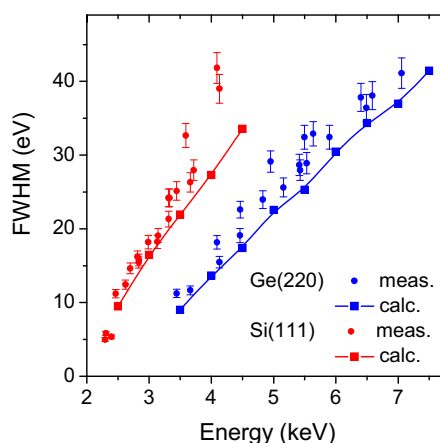


Figure 2. Energy resolution of the spectrometer with a Si(111) (in red) and Ge(220) (in blue) crystals: measured (circles) and calculated with the Monte-Carlo simulations (squares).

References

- [1] J. Szlachetko, *et al.*, "Wavelength-dispersive spectrometer for x-ray micro-fluorescence analysis at the X-ray Microscopy beamline ID21 (ESRF)", *J. Synchrotr. Rad.* **17** (2010) 400–408.

INFLUENCE OVERGROWTH PARAMETERS ON THE LOCAL STRUCTURE IN CdSe QUANTUM DOTS STUDIED BY FINE STRUCTURE METHOD

**E. Piskorska-Hommel^{1,2*}, V. Holý³, A. Wolska¹, A. Gust¹, C. Kruse¹, H. Kröncke²,
J. Falta², D. Hommel², H. Renevier⁴, and F. d'Acapito⁴**

¹ *Institute of Physics, Polish Academy of Sciences, Warsaw, Poland*

² *Institute of Solid State Physics, University of Bremen, Bremen, Germany*

³ *Department of Condensed Matter Physics, Charles University, Prague, Czech Republic*

⁴ *European Synchrotron Radiation Facility, Grenoble, France*

Keywords: CdSe, quantum dots, exafs, dafs

*) *e-mail: e.piskorska@ifp.uni-bremen.de*

The II–VI quantum dots have attracted interest due to application in red, green and blue laser diodes, as well in fundamental physics [1]. The ZnSe-based laser diodes are not long-term stable under electrical operation. Nevertheless, it has been shown that such green emitting ZnSe lasers are significantly more stable when replacing the ZnCdSse quantum well by a stack of CdZnSe/ZnSse quantum dots [2].

CdSe quantum dots can be formed in a ZnSe matrix by molecular beam epitaxy (MBE). This system has a high lattice mismatch (~7%) resulted in self-assembled quantum dots (QDs) during epitaxial growth [3].

Since the self-organization process has a stochastic nature, the resulting nanostructures have a certain dispersion of their sizes and shapes and, in addition, the dots are chemically inhomogeneous. Therefore, a reliable and non-destructive characterization of the structure of quantum dots is of a crucial importance to improve their applicability. Several characterization techniques such as transmission electron microscopy (TEM), scanning tunneling microscopy (STM) and atomic-force microscopy (AFM) have been employed to aid the understanding of the growth mechanisms and to determine optimal growth conditions.

The structural investigations of CdZnSe/ZnSe quantum dots were mainly performed by high-resolution x-ray diffraction (HRXRD) using synchrotron radiation, high-resolution transmission electron microscopy (HRTEM) and luminescence [4, 5], yielding the structure and the correlations of the positions of CdSe quantum dots.

The capping process of quantum dots plays an important role for their optical properties; however the capping layer introduces additional strain and changes in the chemical composition by intermixing during the deposition of the capping layer. To get information about the intermixing of substrate and capped layer a key issue is to determine the optimal technological conditions in

order to obtain the nanostructure with demanded optical and electrical properties.

In order to explain the influence of the overgrowth parameters on the structure of the formed CdSe quantum dots Extended X-ray Absorption Fine Structure (EXAFS) and Diffraction Anomalous Fine Structure (DAFS) were employed. Due to its selectivity for a chosen element, EXAFS is well suited to determine the bond lengths Cd-Se, Cd-Cd and Cd-Zn and atomic ordering within strained CdSe/ZnMgSSe quantum dot layers. However, the EXAFS signal provides structural information averaged over all absorber atoms selected. To obtain the bond lengths and the atomic ordering within regions with a chosen elastic strain, the DAFS technique was used. From the DAFS spectra we determined the structure of the neighborhood of absorbing atoms in a region of the dot volume with given strain (iso-strain volume). Therefore, local atomistic structural parameters for this volume are obtained as results. The advantage of the DAFS method is that the EXAFS-like information can be obtained "locally," allowing us to detect possible atomic ordering in CdSe/ZnMgSSe alloys.

A series of CdSe/ZnSe/MgS single quantum dots layers grown by molecular beam epitaxy (MBE) on GaAs(001) substrates were studied. The CdSe monolayers (ML) were embedded in a 1.4 nm ZnSe layer surrounded by 2 nm MgS barriers grown on a GaAs substrate with 50 nm ZnSe underneath and 25 nm above this dot structure. The investigated samples differ in the amount of deposited CdSe monolayers.

The EXAFS spectra at the Cd K edge (~27 keV) were collected at fluorescence mode using a multi-element Ge detector.

The DAFS spectra at the Se K-edge (~12.7 keV) were collected in grazing-incidence geometry at different positions in reciprocal space near the (800) diffraction spot (for various deviations q_r from the reciprocal lattice

point) in order to obtain local chemical information and information on the atomic ordering in a particular iso-strain volume. The q_r axis was chosen along the ($h00$) line (radial direction). The DAFS signal stems from an iso-strain volume, the position of which is determined by the value of the q_r coordinate, where the DAFS signal was collected. The grazing incidence geometry allowed us to reduce the contribution of the substrate to the scattered intensity and enhances the contribution of the quantum dots to the measured signal. To avoid the oxidation, the samples were kept in He atmosphere during the measurement.

The Athena program was used to subtract the pre-edge background, normalize to the experimental edge step and absorption data from the EXAFS data [6]. The DAFS spectrum $\chi(E)$ depends on the real (χ') and imaginary (χ'') parts of the anomalous form-factor of the Se atoms. The numerical Kramers-Kronig transformation was used to extract the imaginary part $\chi''(E)$ of the DAFS spectrum [7]. Then, the data were transformed to the direct R-space and both EXAFS and DAFS data were fitted in R-space to theoretical curves generated by the FEFF 8 code for the Cd-Se, Cd-Cd and Cd-Zn pairs [8]. Then, the Artemis program was used to obtain the structure parameters, *i.e.*, bond lengths (R), Debye-Waller factors (σ^2) and coordination numbers (N) [9]. The EXAFS and DAFS results are discussed in details.

References

- [1] T. Passow, K. Leonardi, D. Hommel, "Optical and Structural Properties of CdSe/Zn(S)Se Quantum Dot Stacks", *Phys. Stat. Sol. (b)* **224** (2001) 143–.
- [2] M. Klude, T. Passow, R. Kröger, D. Hommel, "Electrically pumped lasing from CdSe quantum dots", *Electr. Lett.* **37** (2001) 1119–1120.
- [3] K. Leonardi, H. Heinke, K. Ohkawa, D. Hommel, H. Selke, F. Gindele, U. Woggon, "CdSe/ZnSe quantum structures grown by migration enhanced epitaxy: Structural and optical investigations", *Appl. Phys. Lett.* **71** (1997) 1510–1512.
- [4] Th. Schmidt, T. Clausen, J. Falta, G. Alexe, T. Passow, D. Hommel, S. Bernstorff, "Correlated stacks of CdSe/ZnS quantum dots", *Appl. Phys. Lett.* **84** (2004) 4367–1569.
- [5] G. Bacher, H. Schömiß, M.K. Welsch, S. Zaitsev, V.D. Kulakovskii, A. Forchel, S. Lee, M. Dobrowolska, J. Furdyna, B. König, W. Ossau, "Optical spectroscopy on individual CdSe/ZnMnSe quantum dots", *Appl. Phys. Lett.* **79** (2001) 524–526.
- [6] <http://cars.uchicago.edu/ifeffit>
- [7] M.G. Proietti, H. Renevier, J. Hodeau, J. Garcia, J. Béar, P. Wolfers, "Diffraction-anomalous-fine-structure spectroscopy applied to the study of III-V strained semiconductors", *Phys. Rev. B* **59**, 5479 (1999); J.O. Cross, *Ph.D. thesis*, (University of Washington, Seattle, 1996); J. Coraux, V. Favre-Nicolin, M.G. Proietti, B. Daudin, H. Renevier, "Grazing-incidence diffraction anomalous fine structure: Application to the structural investigation of group-III nitride quantum dots", *Phys. Rev. B* **75** (2007) 235312.
- [8] S.I. Zabinsky, J.J. Rehr, A. Ankudinov, R.C. Albers, M.J. Eller, "Multiple-scattering calculations of x-ray-absorption spectra", *Phys. Rev. B* **52** (1995) 2995–3009.
- [9] B. Ravel, M. Newville, "ATHENA, ARTEMIS, HEPHAESTUS: data analysis for X-ray absorption spectroscopy using IFEFFIT", *J. Synchrotr. Rad.* **12** (2005) 537–541.

EXAFS AND XRD STUDIES OF CRYSTALLOGRAPHIC GRAINS IN NANOCRYSTALLINE FePd:Cu THIN FILMS

M. Krupinski*, M. Perzanowski, A. Polit, Y. Zabala, A. Zarzycki, and M. Marszalek

*The Henryk Niewodniczanski Institute of Nuclear Physics, Polish Academy of Sciences,
Radzikowskiego 152, 31-342 Krakow, Poland*

Keywords: thin films, magnetic alloys, absorption spectroscopy

**) e-mail: Michal.Krupinski@ifj.edu.pl*

The FePd L1₀ phase alloys belong to the systems, which are very interesting due to their promising magnetic properties and forthcoming applications in recording devices [1]. The magnetism of the system is correlated very strongly with crystallographic structure, in particular with grain size and grain shape [2].

[Fe(0,9nm)/Pd(1,1nm)/Cu(*d* nm)]×5 multilayers were prepared by thermal deposition at room temperature in UHV conditions on Si(100) substrates covered by 100 nm SiO₂. The thickness of copper layer has been changed from 0 to 0.4 nm. After the deposition, the multilayers have been rapidly annealed at 600°C in nitrogen atmosphere, what resulted in the creation of FePd:Cu alloy.

The structure of obtained alloy films was determined by x-ray diffraction (XRD), glancing angle x-ray diffraction (GAXRD), and x-ray absorption fine structure (EXAFS). The chemical composition of the films was checked by Rutherford backscattering (RBS). The measurements clearly showed that for all investigated

copper compositions the L1₀ FePd:Cu nanocrystalline phase has been formed during the annealing process.

The paper concentrates on crystallographic grain features analysis of obtained alloys and illustrates how the EXAFS technique can help to extend the information about grain size and grain shape of poorly crystallized materials. The comparison of EXAFS and XRD results gives a reasonable agreement. Using appropriate models we show the reasons of possible differences between the results obtained from XRD and more challenging EXAFS analysis applied to FePd:Cu system.

References

- [1] S.N. Piramanayagam, "Perpendicular recording media for hard disk drives", *J. Appl. Phys.* **102** (2007) 011301.
- [2] H. Naganuma, K. Sato, Y. Hirotsu, "Fabrication of oriented L1₀-FeCuPd and composite bcc-Fe/L1₀-FeCuPd nanoparticles: Alloy composition dependence of magnetic properties", *J. Appl. Phys.* **99** (2006) 08N706.

THYMIDYLATE SYNTHASE IN COMPLEX WITH N(4)-HYDROXY-2'-DEOXYCYTIDINE 5'-MONOPHOSPHATE: CRYSTAL STRUCTURE AND MOLECULAR MODELING

**Adam Jarmuła^{1*}, Anna Dowierciał^{1*}, Piotr Wilk¹,
Wojciech R. Rypniewski², and Wojciech Rode¹**

¹ *Nencki Institute of Experimental Biology, Polish Academy of Sciences, Pasteura 3, 02-093 Warszawa, Poland*

² *Institute of Bioorganic Chemistry, Polish Academy of Sciences, Noskowskiego 12/14, 61-704 Poznań, Poland*

Keywords: thymidylate synthase (TS), N(4)-OH-dCMP, crystal structure, molecular dynamics, inhibitors of TS

**) E-mail: a.jarmula@nencki.gov.pl, a.dowiercial@nencki.gov.pl*

Thymidylate synthase (TS) catalyzes the reductive methylation of dUMP, the reaction being the sole intracellular *de novo* source of thymidylate required for DNA synthesis. TS is an important target in chemotherapy, as its inhibition blocks DNA synthesis and prevents cellular proliferation. An analogue of dUMP, N(4)-hydroxy-2'-deoxycytidine 5'-monophosphate (N(4)-OH-dCMP), exhibited in the presence of the cofactor, N⁵,N¹⁰-methylene tetrahydrofolate (mTHF), a strong, time-dependent inhibition of TS [1]. In order to elucidate the inhibitory mechanism of N(4)-OH-dCMP on TS, X-ray crystallographic and molecular modeling studies were carried out.

The protein complex of mouse thymidylate synthase (mTS) with N(4)-OH-dCMP was crystallized by the vapor diffusion method. Diffraction data to 1.75 Å resolution were collected on the BESSY synchrotron in Berlin and processed with DENZO and SCALEPACK. The structure was refined with REFMAC5 of the CCP4 program suite using the 3IHI crystal structure of mTS as the search model. The quality of the final structure, with an *R*-factor of 21.5%, was analyzed with PROCHECK and SFCHECK.

The structure, consisting of one dimer per asymmetric part of the unit cell (Fig. 1), showed a strong similarity to the crystal structure of the complex mTS□dUMP, reflected by the backbone RMSD of 0.36 Å. The molecule of N(4)-OH-dCMP, which is defined by very good electron density, exhibits similar binding as the molecule of dUMP. Both molecules are anchored in the active site by several H-bonds to their phosphate moieties from four arginine and single serine residues. The orientation of N(4)-OH-dCMP, which is secured by H-bonds between the conserved Asn 220 of the enzyme and N(3)-H and N(4) moieties of the pyrimidine ring in N(4)-OH-dCMP, is the same as that of dUMP, with the positions of the pyrimidine rings in both molecules slightly shifted away from each other.

Molecular dynamics simulations were performed with SANDER module of AMBER8 for the complexes between TS from different sources, including human, rat, *E.coli* and *L.casei*, and (i) N(4)-OH-dCMP (binary systems), and (ii) N(4)-OH-dCMP and tetrahydrofolate

(THF; analogue of mTHF) (ternary systems). The simulations were started from the respective crystal structures after replacing the molecule of dUMP with the one of N(4)-OH-dCMP. The binding mode of N(4)-OH-dCMP in each simulated complex was analyzed and compared with all other ones in the search for conformational and/or structural differences. The analysis revealed some differences in (i) the binding positions of N(4)-OH-dCMP among the binary systems and (ii) the binding alignments between N(4)-OH-dCMP and THF among the ternary systems. Those observations will help to construct a comprehensive model of the interaction of N(4)-OH-dCMP with TS and, in turn, to suggest a possible mechanism of the inhibitory action of this analogue of dUMP.

References

- [1] W. Rode, Z. Zieliński, J.M. Dzik, T. Kulikowski, M. Bretner, B. Kierdaszuk, J. Cieśla, D. Shugar, "Mechanism of inhibition of mammalian tumor and other thymidylate synthases by N4-hydroxy-dCMP, N4-hydroxy-5-fluoro-dCMP, and related analogs", *Biochem.* **29** (1990) 10835–10842.

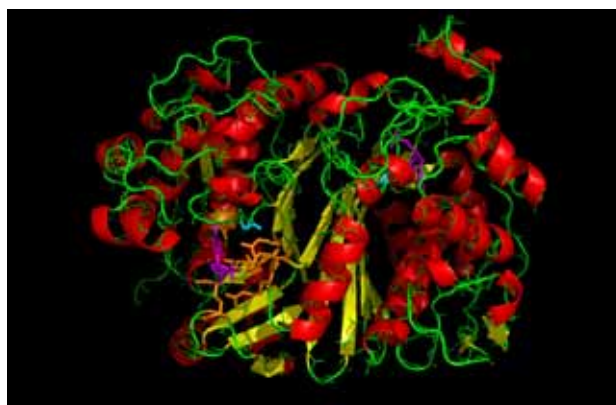


Figure 1. Crystal structure of mTS□N(4)-OH-dCMP (chains A and B). The ligand molecule depicted in magenta; Cys 189 in cyan; Arg 44, Arg 209, Ser 210, Arg 169, Arg 170 and Asn 220, the amino acids crucial in proper ligand binding and orientation, in orange.

DOMAIN CONFIGURATIONS AND CONDUCTIVITY IN LSGM

T. Tataryn^{1*}, **D. Savytskii**¹, **E. Schmidbauer**², **C. Paulmann**³, and **U. Bismayer**⁴

¹Lviv Polytechnic National University, 12 Bandera St., 79013 Lviv, Ukraine

²Geophysics, Munich University, Theresienstr. 41, D-80333 Munich, Germany

³HASYLAB, DESY, Notkestr. 85, D-22603 Hamburg, Germany

⁴Mineralisch-Petrographisches Institut, Universität Hamburg, Grindelallee 48, D-20146 Hamburg, Germany

Keywords: twin structure, solid electrolyte, ionic conductivity

*) e-mail: tataryn.taras@gmail.com

The aim of our investigations was to study the arrangement and distribution of twin boundaries during mechanical and thermal treatment in order to examine reversibility phenomena in larger ferroelastic crystal plates ($5 \times 6 \times 0.87 \text{ mm}^3$) as well as the influence of the domain structure on ionic conductivity. In the selected plate of $\text{La}_{0.95}\text{Sr}_{0.05}\text{Ga}_{0.9}\text{Mg}_{0.1}\text{O}_{3-x}$ (LSGM) with thickness of 0.87 mm a submicron twin structure was abundant. Diffraction studies were performed using white synchrotron radiation and the Kappa-diffractometer, beamline F1 at HASYLAB, DESY in Hamburg. Using a MAR CCD-detector system the orientation of individual domains (twins) was determined. Scanning of the sample under the beam ($0.05 \times 0.05 \text{ mm}^2$) and collecting diffraction data at each step 45 micron spatial resolution was used to map thin domain patterns in the LSGM plate after mechanical as well as thermal treatment. Conductivity measurements were done between $\sim 70^\circ\text{C}$ and 710°C in air. Impedance spectroscopy was applied using a HP4284 LCR-meter in the range 20 Hz – 1 MHz.

Data were recorded applying AC amplitudes of 80 mV and 1V to the electrode.

Analysis of Laue patterns collected in the same area of the plate has shown that the twin structure changed after the treatments described above. For example, a chevron-like 4 domain configuration was observed in 89% of the scanned area in the virgin sample, after grinding and polishing the plate in 37% and after further heating/cooling in approximately 69% of the same sample area (Fig. 1). It was shown that before mechanical treatment mainly twin walls normal to the largest surface of the plate occurred. The observed domain structure was partially switched to another twin configuration with domain walls parallel to the surface or to certain domain states during polishing. After annealing the domain configuration with prevalent domain walls normal to the largest plate surface was fully restored. The mechanism of twinning under mechanical treatment is shown in Fig. 2.

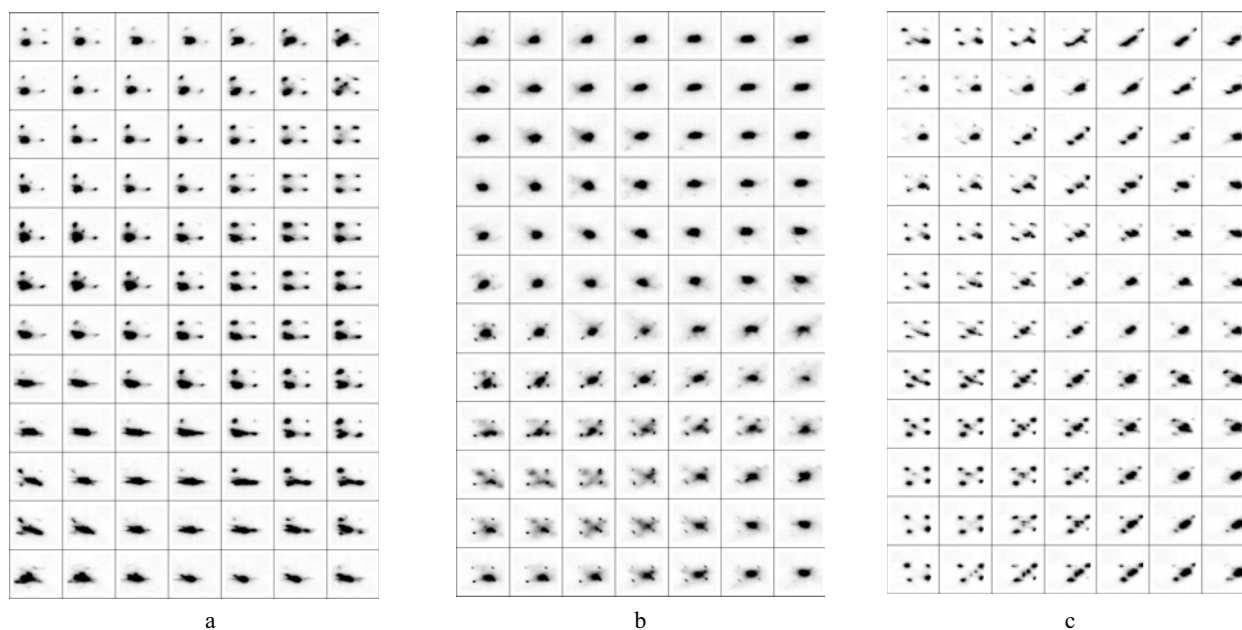


Figure 1. The part of scanned area of the plate (a) before treatment, (b) after grinding and polishing and (c) after further heating/cooling.

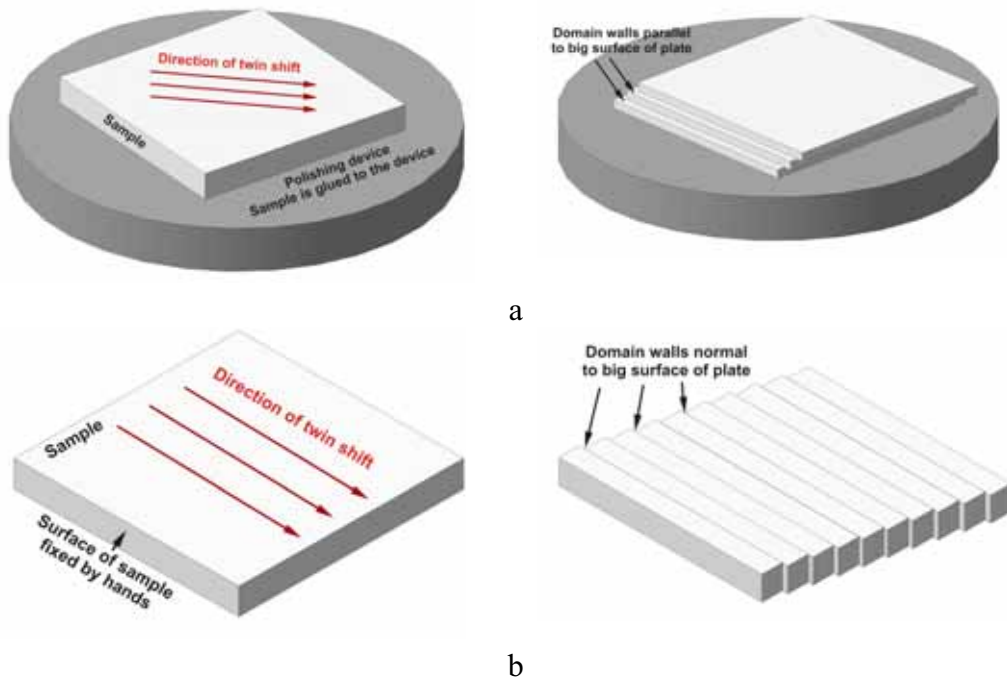


Figure 2. Twinning of a plate under mechanical treatment: a) the crystal plate is glued to the metal cylinder; b) the surface of the plate is simply fixed by hand.

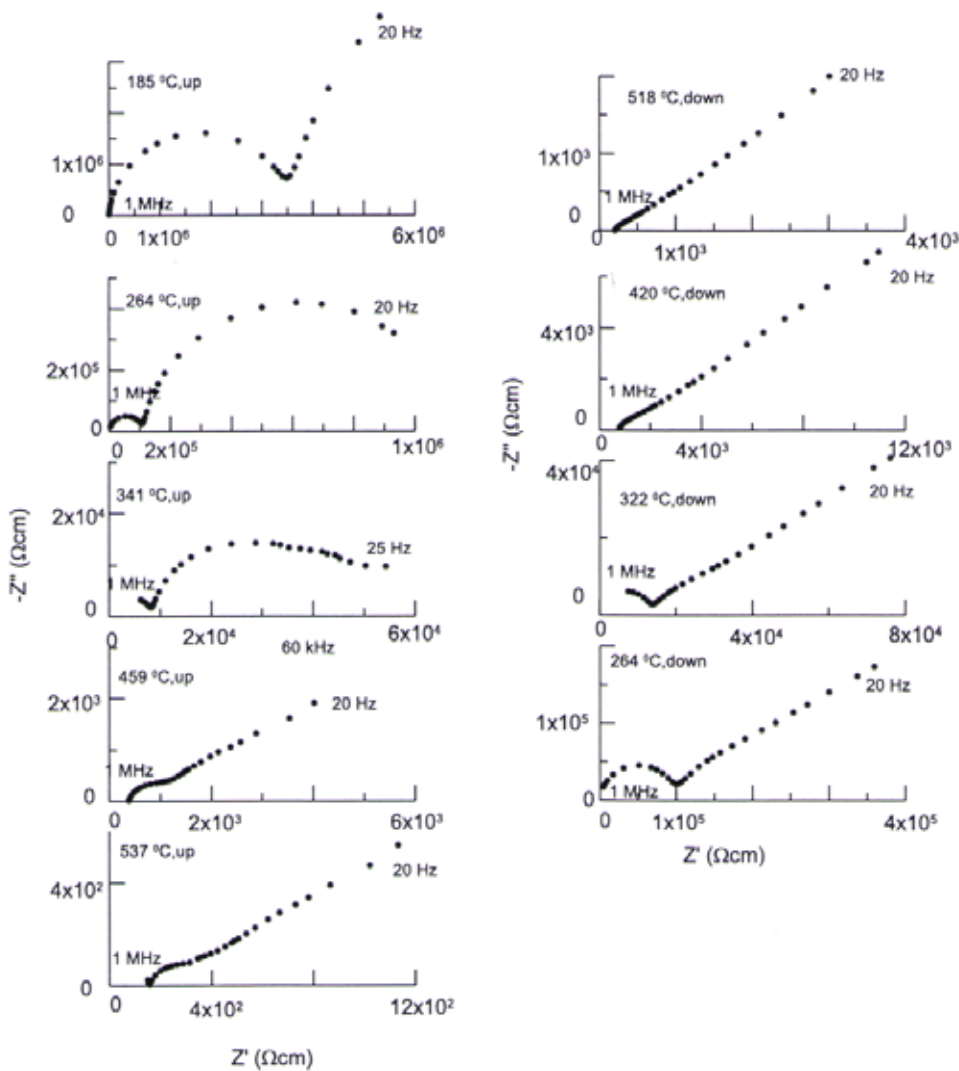


Figure 3. Complex plane impedance plots as a function of temperature during heating and cooling in air.

Impedance plots show two semicircular arcs (Fig. 3). The first high frequency arc corresponds to the bulk conductivity while the second low frequency one corresponds to the conductivity on domain boundaries.

Our results show that the specific chevron-like twin pattern allows for reproducibility of wall configurations in heavy defect LSGM crystals [1]. The stress can relax completely by forming phase-specific domain wall configurations, and hence, reorientations occur during thermal cycling. This feature may be of practical use as the preparation of electrolyte and electrode ceramics for SOFC includes compaction during one of the synthesis stages. Compaction, however, leads to unidirectional mechanical stress. Ceramics of LSGM can be approximated by an ensemble of small crystallites. Mechanical pressure imposed to such an electrolyte pellet causes the rearrangement of the twin structure of "chevron cells" in ceramic grains along the direction parallel or nearly parallel to the imposed pressure. Hence, such pressure will cause memory texturing of twin "chevrons" in electrolyte layers along the direction

of oxygen diffusion in the SOFC structure. Keeping in mind the influence of twin walls on the conductivity and the high density of twin walls in LSGM solid solutions, it is supposed that texturing of the twins, e.g. reorientation of "chevron cells" increases the conductivity of the perovskite-type electrolyte LSGM along the cathode-anode direction. The improved knowledge of twin distributions allows to tailor conductivity properties of electrolyte materials.

Acknowledgments: The work was supported by WTZ (UKR 07/009) and the Ukrainian Ministry of Education and Science (project "Tern"). T. Tataryn acknowledges financial support of the Deutscher Akademischer Austauschdienst (Leonhard-Euler program).

References

- [1] D. Savytskii, U. Bismayer, "Strains at junctions in multidomain configurations", *Phase Transi.* **81** (2008) 431–447.

XAFS AND X-RAY DIFFRACTION STUDY OF THE CUBIC PHASE OF $\text{Ni}_3\text{B}_7\text{O}_{13}\text{Br}$

V.A. Shuvaeva^{1*}, **Y.V. Zubavichus**², **A.A. Chernyshov**², and **K.A. Lyssenko**³

¹ *Institute of Physics, Southern Federal University, 194, Stachki Str, Rostov-on-Don, 344090, Russia*

² *RRC "Kurchatov Institute", KCSRNT, Kurchatov sq. 1, 123182, Moscow, Russia*

³ *Institute of Organoelement Compounds, Russian Academy of Sciences, 28 Vavilov Str., B-334, Moscow, Russia*

Keywords: boracite, XAFS, diffraction, structure, disorder, phase transition, ferroelectric

*) e-mail: v_shuvaeva@mail.ru

Application of advanced experimental methods using synchrotron radiation makes it possible to resolve many long-standing challenging problems. One of such problems is the atomic structure of the cubic paraelectric phase of compounds belonging to the family of boracites (general formula $\text{Me}_3\text{B}_7\text{O}_{13}\text{X}$, where M is one of the divalent metals Mg, Cr, Mn, Fe, Co, Ni, Cu, Zn or Cd, and X is a halogen Cl, Br, or I). Nearly all boracites undergo phase transitions to lower symmetry ferroelectric phases. The structures of most of known phases of boracites have been carefully studied using X-ray diffraction. As a result of the studies several alternative structural models of the paraelectric phase were proposed. Models assuming disorder of both halogen and metal atoms were intensively discussed along with generally accepted ideal cubic structure [1,2], however no clear evidences in favor of any of the proposed models were obtained. Application of X-ray absorption spectroscopy (XAS) allows to clearly reveal a disorder in this case, since the difference of metal-halogen distances in the alternative models is about 0.3 Å. By combining spectroscopic data with diffraction, a comprehensive model of atomic arrangements can be worked out. However only one boracite compound, namely $\text{Fe}_3\text{B}_7\text{O}_{13}\text{Br}$ has been studied so far by XAFS [3].

We studied the local environment around Br ion in the cubic phase of $\text{Ni}_3\text{B}_7\text{O}_{13}\text{Br}$ at the temperature of about 200° C using XAFS technique. The experiment was performed at the K1.3b station of synchrotron radiation source "Siberia-2" at Kurchatov Institute (Moscow). Spectra were collected in transmission mode at Br K -edge.

The Fourier transform of Br K-XAFS of the cubic phase is shown in the Fig. 1 together with the one obtained for the orthorhombic ferroelectric phase of the compound. It can be clearly seen that the phase transition from ferroelectric to the paraelectric phase does not result in any significant change of the shortest Br-Fe distance, which was found to be 2.61 Å for the ferroelectric phase and 2.63 Å for the cubic paraelectric one.

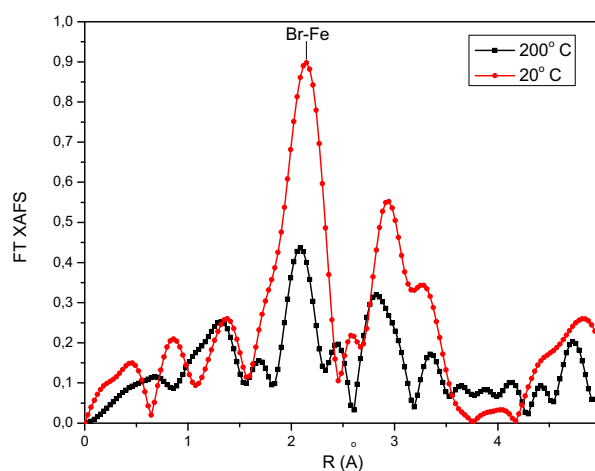


Figure 1. The Fourier transform of Br K-XAFS of $\text{Ni}_3\text{B}_7\text{O}_{13}\text{Br}$ measured at 20° and 200°C.

These results were incorporated into refinement of the structure of the cubic phase of the compound basing on the X-ray diffraction data, obtained from a single-crystalline sample. The study showed that only the model assuming disorder of both Fe and Br positions is in agreement with the data of both XAFS and X-ray diffraction. Besides the distribution of Br-Fe distances obtained from XAFS suggests a strong correlation of Fe and Br displacements in the cubic phase.

Thus a solid proof has been obtained that ferroelectric-to-paraelectric phase transition in $\text{Ni}_3\text{B}_7\text{O}_{13}\text{Br}$ boracite has an essential order-disorder component.

References

- [1] P. Felix, M. Lambert, R. Comes, H. Schmid, *Ferroelectrics* **7** (1974) 131–133.
- [2] D.J. Lockwood, *Ferroelectrics* **36** (1981) 443–446.
- [3] T.I. Nedoseykina, V.A. Shuvaeva, I.V. Pirog, A.T. Shuvaev, K. Yagi, Y. Azuma, H. Terauchi, *Ferroelectrics* **284** (2003) 175–184.

EXAFS AND XMCD INVESTIGATIONS ON THE Mn⁺ IMPLANTED SILICON CRYSTALS

A. Wolska^{1*}, **M.T. Klepka**¹, **K. Lawniczak-Jablonska**¹, **D. Arvanitis**², and **A. Misiuk**³

¹ *Institute of Physics PAS, al. Lotników 32/46, 02-668, Warsaw, Poland*

² *Physics Department, Uppsala University, Box 530, 75121 Uppsala, Sweden*

³ *Institute of Electron Technology, Al. Lotnikow 46, 02-668 Warsaw, Poland*

Keywords: EXAFS, XMCD, implantation, silicon

**) e-mail: wolska@ifpan.edu.pl*

Semiconductor devices using the spin of electrons have attracted much attention because of their expected applications in spintronics. The key to the spintronic's success is availability of suitable materials for device manufacturing. Diluted magnetic semiconductors (DMS) have been shown to be the best materials for such purpose. Usually, the Mn-doped III-V and II-VI compounds forming DMS have been in the center of attention. However, there is another interesting class of materials, namely the Si-based DMS. Among them, silicon implanted with Mn ions seems to be a promising combination. The implantation of Mn⁺ ions into a silicon matrix is a good way of exceeding the solubility limit of Mn in Si. Moreover, it has been already shown that the Mn-implanted Si samples can be ferromagnetic with a Curie temperature (T_C) higher than 400 K [1]. On the other hand, the ferromagnetic properties were also reported for silicon samples implanted with non-magnetic ions, *e.g.* Si. Therefore, it is important to find out the origin of the magnetic properties in this kind of materials.

A direct way to check whether the magnetism is related with the Mn atom cores is to perform core level X-ray magnetic circular dichroism (XMCD) studies, which allow to detect the local magnetic moments for the specific element what is not possible in the superconducting quantum interference device (SQUID) measurements.

The samples were prepared by Mn⁺ implantation into silicon wafers grown by Czochralski method (Cz-Si) or by floating zone method (Fz-Si). The energy of Mn⁺ ions was of 160 keV and a dose of 1×10^{16} cm⁻². The implanted samples were subsequently annealed at temperatures from 275°C to 1000°C under pressures of 1 bar or 11 kbar. The SQUID measurements showed that samples after low temperature annealing (up to 450°C) exhibited ferromagnetic properties [2].

The Extended X-Ray Absorption Fine Structure (EXAFS) measurements, as an element specific method, provides information about the local atomic structure around the chosen element, Mn in this case, and enables to monitor the results of the annealing.

The EXAFS measurements at the Mn K-edge were carried out at Hasylyab (A1 and E4 stations) using a seven element silicon fluorescence detector. The samples were

cooled to liquid nitrogen temperature in order to minimize thermal disorder.

The XMCD spectra at the Mn L_{3,2}-edges were measured at MAX-lab (beamline I-1011). The measurements were carried out at room (RT ~300 K) and liquid nitrogen (LN ~100 K) temperatures under an applied magnetic field of 0.1 T, along the x-ray path. The total electron yield detection mode was used. Two angles of incidence were chosen as follows: grazing (20° to the sample surface) and normal (90° to the surface).

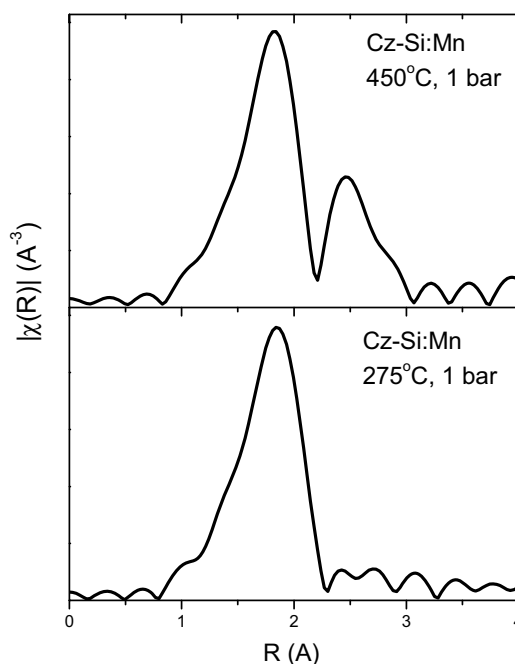


Figure 1. Magnitude of the Fourier Transform of the EXAFS spectra of the Cz-Si:Mn samples annealed at 275°C and 450°C (1 bar).

The local structure around the Mn atoms, as found out by the EXAFS analysis at the K-edge of Mn, exhibits the differences between the samples prepared by both methods and annealed at 275°C. In the case of Fz-Si:Mn sample, the Mn atoms gather together forming nanoinclusions consisting of a Mn_xSi_y compound [3]. In

the case of Cz-Si:Mn annealed at low temperature, the EXAFS analysis showed only silicon neighbors. [4]

Figure 1 presents the Fourier Transformed EXAFS oscillations of the Cz-Si:Mn samples annealed at 275°C and 450°C (1 bar). It is easily seen, that the local crystallographic environment of the Mn atoms, depends on the heat treatment. For the sample annealed at 275°C, only the nearest neighbor shell is visible. In the case of the Cz-Si:Mn sample annealed at 450°C, a second neighbor shell appears, a fact which suggests that the crystallization of the inclusions already starts. For the Fz-Si:Mn sample, only the first shell can be distinguished for both annealing temperatures (Fig. 2). It seems that the temperature of the inclusions formation process depends on the method of the sample growth.

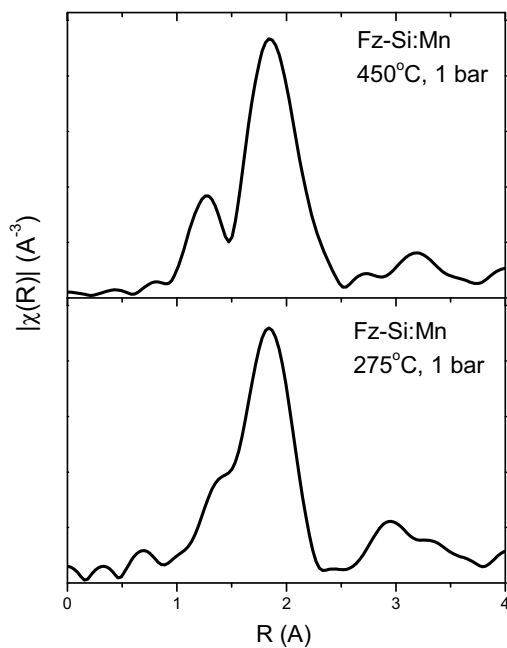


Figure 2. Magnitude of the Fourier Transform of the EXAFS spectra of the Fz-Si:Mn samples annealed at 275°C and 450°C (1 bar).

The XMCD measurements are presented in Fig. 3. A dichroic signal is not found for the considered Si:Mn samples. It seems that the Mn atom cores are not the main source of ferromagnetism in these samples. It is possible that ferromagnetism in these samples is mainly induced by the defects in the matrix caused by the ion implantation. This conclusion is supported by the fact that the high temperature treatment leading to recrystallization of the matrix seems to eliminate the ferromagnetic response in the investigated samples.

Acknowledgments: The research leading to these results has received funding from the European Community under Contract RII3-CT-2004-506008 (IA-SFS) and the European Community's Seventh Framework Programme (FP7/2007-2013) under grant agreement n° 226716.

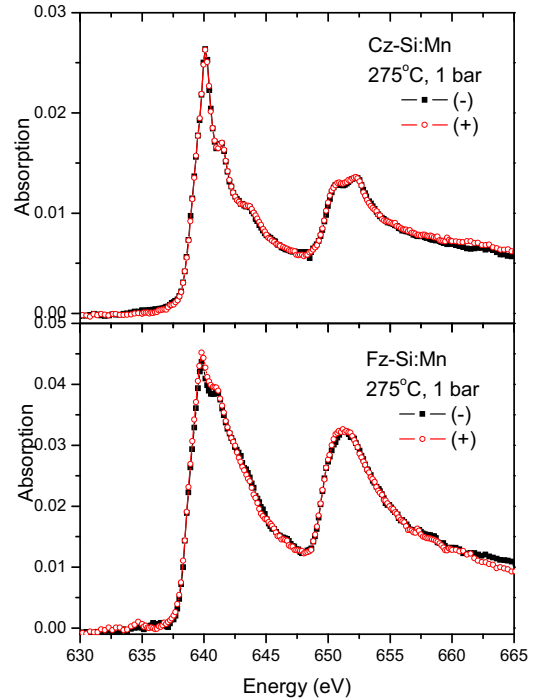


Figure 3. XANES spectra of Mn $L_{3,2}$ edges for Cz-Si:Mn and Fz-Si:Mn samples annealed at 275°C. Measurements were performed at normal incidence at RT by inverting the magnetic field direction.

References

- [1] M. Bolduc, C. Awo-Affouda, A. Stollenwerk, M.B. Huang, F.G. Ramos, G. Agnello, V.P. LaBella, "Above room temperature ferromagnetism in Mn-ion implanted Si", *Phys. Rev. B* **71** (2005) 033302.
- [2] A. Misiuk, J. Bak-Misiuk, B. Surma, W. Osinniy, M. Szot, T. Story, J. Jagielski, "Structure and magnetic properties of Si:Mn annealed under enhanced hydrostatic pressure", *J. Alloys Compds.* **423** (2006) 201–204.
- [3] A. Wolska, K. Lawniczak-Jablonska, M.T. Klepka, M.S. Walczak, A. Misiuk, "Local structure around Mn atoms in Si crystals implanted with Mn^{+} studied using x-ray absorption spectroscopy techniques", *Phys. Rev. B* **75** (2007) 113201.
- [4] A. Wolska, K. Lawniczak-Jablonska, S. Kret, P. Dłużewski, A. Szczepańska, M.T. Klepka, M.S. Walczak, Y. Lefrais, M.J. Hýtch, A. Misiuk, "Atomic order in magnetic inclusion of Mn in Si crystal: XAS and TEM studies", *J. Non-Cryst. Solids* **354** (2008) 4189–4192.

ANOTHER APPROACH TO THE Mn ION IMPLANTATION INTO THE GaSb CRYSTALS

A. Wolska^{1*}, K. Lawniczak-Jablonska¹, M.T. Klepka¹, M. Kulik², and R. Jakiela¹

¹*Institute of Physics PAS, al. Lotników 32/46, 02-668 Warsaw, Poland*

²*Institute of Physics, University Maria Curie-Skłodowska, Pl. Marii Curie Skłodowskiej 1, 20-031 Lublin, Poland*

Keywords: XAFS, implantation, GaSb

*) *e-mail: wolska@ifpan.edu.pl*

The quest for materials ferromagnetic at room temperature that can be used for spintronic applications is still going on. Different compounds obtained with different methods are investigated. One of the most popular materials is GaMnAs. It has been examined in the form of the uniform ternary alloys as well as the material containing precipitations of ferromagnetic MnAs. The interest in precipitations opened the way for the implantation methods. Different types of magnetic inclusions (Ga_xMn_y , MnAs hexagonal and GaMnAs cubic) were formed in the GaAs crystals depending on the applied Mn ion energy, dose and post implantation annealing procedures [1,2]. On the other hand, also MnSb inclusions show promising magnetic properties at room temperature. It is possible to obtain such inclusions during the MBE growth but the implantation method is cheaper and easier to carry out within the industrial production process. Therefore, it would be important to find an optimal way of producing the MnSb inclusions with the desirable properties by Mn ions implantation as it has been done in the MnAs case.

Unfortunately, the recipe for the formation of the MnSb inclusions in the GaSb substrates during Mn ion implantation is not simple. Implantation tends to remove Sb atoms from the Mn atoms' neighborhood and the Mn atoms prefer to bond to Ga or O atoms [3]. Therefore, processes with more steps should be investigated in order to establish the proper procedures.

The samples were prepared by co-implantation of the Ne^+ , He^+ , Mn^+ and Sb^+ ions into the GaSb(100) crystals. The He^+ and Ne^+ ions were used to make the matrix disordered in order to prevent the escape of Sb atoms. The substrates' temperature during the implantation processes was kept at 80 K. Four series of implantation were prepared:

1. *NeMn* where the substrate was implanted with Ne^+ ions (250 keV, dose $5 \times 10^{16} \text{ cm}^{-2}$) first and then with Mn^+ ions (150 keV, dose $9 \times 10^{14} \text{ cm}^{-2}$).
2. *NeMnSb* where after the procedure described above the Sb^+ ions (250 keV, dose $9 \times 10^{14} \text{ cm}^{-2}$) were added.
3. *HeMn* where the substrate was implanted with He^+ ions (80 keV, dose $5 \times 10^{13} \text{ cm}^{-2}$) first and then with Mn^+ ions (150 keV, dose $9 \times 10^{14} \text{ cm}^{-2}$).
4. *HeMnSb* where after the procedure described above the Sb^+ ions (250 keV, dose $9 \times 10^{14} \text{ cm}^{-2}$) were added.

The energy and doses of Mn and Sb ions were chosen according to the depth profile ion distribution simulated by code SRIM2008 [4,5] in order to locate the Mn and Sb ions in the distance from 50 to 150 nm from the surface. The implantation of noble gases was not supposed to influence the GaSb matrix density.

Each of the implanted samples was subsequently divided in three parts. One part was left as such, the second part was subject to rapid thermal annealing for 5 min. in the Ar atmosphere at the temperature 350°C and the third one at 400°C.

The X-ray Absorption Near Edge Structure (XANES) and Extended X-ray Absorption Fine Structure (EXAFS) measurements at the Mn K-edge were carried out at Hasylab (A1 station) in fluorescence mode using a silicon drift detector. The samples were cooled to liquid nitrogen temperature in order to minimize thermal disorder. In order to check the distribution of the atoms in the crystals, the Secondary Ion Mass Spectroscopy (SIMS) measurements using a CAMECA IMS6F micro-analyzer were also carried out.

Figure 1 presents the XANES spectra of the samples annealed at 350°C compared with the MnSb standard spectrum. The shapes of the spectra of the investigated samples are quite similar to each other. However, the possibility of MnSb formation has to be excluded since they are significantly different from the MnSb spectrum.

More specific information about the local neighborhood of the Mn atoms can be obtained from the EXAFS analysis. As can be seen in Figure 2, the Mn neighborhood is rather amorphous, only the first shell consisting of oxygen atoms is formed. The MnO standard spectrum is shown for comparison.

The distribution of the elements in the *NeMnSb* sample annealed at 350°C measured by SIMS is presented in Figure 3. SIMS data confirm that high amount of oxygen was introduced during the procedure and, as it was shown above, this resulted in formation of Mn oxides.

Concluding, it seems like the implantation into the cold and amorphous substrate prevented the Sb atoms from escaping but still the oxygen atoms were incorporated deeply into the matrix and the Mn oxides were formed.

Acknowledgements: This work was partially supported by national grant of Ministry of Science and High Education N202-052-32/1189. The research leading to these results has received funding from the European Community's Seventh Framework Programme (FP7/2007-2013) under grant agreement n° 226716.

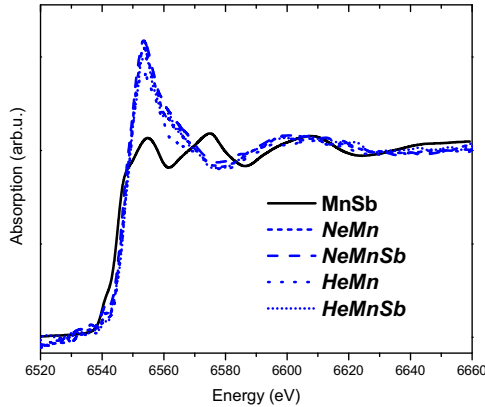


Figure 1. XANES of the samples annealed at 350°C compared with MnSb standard spectrum.

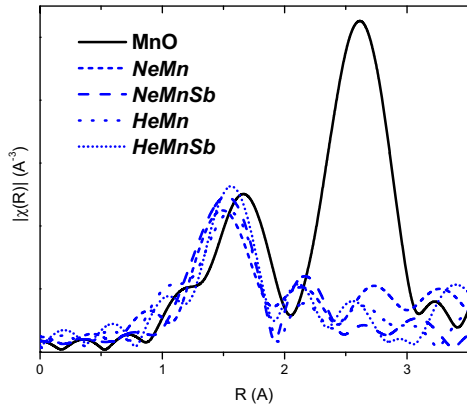


Figure 2. Magnitude of Fourier transform of the EXAFS spectra of the samples annealed at 350°C compared with the MnO standard.

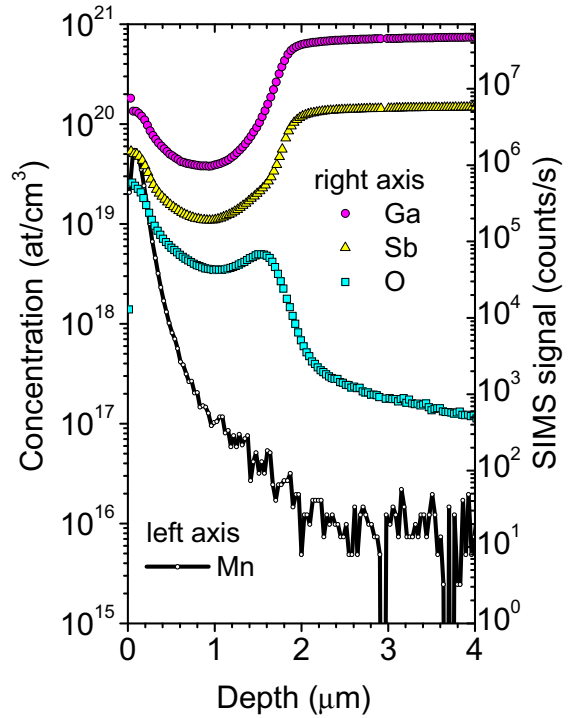


Figure 3. SIMS depth profiles of the element distribution in the *NeMnSb* sample annealed at 350°C.

References

- [1] C. Chen, M. Cai, X. Wang, S. Xu, M. Zhang, X. Ding, Y. Sun, "Ferromagnetic properties and structures of the Mn-implanted GaAs semiconductor", *J. Appl. Phys.* **87** (2000) 5636–5638.
- [2] S.-L. Songa, N.-F. Chen, J.-P. Zhou, Z.-G. Yin, Y.-L. Li, S.-Y. Yang, Z.-K. Liu, "Mn implanted GaAs by low energy ion beam deposition", *J. Cryst. Growth* **264** (2004) 31–35.
- [3] A. Wolska, K. Lawniczak-Jablonska, M.T. Klepka, A. Barcz, A. Hallen, D. Arvanitis, "Study of the local environment of Mn ions implanted in GaSb", *Acta Phys. Polon. A* **117** (2010) 286–292.
- [4] J.F. Ziegler, J.P. Biersack, U. Litmar, *The Stopping and Range of ions in Solid*, (Pergamon Press, New York, Oxford, Toronto Sydney, Frankfurt Tokyo 1985).
- [5] J.F. Ziegler, J.P. Biersack, D.M. Ziegler, *SRIM The stopping and range of ions in solid*, (SRIM Co. 2835 Cox Nec Rd. Chester, Maryland, 21619 U.S.A.).

EXAFS INVESTIGATIONS ON NOVEL LAVES PHASE HYDRIDES

M.T. Klepka^{1*}, **A. Wolska**¹, **K. Lawniczak-Jablonska**¹, **S. Filipek**², and **R. Sato**²

¹*Institute of Physics, PAS, al. Lotnikow 32/46, PL-02668 Warsaw, Poland*

²*Institute of Physical Chemistry, PAS, ul. Kasprzaka 44/52, PL-01224 Warsaw, Poland*

Keywords: EXAFS, Laves phase, hydrides

**) e-mail: mklepka@ifpan.edu.pl*

The Laves phases are interesting materials for future hydrogen energy development. They represent a group of intermetallic compounds that, besides of very interesting physical and chemical properties, are considered as important hydrogen storage materials. Generally, they are stable for a long time at normal conditions [1]. Recently a number of novel hydrides/deuterides materials were synthesized by treating various Laves compounds under high hydrogen/deuterium pressure. The most interesting is the group of YMn_2D_6 complex deuterides doped with Cr or Fe.

Although their properties were intensively investigated, the position of Mn and Cr/Fe atoms in the crystal structure and electronic structure of these compounds is not completely clear yet.

Submitting YMn_2 to high hydrogen pressure leads to the formation of a novel, unique YMn_2D_6 deuteride with $Fm-3m$ symmetry (see Fig. 1) [2]. The YMn_2D_6 was synthesized for the first time by submitting YMn_2 to deuterium at 1.7 kbar pressure at 473 K. According to X-ray (XRD) and Neutron Powder Diffraction (NPD) experiments, YMn_2D_6 crystallizes in the K_2PtCl_6 – type cubic structure with $a = 6.709(1)$ Å at 300 K. The Y and half of the Mn atoms occupy the $8c$ site whereas the

other Mn atoms are located in $4a$ site and are surrounded by 6 D atoms ($24e$). The Mn($4a$)-D distances are around 1.65 Å [2].

Investigated materials were synthesized at the Institute of Physical Chemistry PAS in Warsaw in collaboration with French and Taiwanese Partners. Among obtained materials especially interesting is the group of YMn_2D_6 complex deuterides additionally doped with Cr or Fe atoms.

Despite large number of reports about properties of Laves hydrides, there is not much reported about structural changes under high pressure especially local atomic structure around Cr or Fe dopants.

The X-ray Absorption Spectroscopy (XAS) offers unique possibility to localize the position of atoms inside the crystal structure and to estimate the chemical bonding of elements as well as changes introduced by different treatments. Therefore, it is an ideal tool for study these novel hydrides of Laves phase.

EXAFS measurements of Mn, Cr and Fe K edge were performed at HasyLab at E4 station. Transmission and fluorescence modes of detection at LN temperature were used. Samples were powders and were prepared under Ar atmosphere in order to avoid oxidation.

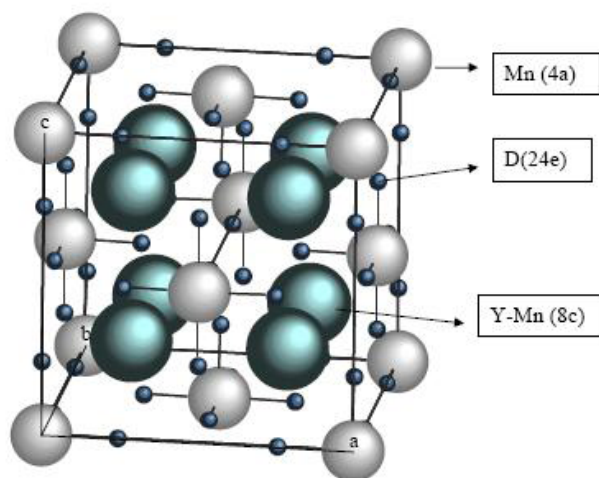


Figure 1. Crystal structure of YMn_2D_6 in $Fm-3m$ space group.

EXAFS data analysis confirmed change of YMn_2 crystal structure after deuteration (see Fig. 2). Moreover, two equivalent positions of Mn atoms in YMn_2D_6 were also identified [Mn (0, 0, 0) and Mn ($\frac{1}{4}$, $\frac{1}{4}$, $\frac{1}{4}$)].

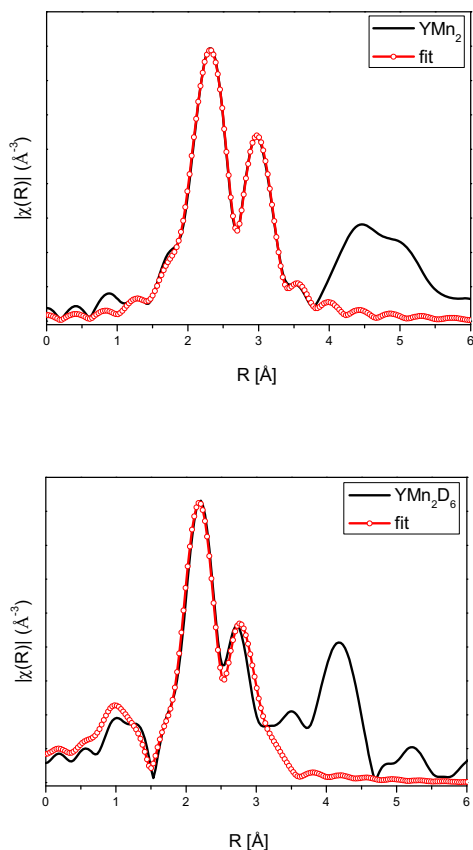


Figure 2. Fourier transformed experimental EXAFS spectra, for Mn K-edge, together with fitting result for YMn_2 and YMn_2D_6 .

Furthermore, Mn K edge investigation indicated that addition of Cr atoms up to 10% did not change distribution of Mn between two equivalent positions in the lattice. However, when 20% of Cr atoms is incorporated then 90% of Mn were found in the ($\frac{1}{4}$, $\frac{1}{4}$, $\frac{1}{4}$) position (see Fig. 3).

Acknowledgments: The study was supported by Polish Science Foundation as a common investigation of scientific network "New

materials – production and structure investigation" and the European Community under Contract RII3-CT-2004-506008 (IA-SFS).

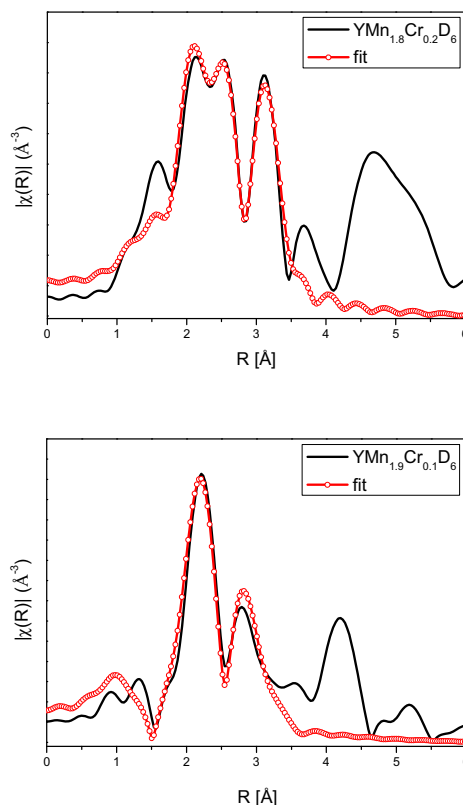


Figure 3. Fourier transformed experimental EXAFS spectra, for Mn K-edge, together with fitting result for $\text{YMn}_{1.8}\text{Cr}_{0.2}\text{D}_6$ and $\text{YMn}_{1.9}\text{Cr}_{0.1}\text{D}_6$.

References

- [1] S.M. Filipek, V. Paul-Boncour, A. Percheron Guegan, I. Jacob, I. Marchuk, M. Dorogova, T. Hirata, Z. Kaszukur, "Synthesis of novel deuterides in several laves phases by using high pressure of gaseous deuterium", *J. Phys. Cond.Matter*, **14** (2002) 11261–11264.
- [2] V. Paul-Boncour, S.M. Filipek, M. Dorogova, F. Bourée, G. André, I. Marchuk, A. Percheron-Guégan, R.S. Liu, "Neutron diffraction study, magnetic properties and thermal stability of YMn_2D_6 synthesized under high deuterium pressure", *J. Sol. State Chem.* **178** (2005) 356–362.

LUMINESCENCE FROM ADENINE IN ARGON MATRICES AT 12 K

K. Polewski^{1*}, **J. Trunk**², and **J.C. Sutherland**²

¹ Dept. of Physics, Life Sciences University, 60-637 Poznan, Poland

² Biology Dept., Brookhaven National Laboratory, Upton, NY 11973, USA

Keywords: adenine, fluorescence, matrix isolation, fluorescence lifetimes

**) e-mail: polewski@up.poznan.pl*

Matrix isolation technique offers a certain advantages compared to the other methods. In a dilute gas matrix each solute is completely surrounded with inert, non-polar hosts, usually argon or nitrogen molecules. Besides minimizing the host-solute interactions, the hosts are transparent to UV radiation (up to 170 nm for N₂) and free of fluorescent impurities.

The synchrotron light from U9B station at National Synchrotron Light Source at Brookhaven National Laboratory has been used to excite adenine embedded into low temperature argon matrix. Measured absorption spectrum is similar to those reported in the other environment with two exceptions: the higher energy part of the spectrum shows much higher intensity than previously reported and weak apparent absorption peak with maximum at 280 nm is present.

Fluorescence spectra recorded at four different excitations show the similarity in peak position and shape of the spectra.

Fluorescence excitation spectra revealed five well resolved peaks which correspond to the features resolved in the absorption spectrum, however with much better resolution.

The obtained fluorescence lifetimes calculated for different excitations were fitted with a double exponential decay with a shorter lifetime between 1.7 and 3.3 ns and longer component with lifetime varying from 15 to 23 ns. At the excitation at 180 nm, monoexponential fit with lifetime of 3.3 ns was required.

It has been also shown that deactivation processes in adenine depend on excitation energy. Excitation at 267 nm and 285 nm, besides fluorescence, produced electronically excited triplet, with a very characteristic structured phosphorescence spectrum.

Matrix isolation technique used with synchrotron radiation from UV range offers insight into photophysical processes, unperturbed by environment, occurring in biologically important molecule of adenine.

MULTI-MODAL X-RAY FLUORESCENCE DETECTION AT THE ID21 X-RAY MICROSCOPY BEAMLINE

J. Szlachetko^{1,2*}, **M. Cotte**^{1,3}, **J. Morse**¹, **M. Salome**¹, and **J. Susini**¹

¹ *European Synchrotron Radiation Facility, Grenoble, France*

² *Institute of Physics, Jan Kochanowski University, Kielce, Poland*

³ *Centre of Research and Restoration of French Museums, UMR171, Paris, France*

Keywords: wavelength-dispersive spectroscopy, micro-fluorescence, x-ray imaging, microscopy, beamline

*) jakub.szlachetko@esrf.fr

The ID21 ESRF beamline is dedicated to micro-X-ray fluorescence (μ XRF) and micro X-ray absorption spectroscopy (μ -XANES) in the X-ray energy domain between 2 keV and 7 keV [1]. The scanning x-ray microscope enables the localization and speciation of trace elements down to the ppm range with a submicrometer beam size. It provides access to the absorption edges of a wide range of elements of interest in the areas of Environmental Sciences, Earth and Planetary Sciences, Life Sciences and Cultural Heritage. Recently, several developments in the field of x-ray detection have been made to enlarge the measurement possibilities available at the beamline and to improve the detection limits for x-ray fluorescence.

The scanning X-ray microscope (SXM) of ID21 was completely refurbished in 2008. It is now a highly versatile instrument in terms of focusing optics, detectors, and sample environment [2]. The X-ray beam spot size ranges from ~ 20 μ m (obtained with a polycapillary optics) to ~ 500 nm (obtained with focusing zone plates or a Kirk-Patrick Baez mirror system). The SXM employs several detectors, which are complementary in terms of count-rate throughput, solid-angle collection efficiency and spectral resolution. For experiments demanding high sensitivity, a single- or a seven-element Ge detector provide large fluorescence detection solid angle, absence of detector K-escape peak contributions, and detector peak-to-valley ratio >5 k. For the case of highly concentrated samples, or for samples where the matrix signal dominates the fluorescence signal, either 30 mm² or 100 mm² silicon drift diode (SDD) detectors can be used at count rates approaching 1 Mcps. Finally, in order to resolve overlapping or

closely spaced fluorescence lines, a polycapillary optic based, scanning wavelength-dispersive spectrometer (WDS) has been developed [3]. In many applications the WDS makes possible detailed elemental and chemical analyses that are simply not accessible with the lower resolution solid state detectors.

We present the operational characteristics, the construction details and the performance achieved with the detectors of ID21. In particular the throughput count rates, spectral resolutions and achievable detection limits are compared. We describe the application of different detection systems for two-dimensional elemental mapping and micro-XANES analysis. The x-ray fluorescence spectra obtained are compared to theoretical simulations and discussed in terms of absorption, re-absorption and scattering phenomena.

References

- [1] J. Susini, M. Salome, B. Fayard, R. Ortega, B. Kaulich, "The Scanning X-ray Microprobe at the ESRF x-ray microscopy beamline", *Surf. Rev. Lett.* **9** (2002) 203–211.
- [2] M. Salome, P. Bleuet, S. Bohic, J. Cauzid, E. Chalmin, P. Cloetens, M. Cotte, V. De Andrade, G. Martinez-Criado, S. Petitgirard, M. Rak, J.A. Sans Tresserras, J. Szlachetko, R. Tucoulou, J. Susini, J. "Fluorescence X-ray micro-spectroscopy activities at ESRF", *J. Phys.* **186** (2009) 012014.
- [3] J. Szlachetko, M. Cotte, J. Morse, J. Susini, P. Jagodzinski, J.-Cl. Dousse, J. Hozzowska, Y. Kayser, J. Susini, "Wavelength-dispersive spectrometer for X-ray microfluorescence analysis at the X-ray microscopy beamline ID21 (ESRF)", *J. Synchrotr. Rad.* **17** (2010) 400–408.

LIFETIME BROADENING-FREE L₃ X-RAY ABSORPTION SPECTRUM OF Xe MEASURED BY X-RAY RESONANT INELASTIC SCATTERING

J. Szlachetko^{1,2*}, **M. Kavčič**³, **M. Žitnik**³, and **K. Bučar**³

¹ European Synchrotron Radiation Facility, Grenoble, France

² Institute of Physics, Jan Kochanowski University, Kielce, Poland

³ J. Stefan Institute, Jamova 39, SI-1000, Ljubljana, Slovenia

Keywords: high-resolution spectroscopy, x-ray resonant inelastic scattering, beamline

*) jakub.szlachetko@esrf.fr

The one of the most useful tools for studying the density of unoccupied electronic states of an atom is the x-ray absorption near edge structure (XANES) technique. However, in many cases the resolution of the XANES spectroscopy is limited by the natural broadening originating from the lifetime of atomic states. The x-ray resonant inelastic scattering (RIXS) represents an alternative technique to probe both occupied and unoccupied electronic states of an atom. The RIXS is a photon-in photon-out second order process and therefore is characterized by low scattering probabilities. However, the energy widths of the RIXS spectra depend only on the experimental resolution and not on the natural width of the initial core-hole state. For this reason, the RIXS spectroscopy reveal much more details and features that could not be observed by means x-ray absorption spectroscopy [1,2].

Nowadays, the third generation synchrotron light source combined with modern focusing type crystal spectrometer exhibits sufficient experimental energy resolution and efficiency needed to record high quality RIXS spectra well below the absorption edge thus

yielding the possibility to extract the absorption spectrum with the subnatural line width resolution. For this work, a Johansson type crystal spectrometer of J. Stefan Institute was coupled to the ID26 beamline of the ESRF synchrotron. We have recorded the L₃-N_{4,5} RIXS spectrum of Xe well below the L₃ absorption edge (4770 eV) with relatively small statistical uncertainty. The overall energy resolution was ~1 eV which is below the width given by the Xe L₃ hole lifetime (2.82 eV). The data analysis based on the Kramers-Heisenberg approach was employed to deduce the Xe L₃ absorption edge with the subnatural energy resolution from the measured RIXS spectrum. Energy positions and relative emission rates $f\theta$ if for $[2p_{3/2}]nl$ inner-hole excited states are extracted and compared to the calculated values.

References

- [1] H. Hayashi *et al.*, *Chem. Phys. Lett.* **371** (2003) 125-130.
 [2] H. Hayashi *et al.*, *Anal. Sci.* **24** (2008) 15-23.

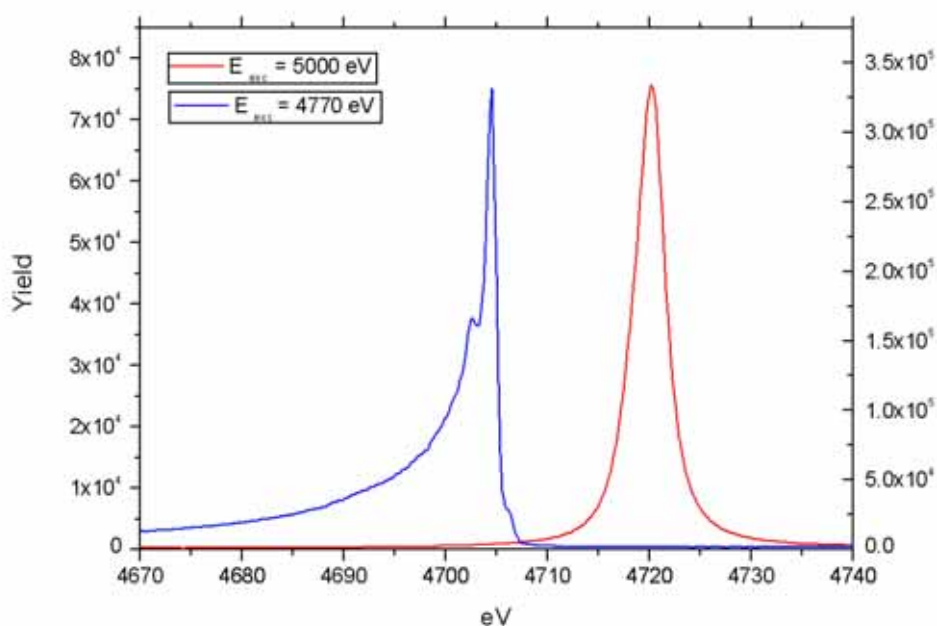


Figure 1. High resolution Xe L₃-N_{4,5} x-ray emission line excited above (5000 eV) and below (4770 eV) the L₃ absorption edge.

EXAFS AND XRD STRUCTURE ANALYSIS OF ZnO NANOCCLUSERS FORMED VIA SELECTIVE OXYGENATION OF ORGANOZINC COMPOUNDS

B. Mierzwa¹, K. Zelga², W. Bury², K. Sokołowski², J. Lewiński^{1,2},
R. Nietubyć³, and Z. Kaszukur^{1*}

¹ Institute of Physical Chemistry Polish Academy of Sciences, 44/52, Kasprzaka, 01-224 Warszawa, Poland

² Faculty of Chemistry Warsaw University of Technology, 3, Noakowskiego, 00-664 Warszawa, Poland

³ Andrzej Soltan Institute for Nuclear Studies, 05-400 Świerk/Otwock, Poland

Keywords: nanocrystals, ZnO, powder diffraction, EXAFS

*) e-mail: zbig@ichf.edu.pl

Sample of nanocrystalline ZnO was obtained from crystalline organo-zinc compound of chemical formula $C_{34}H_{62}N_2O_{12}Zn_3$ crystalizing in monoclinic crystal structure in $P1_21/c1$ space group and lattice parameters $a = 15.652 \text{ \AA}$, $b = 13.973 \text{ \AA}$, $c = 21.833 \text{ \AA}$ and angle $\beta = 114.031^\circ$. The cell view is presented in fig.1. The crystals were ground in nitrogen atmosphere what led to decomposition of crystal structure and formation of ZnO wurtzite nanocrystals of size estimated via Scherrer formula as $\sim 2.5 \text{ nm}$. ZnO nanocrystals in literature were observed in the form of nanorods, nanowires, nanoribbons and $\sim 50 \text{ nm}$ size hollow nanospheres [1,2].

The sample was studied by powder X-ray Diffraction and EXAFS techniques. The results do not fit with regular ZnO crystallite model of certain shape but rather point to models with reduced number of neighbour atoms for small value of neighbour distance (see model 1 and 2 and Figs. 2 and 3 for coordination numbers) as for hollow crystallites.

The EXAFS analysis proved to be capable to distinguish between two models by correct estimation of coordination number (Fig. 3) falling down for the model 2 (hollow) to 50-60% of that of the regular crystallite. The models considered in analysis comprised stack of hexagonal wurtzite structure (space group $P6_3mc$) grown

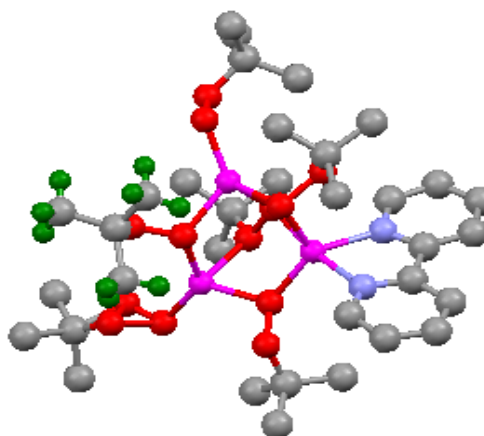


Figure 1. Unit cell view of the crystal serving as a precursor to the studied nanocrystalline sample. Atom colors: Zn atoms- magenta, O in red, C in grey, N in light blue and part of H atoms in green.

in [001] direction of about 2.5nm size (model 1) and the same size crystallite hollowed out (with empty interior) (model 2). The models for illustrative purpose cut by half are presented below (Fig. 4).

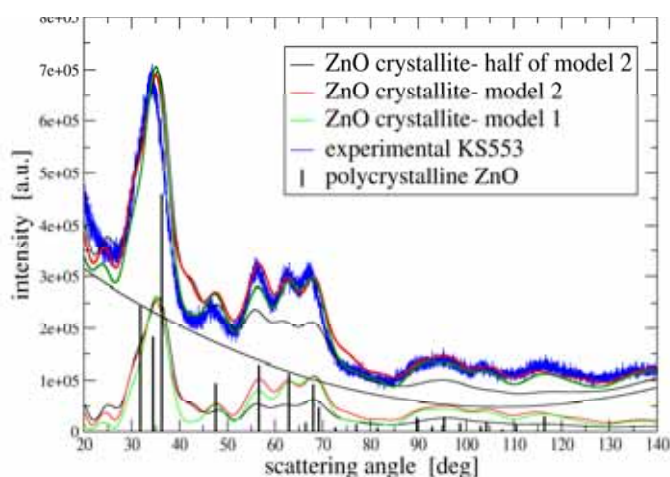


Figure 2. XRD pattern of the nanocrystalline ZnO sample compared to diffractograms of models

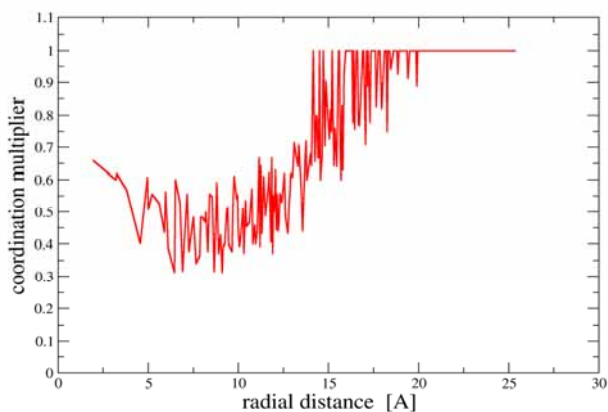
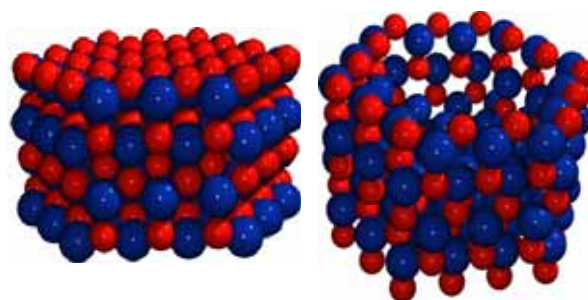


Figure 3. Ratio of Radial Distribution Function (RDF) of model 2 to that of model 1.

The number of neighbours at a distance comparable to the crystallite size is equal for both models. At smaller distances the number of neighbour atoms is for model 2 significantly reduced in comparison to model 1.

Although concluding about the nanocrystal typical morphology can be difficult on the basis of XRD alone, complementing it with EXAFS data may strengthen the conclusions combining arguments based on different physical phenomena.



Half of the model 1: a regular fragment of ZnO lattice. Zn- blue, O- red. Half of the model 2: a crystallite with empty interior.

Figure 4.

References

- [1] Z. Chen, L. Gao, "A new route toward zno hollow spheres by a base-erosion mechanism", *Cryst. Growth Design* **8** (2008) 460–464.
- [2] Z. Fan, J.G. Lu, "Zinc oxide nanostructures: synthesis and properties", *J. Nanosci. Nanotechnol.*; **5** (2005) 1561–1673.

HIGH-PRESSURE DIFFRACTION STUDY OF SmVO₄: COMPRESSIBILITY AND ZIRCON-SCHEELITE PHASE TRANSITION

W. Paszkowicz¹, **P. Piszora**², **Y. Cerenius**³, **S. Carlson**³,
B. Bojanowski⁴, and **H. Dąbkowska**⁵

¹ *Institute of Physics, PAS, Warsaw, Poland*

² *Faculty of Chemistry, A. Mickiewicz University, Poznań, Poland*

³ *MAXlab, Lund University, Lund, Sweden*

⁴ *Institute of Physics, Szczecin University of Technology, Szczecin, Poland*

⁵ *Department of Physics, McMaster University, Hamilton, Ontario, Canada*

Keywords: samarium, orthovanadate, pressure, bulk modulus, phase transition

**) e-mail: paszk@ifpan.edu.pl*

SmVO₄ is considered as a catalytic material suitable for oxidative dehydrogenation of butane [1] and propane [2]. It belongs to the family of RVO₄, (R = Y, Sc, Pr – Lu) orthovanadates, of wakefieldite mineral name, crystallizing in *I4₁/amd* space group. Some of compounds of this family are considered as being suitable for optical waveguides and polarizers, they can be used for remote thermometry, as laser components, as catalysts for oxidative dehydrogenation and are candidates for advanced bio-imaging phosphors and as components of toughened ceramic composites. In this work the elastic properties and structural changes under pressure of SmVO₄ are determined experimentally and compared with literature data of some other RVO₄ compounds.

The SmVO₄ single crystal was grown from PbO/PbF₂ flux by the slow cooling method. The *in-situ* high-pressure measurements were conducted at I711 beamline (MAXlab, Lund, Sweden) using a membrane-driven diamond-anvil cell. A methanol-ethanol-water mixture was applied as pressure transmitting medium.

The experiments performed at room temperature at hydrostatic pressures show that EuVO₄ undergoes a

zircon–scheelite phase transition which starts at 7 GPa and ends at about 9 GPa. Fitting the Birch-Murnaghan equation of state gave the bulk modulus of the zircon-type phase of 118 GPa. The above values differ from those found in a recent study [3] for the EuVO₄ compound being a close neighbor of SmVO₄ in the RVO₄ series. The possible reasons for the similarities and differences in respect to EuVO₄ and other members of the RVO₄ family will be discussed.

References

- [1] D. Patel, P.J. Andersen, H.H. Kung, "Oxidative dehydrogenation of butane over orthovanadate", *J. Catal.* **125** (1990) 132–142.
- [2] C.T. Au, W.D. Zhang, H.L. Wan, "Preparation and characterization of rare earth orthovanadates for propane oxidative dehydrogenation", *J. Catal. Lett.* **37** (1996) 241–246.
- [3] D. Errandonea, R. Lacombe-Perales, J. Ruiz-Fuertes, A. Segura, S.N. Achary, A.K. Tyagi, "High-pressure structural investigation of several zircon-type orthovanadates", *Phys. Rev. B* **79** (2009) 184104.

FIRST APPROACH TO STUDIES OF SULPHUR ELECTRON DOS IN PROSTATE CANCER CELL LINES AND TISSUES STUDIED BY XANES

Wojciech M. Kwiatek^{1*}, **Joanna Czapla**¹, **Magdalena Podgórczyk**¹, **Andrzej Kisiel**², **Jerzy Konior**², and **Antonella Balerna**³

¹*Institute of Nuclear Physics PAN, ul. Radzikowskiego 152, 31-342 Kraków, Poland*

²*Institute of Physics, Jagiellonian University, ul. Reymonta 4, 30-059 Kraków, Poland*

³*INFN - Laboratori Nazionali di Frascati, Via E. Fermi 40, I-00044 Frascati, Italy*

Keywords: prostate cancer, sulphur, DOS, XANES

**) e-mail: wojciech.kwiatek@ifj.edu.pl*

Urological cancers comprise approximately one third of all cancers diagnosed in men worldwide, and out of these prostate cancer is the most common one [1]. Therefore, there is a significant medical need to investigate these diseases with different techniques, as the etiology of them is not well known.

The synchrotron methods already have been applied in the examination of biological samples and these techniques are constantly developed. Hence, prostate cancer cell lines and tissues along with selected organic and inorganic compounds used as standards were studied with X-ray absorption fine structure spectroscopy. The experiment was held at the DRX1 beamline at LNF, Frascati (Italy). The K-edge of sulphur was chosen for the studies because it is an essential biological element and its biochemistry is only partially understood [2]. It is believed that changes to the structure of protein binding sites, where sulphur is present, alter cells metabolism and these changes may play an important role in carcinogenesis.

The previous studies of sulphur K-edge XANES spectra of prostate cancer cell lines and tissues showed the presence of sulphur on –II oxidation state and similarity to Na₂S₂O₃ XANES spectrum [3], as shown in Fig. 1. However, one should notice that out of sulphur atoms present in Na₂S₂O₃, one atom is present in –II oxidation state and the second one is in +VI oxidation state.

For further studies, the comparison is made between the experimental results collected during XANES measurements and the theoretical calculations of electron density of states. In this work, the first results of these studies are presented.

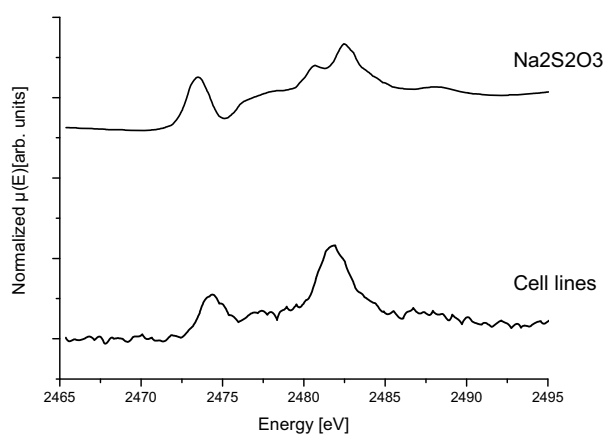


Figure 1. XANES sulphur K-edge spectra of Na₂S₂O₃ and cell lines.

References

- [1] *WHO World Cancer Report 2008*, Peter Boyle, Bernard Levin (eds.), (Lyon 2008).
- [2] I.J. Pickering, R.C. Prince, T. Divers, G.N. George, "Sulfur K-edge X-ray absorption spectroscopy for determining the chemical speciation of sulfur in biological systems", *FEBS Lett.* 441 (1998) 11–14.
- [3] W.M. Kwiatek, M. Podgórczyk, Cz. Paluszkiwicz, A. Balerna, A. Kisiel, "Sulphur XANES analysis of cultured human prostate cancer cells", *Acta Phys. Polon. A* 114 (1010) 463–470.

CHARACTERISATION OF NANOPOROUS POLYMERIC SPME COATINGS WITH USE OF SAXS MEASUREMENTS

P. Olszowy^{1*}, **M. Kozak**², **S. Pikus**³, and **B. Buszewski**^{1*}

¹ Department of Environmental Chemistry and Bioanalytics, Faculty of Chemistry, Nicolaus Copernicus University, 7 Gagarin Str., 87100 Torun, Poland

² Department of Macromolecular Physics, Faculty of Physics, Adam Mickiewicz University, 85 Umultowska Str., 61614 Poznan, Poland

³ Department of Crystallography, Faculty of Chemistry, Maria Curie-Skłodowska University, 3 Maria Curie-Skłodowska Str., 20031 Lublin, Poland

Keywords: solid phase microextraction, electropolymerisation, small angle x-ray scattering

**) e-mail: olszowy@chem.umk.pl*

The recent trend in sample preparation methods are focus on the miniaturization and development of new selective materials. The number of studies set the conducting polymers as one from the most essential group of materials which can be applied with success as an adsorbent in solid phase microextraction (SPME). These kinds of polymers are the area of our interests because of a several important aspect. Mainly due to possibility to synthesis of these polymers on electrochemical polymerization way. This method allows for a broad of variety changing while preparing fibers *i.e.* thickness, existence of counter ions and porosity. Thickness of the fibers may be rapidly measured by use of Scanning Electron Microscope (SEM) (Fig. 1) but porosity investigations of such materials contains very small pore size procure plenty of embarrassment.

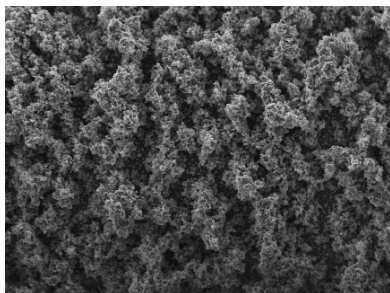


Figure 1. SEM micrographs with structure of polypyrrole SPME fiber obtained on the electrochemical polymerisation way.

First investigation was directed on the measurement with use of low temperature adsorption of nitrogen but with use of this technique we could not obtain a satisfactory results caused by low resolution of apparatus and small pores existed in porous polymeric materials. Simultaneously a rehearsal investigation with applying a Small Angle X-ray Scattering measurement was applied. This examination was performed with use of diffractometer NanoSTAR (Bruker-AXS) and HiSTAR detector with high resolution.

Measurements with use of SAXS were performed for polypyrrole and polythiophene SPME coatings obtained on the electrochemical polymerisation way with thickness in range 90-95 and 145-155 μm , respectively.

Calculated pore size range for these materials were in range from 400 to 1300 \AA both for polypyrrole and polythiophene coatings. Example plot is presented in Fig. 2. However some differences between these materials especially in small and high pore size range were observed.

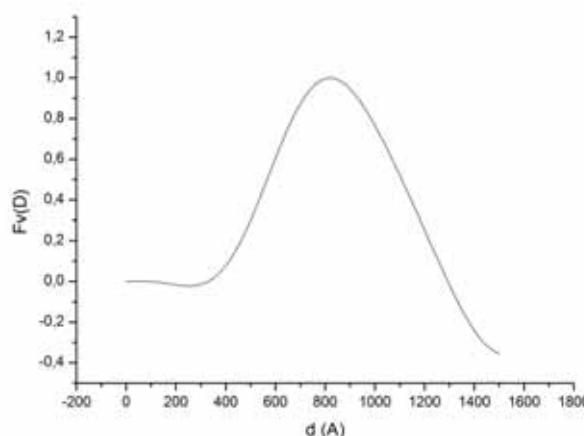


Figure 2. SAXS measurements of polythiophene SPME coating.

Synthesized and characterized fibers were used in SPME for sampling a medically important antibiotics from standard solutions, human plasma and whole blood. These investigations create a possibility to apply the described method in experienced biomedical analysis [1].

Acknowledgments: This work was supported by Ministry of Science and Higher Education (Warsaw, Poland) Grant. No. 2680/B/H03/2010/38 and by European Social Found, Polish National Budget, Kujawsko-pomorskie Voivodship Budget (within Sectoral Operational Programme Human Resources) "Krok w przyszłość" and "Stypendia dla doktorantów 2008/2009-ZPORR".

References

- [1] B. Buszewski, P. Olszowy, T. Ligor, M. Szultka, J. Nowaczyk, M. Jaworski, M. Jackowski, "Determination of adrenolytic drugs by SPME-LC-MS", *Anal. Bioanal. Chem.* **397** (2010) 173–179.

INFLUENCE OF NICKEL DOPING ON PHYSICAL PROPERTIES OF ZnCr_2Se_4

P. Zajdel^{1*}, **I. Jendrzejewska**², **J. Gorau**¹, **H. Duda**¹, **T. Goryczka**³, and **A. Kita**²

¹ *Institute of Physics, University of Silesia, ul. Uniwersytecka 4, 40-007 Katowice, Poland*

² *Institute of Chemistry, University of Silesia, ul. Szkolna 9, 40-006 Katowice, Poland*

³ *Institute of Chemistry and Physics of Metals, University of Silesia, ul. Bankowa 12, 40-006 Katowice, Poland*

Keywords: nickel, spinel, XAS

*) e-mail: pawel.zajdel@us.edu.pl

ZnCr_2Se_4 crystallises in spinel structure (SG 227, $a = 10.48 \text{ \AA}$). At 21 K, it orders magnetically into incommensurate helix with propagation vector $k = (0,0,0.41)$ with a slight tetragonal distortion ($c/a = 0.9995$).

The development of the incommensurate structure is driven by a bond frustration induced by the competition of a nearest neighbour (NN) ferromagnetic superexchange (close to 90° Cr-Se-Cr angle) and numerous NNN antiferromagnetic (AF) interactions. The balance between these interactions can be tuned by doping the system, which may lead to many useful magnetic and electric properties like a spin glass or increased Seebeck effect [1]. But so far, there has been no adequate study of a local structure around the dopant.

We have performed XANES and EXAFS studies of $\text{ZnCr}_{2-x}\text{Ni}_x\text{Se}_4$ in order to elucidate the influence of Ni on the structural and electronic properties of the system. By the comparison with the Ni K and Cr K edges of monoclinic $(\text{NiCr}_2)\text{Se}_4$ and the local structure fits using IFFEFIT package, we have confirmed that the Ni is indeed located on the Cr site, since it is not unusual to observe Ni on tetrahedral one [2]. This is also in agreement with the decrease of the lattice parameters due to smaller radius of nickel.

The remaining problem is the nominal oxidation state of nickel. The analysis of the XANES region of Ni K edge revealed that Ni is incorporated in the structure closer to Ni^{2+} rather than Ni^{3+} state. (We note that the chemical bond in ZnCr_2Se_4 has a strong covalent character, so we cannot strictly speak about the oxidation state in an ionic sense) (Fig. 1).

In order to elucidate this result we have performed FPLO calculations of ZnCr_2Se_4 and $\text{ZnCr}_{1.8}\text{Ni}_{0.2}\text{Se}_4$. The calculated densities of states (DOS) gave a good agreement with the experimental absorption edges. The main nickel contribution to the band structure of the host have been found to be the 3d states located at the Fermi's level, which are polarised opposite to the chromium 3d band (Fig. 2). This is in agreement with the observed decrease of the magnetic moment per formula with increased Ni content.

References

- [1] H. Duda, T. Groń, I. Jendrzejewska, S. Mazur, P. Zajdel, A. Kita, *Phys. Stat. Sol. (c)* **4** (2007) 1309–1312.
[2] H. Itoh, K. Motida, S. Miyahara, *J. Phys. Soc. Jap.* **43**(3) (1977) 854.

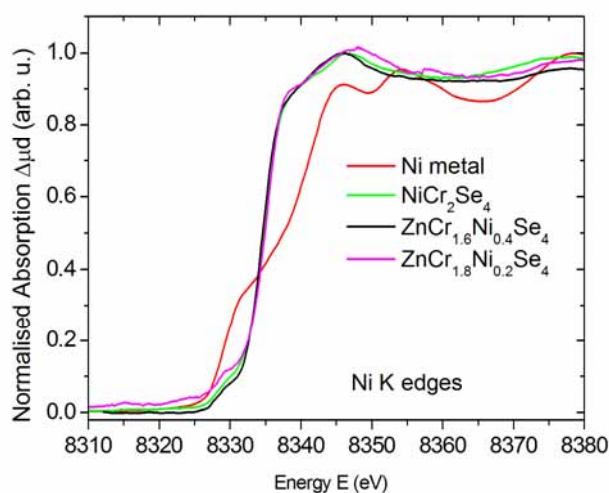


Figure 1. Experimental Ni K absorption edges of $\text{ZnCr}_{2-x}\text{Ni}_x\text{Se}_4$, together with standards: Ni-metal, NiCr_2Se_4 .

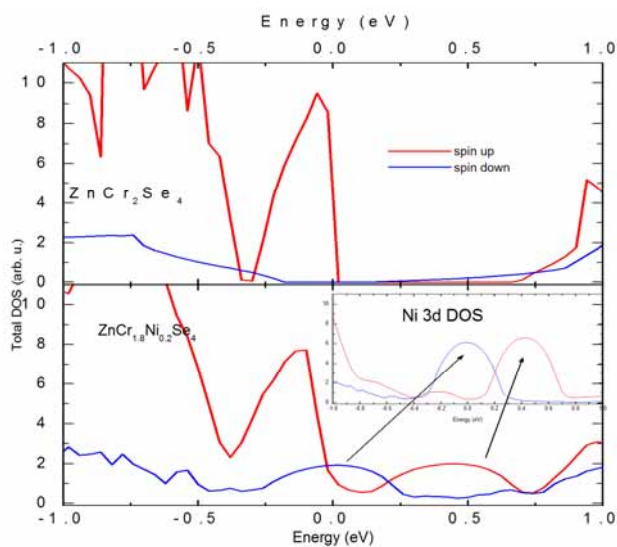


Figure 2. FPLO calculated DOS reveals that Ni 3d levels are situated in the forbidden gap of ZnCr_2Se_4 and polarised opposite to chromium.

RECONSTRUCTION OF THE SPHERICAL ELECTRON MOMENTUM DENSITY DISTRIBUTION IN Mg BY THE MAXIMUM ENTROPY METHOD

M. Brancewicz^{1*}, **A. Andrejczuk**¹, **E. Żukowski**¹, **L. Dobrzyński**^{1,2}, and **S. Kaprzyk**³

¹ Faculty of Physics, University of Białystok, ul. Lipowa 41, 15-424 Białystok, Poland

² The Soltan Institute for Nuclear Studies, 05-400 Otwock-Świerk, Poland

³ Faculty of Physics and Applied Computer Science, AGH University of Science and Technology, Al. Mickiewicza 30, 30-059 Kraków, Poland

Keywords: magnesium, Compton profile, momentum density, maximum entropy method

*) e-mail: brancew@alpha.uwb.edu.pl

One-dimensional projections of the electron momentum density distribution (Compton profiles - CPs) of single crystal magnesium were measured using high-energy (115.6 keV) synchrotron radiation at the beamline BL08W at SPring-8, Japan [1].

Four special directions in Brillouin zone were chosen for investigations: ΓM , ΓK , ΓA and ΓI (lying between ΓM and ΓK). The total experimental resolution of the measured CPs was equal to 0.12 a.u. Taking into account very small anisotropy [2] of directional CPs of magnesium, one can assume that the electron momentum density distribution $n(p)$ is almost isotropic. Within this approximation the spherical electron momentum density of the valence electrons in Mg was reconstructed using maximum entropy method (MEM).

The experimental resolution is taken into consideration in $n(p) \rightarrow CP$ transformation matrix used by

MEM algorithm. Thus the reconstructed $n(p)$ is close to the real one. Using smooth electron momentum density (estimated from experimental CPs) as a starting prior in MEM, reconstructed $n(p)$ clearly shows interesting structure below the Fermi momentum.

References

- [1] Y. Sakurai, M. Itou, "A Cauchy-type X-ray spectrometer for momentum density studies on heavy-element materials", *J. Phys. Chem. Solids* **65** (2004) 2061–2064.
- [2] M. Brancewicz, A. Andrejczuk, Y. Sakurai, M. Itou, L. Dobrzyński, E. Żukowski, S. Kaprzyk, "Electron momentum density of hexagonal magnesium studied by high resolution Compton scattering", *Rad. Phys. Chem.* **78** (2009) 137–139.

STUDIES OF STRUCTURAL CHANGES INDUCED BY UV AND VUV LASER PULSES

D. Klinger¹, R. Sobierajski^{1,8}, M. Jurek¹, J. Krzywinski^{1,5}, J.B. Pelka¹, D. Żymierska^{1*},
R. Minikayev¹, B. Kozankiewicz¹, J. Chalupský^{2,3}, L. Juha², V. Hájková², J. Cihelka²,
T. Burian^{2,3}, L. Vyšín^{2,3}, H. Wabnitz⁴, W. Caliebe⁴, K. Tiedtke⁴, S. Toleikis⁴,
T. Tschentscher⁴, R. London⁵, S. Hau-Riege⁵, K. Sokolowski-Tinten⁶, N. Stojanovic⁶,
J. Hajdu⁷, A.R. Khorsand⁸, A.J. Gleeson⁹, and K. Nowakowska-Langier¹⁰

¹ Institute of Physics, Polish Academy of Sciences, Al. Lotników 32/46, PL-02-668 Warsaw, Poland

² Institute of Physics, Czech Academy of Sciences, Na Slovance 2, 182 21 Prague 8, Czech Republic

³ Czech Technical University in Prague, Břehova 7, 115 19 Praha 1, Czech Republic

⁴ Deutsches Elektronen-Synchrotron DESY, Notkestrasse 85, D-22603 Hamburg, Germany

⁵ Lawrence Livermore National Laboratory, 7000 East Avenue, CA 94550 Livermore, USA

⁶ University of Duisburg-Essen, D-45117 Essen, Germany

⁷ Uppsala University, SE-75124 Uppsala, Sweden

⁸ FOM-Institute for Plasma Physics Rijnhuizen, P.O. Box 1207, 3430 BE Nieuwegein, The Netherlands

⁹ CCRLC Daresbury Laboratory, Warrington, Cheshire, WA4 4AD, UK

¹⁰ Andrzej Soltan Institute for Nuclear Studies, PL-05-400 Świerk/Otwock, Poland

Keywords: laser processing, XUV free electron laser, material modification, laser ablation, synchrotron radiation, X-ray diffraction

*) e-mail: zymier@ifpan.edu.pl

Investigations of the interaction of laser radiation with optical materials have remained strenuous in the last decade. Especially, the interaction of ultra short laser pulse with matter has been studied. In the research the influence of the pulse duration [1, 2] and the material [3-5] on the ablation threshold were taken into account but many questions referred to ablation remain open as before. In order to reveal differences in results of interaction of short (ns) and ultra short (fs) laser pulses with matter, we carried previously out experimental studies by means of the interference-polarizing microscopy using the Nomarski reflection contrast, atomic force microscopy, and theoretical simulation of the process. The interaction with matter of ns laser pulses consists in thermal processes. The energy of laser radiation is transferred into the lattice in the form of a thermal energy in a nanosecond time scale causing melting of the surface layer. Next recrystallisation occurs which is continued after the laser pulse. We investigated these effects in single silicon crystals as well as in implanted samples. In dependence on laser annealing conditions (the energy density and duration) polycrystallisation, structural reordering or creation of microcrystallites on amorphous layer occurs [6,7]. Interaction of fs laser pulse with matter differs from that of ns pulse. XUV radiation permits a high degree of electronic excitation. The temperature of the electronic system grows up rapidly (in a femtosecond time scale, < 100 fs). Further, at a picosecond time scale the electron gas cools down by the heat transfer to the crystal lattice. If the lattice temperature reaches the phase transition point, the damage occurs. The depth of the damaged volume

increases due to the thermal diffusion in the lattice that happens on a nanosecond time scale. We studied the irradiation damage in silicon single crystals [8,9].

The aim of the present work is an X-ray characterisation of materials in which structural modifications were induced with nanosecond pulses generated by excimer laser and the intense XUV femtosecond pulses generated by the TESLA test facility free electron laser (TTF FEL) at DESY, Hamburg. The results were obtained by X-ray diffraction method using synchrotron radiation at the W1.1 beam line at DESY-HASYLAB. The monochromatic X-ray beam of the wavelength $\lambda = 1.54056 \text{ \AA}$ was applied. The measurements were recorded with 2θ scans in the glancing incidence geometry and with $\omega-2\theta$ scans. This method permitted us to determine the quality of crystal structure of samples. The samples were investigated before and after irradiation with laser radiation, this way the changes in crystallographic structure caused by the ablation were revealed, namely the creation of microcrystallites on the amorphous or polycrystalline surfaces of studied samples was observed.

Acknowledgements: This work was supported in part by the Ministry of Science and Higher Education (Poland) under special research project No. DESY/68/2007.

References

- [1] M. Lenzner, "Femtosecond laser-induced damage of dielectrics," *Int. J. Mod. Phys. B* **13** (1999) 1559–1578.

- [2] A. Rosenfeld, M. Lorenz, D. Ashkenasi, P. Rudolph, J. Krueger, W. Kautek, "Femtosecond- and nanosecondpulse laser ablation of bariumaluminumborosilicate glass," *Appl. Phys. A* **69** (1999) 759–761.
- [3] T.Q. Jia, Z.Z. Xu, R.X. Li, D.H. Feng, X.X. Li, C.F. Cheng, H.Y. Sun, N.S. Xu, H.Z. Wang, "Formation of nanogratings on the surface of a ZnSe crystal irradiated by femtosecond laser pulses," *Phys. Rev. B* **72** (2005) 1254291–1254294.
- [4] I.H. Chowdhury, A.Q. Wu, X. Xu, A.M. Weiner, "Ultrafast laser absorption and ablation dynamics in wide-band-gap dielectrics," *Appl. Phys. A* **81** (2005) 1627–1632.
- [5] K. Sokolowski-Tinten, J. Bialkowski, A. Cavalleri, D. von der Linde, A. Oparin, J. Mejer-ter-Vehn, S.I. Anisimov, "Transient states of matter during short pulse laser ablation," *Phys. Rev. Lett.* **81** (1998) 224–227.
- [6] D. Klinger, J. Auleytner, D. Żymierska, B. Kozankiewicz, L. Nowicki, A. Stonert, "Pulsed laser annealing of Sn-implanted Si single crystal", *J. Appl. Phys.* **95** (2004) 2331–2336.
- [7] D. Klinger, E. Łusakowska, D. Żymierska, "Nano-structure formed by nanosecond laser annealing on amorphous Si surface", *Mat. Sci. Semi. Mat.* **9** (2006) 323–326.
- [8] J.B. Pelka, R. Sobierajski, D. Klinger, W. Paszkowicz, J. Krzywiński, M. Jurek, D. Żymierska, A. Wawro, A. Petrouchik, L. Juha, V. Hajkova, J. Cihelka, J. Chalupsky, T. Burian, L. Vysin, S. Toleikis, K. Sokolowski-Tinten, N. Stojanovic, U. Zastra, R. London, S. Hau-Riege, C. Riekel, R. Davies, M. Burghammer, E. Dynowska, W. Szuskiewicz, W. Caliebe, R. Nietubyć, "Damage in solids irradiated by a single shot of XUV free-electron laser: Irreversible changes investigated using X-ray microdiffraction, atomic force microscopy and Nomarski optical microscopy", *Rad. Phys. Chem.* **78** (2009) S46–S52.
- [9] R. Sobierajski, D. Klinger, M. Jurek, J.B. Pelka, L. Juha, J. Chalupský, J. Cihelka, V. Hajkova, L. Vysin, U. Jastrow, N. Stojanovic, S. Toleikis, H. Wabnitz, J. Krzywinski, S. Hau-Riege, R. London, "Interaction of intense ultrashort XUV pulses with silicon", *Proc. SPIE* **7361** (2009) 736107-1–11.

SPONTANEOUS EXFOLIATION AND SELF-ASSEMBLY PHENOMENA IN POLYVINYLPIRROLIDONE/SYNTHETIC LAYERED SILICATE NANOCOMPOSITES

M. Żabska^{1*}, **K. Jaśkiewicz**^{1,2}, **A. Kiersnowski**¹, **K. Szustakiewicz**¹,
S. Rathgeber^{2,3}, and **J. Pięłowski**¹

¹ Polymer Engineering and Technology Division, Wrocław University of Technology, 50 370 Wrocław, Poland

² Department of Polymer Physics, Max Planck Institute for Polymer Research, 55 128 Mainz, Germany

³ Institut für Physik, Johannes Gutenberg University Mainz, 55 099 Mainz, Germany

Keywords: polyvinylpyrrolidone, nanocomposites

*) e-mail: malgorzata.zabska@pwr.wroc.pl

Polyvinylpyrrolidone (PVP) and synthetic montmorillonite (MMT) were used to prepare nanocomposites via the solution intercalation method using water as a solvent. The structural properties of the PVP/MMT nanocomposites were investigated by using wide- and small-angle X-ray scattering (WAXS and SAXS) as well as transmission electron microscopy. The research revealed that at concentrations not exceeding 20 wt.% MMT exfoliates without a necessity of any mechanical treatment. The orientation process needs no external force like shearing or stretching. Orientational structure was investigated by 2D WAXS and 2D SAXS methods. Analysis of diffractograms recorded for samples oriented with edges to the primary beam revealed that silicates platelets were aligned parallel to the surface of polymer film (Fig. 1). From TEM images it can be concluded that nanocomposites of PVP/MMT with 5 wt.% of MMT are exfoliated and distance between montmorillonite platelets average 32 nm (Fig. 2).

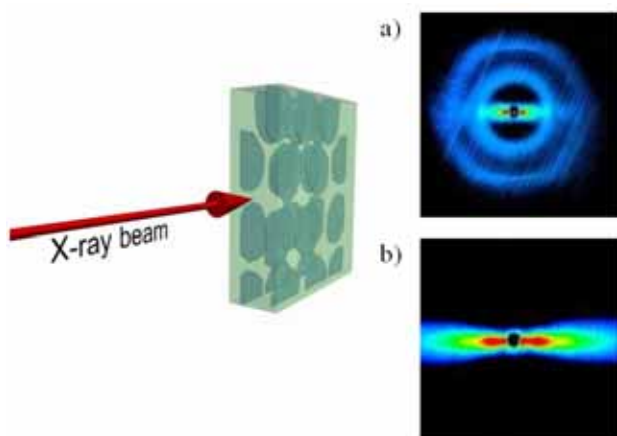


Figure 1. a) 2D WAXS and b) 2D SAXS patterns of PVP/MMT nanocomposites with 10 wt.% MMT.

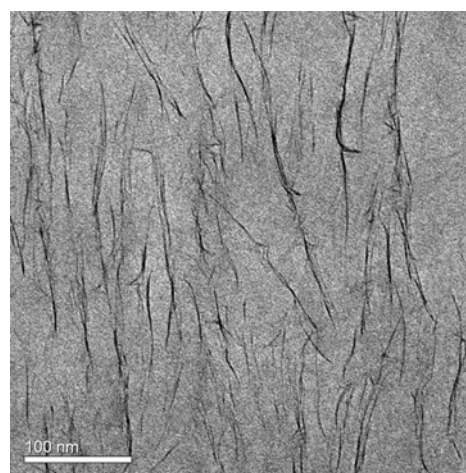


Figure 2. TEM image of PVP/MMT nanocomposite containing 5 wt. % of montmorillonite.

Similar observations were already made by Ogata *et al.* [1,2]. The main difference however is that the authors of the above mentioned article failed to obtain delaminated polymer clay system.

In addition to structural investigations thermal and optical properties of the nanocomposites were investigated. Differential Scanning Calorimetry indicated no significant changes in glass transition temperatures for obtained nanocomposites. TGA research revealed slight decrease of thermal stability in samples containing MMT when compared to pure polymer. UV-VIS transmittance spectra show lower transmittance for nanocomposites than for neat polyvinylpyrrolidone, however PVP/MMT blends still keep the good optical transparency.

References

- [1] N. Ogata, S. Kawakage, T. Ogihara, *J. Appl. Polym. Sci.* **66** (1997) 572–581.
- [2] N. Ogata, G. Jimenez, H. Kawai, T. Ogihara, *J. Polym. Sci. B - Polym. Phys.* **35** (1997) 389–396.

HEXAGONAL BORON NITRIDE AS A PRESSURE TRANSMITTING MEDIUM IN THE HIGH-PRESSURE HIGH-TEMPERATURE X-RAY DIFFRACTION EXPERIMENT

P. Piszora^{1*}, **W. Nowicki**¹, **J. Darul**¹, and **C. Lathe**²

¹ Faculty of Chemistry, Adam Mickiewicz University, Grunwaldzka 6, 60-780 Poznan, Poland

² Helmholtz Centre Potsdam, GFZ German Research Centre for Geosciences,
Telegrafenberg, 14473 Potsdam, Germany

Keywords: high pressure, pressure medium, boron nitride, hBN,

*) e-mail: pawel@amu.edu.pl

Hexagonal boron nitride (*h*-BN) powder is a solid lubricant that compares favourably with, and in some cases exceeds, the performance of other solid lubricants. Its high-temperature stability, low coefficient of friction, extreme pressure performance, high thermal conductivity, high electrical resistivity, inertness in a wide variety of chemical environments, and environmental friendliness make *h*-BN an ideal alternative to other solid lubricants in many high performance applications.

Boron nitride has long been used as a crucible material in inert environments at high temperatures. It has found application as a fibber coating in ceramic-matrix composites. In such applications, it is likely to be exposed to high-temperature oxidizing conditions. However, there are many questions about its oxidation behaviour. The literature contains numerous studies of BN oxidation [1,2], which indicate the oxidation behaviour of BN is complex and dependent on structure.

In our experiment, the hexagonal boron nitride was tested as the pressure-transmitting medium at high-pressure high-temperature conditions in the mixture with LiMn₂O₄.

Lithium-manganese oxide (*Fd3m* space group) sample was obtained by conventional solid-state reaction of Li₂CO₃ with α -Mn₂O₃ (*Ia3*, bixbyite structure) at 1073 K. The synchrotron X-ray powder diffraction data, collected at beamline B2 (Hasylab), at ambient conditions confirmed the cubic spinel structure. The samples were mounted in *h*-BN cylinder, in boron-epoxy cube with the edge length 8 mm. The cube was located in between six anvils of the MAX80 press. In the high-pressure investigations a level of the pressure hydrostaticity due to applied pressure medium is very important [3]. The hexagonal boron nitride is considered to be a relatively 'soft' material and has been often used as the pressure medium; thereat we decided to perform high-pressure experiments on LiMn₂O₄/*h*-BN, with the weight ratio 1:2, in order to get quasihydrostatic conditions. The measurements were performed with the energy dispersive experimental setup and a white synchrotron radiation at F2.1 beamline (Hasylab). The

X-ray detection system was based on a germanium solid-state detector of resolution 135 eV at 6.3 keV. The sample was gradually compressed to required pressure of 3 kbar, at ambient temperature, and then it has been heated quickly to 500°C. After 15 minutes of heating, the sample was quenched by the switching off the power (the initial cooling rate was about 300°C/s). The structural changes have been monitored *in situ* with the energy dispersive XRD method. After the pressure releasing, the recovered sample has been analyzed by powder X-ray diffraction using a Huber image foil camera 670 with a capillary holder at I711 beamline in Max-lab (Lund).

Successful fitting of the XRD pattern of recovered sample with the Rietveld method revealed presence of LiMnBO₃, *h*-BN and MnO crystal phases. This phase composition enables to imply conclusion that, at applied high-pressure/high-temperature conditions, *h*-BN is not chemically resistant to oxidation in the presence of oxide sample. Furthermore, the hexagonal LiMnBO₃ has been recently proposed as a new cathode material for lithium-ion batteries [4] and its HP/HT synthesis route can appear as technologically important. The sample container made of *h*-BN could be applied for oxides in HP/HT experiments only with a special precaution.

Acknowledgements: The research leading to these results has received funding from the European Community's Seventh Framework Programme (FP7/2007-2013) under grant agreement n° 226716.

References

- [1] K. Oda, T. Yoshio, "Oxidation kinetics of hexagonal boron nitride powder", *J. Mater. Sci.* **28** (1993) 6562–6566.
- [2] V.A. Lavrenko, A.F. Alexeev, "High-temperature oxidation of boron nitride", *Ceram. Int.* **12** (1986) 25–31.
- [3] P. Piszora, "In-situ investigations of LiMn₂O₄ at high pressure" *Z. Kristallogr. Suppl.* **26** (2007) 387–392.
- [4] L. Chen, Y. Zhao, X. An, J. Liu, Y. Dong, Y. Chen, Q. Kuang, "Structure and electrochemical properties of LiMnBO₃ as a new cathode material for lithium-ion batteries" *J. Alloys Compds.* **494** (2010) 415–419.

SYNTHESIS OF MULTIMETALLIC LAYERED MATERIALS AND CHARACTERIZATION OF THE CALCINATION PRODUCTS

J. Darul^{1*}, **W. Nowicki**¹, and **D. Trots**²

¹ Faculty of Chemistry, Adam Mickiewicz University, Grunwaldzka 6, PL-60780 Poznań, Poland

² HASYLAB at DESY, D-22603 Hamburg, Germany

Keywords: layered double hydroxides (LDHs), X-ray diffraction, thermal decomposition

*) e-mail: jola@amu.edu.pl

The layered double hydroxides (LDHs), also known as hydrotalcite-like materials or as anionic (more properly speaking, anion exchanging) clays, are a large group of natural and synthetic materials readily produced when suitable mixtures of metal salts are exposed to base. These materials have the general formula $[MII_{1-x}MIII_x(OH)_2] (A^{n-})_x/n mH_2O$. Metal cations are located in coplanar octahedra $[M(OH)_6]$ sharing edges and forming $M(OH)_2$ layers with the brucite (cadmium iodide-like) structure. Partial substitution of the divalent cations by trivalent ones gives rise to a positive charge in the layers, balanced by anions (A^{n-}) located between the hydroxylated layers, where water molecules also exist. The anions and the water molecules are hosted together in the interlayer gallery. The nature of the cations in the brucite-like sheets (which is not restricted to +2/+3 combinations) and the interlayer anions together with the coefficient x value may be varied in a broad range, giving rise to a large class of isostructural materials [1,2]. Decomposition of LDHs at moderate temperatures leads to mixed oxides displaying high specific surface areas, good interdispersion of the metal cations, and reactivity, which are of interest because of their catalytic applications [3].

In this study we used the co-precipitation method at constant pH for the synthesis of layered double hydroxides containing Zn^{2+} , Ni^{2+} and Al^{3+} with cationic ratio 1-4 and carbonate, nitrate or citrate as charge balancing anions. The samples have been characterized by elemental chemical analysis, powder X-ray diffraction, and FT-IR spectroscopy. Their thermal stability has been assessed by thermogravimetric and differential thermal analyses (TG-DTA) and high temperature synchrotron powder X-ray diffraction (PXRD). Investigations on the high temperature phase transitions were carried out at the synchrotron beamline B2 at HASYLAB (DESY, Hamburg). The diffractometer

was equipped with capillary furnace (STOE) and the on-site readable image-plate detector OBI. Samples mounted into quartz capillaries of diameter 0.3 mm were heated and cooled at the temperature range from RT to 800°C. The wavelength was 0.65131 Å.

Thermal decomposition LDHs containing carbonate or nitrate in the interlayer starts at 200–300°C and proceeds through intermediate amorphous phases. The final decomposition product is a mixture of $MIIIMIII_2O_4$ spinel and $MIIO$ oxide because a $MII/MIII$ ratio larger than 1 is required to form a stable hydrotalcite. The thermal stability of these materials is strongly related with several factors, such as both the nature of cations and the cationic ratio in the brucite-like sheets, the nature of the compensating anions and the crystallinity degree of LDH lattice.

Acknowledgements: This research is partially supported by the Ministry of Science and Higher Education (Poland), grant No. NN204330537. The diffraction experiment leading to these results has received funding from the European Community's Seventh Framework Programme (FP7/2007-2013) under grant agreement n° 226716.

References

- [1] G.C. Thomas, A.V. Radha, P.V. Kamath, S. Kannan, "Thermally induced polytype transformations among the layered double hydroxides (LDHs) of Mg and Zn with Al", *J. Phys. Chem. B.* **110** (2006) 12365–12371.
- [2] G.M. Lombardo, G.C. Pappalardo, R. Constantino, U. Constantino, M. Sisani, "Thermal effects on mixed metal layered double hydroxides: Direct modelling of the X-ray powder diffraction line shape through molecular dynamics simulations", *Chem. Mater.* **20** (2008) 5585–5592.
- [3] F. Figueras, "Base catalysis in the synthesis of fine chemicals", *Top. Catal.* **29** (2004) 189–196.

MODIFICATION OF THE LOCAL STRUCTURE OF OXYGEN IN CdO UNDER IRRADIATION

I.N. Demchenko^{1,2,3*}, **T. Tyliczszak**², **M. Chernyshova**⁴, **K.M. Yu**², **J.D. Denlinger**²,
D. Speaks^{2,5}, **P. Olalde-Velasco**⁶, **O. Hemmers**⁷, **W. Walukiewicz**²,
G. Derkachov³, and **K. Lawniczak-Jablonska**³

¹ *University of Nevada Las Vegas, Department of Chemistry,
4505 Maryland Pkwy-Box 454003, Las Vegas, NV 89154-4003, USA*

² *Lawrence Berkeley National Laboratory, 1 Cyclotron Rd, Bldg4R0230, Berkeley, CA 94720-8235, USA*

³ *Institute of Physics PAS, al. Lotnikow 32/46, 02-668, Warsaw, Poland*

⁴ *Institute of Plasma Physics and Laser Microfusion, 23 Hery Street, 01-497 Warsaw, Poland*

⁵ *Department of Materials Science and Engineering, University of California, Berkeley, CA 94720, USA*

⁶ *Instituto de Ciencias Nucleares, UNAM, Mexico, Distrito Federal 04510, Mexico*

⁷ *Harry Reid Center for Environmental Studies, University of Nevada Las Vegas, Las Vegas, NV 89514-4009, USA*

Keywords: cadmium oxide, irradiation, NEXAFS

*) e-mail: INDemchenko@lbl.gov

We have studied the effects of high concentration of point defects on the electronic structure of CdO. The defects were introduced by irradiation with high energy Ne ions. The "as-grown" and "irradiated" samples were investigated at the Advanced Light Source (ALS) Lawrence National Berkeley Laboratory at the beamline 11.0.2. Significant differences between experimental near edge x-ray absorption fine structure (NEXAFS) spectra gathered in total fluorescence yield (TFY, bulk sensitive) and total electron yield (TEY, rather surface sensitive) detection modes are observed. Such observation makes clear that irradiation process drastically modifies the surface layer of investigated films.

An interpretation of NEXAFS spectra at the K-edge of oxygen in "as-grown" and "irradiated" CdO films, within the *ab-initio* real space multi-scattering (RSMS) formalism applying the FEFF8 code, with many-body effects incorporated in terms of final-state potentials and complex energy-dependent self-energy, will be shown.

Different models with point defects (namely oxygen vacancy and cadmium interstitials) in the host CdO matrix were considered and respective theoretical spectra were calculated. Basing on the RSMS theory, we are able to interpret the experimental spectra in terms of changes in the local atomic (geometrical) and electronic structure around oxygen atoms.

Comparison of the experimental ("irradiated" versus "as grown") and theoretical data allows to conclude that electronic levels of defects push the Fermi level into the conductive band, thus modify the charge transfer around the oxygen atoms with the defected local atomic order what leads to the shift of the absorption threshold to a higher energy. The observed leading edge differences of TFY and TEY spectra could be likely explained basing on electron accumulation at the surface of n-type CdO due to the presence of positively charged donor-type surface states. Our conclusions are confirmed by optical absorption measurements.

STUDIES OF MICROSTRUCTURE IN ANNEALED NANOCRYSTALLINE CHROMIUM BY USING SYNCHROTRON RADIATION DIFFRACTION

D. Wardecki^{1*}, **R. Przeniosło**¹, **A.N. Fitch**², **M. Bukowski**³, and **R. Hempelmann**³

¹ *Institute of Experimental Physics, University of Warsaw, Hoża 69, 00-681 Warsaw, Poland*

² *European Radiation Synchrotron Facility, BP 220, F-38043 Grenoble Cedex, France*

³ *Institute of Physical Chemistry, University of Saarland, D66123, Saarbrücken Germany*

Keywords: nano-chromium, synchrotron radiation, powder diffraction, Waren-Averbach method, electrodeposition

*) e-mail: dward@fuw.edu.pl

The kinetics of thermal evolution of the microstructure of electrodeposited nanocrystalline chromium (n-Cr) was studied by using several techniques: synchrotron radiation (SR) diffraction at ESRF ID-31 beamline [1] as well as SEM, TEM and EDX. The as-prepared n-Cr samples show the standard bcc crystal structure of Cr [2] with volume-averaged column lengths varying from 25 nm to 30 nm. The grain growth kinetics and the oxidation kinetics were studied by time resolved SR diffraction measurements with n-Cr samples annealed at 400°C, 600°C and 800°C. The most of microstructure changes *e.g.* crystallite size and microstrain fluctuations' decrease, occur within the first 10 minutes of annealing similar to the results of earlier studies [3]. The final crystallite size depends only on the annealing temperature and not on the initial grain size nor on the oxygen content. The final volume-averaged column lengths observed after 50 minutes annealing are: 40 nm, 80 nm and 120 nm for temperatures 400°C, 600°C and 800°C, respectively. The formation of the Cr₂O₃ [4] and CrH [5] phases is observed during annealing. The kinetics of the oxidation process *i.e.* the

Cr₂O₃ content increase has been also studied with SR diffraction measurements for n-Cr as well as polycrystalline Cr.

References

- [1] A.N. Fitch, "The high resolution powder diffraction beam line at ESRF", *Res. Nat. Inst. Stand. Technol.* **109** (2004) 133.
- [2] A. Hull, "X-Ray crystal analysis of thirteen common metals", *Phys. Rev.* **17** (1921) 571-88.
- [3] G. Chojnowski, R. Przeniosło, I. Sosnowska, M. Bukowski, H. Natter, R. Hempelmann, A. Fitch, V. Urban, "Microstructure evolution and grain growth kinetics in annealed nanocrystalline chromium", *J. Phys. Chem. C* **111** (2007) 5599-5604.
- [4] R.E. Newnham, Y.M. de Haan, "Refinement of the alpha Al₂O₃, Ti₂O₃, V₂O₃ and Cr₂O₃ structures", *Z. Kristallogr.* **117** (1962) 235-237.
- [5] C.A. Snively, A. Dale, D.A. Vaughan, "Unit cell dimension of face-centered cubic chromium hydride and space groups of two chromium hydrides", *J. Am. Chem. Soc.* **71** (1949) 313-314.

A SYNCHROTRON STUDY OF POLYMORPHIC PHASE TRANSITION IN NYLON 6

M. Basiura-Cembala^{1*} and **B. Goderis**²

¹ *Institute of Textile Engineering and Polymer Materials, University of Bielsko-Biala, Willowa 2, 43-309 Bielsko-Biala, Poland*

² *Molecular and Nanomaterials, Catholic University of Leuven, Celestijnenlaan 200 F, 3001 Heverlee, Belgium*

Keywords: nylon 6, polymorphism, WAXD, Brill transition

**) e-mail: mbasiura@ath.bielsko.pl*

Aliphatic polyamides, such as nylon 6 (polyamide 6) are well known for their strong hydrogen bonding ability. The hydrogen bonds are the driving force that locks the crystallizing lamella into one or another crystalline form, satisfying a requirement of complete hydrogen bonding. Hydrogen bonds are also present in the amorphous regions and even in the molten state.

There exist two well resolved and documented crystal structures of PA6, *i.e.* the α and γ forms. It is generally accepted that the monoclinic α form is the thermodynamically most stable and that it is present after cooling slowly from the melt or annealing at high temperatures [1]. The monoclinic γ form, obtained by a treatment with an iodine-potassium iodide solution is also very stable and does not easily convert to the α form [2]. Fast cooling or cold crystallization promotes development of a (pseudo)hexagonal β structure which, depending on cooling rate, can coexist with the α form [1,3]. Most polyamides undergo a reversible transition between the pseudo-hexagonal structure at high and the monoclinic or triclinic form at low temperature. This transition is known as the Brill transition [4]. It is widely accepted that PA6 does not reveal the full Brill transition. However our synchrotron wide angle x-ray diffraction (WAXD) experiment shows that the more rapidly cooled sample the more imperfect the α phase and the more evident is the Brill transition upon heating. Surprisingly, the most clear Brill transition is evident upon heating of a sample annealed for 10 hours at 200°C, *i.e.* close to the melting temperature. This result, shown in Fig. 1, contradicts conventional wisdom that the α form is the thermodynamically most stable, especially when formed during annealing at high temperatures.

We suggest that the β form of nylon 6 is of the same nature as the pseudo-hexagonal phase that occasionally appears during heating (Brill transition). Most likely α crystals during heating convert into the transient mesophase of intermediate order (the β form). Increasing the temperature yields two opposing effects: On the one hand, thermal activation leads towards destruction of crystals and melting. On the other hand, thermal activation accelerates the transition to better ordered states via the β form. The outcome of the interplay of the two local processes depends on the morphology at hand and time allowed in the given temperature window.

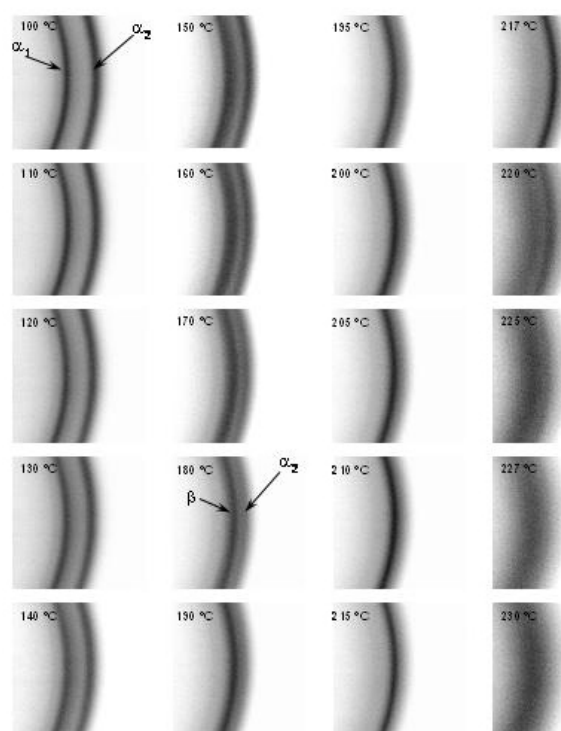


Figure 1. Selected 2D WAXD patterns of the annealed PA6 sample recorded on heating at 5°C/min.

Acknowledgements: This work is supported by the Polish Ministry of Science and Higher Education via research grant no N N508 469034.

References

- [1] D.R. Holmes, C.W. Bunn, D.J. Smith, "The crystal structure of polycapraamide: Nylon 6", *J. Polym. Sci.*, **17** (1955) 159–177.
- [2] H. Arimoto, M. Ishibashi, M. Hirai, Y. Chatani, "Crystal structure of the γ -form of nylon 6", *J. Polym. Sci., Part A 3* (1965) 317–326.
- [3] I. Sandeman, A. Keller, "Crystallinity studies of polyamides by infrared, specific volume and x-ray methods", *J. Polym. Sci.* **19** (1956) 401–435.
- [4] R. Brill, "Über das Verhalten von Polyamiden beim Erhitzen", *J. Prakt. Chem.* **161** (1942) 49–64.

LOW RESOLUTION STRUCTURE IN SOLUTION OF NATIVE HUMAN CYSTATIN C

M. Taube¹, **Z. Pietralik**¹, **A. Szymańska**², **A. Grubb**³, and **M. Kozak**^{1*}

¹ *Department of Macromolecular Physics, Faculty of Physics A. Mickiewicz University, Umultowska 85, 61-614 Poznań, Poland*

² *Department of Medicinal Chemistry, Faculty of Chemistry, University of Gdańsk, Sobieskiego 18, 80-952 Gdańsk*

³ *Department of Clinical Chemistry, Lund University, Sweden*

Keywords: human cystatin C, SAXS, low resolution structure

**) e-mail: mkozak@amu.edu.pl*

Human cystatin C (HCC) protein is a member of the family of the cysteine proteases inhibitors which inhibits proteins belonging to the papain and legumain families. HCC gen is located on chromosome 20 and codes a 120 amino acid protein. The general fold of monomeric form of cystatin has been defined by the crystal structure of chicken cystatin. Crystallographic studies of native HCC have shown that the protein exists in crystal in the form of symmetric three-dimensional domain-swapped dimers [1]. Dimerized human cystatin C has different overall conformation in tetragonal [2] and cubic [1] crystal forms. In tetragonal form (pdb: 1TIJ) HCC dimers present more elongated conformation than in cubic form (pdb:1G96).

This protein is also strictly related to the occurrence of one of the so-called conformational disease - the amyloidosis of the Iceland type. Mutational substitution of leucine to glutamine on position 68 causes protein oligomerization and deposition of amyloid fibrils.

Insoluble amyloid fibrils are found as deposits in patients with a range of diseases, *e.g.* Alzheimer disease, Parkinson disease, reactive amyloidosis, cystatin C amyloidosis, and the prionoses [3-5]. Knowledge of the molecular mechanism causing the transition of physiologically normal and soluble proteins to toxic oligomers and insoluble fibrils is essential for the development of treatment strategies for this group of common, but currently incurable, diseases.

SAXS measurements were performed on the X-33 EMBL beamline at DESY, Hamburg (Germany) using the Pilatus photon counting detector. Protein samples (2.9, 5.8 mg/ml) were measured in 50mM phosphate pH 6.7 buffer using synchrotron radiation (wavelength $\lambda = 0.15$ nm) at temperature 283 K. The sample-to-detector distance was 1.7 m, corresponding to the scattering vector range from 0.06 to 5.2 nm⁻¹ ($s = 4\pi \sin\theta/\lambda$ where 2θ is the scattering angle).

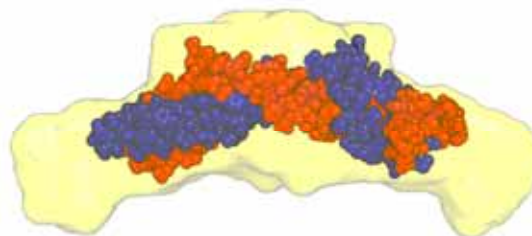


Figure 1. The low resolution model of human cystatin C in solution.

In this study we perform a small angle scattering experiment to probe the conformation and low resolution structure of HCC in solution. Using *ab initio* program DAMMIN we created low resolution 3D model of cystatin C in solution (Fig. 1). HCC form a dimer in solution with elongated conformation as in tetragonal crystal form.

Acknowledgements: The research was supported in part by research grant (No N N202 127237) from the Ministry of Science and Higher Education (Poland). The data collection was supported by European Community - EMBL Hamburg Outstation, contract number: RII3-CT-2004-506008.

References

- [1] R. Janowski, M. Kozak, A. Grubb, M. Abrahamson, M. Jaskolski, *Proteins Struct. Function Bioinform.* **61** (2005) 570–578.
- [2] R. Janowski, M. Kozak, E. Jankowska, Z. Grzonka, A. Grubb, M. Abrahamson, M. Jaskolski, *Nature - Struct. Biol.* **8** (2001) 316–320.
- [3] A.O. Grubb, *Adv. Clin. Chem.* **35** (2000) 63–99
- [4] J.N. Buxbaum, *Trends Biochem. Sci.* **28** (2003) 585–592.
- [5] M. Yamada, *Neuropathol.* **20** (2000) 8–22
- [6] D.I. Svergun, *Biophys. J.* **76** (1999), 2879–2886.

SAXS STUDIES OF DMPC AND DPPC-DIMERIC SURFACTANT LIPOPLEXES

Z. Pietralik¹, M. Taube¹, M. Balcerzak¹, A. Skrzypczak², and M. Kozak^{1*}

¹ *Department of Macromolecular Physics, Faculty of Physics A. Mickiewicz University, Umultowska 85, 61-614 Poznań, Poland*

² *Institute of Chemical Technology and Engineering, Poznan University of Technology, Marii Skłodowskiej-Curie 2, 61-542 Poznań, Poland*

Keywords: dimeric surfactants, lipid bilayers, SAXS

**) e-mail: mkozak@amu.edu.pl*

Dimeric surfactants are a new class of surfactants. They show significantly improved properties in comparison to conventional (monomeric) surfactants. The dimeric surfactants are characterised by critical micellization concentration (CMC) much lower than that of a classic (monomeric) surfactants with equivalent hydrophobic chain length. Dimeric surfactants are also a good surface tension reducers, much more efficient than the corresponding monomeric surfactants [1-3].

The aim of this study was to analyse the effect of different concentrations of dimeric surfactant on the disturbance or stabilisation of particular phases of phospholipids in its mixtures. The study was performed on 1,2-dimyristoyl-sn-glycero-3-phosphocholine (DMPC) and 1,2-dipalmitoyl-sn-glycero-3-phosphocholine (DPPC) and derivative of 1,1'-(alkyl)bis 3-alkyloxymethylimidazolium chloride.

A series of the SAXS data sets were collected in MaxLab, at Beam Line 7-11 (Lund, Sweden) [4]. The data were collected at temperatures from 6 to 30°C for DMPC and from 10 to 45°C for DPPC using the synchrotron radiation ($\lambda = 0.107$ nm) and the Mar 165 CCD detector. The scattering vector range was $0.05 < s < 3.42$ nm⁻¹.

All data sets were processed (normalized to the incident beam intensity, corrected for detector response and the scattering of the buffer was subtracted) using the computer programs BLI7-11 [4] and PRIMUS [5].

The SAXS results implied a gradual disappearance of the lamellar phase typical of DMPC and DPPC and a probable formation of the mixed liposomes. Also the temperature range of the main phase transition in DMPC was shifted towards lower temperatures.

Acknowledgements: The research was supported in part by research grant (No N N202 248935) from the Ministry of Science and Higher Education (Poland). The data collection in MaxLab has received funding from the European Community's Seventh Framework Programme (FP7/2007-2013) under grant agreement n° 226716.

References

- [1] R. Zana, "Dimeric and oligomeric surfactants. Behavior at interfaces and in aqueous solution: a review". *Adv. Colloid Interf. Sci.* **97** (2002) 205–253.
- [2] P. Tyagi, R. Tyagi, "Synthesis, structural properties and applications of gemini surfactants: A review", *Tenside Surfactants Detergents* **46** (2009) 373–382.
- [3] S.K. Hait, S.P. Moulik, "Gemini surfactants: A distinct class of self-assembling molecules", *Curr. Sci.* **82** (2002) 1101–1111.
- [4] M. Knaapila, C. Svensson, J. Barauskas, M. Zackrisson, S.S. Nielsen, K.N. Toft, B. Vestergaard, L. Arleth, U. Olsson, J.S. Pedersen, Y. Cerenius, "A new small-angle X-ray scattering set-up on the crystallography beamline I711 at MAX-lab", *J. Synchrotr. Radiat.* **16** (2009) 498–504.
- [5] P.V. Konarev, V.V. Volkov, A.V. Sokolova, M.H.J. Koch, D.I. Svergun, "PRIMUS: a Windows PC-based system for small-angle scattering data analysis", *J. Appl. Crystallogr.* **36** (2003) 1277–1282.

CHARACTERIZATION OF LuVO₄:Yb SINGLE CRYSTALS

O. Ermakova^{1*}, **W. Wierzchowski**², **K. Wieteska**³, **W. Graeff**⁴, **R.J. Iwanowski**¹,
H. Dąbkowska⁵, **M.H. Heinonen**⁶, **P. Romanowski**¹, **J. Bąk-Misiuk**¹, and **W. Paszkowicz**¹

¹ *Institute of Physics, Polish Academy of Sciences, Al.Lotnikow 32/46, PL-02-668Warsaw*

² *Institute of Electronic Materials Technology, Wólczynska 133, PL-01-919 Warsaw*

³ *Institute of Atomic Energy, PL-05-400 Otwock-Swierk, Poland*

⁴ *HASYLAB at DESY, Notkestr. 85, D-22603 Hamburg*

⁵ *Department of Physics, McMaster University, Hamilton, Ontario, L8S 4M1 Canada*

⁶ *Laboratory of Materials Science, Dept of Physics, University of Turku, Vesilinnantie 5, FI-20014, Turku, Finland*

Keywords: orthovanadate, lutetium, defect structure, electronic structure

**) e-mail: Ermak@ifpan.edu.pl*

Rare earth orthovanadates (RVO₄) have been reported to be applicable, in particular, as laser materials (see e.g. Ref. [1]), for remote thermometry, as catalysts etc. One of recently studied orthovanadates is LuVO₄, due to its optical properties (applicable in laser-diodes [2], optical waveguides [3]). These materials typically crystallize in zircon-type structure. For applications as a single crystal, the defect structure of such crystals has to be studied. Obtaining of defect and electron structure is important for modelling of material properties. Up to now, defect structure of RVO₄ single crystals has not been widely studied. LuVO₄:Nd and a GdVO₄ single crystals of >2 cm size were grown by Czochralski method [3,4], providing 200 rocking curve FWHM of 67 arcsec width; the observed defects included cracks, inclusions (due, in particular, to the interaction with Ir crucible), large voids, and dislocations. Czochralski-grown YVO₄ crystals of >5 cm size exhibit dislocations, glide bands, subgrain boundaries with misorientations of several up to 40 arcmin [5,6].

The needle-shaped (up to 1×2×12 mm³ size) crystals of LuVO₄ were grown from PbO/PbF₂ flux by the slow cooling method. Defect properties of LuVO₄:Yb were studied using x-ray topography and high resolution (HR) diffraction, electronic structure of crystal has been analyzed by x-ray photoelectron spectroscopy (XPS) method.

The examined LuVO₄:Yb crystal was built from two parts, a lighter (transparent) part and a darker part. The HR diffraction study was performed using the PHILIPS-MRD diffractometer equipped with Cu tube ($\lambda = 1.54056 \text{ \AA}$), a four bounce Ge(022) monochromator and a two bounce Ge(022) analyzer. The XPS spectra were recorded in the Perkin-Elmer 5400 ESCA spectrometer, with use of Mg K α (1253.6 eV) excitation mode. Projection reflection topographs were recorded at the F1 beamline (DORIS III, Hasylab).

The HR diffraction curves were obtained for the 002 reflection. The results show that two parts of crystal differed by defect structure: the light part is a true single crystal, whereas the dark part is built from several slightly misoriented blocks. The lattice parameter for light and dark parts is the same $a_{\perp} = 7.0244(2) \text{ \AA}$. The reflection topographs reveal the defect structure in the

vicinity of the (100) oriented crystal surface. A small part of the studied crystal is misoriented by several degrees. The kind of the contrast observed shows that the defects (dislocations or inclusions) are homogeneously distributed along the crystals.

The analysis of the acquired XPS spectra of LuVO₄:Yb showed that the shape of the V 2p spectrum closely resembles the relevant one of a V₂O₅ oxide. No line of the dopant could be detected. This also refers to a full consistency of their bond energies (of V 2p_{3/2} line) and spin-orbit splitting, Δ . Therefore, the bond energies of V 2p core-levels in LuVO₄ remain influenced only by oxygen ligand. The Lu 4f XPS spectrum absolutely dominates the valence band region built of O 2p states. Its shape exhibits close similarity to that of pure Lu. With the same value of spin-orbit splitting, its bond energy of 4f_{7/2} peak remains only shifted by 0.5 eV to higher values as a result of binding with oxygen ligand. This indicates strongly localized character of the Lu 4f level within the valence band.

References

- [1] A.I. Zagumenny, T.V.G. Ostroumov, I.A. Shcherbakov, T. Jensen, J.P. Meyen, G. Huber, "The Nd:GdVO₄ crystal: A new material for diode-pumped lasers", *Sov. J. Quantum Electron.* **22** (1992) 1071–1072.
- [2] L. Qin, X. Meng, J. Zhang, L. Zhu, H. Zhang, B. Xu, H. Jiang, "Growth and defects of Nd:GdVO₄ single crystal", *J. Cryst. Growth* **242** (2002) 183–188.
- [3] X.-L. Wang, K.-M. Wang, G. Fu, S.-L. Li, F. Chen, F. Lu, H.-J. Zhang, H.-K. Kong, J.-Y. Wang, X.-G. Xu, D.-Y. Shen, H.-J. Ma, R. Nie, "Optical planar waveguide fabricated in Nd:LuVO₄ crystal by MeV oxygen implantation", *IOptics Express* **13** (2005) 675–680.
- [4] S. Zhao, H. Zhang, Y. Lu, "Spectroscopic characterization and laser performance of Nd:LuVO₄ single crystal", *Optical Mater.* **28** (2006) 950–955.
- [5] K. Wieteska, W. Wierzchowski, E. Wierzbicka, A. Malinowska, M. Lefeld-Sosnowska, T. Lukasiwicz, W. Graeff, "X-Ray topographic studies of defect structure in YVO₄ crystals", *Acta Phys. Polon. A* **114** (2008) 455–461.
- [6] A. Malinowska, E. Wierzbicka, M. Lefeld-Sosnowska, K. Wieteska, W. Wierzchowski, T. Łukasiewicz, M. Swirkowicz, W. Graeff, "Defect structure formed at different stages of growth process in erbium, calcium and holmium doped YVO₄ crystals", *Acta Phys. Polon. A* **117** (2010) 328–331.

PHOSPHOLIPID/SURFACTANT BICELLAR PHASE STUDIED BY SAXS, FTIR AND DS

K. Szpotkowski, A. Wypych, S. Jurga, and M. Kozak *

*Department of Macromolecular Physics, Faculty of Physics, Adam Mickiewicz University,
Umultowska 85, 61-614 Poznań, Poland*

Keywords: phospholipids, bicellar phase SAXS, DS, FTIR

**) e-mail: mkozak@amu.edu.pl*

Discoidal (bicellar) phase represents intermediate morphology between lamellar and micellar phases. The bicelles are nanodiscs composed of mixture of phospholipids with short and long hydrophobic chains or mixture of phospholipid and surfactants. This phase exhibit the unique properties – very useful in the structural studies of membrane proteins or as a model of biomembranes [1].

Water suspensions of 1,2-dimyristoyl-sn-glycero-3-phosphocholine (DMPC) and 1,2-dipalmitoyl-sn-glycero-3-phosphocholine (DPPC) with different concentrations of the dimeric surfactant GEM-1K1 have been investigated by Small Angle X-ray Scattering (SAXS), Dielectric Spectroscopy in radiofrequency range (DS) and Fourier Transform Infrared Spectroscopy (FTIR).

The SAXS results exhibit that even at very low concentration of the surfactant the transition from lamellar phase to the bicellar phase is realized. The size of bicelles depends on the surfactant concentration.

Dielectric spectroscopy in frequency range from 10^6 Hz to 10^9 Hz was used to study a polar part of phospholipids. The observed small step in the dependence of dielectric constant vs. temperature is connected with a transition from gel to liquid crystalline phase, in accordance with temperature dependencies of

the stretching bands of phosphate and carbonyl groups detected by FTIR. Two characteristic bands from IR spectra, corresponding to symmetric and antisymmetric vibrations of methyl groups, were used to detect changes in the non-polar part of phospholipids bilayer.

Our results show, that the temperatures of the observed main- and pre-transitions' decrease with an increase of the surfactant concentration.

Acknowledgements: The research was supported in part by research grant (No N N202 248935) from the Ministry of Science and Higher Education (MSHE) Poland. A. Wypych expresses her appreciation to the MSHE for a Postdoctoral Fellowship (POL-POST III). The data collection at DESY Hamburg was supported by Integrating Activity on Synchrotron and Free Electron Laser Science to the EMBL Hamburg Outstation, contract number:RII-CT-2004-506008.

References

- [1] C.R. Sanders, R.S. Prosser, "Bicelles: a model membrane system for all seasons?", *Structure* **6** (1998) 1227–1234.
- [2] R. Koynova, M. Caffrey, "Phases and phase transitions of the phosphatidylcholines", *BBA-Rev Biomembranes* **1376** (1998) 91–145.
- [3] J. Katsaras, T.A. Harroun, J. Penczer, M.P. Nieh, "Bicellar" lipid mixtures as used in biochemical and biophysical studies", *Naturwiss.* **92** (2005) 355–366.

SOLUTION SCATTERING STUDIES OF HUMAN CYSTATIN C MUTANTS

M. Taube¹, **Z. Pietralik**¹, **A. Szymańska**², and **M. Kozak**^{1*}

¹ *Department of Macromolecular Physics, Faculty of Physics, A. Mickiewicz University, Umultowska 85, 61-614 Poznań, Poland*

² *Department of Medicinal Chemistry, Faculty of Chemistry, University of Gdańsk, Sobieskiego 18, 80-952 Gdańsk*

Keywords: human cystatin C, SAXS, low resolution structure

**) e-mail: mkozak@amu.edu.pl*

Human cystatin C (HCC) is a cysteine protease inhibitor which, in pathological conditions, undergoes dimerization *via* domain swapping. HCC point mutation Leu68Gln is responsible for occurring of hereditary amyloid angiopathy. The symptoms of this disease includes cerebral hemorrhage, stroke, and dementia as a result of amyloid deposition within arteries in the brain [1].

On the molecular level the crucial step in amyloid formation is dimerization of cystatin C. In this process the monomeric cystatin C molecule partially unfolds and, after exchanging of N-terminal domains, forms a dimer with another cystatin molecule. As a result, new β -sheet structure, consisting of residues Ile56 -Gly59 corresponding to loop L1 in the monomeric molecule is formed between two distinct chains.

Unwinding of L1 is the most pronounced structural change in HCC structure occurring as a result of dimerization because swapped domains reconstitute monomer structure. Circular dichroism and molecular dynamics studies indicate that valine exchange for proline may destabilize the structure of L1 loop while asparagine and aspartic acid may favor more stable conformation [2].

In this study we have performed a small angle scattering experiments on HCC mutants Val57Pro, Val57Asn, Val57Asp to probe the effect of these mutations on cystatin C structure in solution. SAXS measurements were performed on the X-33 EMBL beamline at DESY, Hamburg (Germany) using the Pilatus photon counting detector [3]. On the basis of scattering curve we have determined low resolution structures of Val57Asn and Val57Asp using *ab-initio* modeling software DAMMIN [4].

Val57Pro mutant in solution rapidly forms oligomers in contrast to two other mutants. Val57Asn and Val57Asp have elongated conformation similar to the wild type dimers and undergo slow oligomerization.

Acknowledgements: The research was supported in part by research grant (No N N202 127237) from the Ministry of Science and Higher Education (Poland). The data collection

was supported by European Community - EMBL Hamburg Outstation, contract number: RI13-CT-2004-506008.

References

- [1] A.O. Grubb, *Adv. Clin. Chem.* **35** (2000) 63–99.
- [2] S. Rodziewicz-Motowidło, R. Sosnowska, J. Iwaszkiewicz, P. Juszczyk, E. Sobolewski, A. Szymańska, K. Stachowiak, A. Liwo, *Biopolymers* **91** (2009) 373-383.
- [3] M.W. Roessle, R. Klaering, U. Ristau, B. Robrahn, D. Jahn, T. Gehrmann, P. Konarev, A. Round, S. Fiedler, C. Hermes, D.I. Svergun, *J. Appl. Crystallogr.* **40** (2007) 190-194.
- [4] D.I. Svergun, *Biophysics J.* **76** (1999) 2879-2886.

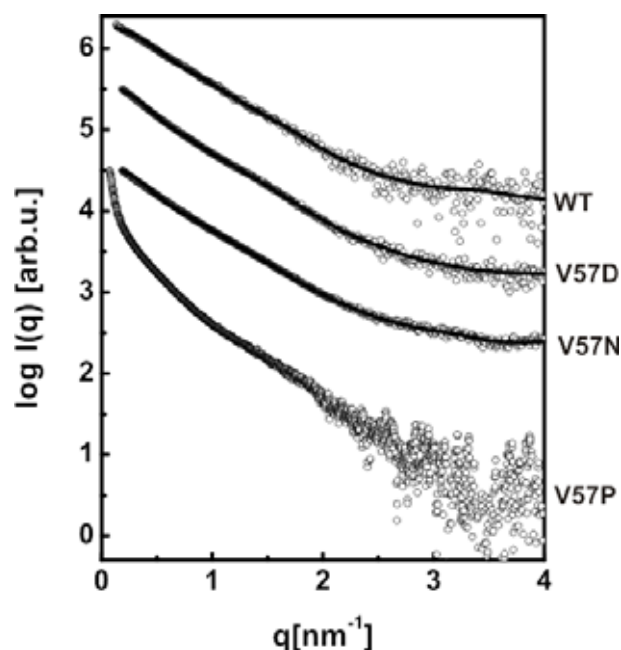


Figure 1. Small angle X-Ray scattering curves (black circles) recorded for wild type (WT) and various Val57 mutants together with fit from models generated by *ab initio* modeling program DAMMIN (black lines).

HIGH-PRESSURE DIFFRACTION STUDY OF SELECTED FOUR-COMPONENT SYNTHETIC GARNETS

E. Werner-Malento^{1*}, **R. Minikayev**¹, **C. Lathe**^{2,3}, **H. Dąbkowska**⁴, and **W. Paszkowicz**¹

¹*Institute of Physics, Polish Academy of Sciences, Al. Lotników 32/46, 02-668 Warsaw, Poland*

²*HASYLAB am DESY, Notkestrasse 85, D-22603 Hamburg, Germany*

³*GFZ German Research Centre for Geosciences, Dept. 5, Telegraphenberg, Potsdam, D-14473, Germany*

⁴*Department of Physics, McMaster University, Hamilton, Ontario, L8S 4M1 Canada*

Keywords: garnet, equation of state, high-pressure diffraction, bulk modulus

**) e-mail: ewerner@ifpan.edu.pl*

The synthetic garnets exhibit physical properties that may lead to various applications. These materials are characterized by low thermal conductivity [1] and by Mohs hardness between 6.5 and 8.5. The garnets containing *e.g.* Fe or Mn as components exhibit anti-ferromagnetic properties [2]. Some of these materials (for example, gadolinium gallium garnet – GGG) can be used for substrates for epitaxy of superconducting films [3]. The garnet-based single crystal films, grown on the garnet substrates (*e.g.* $Y_3Al_5O_{12}$) can be used as scintillation detectors [4]. The doped garnets are applied in solid-state lasers [5], also they can be used as optical high-pressure sensors [6,7]. Elastic properties of garnets (hardness, bulk modulus) are of interest from the point of view of Earth science, because minerals of garnet structure are considered as one of major components of the deep interior of the Earth [8].

Bulk moduli of synthetic three-component garnets are relatively high, for example that for gadolinium gallium garnet equals $K_0 = 169(15)$ GPa [9]. Those for four-component garnets (chemical formula $X_3Y_2Z_3O_{12}$, with divalent X, trivalent Y, and tetravalent Z cations, for example: $Ca_3Fe_2Ge_3O_{12}$, or with trivalent cations, *e.g.* $Gd_3Sc_2Al_3O_{12}$) remain unknown, giving a motivation for the present study.

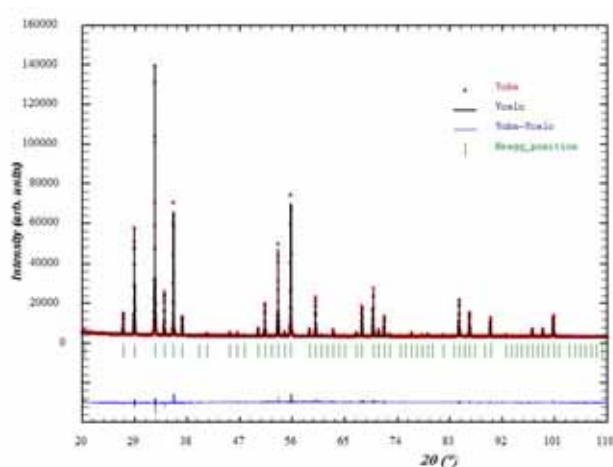


Figure 1. Rietveld refinement plot of the calcium iron germanium garnet (21°C, ambient-pressure data). The lattice parameter for the sample studied is 12.3288(2) Å.

The $Ca_3X_2Ge_3O_{12}$ garnets, where X = Fe, Ga, were characterized at the ambient pressure by X-ray diffraction using a Philips X'pert MRD diffractometer (an example is shown in Fig. 1). The *in-situ* X-ray diffraction experiments were conducted using the energy-dispersive method at the F2.1 beamline equipped with a large-anvil diffraction press, MAX80. The pressures ranging to 8.7 GPa were calibrated using a NaCl equation of state. Lattice parameters of garnets were determined from Le Bail refinements performed with Fullprof2k program.

The analysis of the data collected for the measured garnets shows that their crystal structure is conserved in the studied pressure range. The bulk moduli obtained by fitting the Birch–Murnaghan (BM) equation of state (EOS) are found to be comparable with the values of some other members of the garnet family.

References

- [1] N.P. Padture, P.G. Klemens, "Low thermal conductivity in garnets", *J. Am. Ceram. Soc.* **80** (1996) 1018-1020.
- [2] R. Plumier, D. Estève, "Reinvestigation of the magnetic structure of $Ca_3Mn_2Ge_3O_{12}$ ", *Solid State Comm.* **31** (1979) 921–925.
- [3] P. Mukhopadhyay, "High-Tc films on GGG substrates", *Supercond. Sci. Technol.* **7** (1993) 298–299.
- [4] Yu. Zorenko, I. Konstankevych, M. Globus, B. Grinyov, V. Lyubinskiy, "New scintillation detectors based on oxide single crystal films for biological microtomography", *Nucl. Instrum. Meth. Phys. Res. A* **505** (2003) 93–96.
- [5] M.I. Belovolov, S.I. Derzhavin, D.A. Mashkovskii, K.S. Salnikov, "Diode-pumped solid-state Nd^{3+} : $Ca_3Ga_2Ge_3O_{12}$ crystal lasers", *Quantum Electron.* **37** (2007) 753–759.
- [6] J. Liu, Y.K. Vohra, "Sm:YAG optical pressure sensor to 180 GPa: Calibration and structural disorder", *Appl. Phys. Lett.* **64** (1994) 3386–3388.
- [7] S. Kobyakov, A. Kamińska, A. Suchocki, D. Galanciak, M. Malinowski, " Nd^{3+} -doped yttrium aluminum garnet crystal as a near-infrared pressure sensor for diamond anvil cells", *Appl. Phys. Lett.* **88** (2006) 234102.
- [8] S. Karato, Z. Wang, B. Liu, K. Fujino, "Plastic deformation of garnets: systematics and implications for the Rheology of the mantle transition zone", *Earth Planet. Sci. Lett.* **130** (1995) 13–30.
- [9] A. Durygin, V. Drozd, W. Paszkowicz, E. Werner-Malento, R. Buczek, A. Kamińska, S. Saxena, A. Suchocki, "Equation of state for gadolinium gallium garnet crystals: Experimental and computational study", *Appl. Phys. Lett.* **95** (2009) 141902.

SAXS STUDIES OF $\text{Fe}_3\text{O}_4/\text{SiO}_2$ NANOPARTICLES FOR NANOSENSING

M. Taube¹, M. Hilgendorff², Z. Pietralik¹, M. Giersig², and M. Kozak^{1*}

¹ Department of Macromolecular Physics, Faculty of Physics, A. Mickiewicz University, Umultowska 85, 61-614 Poznań, Poland

² Department of Physics, Freie University Berlin, Arnimallee 14, 14195 Berlin, Germany

Keywords: magnetic nanoparticles, SAXS, nanosensor

*) e-mail: mkozak@amu.edu.pl

Magnetic nanoparticles have been proposed for use as biomedical devices to a large extent for several years. Recently, nanotechnology has developed to a stage that makes it possible to produce, characterize and specifically tailor the functional properties of nanoparticles for various applications. In this lecture we will discuss magnetic nanoparticles before and after their surface modification. The magnetic nanoparticles $\text{Fe}_3\text{O}_4/\text{SiO}_2$ consist of a magnetic core (Fe_3O_4) and SiO_2 shell. These nanoparticles can be manipulated using magnetic fields and therefore they possess attractive properties for biomedical [1,2] and magnetic resonance imaging [3] applications.

SAXS data were collected on the I7-11 beamline at Maxlab, Lund (Sweden) using the Mar 165 CCD detector. Nanoparticle and nanoparticle/DMPC samples were measured in water or 50 mM phosphate pH 6.7 buffer using synchrotron radiation (wavelength $\lambda = 0.107$ nm) at temperature 288 K. The sample-to-detector distance was 1.76 m, corresponding to the scattering vectors range of 0.05 to 3.42 nm^{-1} . All data sets were processed (normalized to the incident beam intensity, corrected for detector response and the scattering of the buffer was subtracted) using the computer programs BL 7-11 [4] and PRIMUS [5]. The pair distance distribution function $p(r)$ was evaluated using GNOM [6].

The values of radii of gyration R_G characterizing the nanoparticles varied from 11.7 to 12 nm and D_{max} was about 34 nm. In mixtures of nanoparticles with biomembrane model systems based on DMPC, the scattering pattern characteristic for the lamellar phase of phospholipids was observed. The incorporation of nanoparticles has not induced phase transition in phospholipid systems.

Acknowledgements: The research was supported in part by research grant (No N N202 127237) from the Ministry of Science and Higher Education (Poland). The data collection in MaxLab has received funding from the European Community's Seventh Framework Programme (FP7/2007-2013) under grant agreement n° 226716.

References

[1] M. Hilgendorff, M. Giersig, Magnetic nanoparticle superstructures, *Eur. J. Inorg. Chem.* **18** (2005) 3571–3583.

- [2] Q.A. Pankhurst, N.K.T. Thanh, S.K. Jones, J. Dobson, "Progress in applications of magnetic nanoparticles in biomedicine", *J. Physics D-Appl. Phys.* **42** (2009) Art. N° 224001.
- [3] P.T. Narasimhan, R.E. Jacobs, "Microscopy in magnetic resonance imaging", *Ann. Rep. NMR Spectrosc.* **55** (2005) 259–297.
- [4] M. Knaapila, C. Svensson, J. Barauskas, M. Zackrisson, S.S. Nielsen, K.N. Toft, B. Vestergaard, L. Arleth, U. Olsson, J.S. Pedersen, Y. Cerenius, "A new small-angle X-ray scattering set-up on the crystallography beamline I711 at MAX-lab", *J. Synchrotr. Radiat.* **16** (2009) 498–504.
- [4] P.V. Konarev, V.V. Volkov, A.V. Sokolova, M.H.J. Koch, D.I. Svergun, "PRIMUS: a Windows PC-based system for small-angle scattering data analysis", *J. Appl. Crystallogr.* **36** (2003) 1277–1282.
- [5] D.I. Svergun, "Determination of the regularization parameter in indirect-transform methods using perceptual criteria", *J. Appl. Crystallogr.* **25** (1992) 495–503.

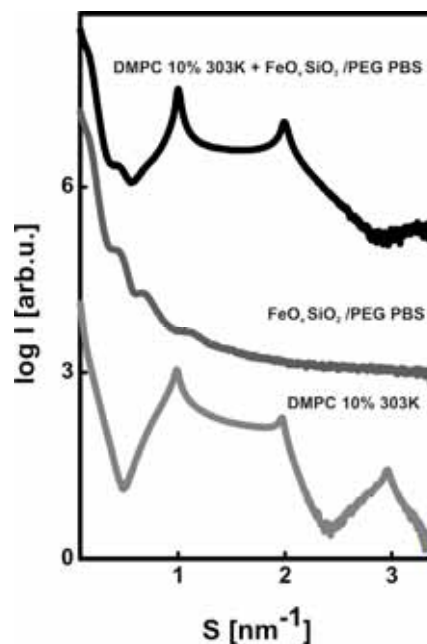


Figure 1. Small angle X-ray scattering curves of magnetic nanoparticles and their mixtures with DMPC.

MAPPING THE PROTEIN WORLD: OVER 1500 BIOMOLECULAR STRUCTURES SOLVED ON-LINE AT EMBL-HAMBURG

Victor Lamzin

EMBL-Outstation c/o DESY Hamburg, Germany

Keywords: protein, diffraction, biomolecular structure

Macromolecular structure determination is an important task in biology because of the intimate relation between the structure and function of biological molecules. This requires good quality X-ray diffraction data and is itself a complex and a multi-step computational process. Several structure-determination software pipelines have been assembled worldwide with different goals and degrees of

built-in automation. However, the best validation of an X-ray diffraction experiment is the arrival at an interpretable density map and a partial structure in a short period of time, ideally during or just after the data collection. Such on-line data evaluation pipeline, Auto-Rickshaw, has been developed at EMBL-Hamburg and has helped to determine over 1500 novel protein structures.

CHALLENGES IN X-RAY OPTICS FOR MODERN X-RAY SOURCES

J. Härtwig *

European Synchrotron Radiation Facility, 6 rue Jules Horowitz, 38360 Grenoble, France

Keywords: X-ray optics, focussing, heat load, X-ray topography, diamond

*) e-mail: haertwig@esrf.fr

The recently launched ESRF upgrade programme 2009–2018 requires a strong, coordinated development program for X-ray optics. High quality X-ray optical systems are critical enabling technologies for delivering appropriately conditioned beams to the end-stations at new and refurbished beamlines (Fig. 1).

Four key aspects drive the new optics instrumentation development:

- Management of the increased heat load and power density on the optical elements due to brilliance and flux improvements,
- Micro- and nano-focusing,
- Beam stability,
- Preservation of wavefront form, coherence properties, beam homogeneity.

High heat load monochromators based on crystals (silicon and diamond) and on wide band-pass

monochromators based on multilayers will represent a direction of strong development.

The various experimental stations need/demand beam dimensions ranging from decimetre size to nanometre size. The upgrade programme aims in particular at improving the focusing capabilities of elements such as mirrors, multilayers, zone plates, and refractive lenses in order to reach the 10nm spot size limit.

To carry out experiments with nanometre sized beams, not only suited optical elements must be available. An environment with high mechanical stability, low temperature fluctuations and low vibration levels will be necessary, including feed back systems using X-ray beam position monitors for white and monochromatic beams.

The quality of the optical elements has to be such that they degrade the beam quality as little as possible.

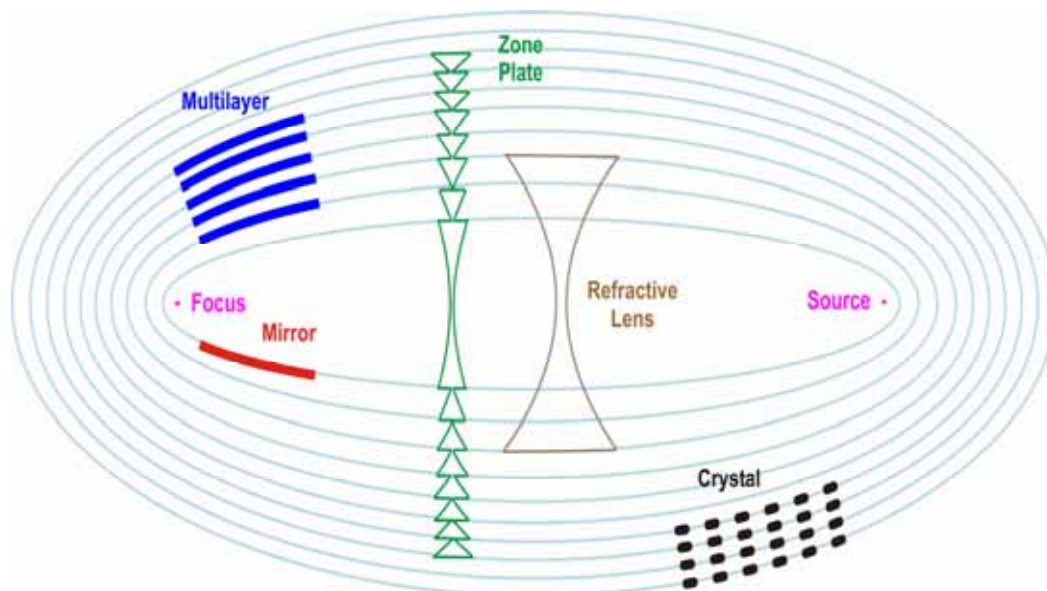
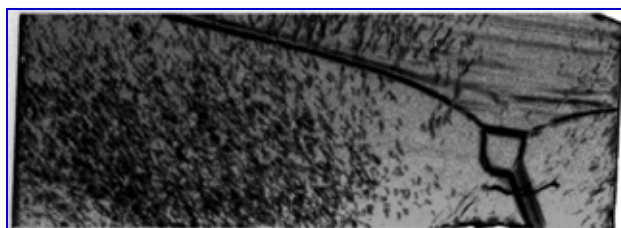
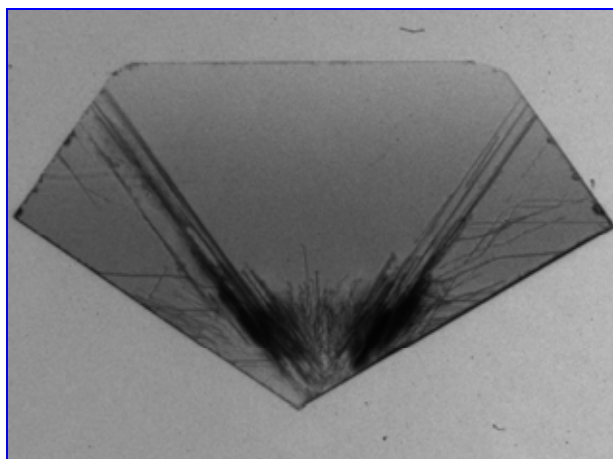


Figure 1. Schematic illustration of various X-ray optical elements for 3rd generation synchrotron beamlines. The upgrade programme aims at improving the focusing capabilities of elements such as mirrors, multilayers, zone plates, and refractive lenses in order to reach the 10 nm spot size limit. High heat load monochromators based on crystals and on multilayers will represent a second direction of strong development



a



b

Figure 2. Comparison of an X-ray topograph of an old, long time ago installed beam splitter out of nitrogen rich type Ib material (a) with an example of a new high quality plate (b).

The lateral (horizontal) dimension of the crystal in (a) is about 5 mm and that in (b) about 11 mm.

Synthetic single-crystalline HPHT-diamond is in principle the best-suited material for Bragg diffracting X-ray optical elements like beamsplitters or monochromators to be used in modern, powerful X-ray sources. Already in the early days of the 3rd generation sources the utilisation of diamonds was discussed, tested and X-ray optical elements were realised. However, a

real break through in their application was not reached. The main reasons were, (and partly still are) by comparison with silicon, the low quality (bulk and surface), the limited availability and the small dimensions of the available material.

Since then a substantial effort was undertaken (and needs to be continued) in the fields of crystal growth, crystal processing and crystal characterisation to develop a high-quality diamond material is needed that combines the extremely high perfection of the crystal bulk with an excellent surface finish [1]. With regard to the quality of the crystal bulk, selected samples became available that locally may be dislocation free, with a very low level of local residual strain. However, at the moment the surface quality appears to be the most critical point to both achieve and study.

High quality type IIa (very low nitrogen impurity concentration) HPHT Diamond plates were investigated with white beam X-ray topography and in particular with high strain sensitive non-dispersive double crystal topography [2]. The results showed and confirmed the excellent local quality of present (selected) plates. This means that they contained large (for diamond) dislocation free regions and an extremely low residual strain level in the range below several 10^{-8} . This is a local strain level like in FZ silicon.

References

- [1] R.C. Burns, A.I. Chumakov, S.H. Connell, D. Dube, H.P. Godfried, J.O. Hansen, J. Härtwig, J. Hozzowska, F. Masiello, L. Mkhonza, M. Rebak, A. Rommeveaux, R. Setshedi, P. Van Vaerenbergh, "HPHT – growth and X-ray characterisation of high-quality type IIa diamond", *J. Phys.: Condens. Matt.* **21** (2009) 364224–1–14.
- [2] R.C. Burns, A. Chumakov, G. Carbone, S.H. Connell, D. Dube, H.P. Godfried, J.O. Hansen, J. Härtwig, F. Masiello, M. Rebak, A. Rommeveaux, R. Setshedi, P. Van Vaerenbergh, A. Gibaud, "Diamonds for X-ray optical applications at 3rd and 4th generation X-ray sources", *Proc. of SPIE Vol.* **6705** (2007) 67050K1–6.

Subject index

activated carbons	105	DNA	47	high-resolution ARPES	48
adenine	132	dopant	91	high-resolution	134
alkali metal	66	DOS	138	spectroscopy	
amorphous materials	111	drug design	17	HRXRD	90, 95,
angiogenesis	22	DS	153		112
angle resolved	81	E-beam	94	human cystatin C	150, 154
photoemission		electrochemical system	2	hydrides	130
spectroscopy		electrodeposition	148	imaging	43
annealing	88	electron spectroscopy	87	implantation	88, 96,
apatite	64	electron-density radial-	61, 116		97, 126,
atherosclerosis	114	distribution function			128
atomic layer deposition	99	electron-density radial-	116	infrared	43
atomic position	85	distribution function		inhibitor of TS	121
modulation		electronic structure	152	insertion device	75
avian magnetometer	2	electropolymerisation	139	in-vivo study	2
system of birds		emittance	51	ionic conductivity	122
azomethine ligands	98	EO-sampling	24, 84	ionomer	102
band structure	52	epilayer	90	iron	103, 114
battery	22	equation of state	155	irradiation	147
beamline	50, 71,	ERL	24, 84	IV-VI crystal	93
	74, 76,	EXAFS	91, 111,	IV-VI semiconductor	52, 92
	133, 134		118, 126,	laser ablation	142
		fast chemical reaction	130, 135	laser alignment	24, 84
beamline productivity	42	Fe nanostructure	58	laser processing	142
beryllium	81	Fe(110)/W(110)	72	laser shaping	24, 84
bicellar phase	153	Fe ₄ complex	86	lattice misfit	90
biomolecular structure	87, 157	ferroelectric	2	Laves phase	130
blends	102	ferromagnetism	125	layered double hydroxide	146
boracite	125	FLASH irradiation	88	(LDH)	
boron nitride	145	fluorescence	73	lead apatite	110
Brill transition	149	fluorescence lifetime	132	lipid bilayer	151
bulk modulus	80, 137,	fluorescence lifetime	132	liquid state	61
	155	focussing	158	low resolution structure	150, 154
cadmium oxide	147	free electron laser	2	LPE	95
calcium	114	freezing criterion	68	lutetium	152
CdSe	118	FTIR	153	macromolecular model	17
chemical composition	112	FT-IR microspectroscopy	2	magnesium	141
close-packed structure	66	fuel cell	2	magnetic alloy	120
cluster	82	gallium arsenide	45, 73,	magnetic molecule	2
collective diffusion	68		91	magnetic moments	85
colloid crystal	68	GaMnSb	101	modulation	
colossal magnetoresistive	108	GaN	90	magnetic nanoparticle	156
perovskites		garnet	155	magnetic properties	101
Compton profile	141	GaSb	96, 128	magnetism	72, 86,
copper	114	genetic algorithm	24, 82,		103
crystal structure	78, 121		83, 84	magnetoelastic coupling	85
crystal structure analysis	67	geometrical confinement	66	malaria	107
crystallographic unit cells	64	GEXRF	115	malarial pigment	107
crystallography	47	GGG	155	manganese	88
cyclohexane derivative	116	GGG films	95	manganite	85
DAFS	118	GISAXS	97	many-body interactions in	48
defect structure	152	glioma circulation	22	solids	
deformation field	73	global optimization	82	material modification	142
density functional theory	105	gold	113	matrix isolation	132
diamond	2, 158	gold surface	2	maximum entropy	141
diffraction	87, 96,	grazing incidence	58	method	
	125, 157	hard X-ray optics	2	metaheuristics	24, 84
dimeric surfactant	151	hBN	145	metal chelate	98
disorder	125	heat load	158	metal cluster	65
disulfiram	94	hemozoin	107	metallic glass	111
DLVO potential	68	heterostructure	112	micro x-ray fluorescence	115
		high pressure	80, 145	micro-fluorescence	79, 133
		high-pressure diffraction	155	microprobe	71

microscopy	43, 87,133	QCL	112	synchrotron	42, 50, 71, 75, 76, 97
MnSb inclusion	56	quantum dots	118	synchrotron design	74
MOCVD	90	quaternary structure	59	synchrotron diffraction	66, 88
modulated crystal	67	radiation damage	90	table-top source	2
molecular dynamic	105, 121	radiation sterilization	94	tellurium	91
momentum density	141	Raman microscopy	64	thermal decomposition	146
Monte-Carlo simulation	117	rare earth	80	thin film	78, 120
mouse	114	rare earth alloys	106	thymidylate synthase (TS)	121
muscle	60, 70	rare earth compounds	106	time-resolved experiment	2
myosin	60	rare-earth	62	transcription regulation	47
myosin motor	70	RBS	90	twin structure	122
N(4)-OH-dCMP	121	reaction mechanism	44	TXRF	115
nano-chromium	148	reactivity	44	ultrathin film	103
nanocomposite	144	remote experiment	59	valence band structure	54, 106
nanocrystal	135	resonance photoemission	106	vicinal surface	81
nanoparticle	113	resonant photoemission spectroscopy	99	Waren-Averbach method	148
nanoporous glass	66	ribosome structure	17	wavelength-dispersive spectroscopy	79, 117, 133
nanoscale	82	Rietveld refinement	110	WAXD	149
nanosensor	156	RIXS	62	WAXS	102
nanowire	82, 45	RNA	47	X ray diffraction	101
NEXAFS	147	samarium	137	XAFS	98, 125, 128
nickel	140	SAXS	102, 150, 151, 153, 154, 156	XANES	108,138
nuclear inelastic scattering	86	scanning tunneling microscopy	82	XFEL	24
nuclear resonant scattering	72, 86, 103	self-assembly	58	XMCD	56, 126
nylon 6	149	semiconductor surface	82	X-ray	88, 96
organic thin films	65	shape anisotropy	56	X-ray absorption spectroscopy (XAS)	44, 62, 107, 113, 120, 140
orthovanadate	80, 137, 152	Si:Mn	88	X-ray diffraction	45, 70, 73,105, 116, 142, 146
oxide materials	106	silicon	73, 88, 97, 126	X-ray diffraction topography	95
p-doping	46	single cells	2	X-ray fluorescence	64
PEO	102	single molecular magnet	2	x-ray imaging	79, 133
perovskite	85	small angle scattering	58	X-ray microfluorescence	77
PETRA III	2	small angle x-ray scattering	139	X-ray microscopy	69, 77
phase transition	80, 125, 137	smectite	69	X-ray optics	158
phospholipids	153	solid electrolyte	122	X-ray photoelectron spectroscopy	54
phosphorus	2, 114	solid phase microextraction	139	x-ray resonant inelastic scattering	134
photo-cathode	24, 84	solid solution	110	x-ray scattering	59, 97
photoelectron spectroscopy	52	solid state	94	X-ray spectromicroscopy	77
photoemission	108	solid state chemistry	44	X-ray standing waves	54
photoemission spectroscopy	65, 92, 92	spectroscopy	46	X-ray topography	158
plant cells	2	spectroscopy	62, 76	XSW imaging	54
Polish Light Source	1, 75	spinel	140	XUV free electron laser	142
polycapillary	117	spintronics	96	zinc	114
polymorphism	149	SQUID	88	zinc oxide	46, 99, 135
polyvinylpyrrolidone	144	stability	51		
powder diffraction	135, 148	standard sample	115		
pressure	137	storage ring	51		
pressure medium	145	structural biology	4, 42		
prostate cancer	138	structural genomics	17		
protein	87	structure	105, 125		
protein	42, 47, 157	sulphur	138		
protein crystallography	4,17	surface phase transition	83		
		surface X-ray diffraction	83		

Authors index

M. Amati	87	D. Carstanjen	47	L. Geelhaar	45	Cz. Kapusta	108
H. Amenitsch	58	Y. Cerenius	50, 137	A. Ghaffar	66	D. Karnaushenko	65
A. Andrejczuk	141	J. Chalupský	142	P. Ghigna	44	Z. Kaszukur	135
A. Antonowicz	91	R. Chałas	64	A. Gianoncelli	77	B. Kaulich	77
J. Antonowicz	111	A.A. Chernyshov	125	M. Giersig	156	M. Kavčič	134
K. Appel	114	M. Chernyshova	147	P. Glatzel	62	Y. Kayser	79, 117
D. Arvanitis	126	S. Chłopicki	114	A.J. Gleeson	142	Y. Kayser	117
R. Bacewicz	91, 111	M. Cholewa	71	A. Gloskovskii	54	M. Kazemian	87
J. Bak-Misiuk	88, 96, 97, 101, 152	P. Cierniak	86	B. Goderis	149	Abyaneh	
T. Balasubramanian	81	J. Cihelka	142	M. Godlewski	99	A.R. Khorsand	142
T. Balcer	73	C.V. Ciobanu	82	J. Goraus	140	A. Kiersnowski	144
M. Balcerzak	151	M. Cotte	79, 133	E. Görlich	76	A. Kisiel	138
A. Balerna	138	J. Czaplá	138	E.A. Görlich	1, 74	M. Kiskinova	77, 87
A. Banaś	114	F. d'Acapito	118	T. Goryczka	140	A. Kita	140
D. Banaś	117	M.M. Dalmiglio	87	G. Goryl	81	J. Klasa	110
K. Banaś	114	J. Darul	145, 146	P. Goryl	75	M.T. Klepka	56, 126, 128, 130
M. Basiura-Cembala	149	Z. Dauter	4	J. Gosk	56	D. Klinger	73, 142
S. Bernstorff	97	A. Davydok	45	W. Graeff	152	W. Knoff	52
M. Bieringer	85	H. Dąbkowska	137, 152, 155	S. Grebinskij	106	A. Kołodziejczyk	108
A. Biermanns	45	I.N. Demchenko	147	L. Gregoratti	87	B. König	47
U. Bismayer	122	J.D. Denlinger	147	A. Grubb	150	J. Konior	138
Z. Błaszczak	61, 116	G. Derkachov	147	A. Gust	118	K. Kopalko	99
D.S. Bohle	107	K. Dettlaff	94	E. Guzewicz	99	J. Korecki	72, 86, 103
B. Bojanowski	137	L. Dobrzyński	141	J. Hajdu	142	A. Kosar	107
V. Bondarenka	106	J. Domagala	101	V. Hájková	142	K. Kosiel	112
O. Borkiewicz	110	V. Domukhovski	93	J. Härtwig	158	R. Kostogrys	114
F. Bottin	54	J.C. Dore	105	S. Hau-Riege	142	A. Kotani	62
M. Brancewicz	141	J.-Cl. Dousse	79, 117	L. Hawelek	105	M. Kowalik	108
W. Braun	65	A. Dowierciał	121	U. Heinemann	47	J. Kowalska	114
S. Breuer	45	H. Drozdowski	61, 116	M.H. Heinson	152	B.J. Kowalski	52, 76, 92, 93
A. Brodka	105	W. Drube	54, 92, 93	O. Hemmers	147	M. Kozak	94, 139, 150, 151, 153, 154, 156
E. Brunello	70	P. Dubček	97	R. Hempelmann	148	B. Kozankiewicz	142
K. Bučar	134	H. Duda	140	M. Hilgendorff	156	A. Koziół	103
M. Bugajski	112	M. Dušek	67	P. Hoffmann	46	G. Krexner	66
M. Bukowski	148	E. Dynowska	78, 96, 101	V. Holý	118	H. Kröncke	118
A. Burian	105	P. Dziawa	92	D. Hommel	118	K. Królas	1, 74
T. Burian	142	D. Einfeld	51	V. Honkimaki	105	M. Krupinski	120
A.S. Burlov	98	M. Eriksson	75	J. Hoszowska	79, 117	C. Kruse	118
W. Bury	135	O. Ermakova	152	M. Irving	60, 70	J. Krzywinski	142
B. Buszewski	139	J. Falta	118	T.C. Irving	70	A. Kubala-Kukuś	115, 117
S.M. Butorin	62	R. Fenger	113	J. Ivančo	65	A. Kuczumow	64
P. Caban	90	S. Filipek	130	R.J. Iwanowski	152	A. Kulik	96
W. Caliebe	88, 96, 101, 142	A.N. Fitch	148	P. Jagodzinski	79, 117	M. Kulik	128
I. Capan	97	J. Flis	110	R. Jakiela	128	K.O. Kvashnina	62
S. Carlson	137	K. Freindl	72, 86	A. Jarmuła	121	W.M. Kwiatek	138, 114
		R.L. Frost	69	M. Jaskólski	4, 17, 28	A. Kwiatkowski	56, 101
		L. Fusi	70	K. Jaśkiewicz	144	V. Lamzin	157
		J. Gaca	90, 112	I. Jendrzewska	140	E. Lanka	47
		M. Gajda	114	V. Joco	81, 83	C. Lathe	145, 155
		J. Gapiński	68	R.L. Johnson	93, 106		
		A.D. Garnovskii	98	L. Juha	142		
		K. Gas	92, 93	M. Jurek	142		
				S. Jurga	153		
				S. Kaprzyk	141		

K. Lawniczak-Jablonska	34, 56, 107, 126, 128, 130, 147	A. Patkowski	68	A. Sienkiewicz	107	H. Tvardauskas	106
T.-L. Lee	54	C. Paulmann	122	M. Sikora	107, 108	A. Twardowski	56
J. Lewiński	135	K. Pagowska	90	A. Skrzypczak	151	T. Tyliczszak	147
M. Linari	70	J. Pełka	73, 78, 92, 142	K. Sliuziene	106	A.I. Uraev	98
V. Lissauskas	106	M. Perzanowski	120	W. Sławiński	85	M.A. Valbuena	81
J.A. Litwin	114	V. Petříček	67	T. Słupiński	91	I.S. Vasilchenko	98
V. Lombardi	60, 70	C. Pettenkofer	46	R. Sobierajski	34, 73, 142	B. Vengalis	106
R. London	142	G. Piazzesi	60, 70	K. Sokolowski-Tinten	142	V.G. Vlasenko	98
M. Lukasiewicz	99	W. Pichl	66	K. Sokolowski	135	L. Vyšín	142
K.A. Lyssenko	125	A. Pietnoczka	91, 111	I. Sosnowska	85	H. Wabnitz	142
A. Łusakowski	52	Z. Pietralik	150, 151, 154, 156	D. Speaks	147	L. Wachnicki	99
E. Majková	65	M.A. Pietrzyk	52, 92, 93	G. Spinolo	44	L. Walczak	81
M. Manecki	110	U. Pietsch	45	N. Spiridis	72	M.S. Walczak	107
A. Marcelli	43	J. Pigłowski	144	M.J. Stankiewicz	1, 74	W. Walukiewicz	147
B. Marciniac	94	S. Pikus	139	P. Starowicz	76	D. Wardecki	148
M. Marszałek	120	S. Pin	44	N. Stojanovic	142	D. Wasik	56
A.J. Martinez-Blanco	83	E. Piskorska-Hommel	118	T. Story	52	A. Wawrzyniak	75
Ł. Mateuszuk	114	P. Piszora	137, 145	W. Strupiński	90	E. Werner-Malento	155
K. Matlak	72, 103	M. Podgórczyk	138	L. Suárez	107	W. Wierzchowski	73, 95, 152
K.E.A. Max	47	K. Polewski	132	J. Susini	79, 115, 133	K. Wieteska	73, 95, 152
K. Mazur	95	A. Polit	120	J.C. Sutherland	132	D. Wilgocka-Ślęzak	72
E.G. Michel	81, 83	R. Przeniosło	85, 148	D.I. Svergun	59	P. Wilk	121
S. Mickievicius	92, 93, 106	C. Quiros	83	J. Szade	76	B.S. Witkowski	99
B. Mierzwa	135	K. Rademann	113	W. Szczerba	113	J. Witkowski	78
R. Minikayev	142, 155	M. Radtke	113	A. Szczerbakow	93	A. Wlodawer	4
W. Minor	42	S. Rathgeber	144	J. Szlachetko	79, 115, 117, 133, 134	T. Wojciechowski	101
R. Mirowski	78	M. Reconditi	60, 70	M. Szot	92, 93	M. Wojcik	90, 112
A. Misiuk	97, 88, 126	U. Reinholz	113	K. Szpotkowski	153	A. Wolska	56, 107, 118, 126, 128, 130
J. Morse	79, 133	H. Renevier	118	K. Szustakiewicz	144	A. Wolska	126
T. Narayanan	70	H. Riesemeier	113	W. Szuszkiewicz	93	K.M. Yu	147
M. Naskrent	94	W. Rode	121	A. Szymańska	150, 154	Y. Zabala	120
R. Nietubyc	34, 52, 78, 135	M. Roessle	59	M. Szymonski	81	D.R.T. Zahn	65
J. Nowak	64	P. Romanowski	78, 88, 96, 97, 101, 152	M. Ślęzak	72, 86, 103	M. Zajac	72, 86, 103
K. Nowakowska-Langier	52, 78, 142	R. Rüffer	72, 103	T. Ślęzak	72, 86, 103	P. Zajdel	140
K. Nowakowski	61, 116	W.R. Rypniewski	121	Cz. Ślusarczyk	102	W. Zalewski	91, 111
W. Nowicki	145, 146	J. Sadowski	52, 56, 99, 101	T. Tataryn	122	A. Zarzycki	120
P. Olalde-Velasco	147	M. Salome	79, 115, 133	M. Taube	150, 151, 154, 156	J. Zegenhagen	54
P. Olszowy	139	J. Sarnecki	95	S. Thiess	54, 92, 93	K. Zelga	135
B.A. Orłowski	29, 76, 92, 93, 106	R. Sato	130	A.F. Thünemann	113	M. Žitnik	134
M. Pajek	79, 115, 117	D. Savytskii	122	K. Tiedtke	142	I. Zizak	66
E. Partyka-Jankowska	86	P. Schäfer	65	S. Toleikis	142	Y.V. Zubavichus	98, 125
W. Paszkowicz	80, 137, 152, 155	E. Schmidbauer	122	K. Tomala	76	M. Żabska	144
		A. Schütz	47	H. Tomizawa	24, 84	M.S. Žbik	69
		P. Segovia	81, 83	D. Trots	146	E. Żukowski	141
		M. Senulis	106	J. Trunk	132	D. Żymierska	29, 32, 142
		A. Shalimov	88	T. Tschentscher	142		
		K. Shimada	48	A. Tuross	90, 95		
		V.A. Shuvaeva	125				

Conference proceedings of meetings organised / co-organised by Polish Synchrotron Radiation Society, 1992-2009: International Schools and Symposia of Synchrotron Radiation in Natural Science (ISSRNS), Polish Meetings of Synchrotron Radiation Users (KSUPS) and other related meetings.

- 1) 1st ISSRNS, Jaszowiec 13-21.05.1992. Eds.: K. Ławniczak-Jabłońska, G. Kowalski, *Acta Physica Polonica A*, Vol. 82, No 1 & No 2, 1992.
- 2) 2nd KSUPS, Mogilany, 1993. Ed. J. Konior, *Universitatis Iagellonicae Folia Physica*, Fasc. XXXVI, 1994.
- 3) 2nd ISSRNS, Jaszowiec 18-26.05.1994. Eds.: K. Ławniczak-Jabłońska, R. Iwanowski, *Acta Phys. Polonica A*, Vol. 86, No 4 & 5, 1994.
- 4) Zastosowanie promieniowania synchrotronowego, 3rd KSUPS, Warszawa, 6-7.06.1995., Ed.: E. Sobczak (Fundacja im. Wojciecha Świątosławskiego, Gliwice, 1995).
- 5) 3rd ISSRNS, Jaszowiec 31.05–8.06.1996. Ed.: J. Konior, *Acta Physica Polonica A*, Vol. 91, No 4 & No 5, 1997.
- 6) Application of Synchrotron Radiation to the Study of Inorganic and Biological Materials, 4th KSUPS, Kraków-Przegorzaly, 18-19.06.1997. Ed.: J. Grochowski, *Universitatis Iagellonicae Folia Physica*, Fasc. XXXIX, 1998.
- 7) 4th ISSRNS, Ustroń-Jaszowiec, 15-20.06.1998. Eds: W. Paszkowicz, E. Sobczak, *Journal of Alloys and Compounds*, Vol. 286, No 1-2, 1999.
- 8) Synchrotron Radiation Studies of Materials, 5th KSUPS, Warszawa, 31.05–1.06.1999. Eds.: M. Lefeld-Sosnowska, J. Gronkowski, (Institute of Experimental Physics, University of Warsaw, Warsaw 1999).
- 9) 5th ISSRNS, Ustroń-Jaszowiec, 12-17.06.2000, eds: Cz. Kapusta, W.M. Kwiatek, J. Konior, M. Stankiewicz, *Journal of Alloys and Compounds*, Vol. 328, No 1-2, 2001.
- 10) Synchrotron Crystallography – from Source to Applications, Synchrotron Crystallography (SYNCRYS) 2001, Krynica-Czarny Potok, 31.08-4.09.2001. Ed.: J. Grochowski in collaboration with W. Paszkowicz, *Acta Physica Polonica A*, Vol. 101, No 5, 2002.
- 11) 6th ISSRNS, Ustroń-Jaszowiec, 17-22.06.2002. Eds.: W. Paszkowicz, A. Burian, J. Gronkowski, B.J. Kowalski, *Journal of Alloys and Compounds*, Vol. 362, No 1-2 (2004).
- 12) Development of Methods for Characterizing the Microstructure of Novel Materials, European Materials Research Society Fall Meeting, Symposium B, 15–19.09.2003, Warsaw. Eds.: W. Paszkowicz, J. Pelka, *Journal of Alloys and Compounds*, Vol. 382, No 1-2, 2004.
- 13) 7th ISSRNS, Zakopane 8-13.06.2004. Eds.: W. Paszkowicz, B.J. Kowalski, E.A. Görlich, Z. Kaszukur, *Journal of Alloys and Compounds*, Vol. 401, No 1-2, 2005.
- 14) 8th ISSRNS, Zakopane 8-13.06.2006. Ed.: W. Paszkowicz, *Synchrotron Radiation in Natural Science*, Vol. 5 No 3, 2006.
- 15) 7th KSUPS, Poznań, 24-36.09.2007. Eds.: M. Kozak, W. Paszkowicz, *Acta Physica Polonica A*, Vol. 115 No. 2, 2008.
- 16) 9th ISSRNS, Ameliówka 15-20.06.2008., Eds.: W. Paszkowicz, B.J. Kowalski, E.A. Görlich, *Radiation Physics and Chemistry*, Vol. 78, Suppl. 10, 2009.
- 17) 8th KSUPS, Podlesice 24-26.09.2009. Eds.: W. Paszkowicz, M. Sikora, W. Szuszkiewicz, *Acta Physica Polonica A*, Vol. 117 No 1-2, 2010.
- 18) 10th ISSRNS, Szklarska Poręba 6-11.06.2010. Eds.: M. Kozak, P. Piszora, Z. Kaszukur, *Radiation Physics and Chemistry*, in preparation.

JOBS AND POSTDOCS

The European Synchrotron Radiation Facility (ESRF) is Europe's most powerful light source. Our fields of research are Physics and Chemistry, Life Sciences and Medicine, Earth and Environmental Sciences, Surface and Materials Sciences. We offer you an exciting opportunity to work with international teams using synchrotron light in Grenoble, in the heart of the

French Alps. Have a look at www.esrf.eu/jobs. We have vacancies for Scientists, Post doctoral fellows, PhD students, Engineers, Technicians and Administrative staff. Contact: ESRF, BP 220, F-38043 Grenoble Cedex 9, FRANCE, Tel.+33476882827, recruitment@esrf.eu, www.esrf.eu.

12 months post-doc "Advanced TEM study of local electronic properties of indium rich nitrides." at the Institute of Physics PAS (Warsaw). Indium-rich nitride heterostructures will be investigated with the use of a monochromatic, image aberration corrected FEI TITAN CUBED 80-300. High-resolution imaging, electron holography, and electron energy loss spectroscopy will be applied for internal electrostatic field and valence band structure characterizations at atomic and nano scales. Development of computer simulations for the interpretation of experimental data will be an important part of the work. The goal is to determine the influence of structural defects on the electronic properties of the investigated materials. The work will be conducted in cooperation with 12 EU groups of the Marie Curie Initial Training Network (EU/FP7) "RAINBOW" <http://rainbow.ensicaen.fr/>. Deadline for applications: 30.06.2010; Duration: 12 months; Gross salary (including employer charge) around 3600 Euro/month.

Requirements: Ph.D. in Solid State Physics, Crystallography or Material Sciences; Defended thesis in the domain of Transmission Electron Microscopy; A high scientific record, publications in international journals; Fluent English in writing and speaking; Documented experience in one of the following techniques: EELS, Electron-holography. The candidates should fulfill the eligibility criteria of the EU/FP7 Marie Curie Initial Training Networks <http://rainbow.ensicaen.fr/spip.php?rubrique12>. For application, the candidate should send a CV. In next steps those selected on the basis of the CV will be invited to send a copy of their PhD thesis, relevant publications, two recommendation letters, as well as a motivation letter. The selection of candidates will be monitored by the training task force of the RAINBOW Initial Training Network. Therefore, each candidate should send a copy of the CV to: Dr. Sławomir Kret (kret@ifpan.edu) as well as to the RAINBOW project manager Ms Claire Durand (claire.durand@ensicaen.fr).

Polskie Towarzystwo Promieniowania Synchrotronowego (PTPS)

Siedziba:

ul. Radzikowskiego 152
31-342 Kraków
tel. (0) 12 662 82 35

Nr konta bankowego:

Bank PeKaO SA | Oddział w Krakowie
80 1240 1431 1111 0000 1045 5083

Adres do korespondencji:

Dr Danuta Żymierska
Instytut Fizyki PAN
al. Lotników 32/46
02-668 Warszawa
tel/fax: (0) 22 843 60 34
[e-mail: zarzadz@synchrotron.org.pl](mailto:zarzadz@synchrotron.org.pl)
<http://www.synchrotron.org.pl>

Roczne składki członkowskie dla członków zwyczajnych:

Wysokość składek członkowskich (od 1 stycznia 2009 r.):
Samodzielni pracownicy nauki – 50 zł
Doktorzy – 40 zł
Pozostali – 30 zł

Zarząd Polskiego Towarzystwa Promieniowania Synchrotronowego (Kadencja: 2008 – 2011)

Prezes:

Prof. dr hab. Krystyna Jabłońska
Instytut Fizyki PAN
al. Lotników 32/46
02-668 Warszawa
e-mail: jablo@ifpan.edu.pl

Wiceprezes:

Prof. dr hab. Andrzej Burian
Instytut Fizyki
Uniwersytet Śląski
ul. Uniwersytecka 4
40-007 Katowice
e-mail: burian@us.edu.pl

Wiceprezes:

Dr hab. Maciej Kozak
Wydział Fizyki
Uniwersytet im. A. Mickiewicza
ul. Umultowska 85
61-614 Poznań
e-mail: mkozak@amu.edu.pl

Sekretarz:

Dr Danuta Żymierska
Instytut Fizyki PAN
al. Lotników 32/46
02-668 Warszawa
e-mail: zymier@ifpan.edu.pl

Skarbnik:

Doc. dr hab. Wojciech Kwiatek
Instytut Fizyki Jądrowej PAN
ul. Radzikowskiego 152
31-142 Kraków
e-mail: wojciech.kwiatek@ifj.edu.pl

Wydawca:

Doc. dr hab. Wojciech Paszkowicz
Instytut Fizyki PAN
al. Lotników 32/46
02-668 Warszawa
e-mail: paszk@ifpan.edu.pl

Członek Zarządu ds. Strony

Internetowej:
Dr inż. Anna Wolska
Instytut Fizyki PAN
al. Lotników 32/46
02-668 Warszawa
e-mail: wolska@ifpan.edu.pl

Członkowie:

Dr hab. Edward A. Górclich
Instytut Fizyki
Uniwersytet Jagielloński
ul. Reymonta 4
30-059 Kraków
e-mail: ufgoerli@cyf-kr.edu.pl

Doc. dr hab. Bogdan Kowalski
Instytut Fizyki PAN
al. Lotników 32/46
02-668 Warszawa
e-mail: kowab@ifpan.edu.pl

Prof. dr hab. Bronisław Orłowski
Instytut Fizyki PAN
al. Lotników 32/46
02-668 Warszawa
e-mail: orbro@ifpan.edu.pl

Dr hab. Paweł Piszora
Wydział Chemii
Uniwersytet im. A. Mickiewicza
ul. Grunwaldzka 6
60-780 Poznań
e-mail: pawel@amu.edu.pl

Zawiadomienie

Walne Zebranie Polskiego Towarzystwa Promieniowania Synchrotronowego

Zapraszamy na Walne Zebranie PTPS, które odbędzie się w trakcie 10. *International School and Symposium on Synchrotron Radiation in Natural Science* w Szklarskiej Porębie w hotelu "LAS Piechowice" w czwartek, 10 czerwca 2010 roku o godz. 11.00 z podanym poniżej porządkiem obrad.

Sekretarz PTPS
D. Żymierska

Prezes PTPS
K. Jabłońska

Porządek obrad:

1. Powitanie uczestników i przyjęcie porządku obrad.
2. Sprawy członkowskie.
3. Sprawozdanie merytoryczne z działalności Zarządu PTPS za okres od 25.09. 2009 r. do 9.06.2010 r.
4. Sprawozdanie finansowe Zarządu.
5. Sprawozdanie Komisji Rewizyjnej.
6. Dyskusja nad sprawozdaniami.

7. Głosowanie nad przyjęciem sprawozdań.
8. Organizacja 9. KSUPS w roku 2011.
9. Organizacja w Polsce Międzynarodowej Konferencji XAFS16 w roku 2015.
10. Plany działalności PTPS.
11. Sprawy bieżące.
12. Wolne wnioski.



Polskie Towarzystwo Promieniowania Synchrotronowego

istnieje od 1991 roku

Naszym celem jest:

Wymiana informacji na temat badań prowadzonych przy użyciu promieniowania synchrotronowego przez polskich naukowców, osiąganych przez nich wyników i publikacji naukowych w czasopismach o zasięgu międzynarodowym

Działania na rzecz szkolenia młodej kadry polskich studentów, doktorantów i naukowców w zagranicznych ośrodkach synchrotronowych

Wymiana doświadczeń w zakresie popularyzacji wiedzy na temat badań prowadzonych przy użyciu promieniowania synchrotronowego

Pomoc w organizowaniu dostępu polskich naukowców do źródeł promieniowania synchrotronowego

Koordinacja działalności informacyjnej dotyczącej możliwości pomiarowych powstającego w Polsce ośrodka synchrotronowego i aktywizacja młodej kadry naukowej w tym zakresie

Organizowanie konferencji i innych imprez naukowych



www.synchrotron.org.pl

